Synthesis and Evaluation of New Ligands for Gallium Radiolabelling

BRADLEY PETER WALDRON

Synthesis and Evaluation of New Ligands for Gallium Radiolabelling

Bradley Peter Waldron

Supervisor:

Professor David Parker

Department of Chemistry

Thesis submitted in fulfilment of Doctor of Philosophy

October 2012

Declaration

The research described herein was undertaken at the Department of Chemistry, Durham University between January 2009 and August 2012. All of the work is my own; no part of it has previously been submitted for a degree at this, or any other, university.

Statement of Copyright

Bradley Waldron: Date:

Professor David Parker: Date:

Abstract

A series of N_3O_3 triaza-tricarboxylate hexadentate ligands, based on the 6-amino-1,4-diazepine scaffold, has been designed and synthesised. An investigation of the suitability of these ligands towards application in ^{68}Ga-PET has been conducted, with particular focus on the efficiency and efficacy of radiolabelling. Subsequently, selectivity for Ga(III) over other relevant cations has been studied, along with exploration of the kinetics of radiolabelling, stability and *in vivo* behaviour of the radiolabelled complexes in healthy rats. The four best candidates quantitatively radiolabel within three minutes at room temperature over the pH range 4 – 7, to give a single ^{68}Ga-radiolabelled species which is sufficiently stable for in vivo application. As a result, these compounds are very promising candidates for use as ligands in ^{68}Ga-PET.

Decoration of the AMPED scaffold amine functionalities yielded a series of chelators, which allowed the ^{68}Ga-radiolabelling properties of this family of ligands to be investigated. The ligands have a mixture of acyclic and cyclic properties, which facilitated rapid binding of the metal and formation of a stable complex. Synthetic details and ^{1}H NMR solution state properties are described. With respect to radiolabelling, the best ligands were those with the least sterically demanding exocyclic amine substituents. However, ligands featuring a mono-alkylated exocyclic amine were prone to internal lactamisation under acidic conditions, which rendered these compounds ineffectual as ligands for ^{68}Ga.

The synthesis and radiochemical evaluation of an additional series of ligands, featuring a modified core structure, designed to inhibit the lactamisation reaction and promote ‘pre-organisation’ of the ligand donors were undertaken. The synthetic methodology developed allows for selective functionalisation of the different amine groups of the ring. Modification of the AMPED core by substitution of the tertiary methyl group for a phenyl moiety increased the steric bulk close to exocyclic amine, which inhibited internal lactamisation. Critically, the methyl-for-phenyl substitution does not have a detrimental effect on the complexation properties.

Finally a study was undertaken of the radiolabelled complex speciation, using NMR spectroscopy and X-ray crystallography. The presence of multiple radiolabelled complex species was attributed to the formation of kinetically trapped complexes of differing stability. The relative population of the two major ligand conformations is controlled by the relative steric demand of the substituents at the quaternary site. The exocyclic amine is subject to protonation (pK_a 5.7), and therefore the relative population of the ligand conformers is pH dependent over the range 3 – 7. By substituting the methyl group for a more sterically demanding phenyl group, the population of the ligand conformation favouring fast and stable gallium binding was increased.

Acknowledgments

I would like to express my sincere gratitude and thanks to Professor David Parker. His enthusiasm, support, hard work and expertise are an example I hope to follow in my future career. He has shown me the importance of doing thoughtful chemistry which makes a contribution. His persistence that I should always aim *to break a leg* will stand me in good stead for future endeavours. I am also thankful for the daily discussion and freedom he has given me to develop ideas. His input during the writing of this thesis has been patient and constructive, guiding me in the right direction.

I would also like to thank Professor Frank Rösch for hosting me in Mainz, and for his invaluable contributions to the project. It has been a pleasure to collaborate with him, and I look forward to doing so in the future. Thanks to Dr Carsten Burchardt and Ms Melanie Zimny, for all the time and effort they spent planning visits, and teaching essential radiochemistry laboratory techniques. Furthermore, I would like to thank the Rösch and Ross research groups for welcoming me during visits.

This research would not have been possible without the excellent analytical services of the Durham University Department of Chemistry. In particular I would like to thank: Dr Alan Kenwright, Dr Ian McKeag, Dr Juan Aguilar, Dr Catherine Hefferman (NMR), Dr Jackie Mosely, Dr Mike Jones (Mass-spec) and Dr Dimtry Yufit (Crystallography) and for their time, patience, expertise and advice.

The DP group has been a family away from home. I will take away many great memories and experiences from an unforgettable few years with them. In particular I would like to thank Dave (*"just now"*), James ("*what?"*), Pete (*x – you know what I mean*), Robek ("you are…"), Stephen (extrapolate this…) for their great friendships. Others that have filled the time with happiness and fun: Rachel, Brian, Nick ,Martina , Alex, Kanthi, Anurag, Kirsten, Liz, Elena, Neil and Katie.

Johanna, thank you for your endless encouragement, support and understanding. I doubt I will ever be able to show my true gratitude and appreciation for everything you have done in the months building up to the end of my PhD. You have made this all worthwhile.

I would like to express my eternal gratitude and love to my Mother and Father for unflinching support, always pushing me to do better and affording me this fantastic opportunity. None of this would have been possible without them.

FOR MOM AND DAD

IN MEMORY OF WES AND CHERYL

Abbreviations

12-N_4	1,4,7,10-tetraazacyclododecane
^{68}Ga	68-Gallium(III)
9-N_3	1,4,7-triazacyclocnonane
AAZTA	6-amino-6-methylperhydro-1,4-diazepinetetraacetic acid
AMPED	6-amino-6-methyl-1,4-diazepine
APPED	6-amino-6-phenyl-1,4-diazepine
ax	axial
Boc_2O	Di-tert-butyl dicarbonate
C	chair conformation (C^x represents a carbon atom)
Cax	chair conformation with alkyl group axial
Ceq	chair conformation with alkyl group equatorial
DAZA	6-amino-1,4-diazepine
DCM	dichloromethane
DOTA	1,4,7,10-tetraazacyclododecane-1,4,7,10-tetraacetic acid
eq	equatorial
ESMS	electrospray mass spectrometry
EtOH	ethanol
HEPES	(4-(2-hydroxyethyl)-1-piperazineethanesulfonic acid)
LC	liquid chromatography
MeOH	methanol
MRI	magnetic resonance imaging
N	Nitrogen
NaHEPES	Sodium (4-(2-hydroxyethyl)-1-piperazineethanesulfonate)
N-CH_2-CH_2-N	ethylene diamine fragment
Nendo	endocyc;lic amine/nitrogen
Nexo	exocyclic amine/nitrogen
NMR	nuclear magnetic resonance
nOe	nuclear Overhauser effect
NOTA	1,4,7-triazacyclocnonane1,4,7-triacetic acid
PBS	phosphate buffered saline
PET	positron emission tomography
Radio-TLC	the technique of detecting the radioactivity on an eluted TLC plate
SPECT	single photon emission computed tomography
t½	radioactive half-life
TBBA	tert-butyl bromo-acetate
TC	twisted-chair conformation
TFA	trifluoroacetic acid
THF	tetrahydrofuran
TLC	thin layer chromatography
α-particle	alpha-particle
β-	electron
β+	positron
γ-ray	gamma-ray

Contents

Chapter 1

Chapter 2

Chapter 3

Chapter 4

Chapter 5

Chapter 6

Structure Reference

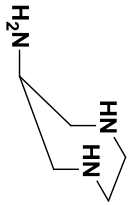

DAZA

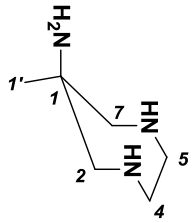

AMPED

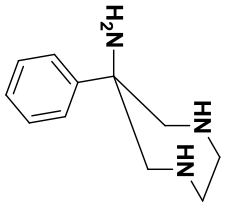

APPED

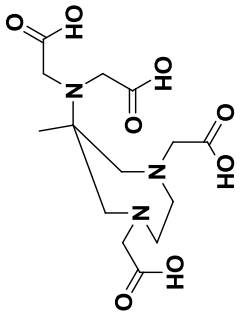

L^1 (AAZTA)

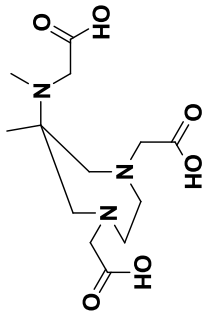

L^2

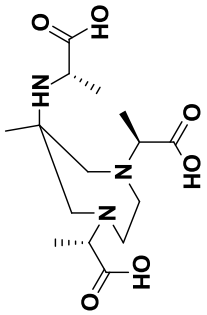

L^3

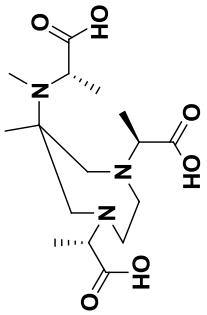

L^4

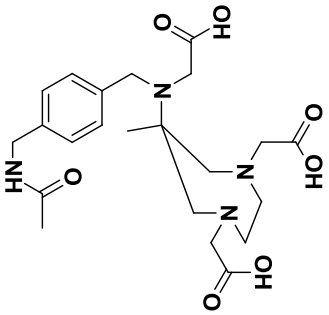

L^5

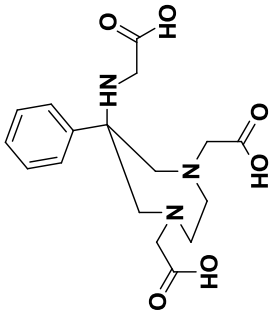

L^6

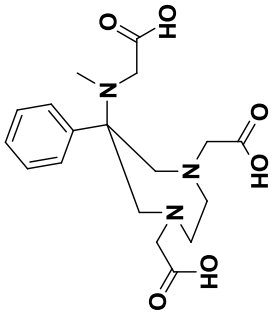

L^7

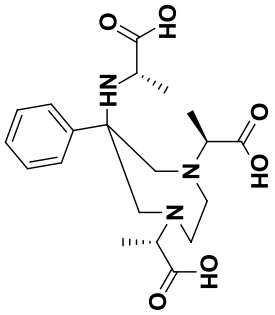

L^8

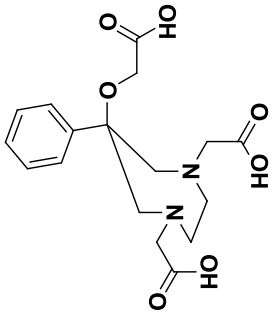

L^9

Chapter 1

Background and Aims of the Project

This chapter introduces medical imaging, with subsequent more detailed, focus on radionuclide imaging. Aspects pertaining to the application of the ^{68}Ga radioisotope in positron emission tomography (PET) are discussed (Sections 1 -5). In section 6 the ligand system of interest is introduced and its literature history reviewed. The aims and specification of the project are outlined in section 7.

1 Medical Imaging Techniques

The effective management of diseases and conditions relies heavily on the accuracy of the investigation and diagnosis. Central to the diagnostic process are the physical techniques used, which are referred to as medical imaging techniques (or modalities). In addition to providing a means for diagnosis, medical imaging techniques also play an important role in the planning and monitoring of the treatment of a disease.[1-3]

Medical imaging techniques are non-evasive methods that allow for the characterisation and measurement of biological morphology, and more recently has facilitated studies of the physiological and biochemical processes taking place in the body.[4-6] As a result, medical imaging techniques can be divided into two categories.

Classical (or "clinical") imaging provides information on the morphology of the body from an internal perspective. Techniques which fall into this category include radiography, X-ray computed tomography (CT), ultrasound imaging, magnetic resonance imaging (MRI) and radioisotope imaging. In contrast, molecular imaging uses cellular probes which provide useful information about the chemical environment.[7] It allows the visualization of biochemical and physiological processes taking place at the molecular and cellular level. Typically, a probe is selected or designed which is sensitive to a specific chemical analyte or process of interest, and is able to report back in a manner which can be detected. Some examples include radioisotope imaging (tracers) and luminescence imaging.[7, 8]

Radiography (commonly known as 'X-ray') was the first medical imaging technique, and followed from the discovery of X-rays in 1985.[9] X-ray images are produced by passing externally generated X-

rays through a region of interest of the patient. As the X-rays pass through the body, they encounter electrons and particles and are consequently absorbed or scattered by the tissue. Certain tissues have higher density than others and will absorb and scatter more X-rays as a result. By placing a detector behind the patient, it is possible to distinguish the regions through which the most X-rays are passing, and therefore identify regions of differing density. X-ray methods also allow for visualization of seemingly hollow structures (intestinal tract, lungs, and vascular system) through the use of certain high molecular weight contrast agents. For example the intestinal tract can be visualized by ingesting barium sulphate.[1, 9]

Computed tomography (CT) is essentially a more advanced form of X-ray imaging. An annular shaped X-ray unit is used to measure a large number of 2D X-ray slices of the patient in the plane of the annulus. Specialised software is then used to process the data into a 3D image showing the internal morphology of the patient.[9]

Ultrasound imaging uses high frequency sound waves directed towards the body to image regions of soft tissue. The sound waves are reflected when they come into contact with micro-bubbles in the tissue, with the tissue density being related to the magnitude of the reflected wave. From the reflected signal, it is possible to determine the different distances at which reflections took place and the relative density of the tissue, allowing an image to be constructed incorporating the tissue densities and relative positioning.[7]

Magnetic resonance imaging (MRI) effectively determines the distribution of water protons inside the patient. The resonant frequency of the water protons depends on their exact location within an applied magnetic field. Thus, by applying a gradient magnetic field over a specific region, it is possible to acquire spatial information about the water relaxation rates within that region. Different tissues have characteristic water relaxation rates, and thus it is possible to construct an image which shows the relative positions of different tissues. Enhanced MRI, which provides better images in a shorter time, can be achieved through the use of paramagnetic contrast agents, which enhance the relaxation rate of the water protons close to the contrast agent. Enhanced relaxation rates result in better contrast between regions, and hence better images.[2, 3, 9]

Radioisotopes, both metals and non-metals, are elements with an unstable nucleus due to an unfavourable ratio of protons and neutrons. In order to obtain a more stable configuration the isotopes undergo radioactive decay, whereby the excess energy is released either as a particle of the

nucleus or one of its electrons.[9, 10] The energy emitted is either in the form of particles (α- or β-particles or Auger electrons) or as electromagnetic radiation (X-rays and/or γ-rays). By detecting these emissions it is possible to determine the location of the radiolabel (administered radioisotope). Photon emitting radionuclides are detected directly by single photon emission computed tomography (SPECT), whereas particle emitters are detected indirectly by positron emission tomography (PET).[1, 9, 10] Radionuclide imaging is only useful when the radiolabel has a bio-distribution profile of interest. Although certain radioisotopes naturally accumulate in specific tissues, the radioisotope is usually attached to some form of targeting agent which determines its fate. For example, iodide has a natural affinity for thyroid tissue, and therefore ^{123}I can be used for imaging of the thyroid gland.[11] The radioisotope ^{82}Sr, on the other hand, tends to accumulate in the bones and liver.[12] Radionuclide imaging can also be used to follow certain physiological process and reactions.

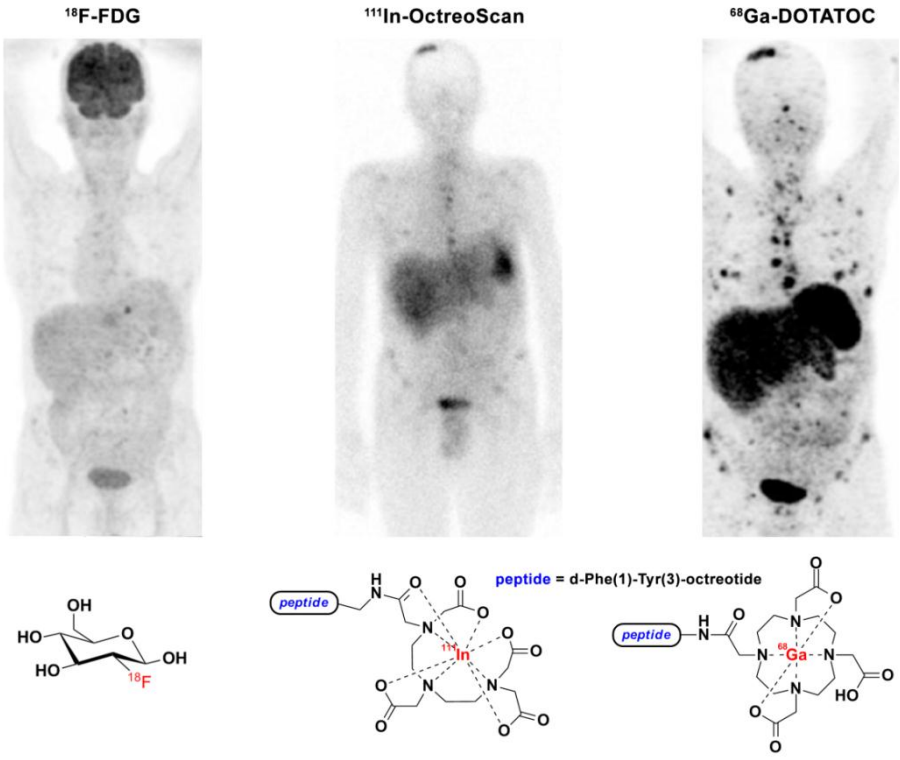

Figure 1.1 *Radionuclide scans (with ^{18}F-FDG, ^{111}In-OctreoScan™ and ^{68}Ga-DOTATOC) of a patient with metastases (chest area) and a neuroendocrine tumour (top of the brain), showing the greater affinity of ^{68}Ga-DOTATOC than ^{111}In-OctreoScan™. Localisation of ^{18}F-FDG occurs in areas* of high metabolic activity, and is far *less useful for the imaging of neuroendocrine tumours. Picture taken from.*[13]

For example, 2-[^{18}F]fluoro-2-deoxy-d-glucose (FDG) is an analogue of glucose which can be used to assess metabolic activity. FDG is taken up by cells which exhibit high metabolic rates (and therefore have a high rate of glucose consumption) such as the brain, kidneys and certain cancer tumours. Once inside a cell, the glucose molecule is phosphorylated which prevents it from leaving, and therefore facilitates PET imaging of the region.[8] A commercially used PET agent, ^{111}In-OctreoScan™, has a peptide fragment which mimics somatostatin (SST), and has affinity for certain SST receptors which are over-expressed by primary neuroendocrine tumours and metastases.[14] However, OctreoScan™ is currently in competition with the more efficient SST PET imaging agent ^{68}Ga-DOTATOC (Figure 1.1).[14]

Whilst all the techniques listed above can provide very useful highly resolved anatomical information, they are limited by the fact that their resolution is insufficient to investigate cellular conditions and function.[3]

Molecular imaging techniques, such as luminescence and nuclear magnetic resonance spectroscopic imaging, are quickly emerging as techniques which can provide useful information on cellular and molecular processes or conditions. The information is derived from the luminescence or magnetic resonance properties of an administered chemical entity. These information providing entities are commonly described as molecular probes, as opposed to imaging agents. The premise is that these molecular probes should report on some process or analyte of interest.

As shown in the preceding discussion, there is a wide range of imaging modalities available. It is important to note that each has advantages and disadvantages in terms of the resolution, measurement time, applicability, costs and additional requirements (i.e. equipment, tracers to make imaging possible). A summary of the different imaging modalities and their characteristics is shown in Table 1.1.

Table 1.1 *Comparison of the key characteristics of different imaging modalities.*[3, 7, 9]

Imaging modality	Tissue penetration	Resolution	Time required for measurement
ultrasound	deep	300 µm	s
Fluorescence microscopy	shallow	500 nm	s
SPECT	deep	2-3 mm	min - h
PET	deep	1-2 mm	min - h
MRI	deep	200 µm	min - h
CT	deep	400 µm	min

Furthermore, some of the techniques are inherently susceptible to outside conditions which may vary. For instance, magnetic resonance imaging (MRI) is temperature sensitive, whereas the signal detected from a radionuclide in PET/SPECT is not. For these reasons, it can be advantageous to apply more than a single imaging modality to a particular study. This has led to a relatively new approach, referred to as multimodal imaging.[7] The basic premise is that for imaging techniques which utilise an imaging agent (to provide a detectable signal or increased contrast), it is possible to incorporate properties required by more than one imaging technique into this single entity. This has obvious benefits in terms of costs and time (licensing of the imaging agents, clinical trials, running costs), and minimizes the effect on the patient. Furthermore, multimodal imaging agents also ensure identical localization of the previously separate tracers.[7, 15] There are a number of obstacles to the synthesis of multi-modal imaging agents, but this is beyond the scope of this discussion.

2 Radionuclide Imaging

2.1 General

The concept of a tracer was first introduced by George de Hevesy (1923), and was defined as a chemical substance, which when introduced into a system can be followed through the course of a process of interest.[16] The tracer should; not influence or disturb the system, and be able to provide information on processes taking place of distribution of a chemical substance.[16] Radiotracers, are widely applied in medicine and research for the study of *in vivo* pharmacokinetics, physiological processes, imaging (diagnosis) and radiotherapy. Often confused, a radioligand and radiotracer have an essential difference in the 'biological' mechanism which makes the imaging targeted. A

radioligand is a radiolabelled molecule that can bind/interact with another molecule in a predictable fashion, thereby allowing the target to be imaged. This differs from a radiotracer which is able to follow/trace the in vivo behaviour of naturally occurring molecule by virtue of its chemical similarity, thereby providing information on a biological process.

The two most prevalent fields of radionuclide research are radio-imaging and radiotherapy. In radiotherapy, the primary objective is to induce cell death by directing radiation at a specific target within the body. Parasitic or infected cells can be dosed with 'lethal' radiation from nuclei which emit α-particles, $\beta^{+/-}$-particles or Auger electrons. For a given radionuclide, the interaction of the emitted radiation with the target tissue should be maximised, and therefore efficient targeting is crucial.[3, 9]

Diagnostic radionuclide imaging (radio-imaging) also relies on the radiolabel being concentrated in or isolated in certain parts or systems of the body. The photons resulting from the radioactive decay are detected by external cameras and the data processed to provide information about the location and shape of the region where the radiolabel has accumulated. This is quite different to X-ray imaging, where external radiation is directed at the patient and regions of differing density determined by the amount of radiation absorbed.

2.2 Advantages and Disadvantages of Radionuclide Imaging

In addition to being independent of the external environment, the very high sensitivity of radio-imaging is a significant advantage over imaging techniques such as MRI and structure-depicting imaging techniques. In a recent study using a ^{13}C-labelled drug, the administered dose required for MRI and radionuclide detection *in vivo* was determined. The study was conducted on a rat, and extrapolated for a 70 kg man.[17] Detection by MRI and radionuclide imaging required 10 g and 1 µg doses of the drug respectively.[17] The high sensitivity of radionuclide imaging arises from the fact that there is no significant background signal.[18] A further benefit of radionuclide imaging is that through appropriate design, and chemical modification of the radiolabelled probe, the radionuclide can be targeted to specific tissues or receptors, thus allowing the disease to be diagnosed more directly than techniques which rely only on anatomy. In addition, it may be possible to investigate biochemical and physiological processes in the body using this technique.[3, 19-21]

In other areas of molecular imaging (luminescence and MRI) there is considerable effort directed towards the development of responsive imaging agents.[22-25] Such imaging agents have the inherent ability to respond to the presence of a chemical substance or stimulus in a manner which can be easily detected. It is not possible to alter the emission properties of a radionuclide, and as a result responsive probes based on radionuclides are not possible. However, attempts are being made to incorporate radionuclides into responsive systems in which they may carry out a tracer function.[7]

2.3 Types of Radionuclide Imaging

Radiolabels which emit γ-rays (electromagnetic radiation) pass through human tissue relatively easily, and can be detected directly using an externally-located Anger camera, by means of single photon emission computed tomography (SPECT). The γ-rays emitted must be sufficiently energetic to penetrate the human tissues and be detected by an externally positioned detector, but not outside the detectable energy range of the detector. The images produced by SPECT, map the radionuclide distribution in one plane, thus producing a two-dimensional map of the radionuclide population distribution.[3, 9, 10]

In contrast, emitted particles (β^+: positrons emitted from neutron deficient radionuclides) only travel a short distance (~ 4 mm) before they encounter an electron.[3, 9, 10] During the collision the masses of the positron and electron are converted into pure energy. The emitted energy is called annihilation radiation, and is characterised by collinear photos (γ-rays of 511 keV each) moving in opposite directions (Figure 1.2).[9, 26] The collinear photons produced by positron emitting radionuclides can be detected simultaneously using two externally located detectors by a technique called positron emission tomography (PET).[9, 26, 27] If two photons are detected along a line at the same time, then the origin of the photons (positron-electron collision) must lie somewhere along that line. The exact location can be determined by the intersection of two such lines, and if a large number of these lines are recorded then a 3D image mapping the radionuclide distribution can be produced (Figure 1.2).[26] The positron only travels a short distance in tissue before it is annihilated, which gives PET images a resolution of approximately 1 - 2 mm. PET has been employed to follow therapeutic response[28], tumour imaging[29], neurotransmission[30] and the measurement of blood flow.[14, 19, 31-33]

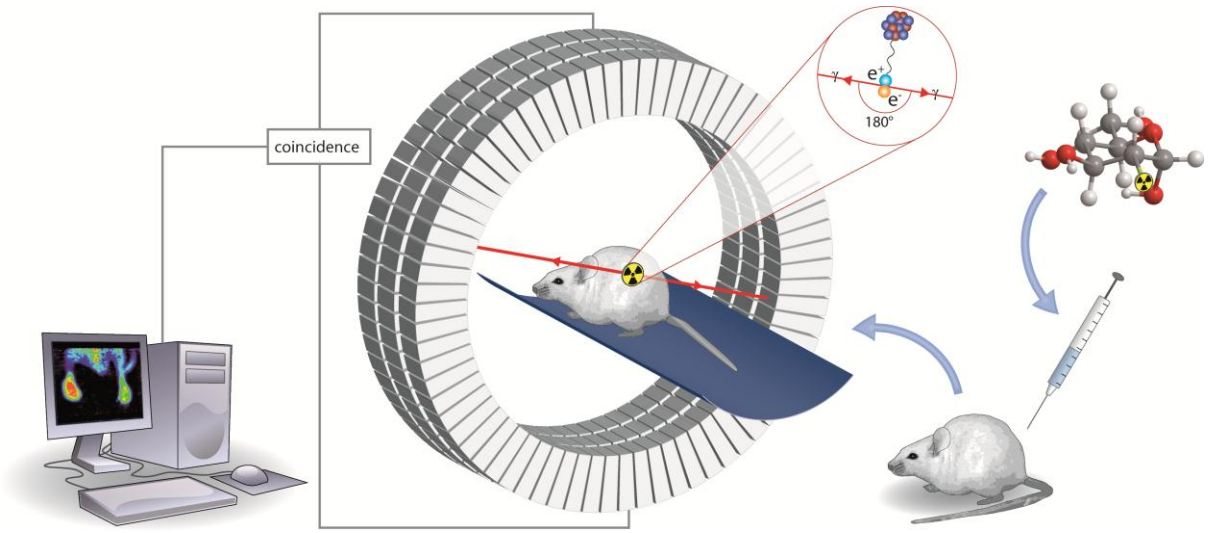

Figure 1.2 *Diagram illustrating β^+-particle emission and annihilation (when it collides with an electron) producing co-linear γ-rays. Detection of coincident emitted γ-rays allows a three-dimensional image of the radiotracer distribution to be constructed. Figure reproduced with the permission of Benedikt Sandhöfer.*

Recently a new 'field' of research, called 'THERANOSTICS', has developed which is effectively a cooperation of radionuclide THERApy and diagNOSTIC imaging. The premise is that, radiopharmaceuticals which prove effective in diagnostic imaging could be utilized in radionuclide therapy by simply changing the identity of the radionuclide that is incorporated. Such an approach is particularly feasible when the radionuclide used has isotopes which are suitable for use in diagnostic and therapeutic applications.[15, 20]

2.4 Choice of radioisotope

The choice of radionuclide is of vital importance, not only in terms of choosing a radionuclide with the appropriate radioactive decay properties, but also in terms of the intended imaging application (i.e., whether the intended application is imaging by SPECT or PET) and radiolabel precursor. For example, different metals have different coordination geometries and preferred coordination sphere sizes; if the intended ligand-radionuclide pair is an unsuitable match, the complex is likely to be unstable and the rate of radiolabelling slow. Dissociation of the metal complex is likely to result in loss of the intended biodistribution, therefore care should be taken to ensure that the chelator and metal ion will give rise to a stable complex *in vivo*. Similarly for non-metal radionuclides, the choice of radionuclide should take into account the intended application (specifically the duration) as well as the radiolabelling protocol.[14, 34]

Of particular interest to this project are targeted radioligands, and therefore some form of targeting vector is essential. A number of biological peptides and antibodies have been shown to be effective in the targeting of certain conditions. These biomolecules are often large, and as a result have very slow pharmacokinetics relating to accumulation (days). Consequently their application requires a radionuclide with a suitably long half-life such as ^{89}Zr (78.4 h) and ^{124}I (100.2 h). The disadvantage of using these radionuclides is the large radiation dose to the patient. Smaller engineered biological 'fragments' have been identified which can serve a similar targeting function has the larger peptides. These fragments are often cheaper and easier to produce, and considerably easier to work with. The faster pharmacokinetics means that a radionuclide with a shorter half-life can be used, thereby decreasing the patient radiation dose, and imaging experiments are considerably shorter. In this regard, the ideal radionuclide for use as an imaging agent possesses the following set of properties:[3, 19, 26, 35-37]

- A high abundance of electromagnetic radiation to be detected. This is also known as the radiative yield, and is important since a radionuclide with a high yield can be administered in smaller amount than one which has a low yield.
- The electromagnetic radiation should have sufficient energy to penetrate the body, yet be sufficiently low to be easily detected.
- In the case of particle emitters, a lower energy particle is preferred. The energy of the emitted particle determines the distance the particle will travel, and is therefore inversely related to the image resolution.
- A low abundance of particulate radiations (α, β) to minimize the harmful radiation dose to the patient.
- A short half-life such that any particulate radiation dose is minimized, but still long enough to permit sufficient time for radiolabelling, administration and detection of the imaging agent. Furthermore, the half-life of the radionuclide should be well suited to the pharmacokinetics of the targeting vector that will be used.
- A decay product which is a stable isotope, will not compromise the stability of the 'active' imaging agent and is non-toxic.
- It should be affordable and readily available.
- Carrier-free and of high chemical purity so that there is no competition from stable isotopes of the same element or others.
- Easy and fast to complex or react (significantly shorter than the half-life of the decaying radioisotope) in a way which renders them useful as imaging agents.

2.5 Metal and non-metal radionuclides for PET

PET employs mainly relatively short lived positron emitting radionuclides.[32] Table 1.2 shows a summary and comparison of the important properties of metal and non-metal radionuclides which could be used in PET. Also included are a three γ-emitting radionuclides (SPECT application) of commercial importance. Properties which are particularly advantageous for PET/SPECT are highlighted in green, while those considered undesirable are in red.

Table 1.2 *Comparison of radionuclides with properties suitable for use in PET and SPECT.*[10, 26, 32, 37-39]

Radionuclide	Half-life	E_{max} (keV)	Radiation type	production
^{11}C	20.3 min	961	β^+ (100 %)	cyclotron
^{13}N	9.97 min	1190	β^+ (100 %)	cyclotron
^{15}O	2.1 min	1732	β^+ (100 %)	cyclotron
^{18}F	109.8 min	634	β^+ (97 %)	cyclotron
^{66}Ga	9.5 h	4153	β^+ (56 %)	cyclotron
^{52}Fe	8.2 h	800	β^+ (57 %)	cyclotron
^{68}Ga	67.6 min	1899 (511)	β^+ (89 %)	generator
^{64}Cu	12.8 h	656	β^+ (19 %)	cyclotron
^{55}Co	17.5 h	1513, 1037	β^+ (77 %)	generator
^{86}Y	14.7 h	2335, 2019, 1603, 1248	β^+ (33 %)	cyclotron
^{89}Zr	78.4 h	897	β^+ (23 %)	cyclotron
^{99m}Tc	6.0 h	141	γ (89 %)	generator
^{111}In	67.9 h	245, 172	γ	cyclotron
^{67}Ga	78.26 h	91, 93, 185, 296, 388	γ	cyclotron

Besides the relevance of the biological application and suitability of the radionuclide the choice of radionuclide depends on a number of other considerations, among which are the cost and convenience of production. Besides substantial cost savings, there are a number of advantages of generator produced radionuclides over cyclotron produced alternatives:[3, 20, 34-36, 40-42]

- The use of cyclotron produced radionuclides requires that there be a cyclotron in the nearby vicinity to allow for synthesis of the radiolabel and subsequent application whilst the radionuclide is still viable.

- Generator produced radionuclides are available almost 'on-demand', whilst cyclotron radionuclides are typically delivered once a day (in the absence of an on-site cyclotron).
- Generator produced radionuclides consist of a long-lived parent nuclide which decays to give the desired, short lived, daughter radionuclide. The daughter radionuclide is easily isolated by solvent extraction or ion exchange.

In some cases short lived radionuclides are desirable. For instance the short half-life of ^{13}N ($t_{½}$ = 9.97 min) allows it to be re-administered in short time frames, or be followed closely with longer lived radionuclides to obtain additional information.[32] PET applications generally prefer longer lifetimes, such that the radiopharmaceutical can be administered, localise and imaged. Radionuclides such as ^{18}F and ^{68}Ga are considered to have suitable decay half-lives for the large majority of biological targeting vectors.[32]

Another important consideration is the radiolabelling method required. Non-metal radionuclides such as ^{18}F and ^{15}N require fast organochemical reactions, which are in some cases not the final step in the synthetic pathway.[32] This can result in significant decay of the radionuclide, and radioactivity exposure. The advantage of this method is that often, the radiolabelled tracer and precursor are chemically similar[32] Metal radionuclides are radiolabelled using chelation chemistry, which requires an appropriate chelating moiety. This may have a negative impact on the biological properties of the targeting vectors present, but has the benefit of radiolabelling being the final step and being conducted in aqueous media (advantageous for large peptides).[32, 36, 42]

3 The 68-Gallium radioisotope and its application

3.1 General

The synthetic benefits of metal radionuclides make them attractive alternatives to non-metal radionuclides such as ^{18}F, ^{123}I and ^{15}O in PET/SPECT. Metal radionuclides which have found application in radionuclide imaging include ^{67}Ga, ^{111}In and ^{99m}Tc. The ^{99m}Tc radionuclide was first used as a radioimaging agent in 1964 and has become the workhorse of radionuclide based diagnostic imaging. This is primarily a result of its favourable nuclear properties (in particular the low particulate emission and $t_{½}$) and generator production.[20, 35, 40] The ^{99m}Tc radionuclide is obtained by decay of the ^{99}Mo radionuclide, which has a half-life of 2.7 days. As a result, the $^{99}Mo/^{99m}Tc$-generator therefore has a short shelf life (~ 1 week). This short shelf-life, coupled with recent

shortages of ^{99}Mo and the benefits of PET over SPECT imaging have necessitated the need for application of other radionuclides.[19, 20, 33, 35, 43] As outlined previously, the important factors to consider when evaluating the suitability of a radionuclide are the half-life, mode of decay, cost and its availability.

Gallium has three radioisotopes, with properties that are conducive to their use as imaging agents in nuclear medicine and research. ^{67}Ga is a γ-ray emitter whose energy (184.6 keV), absence of particulate emission and relatively long half-life (78.27 h) make it ideal for use in SPECT (gamma scintigraphy).[40] However, it is disadvantaged by the fact that its production requires a cyclotron. ^{67}Ga radiolabels have been used for nearly 60 years (with the first production for human use being in 1953) for the imaging of inflammation, infection and, to a lesser extent tumour imaging.[44] It has been administered as gallium citrate, which is quickly dissociated *in vivo* through ligand exchange to the iron binding protein transferrin.[40] Some tumours have receptors for *apo*-transferrin, thus providing a means for non-specific tumour imaging. The mechanism for retention in these tumours is unknown, but it is accompanied by accumulation in the liver, lungs, spleen and bones. ^{67}Ga-transferrin also clears slowly from the blood. The gallium is bound within the iron-binding sites of transferrin.[19, 36] Radioisotopes, ^{66}Ga and ^{68}Ga are both positron emitters and therefore suitable for PET applications. The radioactive properties of the three isotopes are listed in Table 1.3.

Table 1.3 *Radioisotopes of gallium and their nuclear properties.*[21, 35, 40, 41]

Radioisotope	$t_{½}$ (hrs)	β^+ abundance (%)	β^+_{max} (keV)	γ abundance (%)	E_γ (keV)
^{67}Ga	78.27	-	-	37	184.6
^{66}Ga	9.49	56	4153	44	1039, 2572
^{68}Ga	1.13	89	1899	11	(511)*

** two collinear photons produced by positron-electron collision*

^{66}Ga is suitable for radio-imaging due to its relatively long half-life, which allows for measurements over a long time and extended synthetic pathways to the radiolabel. However it is compromised by its low positron abundance and cyclotron source. The ^{68}Ga radionuclide, on the other hand, can be easily obtained from an on-site ^{68}Ge/^{68}Ga generator, has high positron abundance (89%) and intermediate positron maximum energy. With a half-life (1.13 h) which lies between the half-lives of the frequently used ^{11}C (0.33 h) and ^{18}F (1.82 h), it has excellent radioactive decay characteristics. Generator-produced radionuclides are favoured because they are cheaper (with respect to the initial

cost), more convenient and place fewer restrictions on synthetic techniques. The ^{68}Ge parent radionuclide has a long half-life, which gives a generator with a long shelf-life. Furthermore, methods have been developed which allow the ^{68}Ga to be eluted in a high chemical and radioisotope purity.[19, 32, 37, 45-49]

An interesting, and very attractive, advantage of gallium over other radionuclide stems from the variety of gallium isotopes available. The isotopes ^{66}Ga, ^{67}Ga, ^{68}Ga and ^{71}Ga can be used in therapeutic, SPECT, PET and even NMR applications respectively. Thus, once a ligand system has been devised which is able to target a region of interest, it is possible to image or trace (by SPECT, PET and NMR) and subsequently treat the condition simply by changing the isotope used (THERANOSTICS).

The advantages of the ^{68}Ga radionuclide over other radioisotopes are:[19, 32, 34-38, 40, 41, 50, 51]

- The high positron abundance of ^{68}Ga means that acquisition times are considerably reduced in comparison to ^{66}Ga
- The short half-life reduces the particulate dose to the patient, and is between the half-lives of ^{11}C and ^{18}F – the two most commonly used PET radionuclides. It is also well suited to the pharmacokinetics of many biological targeting vectors.
- Availability from a ^{68}Ge/^{68}Ga generator, rendering it cheap and readily available compared to other radioisotopes. Its application allows for PET imaging at facilities without a nearby cyclotron.
- The images obtained from PET (with ^{68}Ga) are more resolved and informative than those obtained from SPECT (with ^{67}Ga).
- It has an intermediate maximum positron energy
- The incorporation of the metal into the ligand is often the last synthetic step, which makes synthesis of the radiolabel potentially faster, safer and easier.

Despite these advantages of ^{68}Ga, the interest in targeted ^{68}Ga radiolabels is relatively recent. Administration of free gallium (as gallium citrate) does allow for some useful imaging.[40, 41] However, it is necessary to influence the biodistribution of the radionuclide by stabilising it as a coordination complex. Furthermore, for the biodistribution of a complex to be driven by its physiochemical properties (size, charge, lipo- / hydro-philicity), it must be kinetically and thermodynamically stable with respect to dissociation under *in vivo* conditions.[19, 34, 40]

The pre-requisites of a complex suitable for ^{68}Ga PET *in vivo* are as follows:

- It should be stable with respect to hydrolysis (formation of hydroxide complexes) and acid-/cation- promoted complex dissociation in the pH range 2-8. If not sufficiently stable precipitation of gallium hydroxide (above pH 3.6) or formation of gallium-transferrin may occur.[40]
- Kinetic inertness to ligand exchange by coordinating proteins such as transferrin. This ligand exchange process is favoured by the high concentration of these ligands *in vivo* and the high stability constants of their complexes (Ga-transferrin: log K = 20.3).[52]

3.2 Elution, preparation and purification of ^{68}Ga

The majority of $\beta^{+/-}$-emitting radionuclides are produced using expensive cyclotrons, which require professional operators. A far more convenient method of radionuclide production is the generator system, which consists of a long lived parent radionuclide which decays to give the daughter (desired) radionuclide.[10, 26] The daughter radionuclide can then be post-processed to remove any unwanted radioactive and non-radioactive metals.

Such a system is very desirable due to the cost effectiveness, almost on demand availability of the radionuclide, ease of use, carrier free nature of the radionuclide and high generator yield.[26, 39, 41, 46, 53] The value of this radionuclide source is evident when it is considered that 80% of SPECT medical examinations make use of ^{99m}Tc, despite the fact that the ^{99}Mo/^{99m}Tc-generator has a shelf life of just over one week.[20, 35]

The long lived parent radionuclide, ^{68}Ge (t½ = 270.6 days), gives the ^{68}Ge/^{68}Ga-generator a shelf life of 2-3 years. This, coupled with the suitability of ^{68}Ga for radiopharmaceuticals, makes it a radionuclide which many consider to have a bright future.[19, 41, 42, 51, 53] Commercial application of this generator has been somewhat hindered by the:[10, 36, 54]

- Chemical form of ^{68}Ga upon elution
- Presence of toxic and competing metal ions
- Low concentration of ^{68}Ga in the generator eluate (high volume)

The ^{68}Ge/^{68}Ga-generators consist of the parent radionuclide immobilised on a column made of inorganic oxides (such as aluminium, tin and titanium) and even in some cases even organic resins.[10, 19, 45, 54] Due to the long half-life of ^{68}Ge it is very important that its removal from eluate is efficient. A considerable amount of work has been done regarding the development of generators and accompanying elution methods that provide carrier free ^{68}Ga in high radiochemical and chemical purity. A detailed discussion of the evolution of ^{68}Ge/^{68}Ga generator design and accompanying elution techniques is beyond the scope of this discussion. For more information the reader is referred to a review by Maecke et al.[19]

The generator widely utilised currently is titanium(IV)dioxide (Cyclotron Co. Obninsk, Russia), which is eluted using 8 mL of 0.1 M hydrochloric acid.[19] The generator is thought to have desirable ^{68}Ga generator yield and ^{68}Ge breakthrough, however also has a number of disadvantages. The eluate volume (8 mL) is relatively high and the eluate itself is strongly acidic, contains measurable amounts of ^{68}Ge activity and metal impurities. Metal impurities include zinc(II) (from ^{68}Ga decay), titanium(IV) (residual column material) and iron(III) (in the column eluate).[19] Removal of metal impurities is of the upmost importance because the majority of radiolabelled precursors have poor metal ion selectivity, and even small amounts of impurities may compete for the precursors because the concentration of ^{68}Ga in the eluate stream is very small (nM).[19, 49]

It is common for groups to develop/adopt automated strategies or protocols for the post-purification and pre-concentration of the generator eluate, which can be categorised into two general techniques.[19]

The first of these is fractionation of the generator eluate directly, which allows the ^{68}Ga to be identified in a smaller volume (pre-concentration) and the presence of any impurities, resulting from generator elution, to be reduced.[55, 56] The more widely applied and reliable protocol is to make use of an ion exchange resin to 'hold' the ^{68}Ga, whilst the impurities are removed.[19] Subsequent removal of the ^{68}Ga from the resin using a smaller solvent volume allows for effective pre-concentration. Velikyan et al have developed an efficient method, based on an anion exchange resin, which has been fully automated and gives a final volume of 200 µL (unknown acidity).[48, 54] Another efficient method described by Zhernosekov et al makes use of a cation exchange resin.[49] The benefit of this method is that the ^{68}Ga is obtained in 400 µL of 98% acetone-0.05 M hydrochloric acid, ready for radiolabelling. The entire process from generator elution to 'ready for radiolabelling' is illustrated in Figure 1.3.

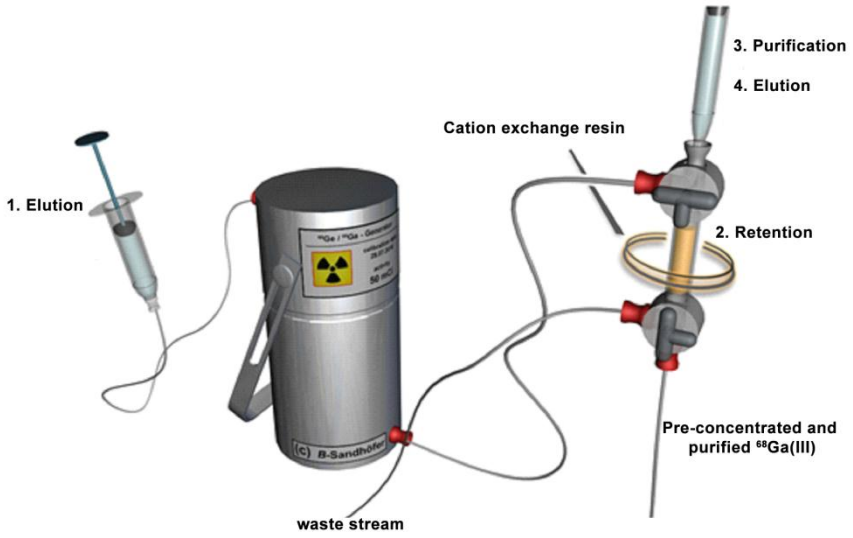

Figure 1.3 *Diagram representing a typical setup for the elution and pre-concentration and purification of ^{68}Ga from a ^{68}Ge/^{68}Ga generator. Figure reproduced with the permission of Benedikt Sandhöfer.*

3.3 Radiolabelling with ^{68}Ga

Incorporation of the radionuclide (radiolabelling) is the key step in the synthesis of a radiopharmaceutical, and considerable effort has focused on minimising the time taken to do so, i.e. increasing the rate of radiolabelling. It is important to minimize the radiolabelling duration mainly due to the short ^{68}Ga half-life, but radiation exposure of the person carrying out the synthesis is also a consideration. It is usually accepted that synthesis, purification and application of the radiopharmaceutical should not exceed 3.5 half-lives (~2.5 h). Even in instances where the application duration is very short, there are obvious advantages to a radiopharmaceutical which has decayed less.

In the case of metal ion radionuclides, radiolabelling is invariably the final step, and thus the synthesis is considered complete when the maximum possible amount of ^{68}Ga is incorporated into the tracer. This yield (experimentally measured radiolabelling yield) does not take into account decay of the radionuclide, and is considered as a compromise between radionuclide decay and actual chemical yield.[10, 46]

3.4 Radiolabelling optimisation

The ideal radiopharmaceutical precursor is one which quantitatively radiolabels at room temperature in less than 10 minutes, and possess a relatively wide pH window of radiolabelling.[32, 46] Such a precursor could be incorporated into a kit-like strategy in which the precursor and any additional chemical substances required (buffers, stabilisers etc.) are lyophilised together in a vial.[19, 48] Radiolabelling protocol would then consist of adding the post-processed generator eluate, shaking the vial and application of the radiopharmaceutical. Radiolabelling is primarily optimised through variations in concentration, temperature and pH.[46] The limiting requirement is that radionuclide incorporation should reach greater than 90% in less than 10 minutes at 90 °C.[35, 39, 46]

Due to the stringent time factors involved, the concentration of the radiolabel precursor (μM) greatly exceeds that of the radionuclide ^{68}Ga (nM). These conditions are used to ensure radiolabelling occurs quickly and completely, i.e. all the available ^{68}Ga is complexed. With such a large excess of the precursor (10000 – 100000 equivalents), the effect of increasing concentration on radiolabelling yield is limited. Typically, groups focus more on determining the concentration of the precursor which can be used without having a negative impact on radiolabelling yield.[39, 46]

Temperature is usually the first consideration, when optimising the rate of radiolabelling yield. As would be expected there is normally an increase in the rate with increasing temperature. Microwave irradiation has also been shown to have significant effect on the radiolabelling yield. In fact, greater yields have been reported for microwave irradiation than those achieved by conventional heating at the same temperature.[46, 57, 58]

The effect of pH on the radiolabelling yield is also well documented.[46, 48] From a ligand design perspective this is not a surprising result. Ligand donor groups have lone electron pairs, which are subject to de/protonation at characteristic pH's. Protonation of a ligand donor groups hinders complexation of the radionuclide, because the energy barrier for removal of the proton has to be overcome. The ideal radiolabelling pH is one at which all the donor groups are deprotonated, and thus primed for complexation of the radionuclide. However, the speciation of the ^{68}Ga radionuclide should also be taken into consideration. Increasing the pH is complicated by the formation of insoluble gallium hydroxide above pH 3.6.[32, 40, 46, 59] If higher pH's are required, a chemical substance capable of weakly binding the ^{68}Ga radionuclide, preventing formation of the hydroxide, but still allowing formation of the desired radiolabel is needed.[46] Buffer anions, such as HEPES, acetate,

glutarate and citrate, have been shown to be effective in this respect.[59] Careful choice of the buffer used allows it to perform a dual function in radiolabelling, i.e. to adjust the pH of the generator eluate and to prevent hydroxide formation.

Many biomolecules are sensitive to pH and temperature, and can be irreversibly damaged (denatured in the case of peptide based biomolecules) if the temperature is too high or the pH too acidic.[20, 32, 43] When the radiopharmaceutical precursor includes some form of biomolecule, which is often the case for bifunctional chelators and macromolecules, the optimisation needs to be carried out within the boundaries set by the biomolecule being used.[10, 32]

4 Biodistribution of the ^{68}Ga Radionuclide

The biodistribution of a ^{68}Ga-radiolabelled species is determined by it chemical form, and falls into one of three categories:

1. The free ion, or the ion weakly bound to labile donors, such that dissociation of the complex occurs *in vivo*).
2. Coordination complexes of Ga(III), where the overall lipophilicity, size and charge determines the biodistribution.
3. Gallium complexes with a tethered targeting moiety, which directs the radiolabel to a specific region, tissue or receptor.

Administration of the free ion results in the formation of ^{68}Ga-transferrin (the natural chelator of Ga(III) *in vivo*) which primarily accumulates at sites of infection, inflammation, bones and, to a lesser extent, tumours.[10, 34, 41]

When a ^{68}Ga coordination complex is administered to a patient, its biodistribution is controlled by the physiological properties of the complex. A relatively large number of ^{68}Ga complexes could be used for imaging of the renal, biliary and reticuloendotheial systems, since these are often the clearance pathways for the complexes.[3, 19] However, probes based on ^{99m}Tc and ^{123}I are currently given preference for such applications.[20, 35, 40]

The PLEB and HBED (Figure 1.4) complexes of ^{68}Ga clear via the renal and biliary system, thus allowing for PET imaging of the liver and kidneys.[60] More lipophilic complexes, such as NOTPR (Figure

1.4), clear via the endogenous biliary route, thereby enabling PET imaging of the respective systems.[61] Lipophilic cationic ^{68}Ga complexes such as TX-TACNH$_3$[62] (Figure 1.6) fall in the same category as heart perfusion agents ^{99m}Tc-Myoview^{TM,63} and ^{99m}Tc-Cardolite^{TM,63}, which are believed to target mitochondrial uptake.[34] ^{99m}Tc-Cardolite® became clinically available in 2008, and is routinely used in clinical practice.

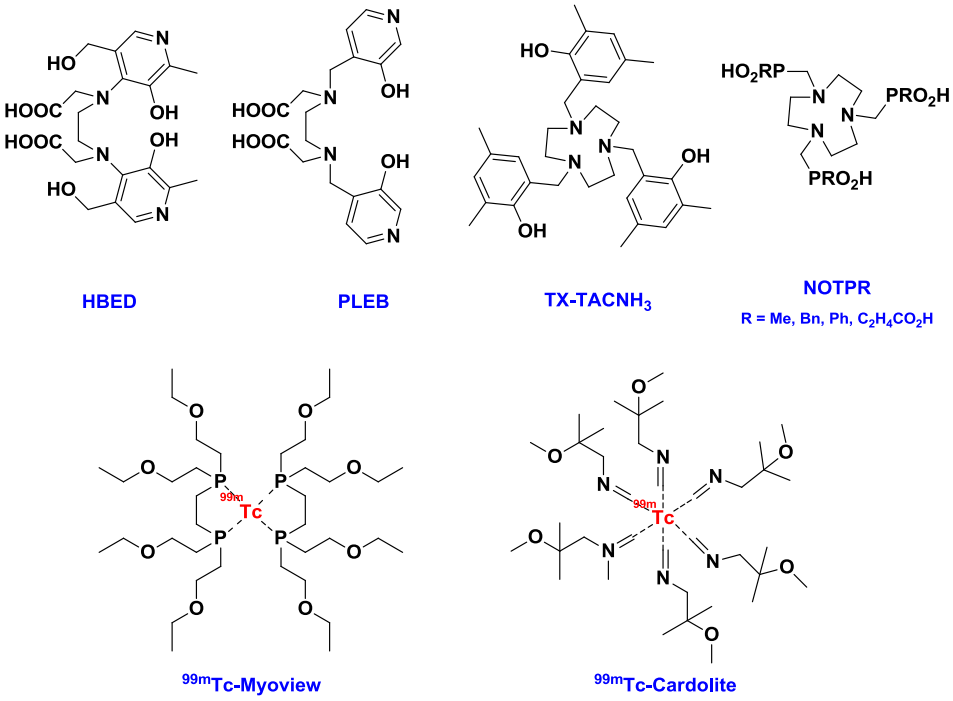

Figure 1.4 *Structures of ^{68}Ga ligands HBED[60], PLEB[60], TX-TACNH$_3$[62] and NOTPR[61]. Also shown are, ^{99m}Tc heart perfusion agents, Myoview^{TM} and Cardolite^{TM}.[63]*

Recently, two lipophilic cationic ^{68}Ga complexes based on the DEDPA framework have been reported (Figure 1.5).[33] The complexes show improved blood, lung and kidney clearance, coupled with persistent heart uptake (compared to the parent DEDPA ligand), displaying myocardial retention (1% initial dose per gram) comparable to ^{99m}Tc-Cardolite^{TM}.[33] Another example of an untargeted biodistribution is the ^{68}Ga complex of the tripodal tetrahedral complex of the ligand NS$_3$, which shows remarkable stability in vivo despite being coordinatively unsaturated (Figure 1.5).[30] The complex crosses the blood-brain-barrier and shows high heart-to-blood ratio; believed to be a result of the complex being neutral, of low molecular weight and lipophilic.[19, 30]

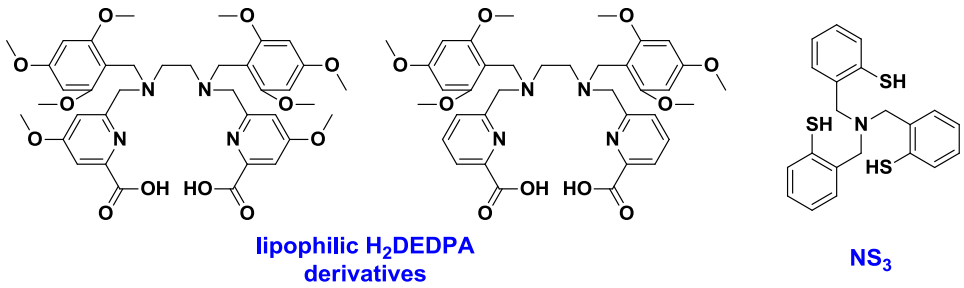

Figure 1.5 *Structures ligands NS_3[30] and H_2DEDPA[33] derivatives, whose ^{68}Ga complexes shown myocardial uptake. [$^{68}Ga.NS_3$] also crosses the blood-brain-barrier.*

Whilst partially effective at accumulating radiolabels within specific regions or systems, these complexes are not targeted radiolabels in the strictest sense. Instead, the biodistribution within the body is "controlled" by modifying the physiochemical properties of the complexes so that they prefer clearance via one pathway over another, or have greater affinity or slower rates of clearance for certain tissues over others.

A more directed approach to modification of the bio-distribution is to use bifunctional chelators.[20, 38, 41, 60, 64-66] A significant amount of work has been done in this field. Bifunctional chelators bind the ^{68}Ga nuclide, and provide a point of attachment for a targeting moiety. Typically, a receptor is identified that is unique or over-expressed with a condition of interest, and then the receptor conjugate is attached to the ^{68}Ga complex.[20, 43, 66-68] The premise of this methodology is that the radiolabel will have a higher affinity for regions where the receptors are found, than for normal tissue.[14, 21, 34, 69] However, targeted radiolabel distribution is not always simply a case of adding a known receptor to a stable complex. For example, hypoxic cells have a tendency (compared to normal healthy tissue) to accumulate charge-neutral electron-poor nitroimidazole, although a NOTA nitroimidazoles derivative showed poorer tumour accumulation than the parent NOTA complex in a hypoxic tumour model.[70]

In both therapeutic and imaging applications of radioisotopes, the *in vivo* stability of the radiolabel is of vital importance. If the radionuclide becomes disconnected, the intended biodistribution will be lost and as a result the signal to background signal ratio will decrease.[19, 20] Furthermore, the radionuclide is potentially harmful to the patient. Thus, the success of a radiolabel depends primarily on the stability of the parent complex *in vivo*. The fate of a released radionuclide depends on its

chemical form. If a metal complex becomes disconnected from its targeting moiety, then the intact complex will be cleared from the body. However, if the metal cation becomes detached from the ligand it will accumulate in the bones and liver, where it will release potentially harmful radiation.[32, 43]

5 Coordination Chemistry of Gallium

5.1 The Ga(III) ion

A detailed knowledge of the coordination chemistry of gallium is crucial to the synthesis of suitable ligands. In aqueous solution, the only stable oxidation state of gallium is +3, and is only present as the Ga(III) aqua ion under strongly acidic conditions. In the pH range 3 – 7, hydrolysis to the insoluble $Ga(OH)_3$ occurs in the absence of suitable stabilizing agents, such as citrate, HEPES, acetate or oxalate.[20, 35] At physiological pH and the gallium concentrations used for radiopharmaceuticals, exclusive formation of the soluble $[Ga(OH)_4]^-$ prevents formation of the insoluble $Ga(OH)_3$.[19, 35] Despite this, the formation of $[Ga(OH)_4]^-$ is equally undesirable in terms of radiolabelling.

The Ga(III) cation has a high charge density and a relatively small ionic radius (0.62 Å) and is classified as a hard Lewis acid.[34, 40] It forms strong dative bonds to highly ionic, non-polarizable hard Lewis bases such as nitrogen and anionic oxygen. Therefore, ligands featuring carboxylate, phosphonate, phosphinate, hydroxamate and amine functional groups are likely to give rise to thermodynamically stable complexes with Ga(III).[34, 35, 38] There are also ligands with softer donor groups like phenolates and thiolates, which give rise to stable complexes.[20, 34, 35, 38] Tetra- and penta-dentate ligands complexes have been reported, but the vacant coordination sites and ability to hold extra donors make them vulnerable to nucleophilic attack (hydrolysis) and ligand exchange.[34] The more characteristic coordination sphere is a distorted octahedron (due to the small size of the ion), which together with the d^{10} configuration of the Ga(III) ion affords excellent stability – provided that suitable ligands are used.[19, 40]

The Ga(III) ion has a unique selectivity issue resulting from its chemical properties. The coordination chemistry (as a result of the ionization potential, ionic radii, electronic configuration and coordination geometry) of the ion are remarkably similar to that of high-spin Fe(III). Transferrin is a plasma protein which has two iron binding sites, and as a consequence a high affinity for Ga(III).

Ligand exchange *in vivo* involving transferrin is a common threat to gallium complexes, and is evident by considering the relative affinities: log K (Ga^{3+}) = 20.3 and log K (Fe^{3+}) = 22.8.[41, 52]

5.2 Ligands for chelating Ga^{3+}

The ^{68}Ga radionuclide has desirable radiochemical properties for use in PET which, coupled with the reliability, convenience and low cost of the $^{68}Ge/^{68}Ga$ generator, make it a radionuclide with exceptionally high potential to make PET more widely available. However, in order to realise this potential suitable ligands are required. A suitable ligand should ideally meet the following criteria:

- The ligand should form complexes with high thermodynamic stability and, more importantly, is kinetically inert to prevent transchelation of the metal. Gallium complexes need to be stable to hydrolysis and more stable than the Ga-transferrin complex.[40]
- Radiolabelling of the ligand should ideally occur rapidly under mild conditions with a low excess of the ligand.[58]
- In order be useful in imaging, the ligand should provide a point of conjugation for targeting vectors. Also useful in this regard is versatility, such that the pharmacokinetics can be adjusted (by changing the overall polarity). Furthermore, conjugation of a biological vector should not cause a significant debilitating effect on the radiolabelling.[57]
- The ligand should be selective for Ga over other metals present. Especially Fe^{3+} (0.05 nM in the hydrochloric acid used to elute the generator), Ca^{2+} (2 mM in serum), Mg^{2+} (1 mM in serum) and Zn^{2+} (^{68}Ga decay).[58, 71] Ideally the synthesis of the ligand should be simple, fast and cost effective.[20, 35]

In order to make ^{68}Ga complexes useful and effective in a variety of ^{68}Ga-PET applications it is widely considered/accepted that conjugation to a suitable targeting vector is necessary using a bifunctional complexing or chelating (BFC) agent.[20, 38, 48, 66] The topic of BFC's for ^{68}Ga is covered in a number of publications, and will not be covered in detail here. *For detailed reviews on this topic the reader is referred to: (a) H. R. Maecke et al, J. Nucl. Med. 2005, **46**, 172S; (b) M. D. Bartholoma, Inorg. Chim. Acta. 2012, 389, 36; (c) M. J. Welch et al, Chem. Rev. 1999, **99**, 2219; (d) H. R. Maecke, Contrast Media Mol. I. 2008, **3**, 53.*

Thus, in order to realise the potential of the ^{68}Ge/^{68}Ga generator, the primary challenges for synthetic chemists are to design ligands which stabilise the Ga(III) ion *in vivo, radio*label rapidly under mild conditions and provide a point of attachment for a targeting vector.[20, 35]

What follows is a brief overview of reported ligands suitable for ^{68}Ga PET. This project is primarily concerned with laying the ground work for novel ligands suitable for ^{68}Ga-PET. In this regard, rapid radiolabelling under mild conditions to give complexes with high *in vivo* stability is of the upmost importance. Modification to yield bifunctional ligands is an important consideration, will however form the basis of work subsequent to this study. Thus the discussion which follows focuses on the radiolabelling properties and stability of the subsequent complexes, as these are pre-requisites for their application. *The discussion which follows is only a brief overview of some of the most promising and prevalent ligands for ^{68}Ga-PET. For a more comprehensive overview which predates the more modern ligands discussed here, the reader is referred to: (a) M. D. Bartholoma et al., Chem. Rev., 2010,* ***110****, 2903; (b) M. J. Welch et al, Chem. Rev. 1999,* ***99****, 2219; (c) H. R. Maecke, Contrast Media Mol. I. 2008,* ***3****, 53; (d) H. R. Maecke et al, J. Nucl. Med. 2005,* ***46****, 172S.*

The efficient and stable complexation of the ^{68}Ga radionuclide has been studied for 4 decades.[36, 72] Early work was dominated by the focused efforts of Martell and Welch, and later succeeded by Maecke and co-workers with the DOTA ligand.[73-75] The current so-called 'gold standard' of ^{68}Ga ligands is the aminocarboxylate ligand DOTA (Figure 1.6). The most well-known ^{68}Ga complex featuring this core is the bioconjugate ^{68}Ga-DOTATOC, which was reported in 2001 by Henze and co-workers (Figure 1.1).[76] It is currently used in clinical practice for the PET-imaging of neuroendocrine tumours and metastases.[43]

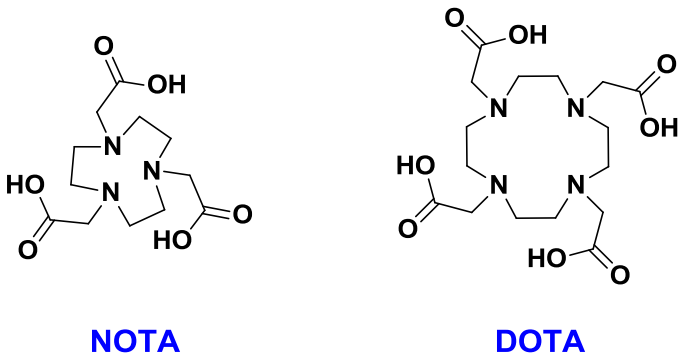

Figure 1.6 *Structure of ligands NOTA and DOTA which have dominated the chelation ^{68}Ga in clinical practice (for ^{68}Ga-PET) and research.*

The 'popularity' of DOTA for ^{68}Ga-PET arises from two features in particular. Firstly, the gallium-DOTA complexes have exceptionally high stability in vivo, with ^{67}Ga-DOTA reported to be stable in serum (*in vitro*) for 1250 h.[77] The stability *in vivo* is largely a result of the macrocyclic effect resulting in a high kinetically stability, whilst the thermodynamic stability (log K = 21.33) is comparable with Ga-transferrin (log K 20.3).[52, 78] The second feature which makes DOTA attractive is the potential for bio-conjugation. DOTA has an N_4O_4 donor system and is more commonly used for chelation of large metal ions, such as the lanthanides, which require octadentate ligands.[79] Crystal structures of [Ga.DOTA] reveal that the ligand binds using an N_4O_2 donor set, with two flailing carboxylate arms.[80] These 'superfluous' functional groups have been exploited by many groups to provide the attachment of targeting vectors yielding BFC's.[19, 20, 66, 79, 80]

Despite these advantages, DOTA has several drawbacks. Optimal radiolabelling with ^{68}Ga is inherently slow (30 min), requires high temperatures (90 °C), high ligand concentrations and rather acidic media (pH 4.6). The long radiolabelling times allow significant radioactive decay, whilst the harsh conditions are unsuitable for many biological targeting vectors. A basic knowledge of coordination chemistry is required to understand why these harsh conditions are required. The DOTA ligand is designed to hold larger metal ions with the N_4 ring of cyclen primed to offer an anti-prismatic square base not ideally suited to the Ga(III) ion. The 12-N_4 ring has pK_a values of 12 and 11 with two bifurcated hydrogen bonds stabilising and rigidifying the ring conformation.[78] Deprotonation of the ligand is the rate limiting step in the metal ion binding, as it is associated with a high energy barrier to the conformational change that allows it to occur. Furthermore, DOTA and its derivatives are difficult and expensive to synthesise, with many groups purchasing BFC precursors from commercial suppliers at a high cost.[79, 81] In fact, the dominance of DOTA derivatives in ^{68}Ga-PET is believed to be related to the commercial availability of DOTA-3^{t}Bu; a useful precursor for the synthesis of BFCs based on DOTA.[20] The drawbacks of DOTA highlighted the need for ligands which radiolabel more quickly and under milder conditions.

Gallium complexes of the macrocycle NOTA (and its derivatives) were first reported in the late 1980's by Parker and co-workers[82], and were subsequently elaborated on by Maecke and co-workers[75] towards the end 1990's. Since then, considerable effort has been expended towards the synthesis of BFC's based on NOTA and its derivatives.[75, 83-85] The ligand benefits from rapid radiolabelling (10 min) at room temperature at pH 3 – 5.5.[48] NOTA has a smaller binding cavity than DOTA and supports octahedral metal ion geometries, which is a better match for the Ga(III) ion. As a result the selectivity for Ga is better, and the complex has high thermodynamic (log K = 31)[64] and

excellent kinetic stability in vivo.[58] One of its derivatives featuring a conjugation facility, NODAGA, has been linked to proteins at pH 4.1 in 7 min.[86] The major drawback of NOTA is that optimal radiolabelling apparently requires acidic conditions, which narrows the window of possible biological vectors. Although a number of NOTA derivatives featuring functionalities for conjugation have been reported, these too are synthetically challenging and can be expensive to prepare.[75, 85, 87]

Structural analogues of NOTA which have shown excellent potential are the phosphinic acid derivatives (Figure 1.7). Despite gallium complexes of these related ligands first being reported back in 1994 by Parker and co-workers[61] for ^{67}Ga complexation, their potential as ^{68}Ga-PET BFCs has only been exploited in the last 2 years by Notni and co-workers.[57, 58, 71, 88] NOTA derivatives featuring phosphinic acids allegedly radiolabel at 95°C in less 5 minutes over the pH range 1 – 5.[57, 58] Radiolabelling at room temperature occurs at lower ligand concentrations than NOTA (at pH 3.3), but the difference is not considerable. The unique feature of these complexes is their ability to label under strongly acidic conditions (pH 1), and at much lower ligand concentrations (1 µM), albeit at high temperature (95°C). This is made possible through the use of the phosphinic acid groups as the primary donor. Their lower pK_a (~ 1) than carboxylates (~ 3.5) means they are protonated at much lower pH, and hence able to bind Ga at much lower pH's.[58] However, the same is not true for the nitrogen donors of the 9-N_3 ring. In this case the energy barrier to deprotonation (at pH 1) is very high. Under these conditions it is highly unlikely that the N_3 donor set will be involved in metal binding. A more likely scenario is that, under acidic conditions, the gallium ion is being bound weakly by the three anionic phosphinate groups in an 'out-of-cage' manner. Radiolabelling may be observed, but not to give the intended N_3O_3 species. It is possible that a subsequent increase in pH may deprotonate the $9N_3$ scaffold, alllowing the Ga ion to 'drop' into the cavity and be bound as a stable N_3O_3 complex. Realistically, the radiolabelling of ligands with polyaza rings at pH < 2 to give a stable complex is not feasible. Furthermore, it lacks any real practical relevance. The original benefit was thought to be the ability to label the strongly acidic generator eluate directly, thus reducing the overall radioactive decay. However, the eluate volume is too large for practical labelling and requires pre-concentration anyway. Furthermore, radiolabelling and storage of BFCs featuring biological vectors under strongly acidic conditions is not feasible.[58] Complexation of ^{68}Ga using TRAP-type ligands which possess carboxyethyl substituents at phosphorus (TRAP-Pr), is further complicated by the tendency to form less stable 'out-of-cage' complexes.[88] Notwithstanding these drawbacks, TRAP ligands are well-suited for ^{68}Ga-PET, and BFCs derivatives have shown promise during *in vivo* evaluation. Although too acidic for most applications, the radiolabelling pH range makes radiolabelling procedures more robust.[58] The real value of these ligands is their ability to label faster

at lower ligand concentration than NOTA, rather than the labelling pH range. However, this value is only realised at very high temperature. Furthermore, labelling at room temperature is not practical because this requires high ligand concentrations (100 µM) and long labelling times (20 min).

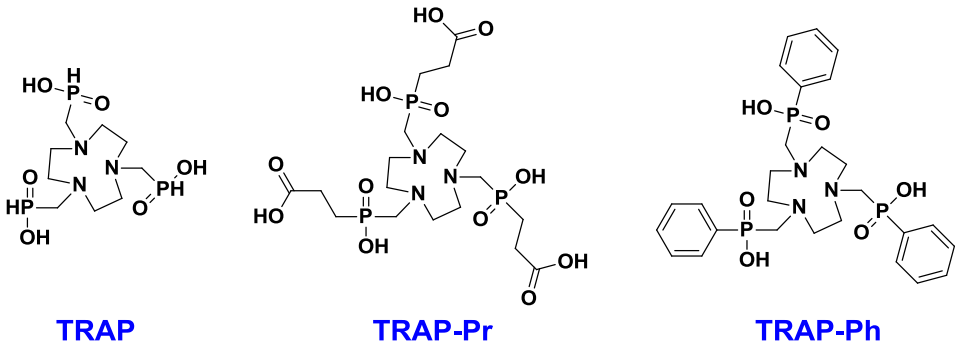

Figure 1.7 *Structure of the TRAP ligand, and two derivatives, which label rapidly at room temperature. By virtue of the phosphinate donors these TRAP radiolabels more quickly, and with a lower ligand concentration, than NOTA.*[57, 58, 88]

The 'renaissance' of the ^{68}Ge/^{68}Ga generator[37] and dominance of NOTA and DOTA (Figure 1.6) in ^{68}Ga-PET, is evident in the number of promising chelators that have been reported in the last 5 years alone.[10, 19, 20, 35] It is interesting to note that, with few exceptions, trends have seen a deviation away from rigid cyclic chelators towards more flexible acyclic ligands.[19, 20] Acyclic chelators are typically synthetically less challenging and tend to radiolabel rapidly, but the absence of the macrocyclic effect can render them less kinetically stable and less metal-ion selective.[20, 34, 35]

The acyclic ligand HBED (Figure 1.8), which is based on an EDTA-type framework, forms very stable ^{68}Ga complexes (log K = 39).[86, 89] The ligand shows ~ 95 % radiolabelling at pH 4.6 in 10 minutes at room temperature with a ligand concentration of 10 µM.[86] More recently, the ligand has been modified (HBED-CC: Figure 1.8) to give a BFC with conjugated proteins that have shown quantitative radiolabelling at pH 4.1 and room temperature in 4 min in some cases.[90] However, in most BFC's of HBED-CC radiolabelling yields of ~ 85 % at 40°C are reported.[86, 91] Whilst a good result, the drawback of non-quantitative radiolabelling is that the radiolabelled BFC will have to undergo a more complex purification prior to application. This adds to the radioactive decay, and can be challenging when biological vectors are present.

Another acyclic ligand with promise is H_2DEDPA[81] (Figure 1.8), which radiolabels quantitatively at room temperature and pH 4.5 in less than 10 min. The complex has relatively high thermodynamic stability (log K = 28) and is sufficiently stable *in vivo*.[81] The H_2DEDPA ligand also has the highest reported specific activity (9.8 ± 0.1 mCi.mol^{-1}) of any ligand which does not require purification.[33] Certain conjugated derivatives of H_2DEDPA have shown similar properties, although a greater ligand concentration (100 µM) is required to maintain the favourable radiolabelling behaviour.[67] Two more lipophilic derivatives (Figure 1.5), which also have favourable radiolabelling properties and stability profiles, show persistent heart uptake (> 1 % ID.g^{-1} over 2 h) in mice.[33]

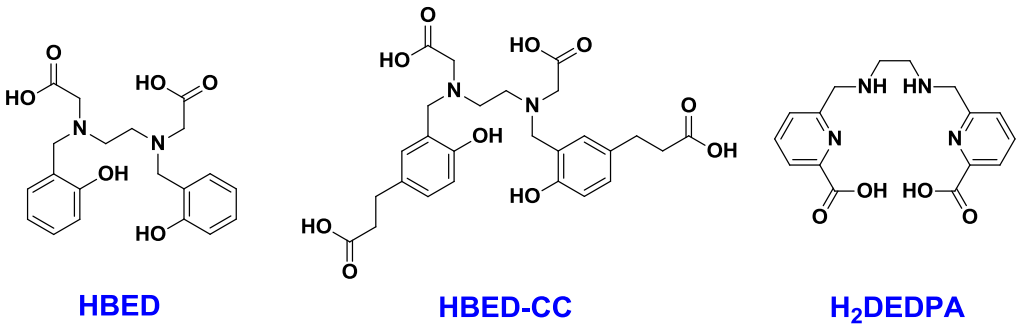

Figure 1.8 *Structures of ligands HBED[89] (and HBED-CC[91] its derivative for biomolecule conjugation) and H_2DEDPA.[81] Each of these ligands displays favourable radiolabelling behaviour, and form radiolabelled complexes of sufficient stability. Furthermore, each has been elaborated to yield BFC's with similar radiolabelling and stability profiles.*

One drawback shared by all of the ligands described is the fairly acidic pH required for radiolabelling. A larger radiolabelling pH window would allow for greater diversity in the biological vectors investigated. Blower and co-workers[43] recently presented the acyclic ligand, CP256 (Figure 1.9), which makes use of defriprone functional groups use in the sequestration of Fe(III).[92] The ligand consists of three Defriprone moieties which bind in an *O,O*-bidentate fashion to give a neutral complex with Ga(III).[43, 92] The parent ligand radiolabels in less than 5 min at room temperature over the pH range 5.5 – 6.5 in less than 5 min, with a ligand concentration of 10 µM, to give a radiolabelled complex which is stable to decomplexation and transchelation in human serum the presence of *apo*-transferrin. The ligand CP256 radiolabels ^{68}Ga quantitatively, more quickly and under milder conditions than any of the ligands reported to date. Given that the CP256 is structurally based on donor groups used in the treatment of Fe(III) overload, an area of possible concern is the high affinity of the ligand for Fe(III). The authors have not reported any Fe(III) challenge experiments, and the possibility of transchelation should not be ruled out. A BFC derivative has been reported,

YM103-C2Ac (Figure 1.9), and shows very similar radiolabelling behaviour and complex stability.[43] A PET imaging study of the BFC derivative was carried out in a normal mouse. The radiolabelled complex had accumulated almost exclusively in the kidneys, with a small amount of excretion to the bladder at 90 min post-injection.[43] Accumulation of the radiolabelled complex in the kidneys may be a further area of concern, especially when the iron sequestration properties of the ligand are taken into account. In some instances, *in vivo* kidney uptake is an indication that the BFC has been degraded.[65]

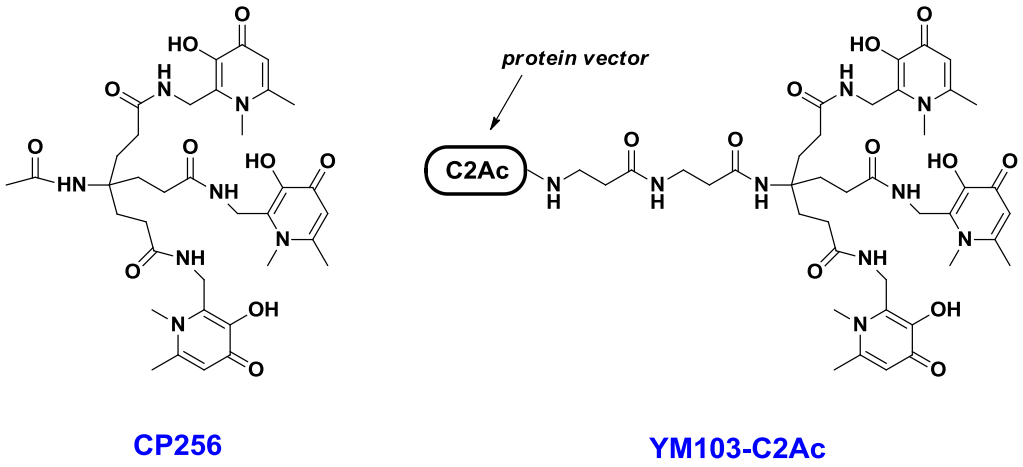

Figure 1.9 *Structure of ligands CP256 and its BFC derivative, YM103-C2Ac. Both ligands display favourable radiolabelling behaviour, and form a ^{68}Ga radiolabelled complex which is stable in vitro.*[43]

6 Ligands based on the AAZ scaffold

6.1 Introduction to AAZ

A review of the literature surrounding the 6-amino-1,4-diazapine (DAZA) reveals that it was first reported in 2004, in its capacity as a ligand.[93] The core was used as a scaffold for aminocarboxlate groups to give heptadentate ligands which continue to show promise as ligands for Gd-MRI imaging agents.[68, 94-100] It is interesting to note that prior to this, Rossignoli[101] (1997) and Hegetschweiler[102] (2000) had suggested that this tridentate ligand would be suitable for the coordination of octahedral metal ions. Hegetschweiler went on to publish a comprehensive report on the coordination chemistry of DAZA and its 6-methylperhydro derivative (AMPED: Figure 1.10).[103, 104] This followed work by Neves and co-workers that investigated the use of AMPED as a mimic of triazacyclononane (9-N_3) in terms of it metal chelating ability.[105] The AMPED ligand consists of three amines, two of

which are endocyclic incorporated within the seven membered ring, the third nitrogen exists as an exocyclic primary amine at the 6-position (Figure 1.10).

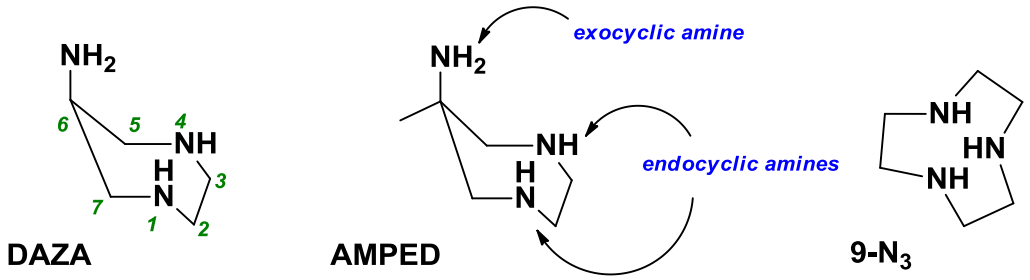

Figure 1.10 *structures of relevant tridentate ligands 6-amino-1,4-diazepine (DAZA), 6-amino-6-methylperhydro-1,4-diazepine (AMPED) and 1,4,7-triazacyclononane (9-N_3).*

As a result of the early endeavours of Aime and co-workers, interest in the tridentate ligand scaffold was sparked on three fronts:

- Coordination of metal ions requiring octahedral ligand fields. [103-107]
- As an ancillary ligand in catalysis using rare earth metals.[108-111]
- As a ligand for metal enhanced MRI applications.[68, 98, 100, 112, 113]

What follows is a brief review of the literature surrounding the use of DAZA and its derivatives as metal chelators, covering the applications relevant to this project

6.2 DAZA as a chelator for metals requiring a hexadentate ligand field

Nitrogen based facial tridentate (*fac*-N_3) ligand moieties such as 9-N_3 (Figure 1.10) have seen wide applications in coordination chemistry including modeling of the active sites of metallo-enzymes, stabilization of catalytically active metal centres and transition metal complexes.[103, 114, 115]

Cyclic chelators like those based on 9-N_3 are attractive because they possess restricted and well defined modes of coordination which allow for the easy design of a desired coordination sphere. In many cases, the coordination geometry enforced is distorted from a regular configuration, a feature which often gives rise to very interesting properties. [99-103, 112] Furthermore, the amine groups can be elaborated or decorated to multidentate ligands.[103-107, 116]

The major disadvantages of these chelators is that their synthesis, modification and extension (functionalisation) is both time consuming and expensive.[105] Thus, chelators mimic the structural characteristics, of 9-N_3 in particular, are of considerable interest.[103, 105] Neves concluded that, based on the structural and physiochemical properties of DAZA and TACN complexes, that the DAZA ligand was a ligand that could potentially mimic the important properties of 9-N_3.[105] It is interesting to note that this statement was made despite their report that Ni(9-N_3)$_2$ was approximately five orders of magnitude more thermodynamically stable than Ni(DAZA)$_2$.[105] The inherent advantages of DAZA are a two-step facile synthesis from readily available starting materials, and a synthetic route that enables selective functionalisation of the primary amine.[93]

Hegetschweiler and co-workers compiled a comprehensive report on the coordination chemistry of a series of complexes of divalent first row transition metal complexes [Ni(II), Cu(II), Zn(II), Cd(II), Co(II)] of the form $[M(DAZA)]^{2+}$ and $[M(DAZA)_2]^{2+}$, making direct comparisons to analogous *fac*-N_3 complexes. There are two interesting features of DAZA and its derivatives when the crystal structure of the free ligand is compared to that of the bound ligand. Firstly, it is apparent that there is a degree of flexibility in the position adopted by the exocyclic amine (N_{exo}) relative to the ring.[103] In the free ligand it takes up an equatorial orientation, but adopts an axial orientation when bound to a metal ion (Figure 1.11). This change in orientation is a reflection of the inherently flexibility of seven membered rings, which typically have a large number of low energy conformations.[103] The N_{exo} functional group is more sterically demanding than a proton, therefore in free DAZA, the lowest energy conformation/s are invariably those in which the amine adopts the less sterically demanding equatorial position. However, tridenate binding of DAZA necessitates that the N_{exo} adopt an axial position. Secondly, when acting as a tridentate ligand, DAZA almost always adopts a chair conformation.[103] This conformation is under considerable torsional strain, as evidenced by the eclipsed conformation of the N-CH_2-CH_2-N ring fragment.[103]

In a later publication, Hegetschweiler hypothesised that it may be possible to improve the ligating properties of DAZA by addition of a methyl group at the 6-position. This ligand is commonly known as AMPED (Figure 1.10).[104] Similar modification had been found to be beneficial with the ligand TACH (Figure 1.12), where the addition of methyl groups onto the ring (Me_3TACH) promoted axial orientation of the nitrogen donors thus improving the ligand kinetics and complex stability (Figure 1.9).[117-119] However, only a weak gain in stability was observed for the DAZA-AMPED modification. In contrast to the findings of Neves, Hegetschweiler went on to state that DAZA is only a mimic of

TACN insofar as the manner in which they bind metals.[103, 104] Both can form complexes with large metal ions (such as lanthanides), because the 5 remembered chelate rings they form are well suited to such metals.[97, 103, 104] In terms of metal binding ability, TACN and Me_3TACH are very efficient, whereas AMPED (and even more so DAZA) is not.[104] The complexes $[M(DAZA)]^{2+}$ and $[M(AMPED)]^{2+}$ were found to have among the lowest stability constants (log K_1) when compared with similar cyclic tri-amine complexes. This was thought to be largely due to the torsional strain resulting from the unfavourable ring conformation.

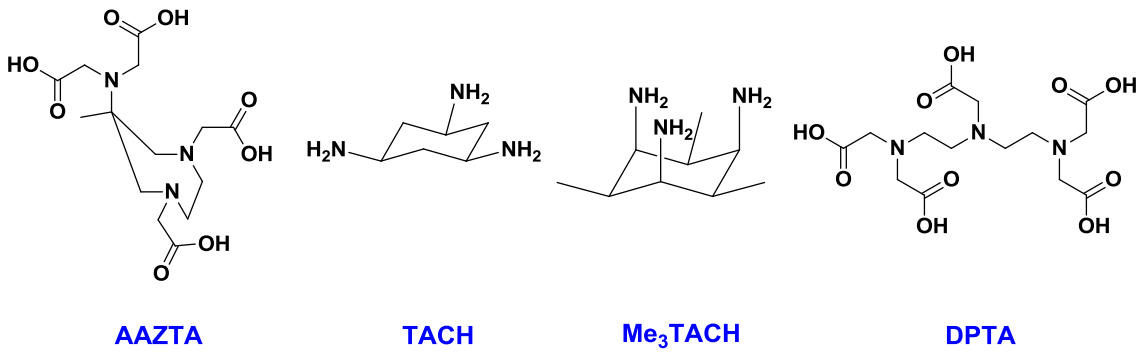

Figure 1.12 *Structures, and abbreviated names, of ligands to which reference is made in the text.*

Aime and co-workers have reported the stability constant for a variety of metal complexes with the tetra-acetate derivative of AMPED (AAZTA: Figure 1.12). For Mg(II), Ca(II), Sr(II) and Mn(II) the log K_{ML} values were between 8.3 and 15.4, whereas with larger Cu(II), Zn(II), Pb(II) and Cd(II) ions complexes have considerably lower values (18 – 21).[97] With the larger lanthanide ions, values were between 18 and 22, i.e. slightly higher than most of the non-lanthanide metal ions. The increasing log K_{ML} with size of the metal ion, indicates that the binding pocket of AAZTA is better suited towards smaller metal ions.[97] It is interesting to note that, compared to the more flexible DPTA ligand (Figure 1.12), the lanthanide complexes of AAZTA are less stable whereas the non-lanthanide complexes are slightly more stable.[97] This indicates that AAZTA has a 'blend' of cyclic (due to the ethylene diamine diacetate fragment) and acyclic (due to the iminoadicetate group) properties.[97, 100, 103, 104] The acyclic properties afford the ligand rapid ligation kinetics characteristic of aminopolycarboxylates. The acyclic portion contributes to the complexes being thermodynamically stable and kinetically inert which is characteristic macrocyclic polyazacarboxylates.[95, 100] As a result, the coordination cage of AAZTA is more rigid than DTPA, but more flexible than the likes of NOTA.[95, 97]

Despite being found to be largely unsuitable as a tridentate ligand, a number of researchers recognised potential in the AAZTA ligand.

6.3 Imaging related applications of AMPED based ligands

In this section metal complexes incorporating the DAZA ligand are discussed. Complexes with potential use as imaging agents are of particular interest, because some of the desirable ligand properties are in-line with those of this project. For an imaging agent to be considered 'promising', the primary concern is stability in vivo. The ability to conjugate the ligand to a moiety which provides some form of optimization is of interest in most imaging applications, and of relevance to this work.

Aime et al reported the synthesis, characterization and relaxometric properties of a Gd diaqua ligand complex, which uses an AMPED core decorated with 4 acetate groups from the three nitrogen atoms to give AAZTA (Figure 1.12).[93] The synthesis of AAZTA follows a simple, high yielding route which uses cheap and readily available starting materials. Furthermore, the extension and modification is relatively simple in comparison to other ligand systems used in the past.[112] This feature of AAZTA has subsequently been exploited by numerous groups.[68, 94, 96, 99, 112]

The $[Gd(AAZTA)(H_2O)]^-$ complex has a stability constant (log K) of 19.3 which is comparable with that of [Gd.DPTA] – a commercially used MRI contrast agent.[93] Furthermore, $[Gd(AAZTA)(H_2O)]^-$ shows no signs of transmetallation and is virtually unaffected by the presence of endogenous anions. $[Gd(AAZTA)(H_2O)]^-$ displayed a relaxivity of 7.1 $mM^{-1}s^{-1}$ at 20MHz and 298 K over the pH range 2-11, which is better than the relaxivities of most commercially used MRI CA's (4-5 $mM^{-1}s^{-1}$).[93] Interest in AAZTA, and its derivatives, for use in Gd-enhanced MRI was sparked by this complex, which displayed good magnetic properties coupled with high thermodynamic and kinetic stability.[93] In fact, all reported gadolinium complexes (for MRI applications) based on the DAZA scaffold feature the same N_3O_4 7-membered core, first reported in 2004.

The crystal structure of the free ligand reveals two nearly identical crystallographic independent molecules, which differ slightly in the conformation of the ring (Figure 1.13). The structure was described as chair-like with the exocyclic nitrogen in an axial position.[95] This is not strictly true, with the conformation more accurately described as a twisted-chair conformation in which the exocyclic-nitrogen takes up a pseudo-axial orientation. The C-O bond distances reveal that only two of the

acetate groups are deprotonated, with the charge being balanced by protonation of their respective amines, to give a zwitterion.[95]

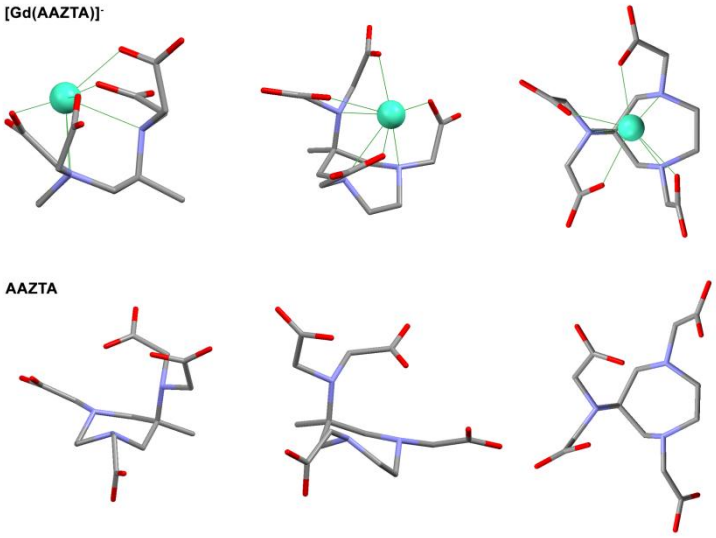

Figure 1.13 *Various views of the crystal structures of the the [Gd(AAZTA)(H$_2$O)]$^-$ complex (top), and AAZTA free ligand (bottom). Hydrogen atoms and water molecules have been excluded for clarity. Note: the regular chair conformation adopted by the AMPED scaffold, eclipsed nature of the ethylene diamine bridge, and how the Gd(III) ion "stands out" of the AAZTA binding cavity in the Gd(AAZTA)$^-$ complex. In contrast the free ligand is considerably more twisted, with N$_{exo}$ adopting a pseudo-axial orientation. In the case of the metal complex, only one half of the dimer is shown.*[95]

The [Gd(AAZTA)(H$_2$O)]$^-$ anion crystallizes as a dimer in the form M$_2$L$_2$, consisting of two ligands in similar conformations. It has been suggested that formation of the dimeric species is favoured by the exposed Gd core (a result of the restricted coordination sphere of AAZTA) which is presented to the acetate groups of another complex.[100] The structure reveals interesting details about the conformation of the AMPED core. As expected, it adopts a near perfect regular chair conformation (the N-CH$_2$-CH$_2$-N fragment has a deviation 3.0 ° from perfectly eclipsed), with its seven donor groups encompassing just over half the coordination sphere of the metal centre (Figure 1.13). The coordination geometry is labelled as a distorted bicapped pentagon, with 3 nitrogen donors, 4 oxygen (acetate) donors and 2 bridging oxygen donors – shared between two adjacent Gd centres.[95] A single water molecule is included to make each Gd centre formally decacoordinate.[95] The Gd-N$_{exo}$ distance (2.599 Å) is slightly shorter than the Gd-N$_{endo}$ distance (2.778 and 2.681 Å), which is not entirely surprising given the inherent flexibility of the exocyclic amine and the presence of two attached acetate groups.[95, 100] This is a consistent feature for metal complexes featuring tridenate

DAZA ligand derivatives.[103, 104] These distances are significantly longer than those reported for cobalt(II), copper(II), nickel(II) and zinc(II) complexes (M-N: 1.946-2.108 Å) with DAZA, as should be expected based on the relative ionic radii.

The conformation adopted by the DAZA core (equivalent atoms of the ring are eclipsed: Figure 1.13) and the exposed metal ion hardly seem conducive to formation of a stable complex. The author attributes the high stability of $[Gd(AAZTA)(H_2O)]^-$ to three structural features:

1. The four anionic acetate groups form a shallow convex surface through the Gd centre, which contributes to the stability of the compound with respect to anion approach and binding.
2. The lack of strain within the complex.
3. The flexibility of the four acetate arms.

This is in contrast to the findings of Hegetschweiler, who attributed the observed low stability of the metal complexes to the torsional strain within the bound ligand.[103, 104] It is likely that, the anionic oxygen donors enhance the stability of the complexes formed, relative to the unfunctionalised DAZA based complexes. However, this does not detract from the fact that there is inherent structural strain in the bound ligand. In fact, a crystal structure of a very similar europium complex (only modified by the addition of a hydroxyl group onto the tertiary methyl) reveals a pseudo-twisted-chair conformation of the ring, a conformation which is expected to have less inherent structural strain than the $[Gd(AAZTA)(H_2O)]^-$ complex (Figure 1.13).[100] It is noteworthy that whilst there is a bridging of two Gd centres in the solid state structure, in solution the anion almost certainly exists as the monomeric species with two bound water molecules – as suggested by ^{17}O NMR studies.[95]

The sufficient stability, facile synthesis and good relaxometric properties of $[Gd(AAZTA)(H_2O)]^-$ has fostered considerable interest in the use of AAZTA as a chelator for Gd MRI contrast agents. Wiener *et al* have illustrated the synthetic flexibility and modification potential of the AMPED core for use as a bifunctional MRI probe.[100] Provision for the attachment of a targeting moiety was made by replacing the exocyclic methyl with an oxyethyl substituent.[100] Vitally, this new binding site does not result in any unwanted side reactions, and does not become involved in complexation.[100] A large number of ligands, with a variety of conjugation functionalities, have been reported.[68, 94, 96, 99, 120] The vast majority use the tertiary ring carbon of AAZTA as a point of attachment. These examples are not discussed in detail here, but some examples are illustrated in Figure 1.14.

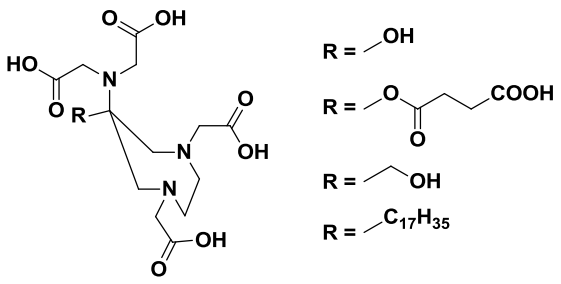

Figure 1.14 *Examples of DAZA based heptadentate ligands used for complexation of Gd(III), which feature functionalisation at the quaternary carbon of the ring.*[94, 96, 100, 112]

From the preceding literature survey, it is evident that other research groups have focused on modification at the exocyclic methyl position to induce higher relaxivities (through reduced molecular rotation primarily) and seek a targeted bio-distribution.

The approach at Durham has been somewhat different, in that we have sought to take advantage of the different amine groups of the AMPED ring to synthesise complexes where the substituents at the endocyclic nitrogen's are varied, whilst the N_{exo} acetate groups are maintained. This approach was for the most part chosen because this chemistry had not been explored.

The mono- and di-glutarate derivatives of AAZTA (Figure 1.15) were synthesised, with the premise that the glutarate groups could alter the water exchange dynamics, and provide a means for the addition of hydrophilic groups. A range of optically pure di- and mono-glutarated Gd(AAZTA) derivatives have been synthesised, each of which contained two coordinated water molecules. It was thought that the glutarate derivatives influence the second hydration sphere in a manner conducive to increasing relaxivity.[98] The complexes only showed small improvements compared to the relaxivity of the parent complex. The author suggested that overcrowding at the metal centre, inhibits the approach of water molecules, thereby slowing the water exchange.[98] As a result, the relaxivities of the glutarate derivatives are not very different from the parent complexes.

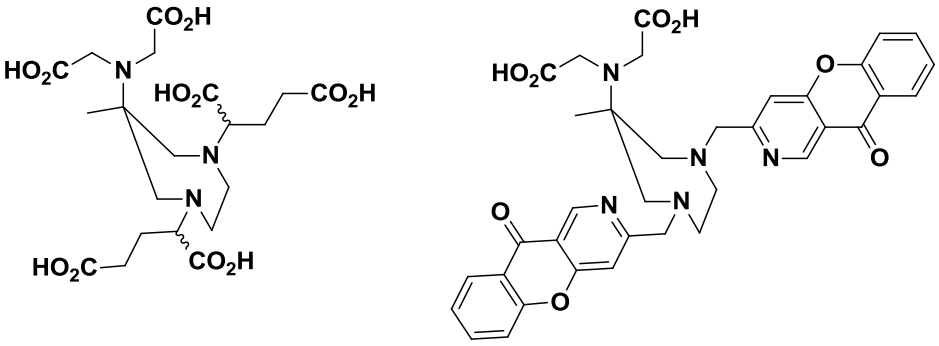

Figure 1.15 Modification of the AAZTA at the endocyclic amines. The diglutarate[98] (left) and di-azaxanthone[121] (right) derivatives of AAZTA. Conformations of the two chiral centres in the di-glutarate can be the same [(*R,R*) or (*S,S*)] or different [(*S,R*)].

Directly following this work the suitability of the scaffold was evaluated in other fluorescence imaging applications aimed at anion sensing. This was facilitated by the substitution of the endocyclic acetate groups for azaxanthone moieties, which acted as sensitizing chromophores and provided the necessary donor groups (pyridyl nitrogens: Figure 1.15).[121] In a screening protocol the overall stability was lower than a DOTA equivalent, and thus only of use *in vivo* under controlled conditions.[121] Interestingly, these are the only two modified AAZTA ligands in which functionalisation has occurred at a position other than the tertiary carbon of the ring.

During the course of this research two publications appeared which correspond closely to work carried out in this project. In 2011 Botta et al reported a series of manganese complexes featuring hexadentate AAZTA-like ligands (Figure 1.16).[113] The complexes were evaluated in terms of their thermodynamic and relaxometric properties as potential MRI contrast agents. In comparison to the [Mn.AAZTA] complex (log K = 14) the hexadentate complexes were three orders of magnitude less stable, and thus are not sufficiently stable for use *in vivo*. Manganese(II) has coordination numbers of six or seven, which led the author to believe that the difference was attributed to the glycine moiety of the hexadentate ligands being a weaker coordinating group than the iminodiacetate of AAZTA.[113] Given the apparent wealth of octahedral manganese(II) complexes in the literature, this may not be the only contributing factor. Inherent strain within the ligand, and different donor sets may also play a role.

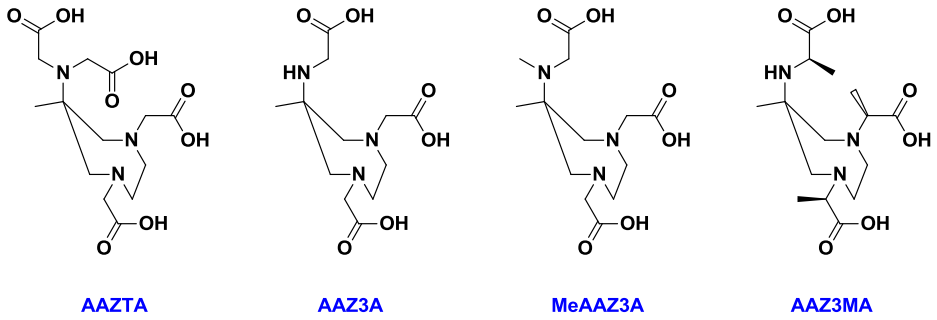

Figure 1.16 *AAZTA and hexadentate 'AAZTA-like' ligands synthesised by Botta et al (2011) as potential ligands for Mn(II) MRI contrast agents.*[113]

In 2012 Manzoni et al[68] published the first example of a gallium complex featuring the DAZA scaffold. Specifically they used the parent AAZTA ligand tethered to an RGB peptidomimetic via the 6-carbon of the ring (Figure 1.17). The peptide used has been shown to have high affinity for $\alpha_v\beta_3$ receptors, which are overexpressed in a variety of cancers. The gallium complex was not investigated in detail, but rather used as a proof of principle for the gadolinium equivalents.

The resulting radiolabelled complex was stated to be more stable than the DTPA equivalent, and sufficiently stable for in vivo testing.[68] Radiolabelling of AAZTA and the conjugate was carried out at pH 3.8 (no further detail was provided), and injected into rats bearing a glioblastoma tumour model. The untargeted radiolabel, [^{68}Ga.AAZTA], was eliminated rapidly from the blood and accumulated in the bladder. The radiolabel was visible in the tumour at 20 min post injection, and undetectable at 50 min. Consistent with the larger size of the radiolabelled complex, [^{68}Ga.AAZTA]-DB58, the kinetics of clearance were slower. Tumour accumulation was highlighted at 40 min, largely due to reduced background signal, and was still visible at 70 min.[68]

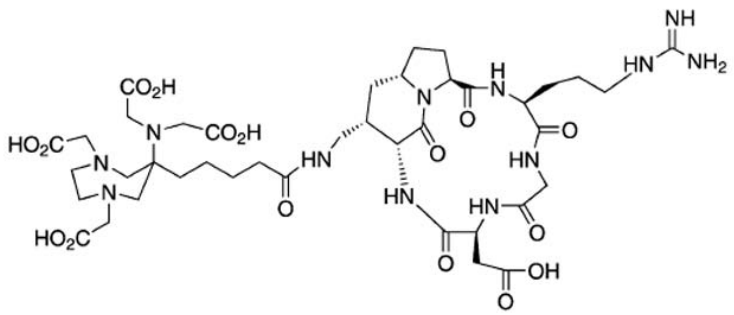

Figure 1.17 *The AAZTA ligand BFC derivative, AAZTA-DB58, used in ^{68}Ga-radiolabelling and subsequent in vivo glioblastoma tumour model trails. Picture from* [68].

Prior to the ^{68}Ga-study, evaluations of the relative affinity of the free DB58, [Gd.DPTA-DB58] and [Gd.AAZTA-DB58] were carried out. It was found that the DTPA analogue produced chelates with satisfactory $\alpha_v\beta_3$ receptor affinity, whereas the AAZTA analogue did not. Subsequent efforts to transfer these findings from Gd complexes to ^{68}Ga complexes for PET studies, found that only the [^{68}Ga.AAZTA-DB58] was sufficiently stable *in vivo* to warrant further testing.[68] The stability of the [^{68}Ga.AAZTA] complex is favourable; however, for in vivo application the detrimental effect of the AAZTA ligand on the binding affinity of DK58 to the $\alpha_v\beta_3$ receptor is undesirable. It is evident that modifications to the AAZTA ligand are required, in order for the ligand to be useful.[68]

The choice of AAZTA in this regard is interesting. In addition to having a detrimental effect on the binding affinity, AAZTA also is not ideally suited to the chelation of gallium(III). The heptadentate ligand has one too many donor groups, which could result in coordinative promiscuity within the ligand complex. This could result in speciation problems, which may influence the pharmacokinetics of the radiolabel. On the other hand, if unused, the additional acid group could be seen as beneficial in terms of the pharmacokinetic properties of the complex.

6.4 Summary: DAZA as a potential ligand for ^{68}Ga-PET

It is apparent from the discussion that, as a ligand, DAZA and its derivatives have had mixed fortunes. Besides its potential application in Gd-enhanced MRI as the AMPED scaffold with four acetate donors, the ligand has found little use. In its simplistic triamine form, a series of comprehensive publications by Hegetschweiler[103, 104], not only found the ligand to be a poor mimic for 9-N_3, but in general a poor chelator of metals requiring an octahedral coordination geometry. Furthermore, subsequent efforts to improve its binding properties through modification of the core (to give AMPED), have proven largely unsuccessful.[104] The DAZA core was evaluated as an ancillary ligand in rare earth metal catalysis[108-110], however interest in the tetra- and penta-dentate derivatives subsided. Hexadentate AAZTA-like ligand derivatives were evaluated for potential application as manganese MRI contrast agents, but the complexes are not sufficiently stable for *in vivo* application.[113]

Although interest in these ligands in Gd MRI applications continues, it could be argued that even here the ligand is not particularly well suited. Reported stabilities are not better than DTPA equivalents, which probably isn't good enough for clinical application in spite of the favourable

magnetic properties. Structural data suggests that the favourable magnetic properties observed, partly arise from the fact that AAZTA is not a suitable ligand for Gd. The gadolinium ion is too big for the cavity of AAZTA, and as a result the metal ion is significantly exposed. This makes the Gd centre accessible to coordinating water molecules, and gives rise to the favourable relaxation properties. The exposed metal ion, coupled with the inherent strain in the coordinated ligand, means complexes like these are likely to be on the border of what is acceptable in terms of stability.

Tumour binding affinity studies indicate that the AAZTA ligand has a detrimental effect on receptor-vector binding affinity. In order to overcome this problem, the AAZTA ligand requires modification to alter its pharmacokinetics.[68] Doing so could be problematic considering the cramped nature of the ligand, especially at the iminodiacetate. Furthermore, there is evidence that modification of the endocyclic amines effects stability and magnetic properties.[98, 121]

At the outset of this research, there were no reports of gallium complexes which incorporate the AMPED core structure. In terms of coordination geometry, 'AAZTA-like' ligands should be well suited to octahedral coordination geometry requirements of ^{68}Ga(III). Crystal structural data of DAZA and 9-N_3 based complexes show that the core *fac*-N_3 structures are very similar.[103-105] This suggests that hexadentate derivatives of DAZA (similar in form to NOTA) should give rise to sufficiently stable complexes for use *in vivo*, provided that the metal ion is of suitable size and nature. Furthermore, it has already been shown that the AMPED ring has considerable conformational flexibility, giving the ligand a mixture of cyclic (stability) and acyclic (flexibility).[95, 97] These features may promote fast ^{68}Ga radiolabelling. Ln-AAZTA crystal structures show that the chelator takes up approximately half of the coordination sphere of the metal. However, it should be noted that the Gd(III) ion is significantly larger than Ga(III). Therefore, it is expected that Ga(III) would fit better for the binding site of AAZTA (or its derivatives). Despite some complications, the ligand has been shown to be extremely versatile in terms of conjugation, it is easy and cheap to synthesize and gives complexes that are sufficiently stable for *in vivo* application.[93, 112] In addition, the lower ligand denticity required by gallium(III) may permit greater ligand modification. This may become important in terms of optimising the pharmacokinetics of the gallium complexes.

7 Aims and specification

The objective of this project is to evaluate the suitability of hexadentate ligands based on AMPED for ^{68}Ga-PET. Specifically, the aim is to design, synthesise and characterise a series of novel hexadentate ligands based on the AMPED scaffold for radiochemical evaluation with ^{68}Ga. Initial evaluation would take the form of radiolabelling and stability studies, with subsequent in vivo evaluations of suitable candidates. Further work would look to improve upon these ligands.

Radionuclide imaging with ^{68}Ga, both in research and clinical practice, is dominated by the use of the ligand derivatives of NOTA and DOTA. The high temperatures required for radiolabelling of DOTA, are largely addressed with NOTA without detriment to the stability of the resulting complex. However, its application is hindered by the acidic pH required for radiolabelling, cost and difficult syntheses. Whilst they serve the purpose, improvements to increase efficiency, suitability, application and costs are required to realise the potential of the favourable ^{68}Ga-radionuclide. Specific areas of improvement include quantitative radiolabelling at milder pH and room temperature, whilst maintaining sufficient in vivo stability.

The specification for a ligand ideal for application in ^{68}Ga-PET is as follows:[10, 19, 20, 35, 39, 41]

1. A derived gallium(III) complex which is sufficiently kinetically inert and thermodynamically stable in vivo over a period of 2 hours.
2. Quantitatively radiolabels with ^{68}Ga within 10 minutes at room temperature over a wide pH range, which includes mildly acidic environments.
3. Follows a synthetic procedure which is cheap, fast and simple.
4. Provides a point of attachment for biological vectors. Synthetic flexibility to adjust the pharmacokinetics of the complex is also favourable.
5. The ligand should display selectively for gallium, over other metal ions it may experience in vivo and during radiolabelling.
6. Synthesis of the ligand should be conducted in a manner such that the radiolabel precursor meets all quality control requirements. Specifically, the final product should have known composition and be of very high purity.

8 References

1. S. Webb, *The Physics of Medical Imaging, Second Edition*, Taylor & Francis Group, LLC, U.S.A, 2012.
2. I. N. Bankman, *Handbook of Medical Imaging: Processing and Analysis Management*, Academic Press, California, U.S.A, 2000.
3. D. Parker, J.-M. Lehn, J. L. Atwood, J. E. D. Davies and D. D. MacNicol, *Comprehensive Supramolecular Chemistry - Imaging and Targeting*, Pargamon, Oxford, United Kingdom, 1996.
4. P. Hermann, J. Kotek, V. Kubicek and I. Lukes, *Dalton Transactions*, 2008, 3027-3047.
5. R. Weissleder and U. Mahmood, *Radiology*, 2001, **219**, 316-333.
6. T. F. Massoud and S. S. Gambhir, *Genes & Development*, 2003, **17**, 545-580.
7. F. L. Thorp-Greenwood and M. P. Coogan, *Dalton Transactions*, 2011, **40**, 6129-6143.
8. R. C. Knowlton, *Epilepsy & Behavior*, 2006, **8**, 91-101.
9. J. T. Bushberg, J. A. Seibert, E. M. Leidholdt and J. M. Boon, *The Essential Physics of Medical Imaging*, Lippincott Williams & Wilkins, Philadepphia, U.S.A, 2002.
10. I. Velikyan, *Medicinal Chemistry*, 2011, **7**, 345-379.
11. J. P. Mach, F. Buchegger, J. C. Volant, J. P. Grob, V. Vonfliedner, A. Bischofdelaloye and B. Delaloye, *Cancer Drug Delivery*, 1985, **2**, 214-214.
12. G. B. Stillwagon, S. E. Order, C. Guse, J. L. Klein, P. K. Leichner, S. A. Leibel and E. K. Fishman, *International Journal of Radiation Oncology Biology Physics*, 1989, **17**, 1223-1229.
13. IAEA, *Production of Long Lived Parent Radionuclides: 68Ge, 82Sr, 90Sr abd 188W*, IAEA, Vienna, Austria, 2010.
14. M. U. Khan, S. Khan, S. Ei-Refaie, Z. Win, D. Rubello and A. Al-Nahhas, *Ejso*, 2009, **35**, 561-567.
15. I. Velikyan, *Theranostics*, 2012, **2**, 424-426.
16. G. Hevesy, *Biochemical Journal*, 1923, **17**, 439-445.
17. D. Artemov, Z. M. Bhujwalla, R. J. Maxwell, J. R. Griffiths, I. R. Judson, M. O. Leach and J. D. Glickson, *Magnetic Resonance in Medicine*, 1995, **34**, 338-342.
18. T. Jones, *European Journal of Nuclear Medicine*, 1996, **23**, 207-211.
19. M. Fani, J. P. Andre and H. R. Maecke, *Contrast Media Mol Imaging*, 2008, **3**, 67-77.
20. M. D. Bartholomae, *Inorganica Chimica Acta*, 2012, **389**, 36-51.
21. A. Al-Nahhas, Z. Win, T. Szyszko, A. Singh, S. Khan and D. Rubello, *Eur J Nucl Med Mol Imaging*, 2007, **34**, 1897-1901.
22. R. Yuste, *Nature Methods*, 2005, **2**, 902-904.
23. J. L. Lakowicz, *Principles of Fluorescence Spectroscopy*, Academic/Plenum Press, New York, U.S.A, 1999.
24. B. Valeur, *In Molecular luminescence Spectroscopy: Methods and Applications*, John Wiley & Sons, New York, U.S.A, 1993.
25. Y. Bretonniere, M. J. Cann, D. Parker and R. Slater, *Organic & Biomolecular Chemistry*, 2004, **2**, 1624-1632.
26. B. N. Ganguly, N. N. Mondal, M. Nandy and F. Roesch, *Journal of Radioanalytical and Nuclear Chemistry*, 2009, **279**, 685-698.
27. F. Roesch and P. J. Riss, *Current Topical Medicinal Chemistry*, 2010, **10**, 1633-1668.
28. J. F. Eary and K. A. Krohn, *European Journal of Nuclear Medicine*, 2000, **27**, 1737-1739.
29. P. Price, *Trends in Molecular Medicine*, 2001, **7**, 442-446.
30. C. S. Cutler, M. C. Giron, D. E. Reichert, A. Z. Snyder, P. Herrero, C. J. Anderson, D. A. Quarless, S. A. Koch and M. J. Welch, *Nuclear Medicine Biology*, 1999, **26**, 305-316.
31. B. J. Pichler, A. Kolb, T. Nagele and H. P. Schlemmer, *J Nucl Med*, 2010, **51**, 333-336.

32. K. Serdons, A. Verbruggen and G. M. Bormans, *Methods*, 2009, **48**, 104-111.
33. E. Boros, C. L. Ferreira, B. O. Patrick, M. J. Adam and C. Orvig, *Nucl Med Biol*, 2011, **38**, 1165-1174.
34. G. Bandoli, A. Dolmella, F. Tisato, M. Porchia and F. Refosco, *Coordination Chemistry Reviews*, 2009, **253**, 56-77.
35. M. D. Bartholoma, A. S. Louie, J. F. Valliant and J. Zubieta, *Chem Rev*, 2010, **110**, 2903-2920.
36. H. R. Maecke and J. P. Andre, *Ernst Schering Res Found Workshop*, 2007, 215-242.
37. F. Roesch and P. J. Riss, *Current Topics in Medicinal Chemistry*, 2010, **10**, 1633-1668.
38. T. J. Wadas, E. H. Wong, G. R. Weisman and C. J. Anderson, *Chem Rev*, 2010, **110**, 2858-2902.
39. C. J. Anderson and M. J. Welch, *Chem Rev*, 1999, **99**, 2219-2234.
40. D. E. Reichert, J. S. Lewis and C. J. Anderson, *Coordination Chemistry Reviews*, 1999, **184**, 3-66.
41. M. A. Green and M. J. Welch, *International journal of radiation applications and instrumentation. Part B, Nuclear medicine and biology*, 1989, **16**, 435-448.
42. M. I. Prata, *Curr Radiopharm*, 2012, **5**, 142-149.
43. D. J. Berry, Y. Ma, J. R. Ballinger, R. Tavare, A. Koers, K. Sunassee, T. Zhou, S. Nawaz, G. E. Mullen, R. C. Hider and P. J. Blower, *Chem Commun (Camb)*, 2011, **47**, 7068-7070.
44. H. D. Bruner, R. L. Hayes and J. D. Perkinson, *Radiology*, 1953, **61**, 602-613.
45. F. Roesch and F. F. Knapp, *Radionuclide generators: Handbook of Nuclear and Radiochemistry*, Kluwer Publishers, 2002.
46. P. J. Riss, C. Burchardt and F. Roesch, *Contrast Media Mol Imaging*, 2011, **6**, 492-498.
47. F. Roesch, *Curr Radiopharm*, 2012, **5**, 202-211.
48. I. Velikyan, H. Maecke and B. Langstrom, *Bioconjug Chem*, 2008, **19**, 569-573.
49. K. P. Zhernosekov, D. V. Filosofov, R. P. Baum, P. Aschoff, H. Bihl, A. A. Razbash, M. Jahn, M. Jennewein and F. Roesch, *Journal of Nuclear Medicine*, 2007, **48**, 1741-1748.
50. W. A. P. Breeman and A. M. Verbruggen, *Eur J Nucl Med Mol Imaging*, 2007, **34**, 978-981.
51. M. Pagou, I. Zerizer and A. Al-Nahhas, *Hell J Nucl Med*, 2009, **12**, 102-105.
52. W. R. Harris and V. L. Pecoraro, *Biochemistry*, 1983, **22**, 292-299.
53. M. Asti, G. De Pietri, A. Fraternali, E. Grassi, R. Sghedoni, F. Fioroni, F. Roesch, A. Versari and D. Salvo, *Nucl Med Biol*, 2008, **35**, 721-724.
54. I. Velikyan, G. J. Beyer and B. Langstrom, *Bioconjug Chem*, 2004, **15**, 554-560.
55. W. A. P. Breeman, M. de Jong, E. de Blois, B. F. Bernard, M. Konijnenberg and E. P. Krenning, *European Journal of Nuclear Medicine and Molecular Imaging*, 2005, **32**, 478-485.
56. D. Mueller, I. Klette, R. P. Baum, M. Gottschaldt, M. K. Schultz and W. A. P. Breeman, *Bioconjug Chem*, 2012, **23**, 1712-1717.
57. J. Notni, P. Hermann, J. Havlickova, J. Kotek, V. Kubicek, J. Plutnar, N. Loktionova, P. J. Riss, F. Rosch and I. Lukes, *Chemistry*, 2010, **16**, 7174-7185.
58. J. Notni, K. Pohle and H. J. Wester, *EJNMMI Res*, 2012, **2**, 28.
59. M. Bauwens, R. Chekol, H. Vanbilloen, G. Bormans and A. Verbruggen, *Nuclear Medicine Communications*, 2010, **31**, 753-758.
60. C. J. Mathias, Y. Z. Sun, M. J. Welch, M. A. Green, J. A. Thomas, K. R. Wade and A. E. Martell, *Nuclear Medicine and Biology*, 1988, **15**, 69-&.
61. E. Cole, R. C. B. Copley, J. A. K. Howard, D. Parker, G. Ferguson, J. F. Gallagher, B. Kaitner, A. Harrison and L. Royle, *Journal of the Chemical Society-Dalton Transactions*, 1994, 1619-1629.
62. D. A. Moore, P. E. Fanwick and M. J. Welch, *Inorganic Chemistry*, 1989, **28**, 1504-1506.
63. L. Maria, C. Fernandes, R. Garcia, L. Gano, A. Paulo, I. C. Santos and I. Santos, *Dalton Transactions*, 2009, 603-606.
64. R. Delgado and J. Dasilva, *Talanta*, 1982, **29**, 815-822.
65. B. E. Rogers, C. J. Anderson, J. M. Connett, L. W. Guo, W. B. Edwards, E. L. C. Sherman, K. R. Zinn and M. J. Welch, *Bioconjugate Chemistry*, 1996, **7**, 511-522.

66. H. R. Maecke, M. Hofmann and U. Haberkorn, *Journal of Nuclear Medicine*, 2005, **46**, 172S-178S.
67. E. Boros, C. L. Ferreira, D. T. Yapp, R. K. Gill, E. W. Price, M. J. Adam and C. Orvig, *Nucl Med Biol*, 2012, **39**, 785-794.
68. L. Manzoni, L. Belvisi, D. Arosio, M. P. Bartolomeo, A. Bianchi, C. Brioschi, F. Buonsanti, C. Cabella, C. Casagrande, M. Civera, M. De Matteo, L. Fugazza, L. Lattuada, F. Maisano, L. Miragoli, C. Neira, M. Pilkington-Miksa and C. Scolastico, *Chemmedchem*, 2012, **7**, 1084-1093.
69. P. J. Riss and F. Roesch, *Bioorg Med Chem*, 2009, **17**, 7630-7634.
70. T. J. Norman, F. C. Smith, D. Parker, A. Harrison, L. Royle and C. A. Walker, *Supramolecular Chemistry*, 1995, **4**, 305-308.
71. J. Simecek, M. Schulz, J. Notni, J. Plutnar, V. Kubicek, J. Havlickova and P. Hermann, *Inorg Chem*, 2012, **51**, 577-590.
72. H. O. Anger and A. Gottschalk, *Journal of Nuclear Medicine*, 1963, **4**, 326-330.
73. T. M. Joneswilson, R. J. Motekaitis, Y. Z. Sun, C. J. Anderson, A. E. Martell and M. J. Welch, *Nuclear Medicine and Biology*, 1995, **22**, 859-868.
74. G. I. Gleason, *The International journal of applied radiation and isotopes*, 1960, **8**, 90-94.
75. J. P. Andre, H. R. Maecke, M. Zehnder, L. Macko and K. G. Akyel, *Chemical Communications*, 1998, 1301-1302.
76. J. Kowalski, M. Henze, J. Schuhmacher, H. R. Macke, M. Hofmann and U. Haberkorn, *Molecular imaging and biology : MIB : the official publication of the Academy of Molecular Imaging*, 2003, **5**, 42-48.
77. A. Heppeler, S. Froidevaux, H. R. Macke, E. Jermann, M. Behe, P. Powell and M. Hennig, *Chemistry-a European Journal*, 1999, **5**, 1974-1981.
78. E. T. Clarke and A. E. Martell, *Inorganica Chimica Acta*, 1991, **190**, 37-46.
79. R. Delgado, V. Felix, L. M. P. Lima and D. W. Price, *Dalton Transactions*, 2007, 2734-2745.
80. T. Mukai, J. Suwada, K. Sano, M. Okada, F. Yamamoto and M. Maeda, *Bioorganic & Medicinal Chemistry*, 2009, **17**, 4285-4289.
81. E. Boros, C. L. Ferreira, J. F. Cawthray, E. W. Price, B. O. Patrick, D. W. Wester, M. J. Adam and C. Orvig, *J Am Chem Soc*, 2010, **132**, 15726-15733.
82. A. S. Craig, D. Parker, H. Adams and N. A. Bailey, *Journal of the Chemical Society-Chemical Communications*, 1989, 1793-1794.
83. C. L. Ferreira, E. Lamsa, M. Woods, Y. Duan, P. Fernando, C. Bensimon, M. Kordos, K. Guenther, P. Jurek and G. E. Kiefer, *Bioconjugate Chemistry*, 2010.
84. K. P. Eisenwiener, M. I. M. Prata, I. Buschmann, H. W. Zhang, A. C. Santos, S. Wenger, J. C. Reubi and H. R. Macke, *Bioconjugate Chemistry*, 2002, **13**, 530-541.
85. P. J. Riss, C. Kroll, V. Nagel and F. Rosch, *Bioorg Med Chem Lett*, 2008, **18**, 5364-5367.
86. Y. Sun, C. J. Anderson, T. S. Pajeau, D. E. Reichert, R. D. Hancock, R. J. Motekaitis, A. E. Martell and M. J. Welch, *J Med Chem*, 1996, **39**, 458-470.
87. R. C. Matthews, D. Parker, G. Ferguson, B. Kaitner, A. Harrison and L. Royle, *Polyhedron*, 1991, **10**, 1951-1953.
88. J. Notni, J. Plutnar and H. J. Wester, *EJNMMI Res*, 2012, **2**, 13.
89. A. E. Martell, R. J. Motekaitis and M. J. Welch, *Journal of the Chemical Society-Chemical Communications*, 1990, 1748-1749.
90. M. Eder, A. V. Krivoshein, M. Backer, J. M. Backer, U. Haberkorn and M. Eisenhut, *Nuclear Medicine and Biology*, 2010, **37**, 405-412.
91. M. Eder, B. Wangler, S. Knackmuss, F. LeGall, M. Little, U. Haberkorn, W. Mier and M. Eisenhut, *Eur J Nucl Med Mol Imaging*, 2008, **35**, 1878-1886.
92. R. Galanello, *Ther Clin Risk Manag*, 2007, **3**, 795-805.
93. S. Aime, L. Calabi, C. Cavallotti, E. Gianolio, G. B. Giovenzana, P. Losi, A. Maiocchi, G. Palmisano and M. Sisti, *Inorg Chem*, 2004, **43**, 7588-7590.

94. E. Gianolio, G. B. Giovenzana, D. Longo, I. Longo, I. Menegotto and S. Aime, *Chemistry-a European Journal*, 2007, **13**, 5785-5797.
95. S. Aime, G. Bombieri, C. Cavallotti, G. B. Giovenzana, D. Imperio and N. Marchini, *Inorganica Chimica Acta*, 2008, **361**, 1534-1541.
96. S. Aime, P. Bardini, C. Cabella, E. Gianolio, F. Arena, A. Maiocchi, F. Tedoldi, F. Uggeri, G. Valbusa and M. Visigalli, *Contrast Media & Molecular Imaging*, 2009, **4**, 276-277.
97. Z. Baranyai, F. Uggeri, G. B. Giovenzana, A. Benyei, E. Brucher and S. Aime, *Chemistry*, 2009, **15**, 1696-1705.
98. E. M. Elemento, D. Parker, S. Aime, E. Gianolio and L. Lattuada, *Organic & Biomolecular Chemistry*, 2009, **7**, 1120-1131.
99. E. Gianolio, K. Ramalingam, B. Song, F. Kalman, S. Aime and R. Swenson, *Inorganic Chemistry Communications*, 2010, **13**, 663-665.
100. R. S. Sengar, A. Nigam, S. J. Geib and E. C. Wiener, *Polyhedron*, 2009, **28**, 1525-1531.
101. M. Rossignoli, T. W. Hambley, G. A. Lawrance and M. Maeder, *Aust. J. Chem.*, 1997, **50**, 241 - 245.
102. J. W. Pauly, J. Sander, D. Kuppert, M. Winter, G. J. Reiss, F. Zürcher, R. Hoffmann, T. F. Fässler and K. Hegetschweiler, *Chemistry – A European Journal*, 2000, **6**, 2830-2846.
103. J. Romba, D. Kuppert, B. Morgenstern, C. Neis, S. Steinhauser, T. Weyhermuller and K. Hegetschweiler, *European Journal of Inorganic Chemistry*, 2006, 314-328.
104. C. Neis, D. Petry, A. Demangeon, B. Morgenstern, D. Kuppert, J. Huppert, S. Stucky and K. Hegetschweiler, *Inorganic Chemistry*, 2010, **49**, 10092-10107.
105. R. A. Peralta, A. Neves, A. J. Bortoluzzi, A. Casellato, A. Dos Anjos, A. Greatti, F. R. Xavier and B. Szpoganicz, *Inorg Chem*, 2005, **44**, 7690-7692.
106. A. J. Bortoluzzi, A. Neves and G. G. Terra, *Acta Crystallographica Section E-Structure Reports Online*, 2006, **62**, M2965-M2966.
107. N. A. Rey, A. Neves, A. J. Bortoluzzi, C. T. Pich and H. Terenzi, *Inorganic Chemistry*, 2007, **46**, 348-350.
108. S. Ge, S. Bambirra, A. Meetsma and B. Hessen, *Chemical Communications*, 2006, 3320-3322.
109. S. Ge, A. Meetsma and B. Hessen, *Organometallics*, 2007, **26**, 5278-5284.
110. S. Ge, A. Meetsma and B. Hessen, *Organometallics*, 2009, **28**, 719-726.
111. P. Comba, C. Haaf and H. Wadepohl, *Inorganic Chemistry*, 2009, **48**, 6604-6614.
112. G. Gugliotta, M. Botta and L. Tei, *Organic & Biomolecular Chemistry*, 2010, **8**, 4569-4574.
113. L. Tei, G. Gugliotta, M. Fekete, F. K. Kalman and M. Botta, *Dalton Trans*, 2011, **40**, 2025-2032.
114. R. I. Haines, *Reviews in Inorganic Chemistry*, 2001, **21**, 165-205.
115. P. Chaudhuri and K. Wieghardt, in *Progress in Inorganic Chemistry, Vol. 50*, Editon edn., 2001, vol. 50, pp. 151-216.
116. R. A. Peralta, A. Neves, A. J. Bortoluzzi, A. Casellato, A. dos Anjos, A. Greatti, F. R. Xavier and B. Szpoganicz, *Inorganic Chemistry*, 2005, **44**, 7690-7692.
117. L. Fabbrizzi, M. Micheloni and P. Paoletti, *Inorganic Chemistry*, 1976, **15**, 1451-1452.
118. S. Deangelis, A. Batsanov, T. J. Norman, D. Parker, K. Senanayake and J. Vepsalainen, *Journal of the Chemical Society-Chemical Communications*, 1995, 2361-2363.
119. D. Parker, K. Senanayake, J. Vepsailainen, S. Williams, A. S. Batsanov and J. A. K. Howard, *Journal of the Chemical Society-Perkin Transactions 2*, 1997, 1445-1452.
120. US Pat., 07988950, 2011.
121. D. Imperio, G. B. Giovenzana, G.-l. Law, D. Parker and J. W. Walton, *Dalton Transactions*, 2010, **39**, 9897-9903.

Chapter 2

AMPED Based Ligands for ^{68}Ga(III)

This chapter discusses the synthesis and solution NMR behaviour of a series of hexa- and hepta-dentate aza-carboxylate ligands (Section 1 and 2), followed by an assessment of their suitability for application in ^{68}Ga-PET (Section 3).

1 Synthetic Aspects

Three main methods have been described for the synthesis of 6-amino-1,4-diazepines for use as ligands in metal complexes.[1-3] This *fac*-N_3 7-membered ring features a single exo- and two endocyclic amines, which can be functionalised to increase the ligand denticity. In particular, interest in this tri-amine has focused on its use in complexes of transition[3-7] (titanium, scandium, manganese) and lanthanide[2, 8-15] (gadolinium, europium) metal ions.

The ligand AAZTA, which has been shown to produce stable complexes with lanthanide metal ions, features the tribasic core modified by the addition of a methyl group at the 6-position to yield 6-amino-6-methylperhydro-1,4-diazepine (AMPED; see Scheme 2.1). Synthesis of this core is both cheap and synthetically facile, with modification to alter the characteristics of the ring for bio-conjugation seemingly straightforward.[2, 13, 14] Gugliotta was the first to show how 6-hydroxylalkyl derivatives can be used to form a range of 6-substituted AMPED scaffolds.[13] Following the success obtained with the stable coordination of lanthanide ions and the relatively facile ligand synthesis, this published synthetic protocol[2] seemed a sensible starting point for the synthesis of ligands suitable for the formation of stable gallium complexes. Furthermore, the other syntheses described require a greater number of steps and are potentially hazardous.[3, 6] Each ligand discussed in this section features the AMPED scaffold, with modifications to the structure being made exclusively through functionalisation of the amines. This approach was chosen as it would allow assessment of the suitability and potential of the triamine core, whilst making relatively simple structural changes. The intention was to optimise the N-substituents in the first instance (Chapter 2), and subsequently consider modifications to the core structure (Chapter 3) which could further improve the ligands ability to bind Ga(III) rapidly, yet form kinetically stable complexes.

A series of six ligands were initially identified as synthetic targets (Figure 2.1). In spite of the fact that the ligand AAZTA (**L**[1]) is likely to be unsuitable, given that it is heptadentate, it was evaluated as the parent ligand of the series. Thought to be better suited for the complexation of gallium(III), the remaining targets present N_3O_3 hexadentate donor systems. An important consideration of potential ligands for PET is the lipophilicity of the radiolabelled complex. To explore the effect of varying lipophilicity on the complexation bahaviour of the ligands, the ligands have been elaborated with methyl groups at various positions (**L**[2-4]). The potential of the system for the development of bi-functional chelators was also investigated through N_{exo}-substitution with a masked benzylamine (**L**[5]).

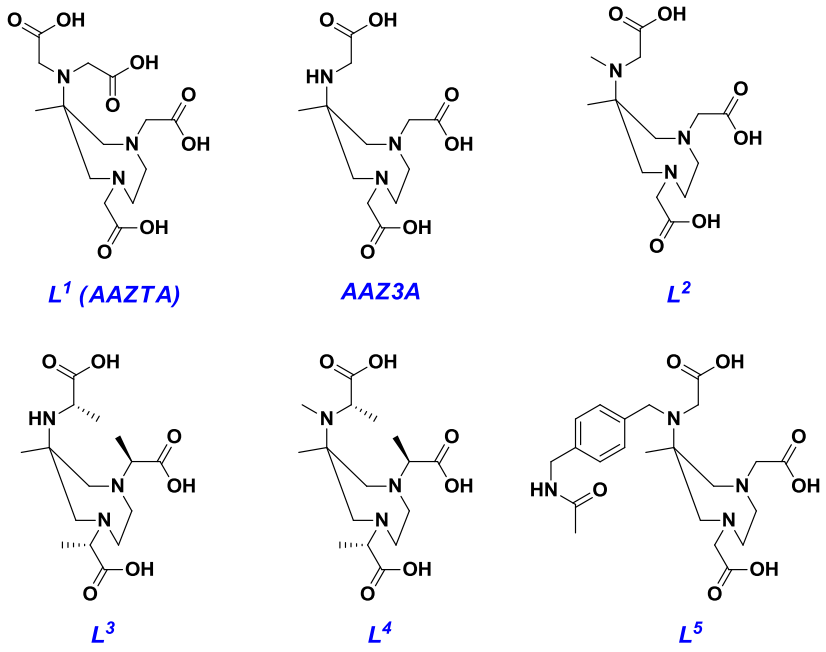

Figure 2.1 *Synthetic targets featuring the AMPED core.*

In this section, an overview and discussion of the synthetic techniques used to make these ligands will be given. The discussion will initially focus on the synthesis of AMPED which is central to every target, and will be followed by a discussion of its functionalisation to yield the desired ligands.

During the course of this research ligands (specifically **AAZ3A**, **L**[2] and the (*RRR)* enantiomer of **L**[3]) have been published elsewhere, for the complexation of manganese(II) with aim of developing MRI imaging agents.[7]

1.1 Synthesis of the AMPED Core

The synthesis of AMPED is a well-established and high yielding two-step procedure that uses relatively cheap and readily available starting materials, allowing per gram-scale batches being to be prepared in an overall yield of 71 % (Scheme 2.1).[2] Numerous research groups have made use of this synthetic strategy, or ones adapted from it, for the synthesis of ligands suitable for the complexation of metal ions – most often heptadenate ligands for lanthanide metal ions.[2]

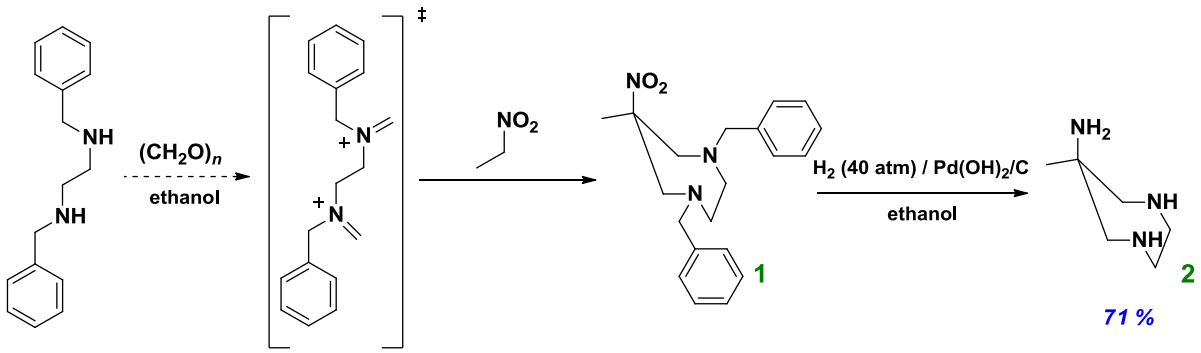

Scheme 2.1 *Synthesis of the AMPED core, with intermediates shown. Method adopted from Aime and co-workers.*[2]

Other methods for the synthesis of very similar rings have been described. However, they require a greater number of steps, give poorer yields and in some cases are potentially hazardous.[3, 5, 6] A further benefit of the method of Aime and co-workers, is that functionalisation of the quaternary carbon is possible through small modification to the reactants used in the first step. This modification has been exploited by numerous groups for the synthesis of derivatives suitable for bio-conjugation.[14-18]

The key step is the formation of the seven-membered ring, which is accomplished by a nitro-Mannich type co-condensation reaction (Scheme 2.1). Initial reaction between paraformaldehyde and the bis-benzyl protected ethylenediamine affords a di-iminium intermediate, which in turn reacts with nitroethane to form the seven-membered ring. The choice of benzyl groups is convenient (and necessary, as became apparent later) since catalytic hydrogenation (using $Pd(OH)_2/C$) of 1,4-dibenzyl-6-methyl-6-nitroperhydro-1,4-diazepine (**1**) results in concomitant reduction of the nitro group and *bis*-N-debenzylation, leading to formation of AMPED. Whilst convenient, this synthetic strategy does have its shortcomings. As noted by Parker[8] and Botta[16], differential N-substitution of

the N_{exo} and N_{endo} amines is possible, but the procedure is non-trivial and inefficient. Taking into consideration the nature of the synthetic targets this is not of concern at this stage, however when differential N-substitution is required, selective deprotection would be more versatile. The synthesis of modified derivatives of these ligands tailored towards bio-conjugation would benefit significantly from a more flexible synthetic strategy.

The product of the hydrogenolysis reaction, AMPED (**2**), following filtration through Celite® and removal of solvent under reduced pressure, is a golden yellow oil which forms an oily white solid upon standing in an inert environment. If left open to the atmosphere, the oil/solid gradually changes form and darkens over the course of a week. The triamine, **2**, is strongly basic, which suggests that the compound reacts with carbon dioxide to yield a carbamate. In support of this, Hegtschweiler et al have shown that bubbling carbon dioxide through a solution of AMPED results in formation of its dicarbamate.[19]

It is possible to reverse this reaction by stirring the carbamate in concentrated hydrochloric acid (7 M) to give the protonated chloride salt of AMPED. This chloride salt is stable in air, and can be converted back to the free amine as required. Despite the benefits of producing the protonated chloride salt, praparing fresh AMPED as required was found to be more time efficient and reliable. A further difficulty experienced with handling and synthesis of AMPED is that the free triamine is relatively volatile, and evaporates under the reduced pressure of a high vacuum line.

1.2 Functionalisation of the AMPED Scaffold

Synthesis of Ligand L^1

The synthesis of ligand $\mathbf{L^1}$ was achieved using the method described by Aime and co-workers (Scheme 2.2).[2] This entailed the per-N-alkylation of the endo- and exo-cyclic amines using an excess of *t*-butyl bromo-acetate and potassium carbonate, in acetonitrile at 368 K. Hydrolysis of the t-butyl esters using trifluoroacetic acid gave the final product ($\mathbf{L^1}$), as the protonated bis-trifluoroacetate salt, in a good yield.

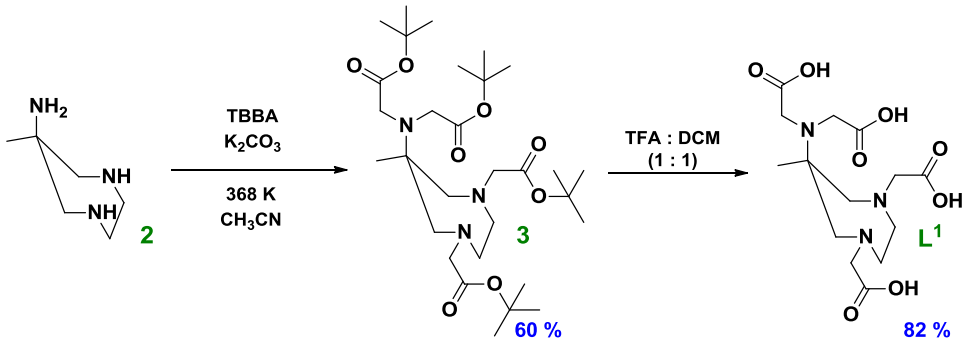

Scheme 2.2 *Synthesis of* ***L*** ^{1} *(AAZTA) as described by Aime and co-workers.*[2]

Attempted Synthesis of AAZ3A

Synthesis of the remaining targets revealed some interesting characteristics relating to the reactivity and accessibility of the endocyclic amine of AMPED. The attempted synthesis of AAZ3A is a good example of some of these characteristics. Initial attempts directed towards the synthesis of the intermediate tris-N-substituted t-butyl acetate ester, **5**, used three equivalents of t-butyl bromo-acetate and potassium carbonate at 368 K. Under these conditions only a small amount of **5** was obtained (~ 10 %) with a considerably larger portion of the tetra-alkylated product, **3** (~ 30 %). In our experience, it was not possible to exclusively produce **5** in an acceptable yield. The optimal yield was obtained when the reaction was carried out with 2.5 equivalents of t-butyl bromo-acetate, 2.5 equivalents of potassium carbonate in acetonitrile at room temperature.

Subsequent hydrolysis of the t-butyl esters using trifluoroacetic acid to give the final product also proved problematic. Whilst the ^{1}H NMR spectrum could be interpreted in a manner consistent with the structure, HR MS-ES^{+} revealed that the compound had a molecular ion peak approximately 18 mass units smaller than that of the theoretical mass. LC ESMS data revealed that during the course of the experiment there was rapid conversion of the desired tri-acid into the isolated product, **6**. We believed that this conversion corresponded to an internal lactamisation reaction involving the exocyclic amine and N_{endo}-acetate substituent (Scheme 2.3). Such a reaction is consistent with the observed change in mass, and during 2011 was reported by other research groups for the same compound.[7] The formation of this lactam ring is essentially irreversible. The reaction is acid catalysed, and therefore it is possible to suppress its formation through the use of base-labile esters. Indeed, Botta and co-workers have shown that by replacing the t-butyl esters with methyl esters it is possible to isolate AAZ3A.[7] Taking into consideration that the radiolabelling experiments would all be conducted at pH < 7 and the apparent ease with which the lactam formed, it is evident that

AAZ3A would not be sufficiently stable for use as a ligand under radiolabelling conditions. The attempted synthesis of AAZ3A did bring to light two interesting features of the exocyclic amine; it is very reactive and easily accessible to incoming nucleophiles.

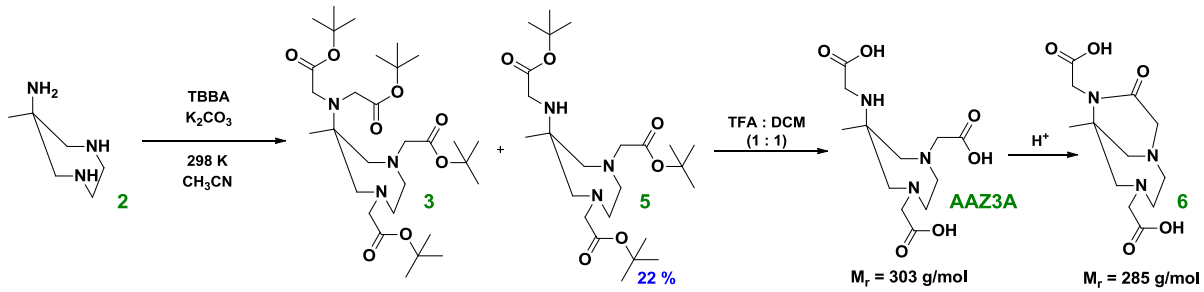

Scheme 2.3 *Attempted synthesis of AAZ3A resulting in lactamisation to give **6**. The free triacid, AAZ3A, is shown as an intermediate, but was not isolated.*

Synthesis of Ligand L^2

Fortuitously, a target chelator structurally very similar to that of the AAZ3A, which will not undergo lactamisation had already been identified. The N-methylated triacid, **L^2**, only differs from AAZ3A by the presence of an N-methyl substituent. The N-methyl group, prevents formation of the lactam ring. The logical procedure for the synthesis of **L^2** was to methylate the already synthesised tri-ester (**5**), with acid hydrolysis of the subsequent ligand precursor no longer viewed as problematic in the absence of the N-H functional group. Due to the accessibility and reactivity of the terminal amine, direct alkylation was avoided initially, thinking that this could result in formation of a quaternary ammonium salt resulting from over-methylation. The Eschweiler-Clarke reaction uses excess formic acid and formaldehyde to methylate the nitrogen of primary or secondary amines, and has been used with considerable success for the methylation of cyclen endocyclic amines. The main benefit of this method is that methylation occurs via reductive amination, which cannot result in the formation of quaternary salts. This is because the intermediate product is an iminium salt, which cannot form at a tertiary amine site. This method is also attractive because it would enable simultaneous N-methylation and ester hydrolysis, due to the presence of formic acid. The desired product was observed by ES-MS along with that of the un-methylated lactamised product seen previously. This result is perhaps not surprising given the propensity for lactamisation of **5** under acidic conditions, and indicates that the rate of methylation and rate of ester hydrolysis (followed by lactamisation) are comparable. Reaction workup and separation of these compounds proved exceedingly difficult, so it was decided to explore alternative methods.

Attempts at direct methylation of **5** were tentative, given the likelihood for formation of a quaternary ammonium salt, due to the high reactivity of methyl iodide and the exocyclic amine of **5**. Indeed, even with one equivalent of methyl iodide and 0.5 equivalents of potassium carbonate at room temperature in acetonitrile a significant amount of the di-methylated ammonium salt was obtained. Separation of the di- and mono-methylated products was difficult, and instead a milder method was sought which suppresses formation of the ammonium salt. This was achieved with a yield of 41 % using a single equivalent of methyl iodide and potassium carbonate in the less polar solvent dichloromethane (Scheme 2.4). Subsequent ester hydrolysis of **7** was carried out using dichloromethane : trifluroacetic acid (1 : 1) to afford $\mathbf{L^2}$ as the protonated bis-trifluoroacetate salt. During the course of this research Botta et al have published a different method for the synthesis of the $\mathbf{L^2}$. The triester **5** is also utilized, however methylation to produce **7** is carried out by reductive amination with formaldehyde and H_2 over Pd/C.[7]

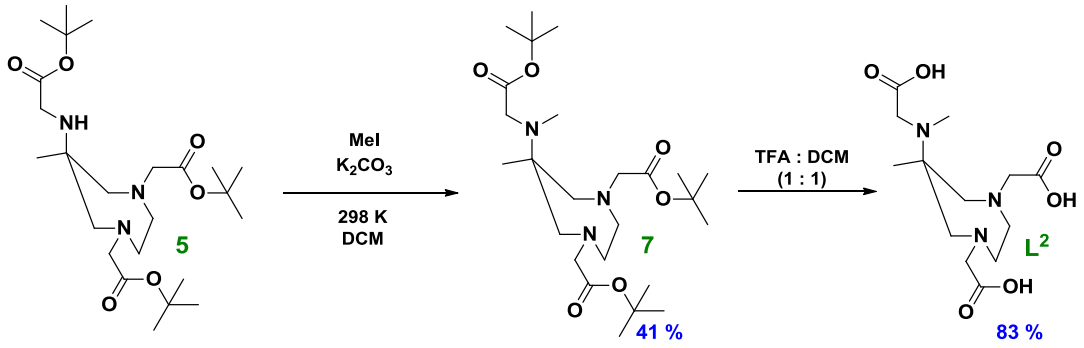

Scheme 2.4 *Conditions used for methylation, and subsequent ester hydrolysis to yield* $\boldsymbol{L^2}$.

Synthesis of Ligand $\boldsymbol{L^3}$

The tri-propionic acid derivative, $\mathbf{L^3}$, features a 'vacant' exocyclic amine position and is therefore at risk of internal lactamisation under acidic conditions. It was thought that the steric bulk afforded by the α-methyl groups of the propionate N-substituents might prevent lactamisation through both hindrance of the reaction at the exocyclic amine, and the preferred adoption of a solution conformer that does not favour the ring closure reaction.

Formation of the ligand precursor, **9**, was relatively simple with N-substitution with the ethyl propionate esters, using an excess of the enantiomerically pure (*R*)-trifluoromethyl-sulphonate, producing the tri-N-substituted *(SSS)*-product (**9**) exclusively (Scheme 2.5).

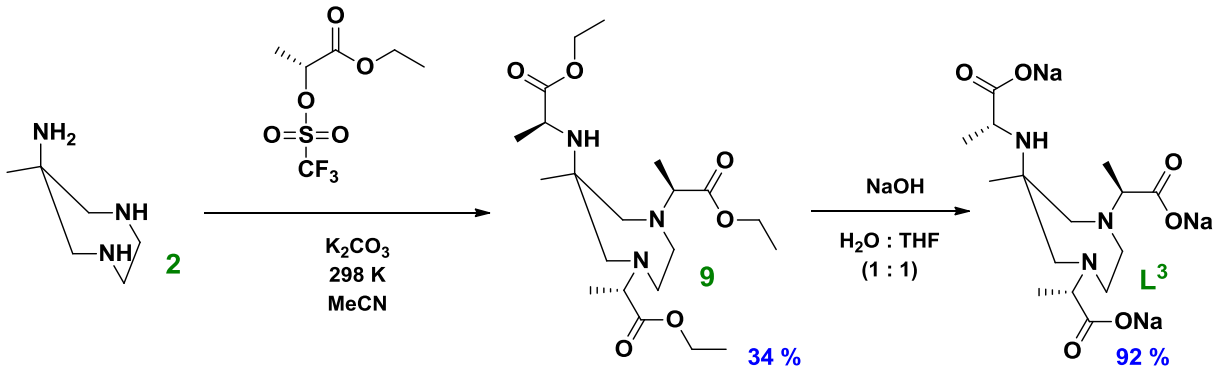

Scheme 2.5 *Synthesis of ligand* ***(SSS)-L³*** *from AMPED.*

Presumably, the absence of the tetra-N-substituted derivative is associated with an increase in the extra steric bulk about the exocyclic amine imparted by the α-methyl groups of the incoming nucleophile. Hydrolysis of the esters was an area of concern, because there are undesirable side reactions which need to be avoided. Taking into account the potential for internal lactamisation under acidic conditions, base hydrolysis of the esters was considered to be a more sensible approach as opposed to acid catalysed hydrolysis. However, it is possible that under basic conditions the chiral propionate arms could form enolates leading to racemisation at each chiral centre. Provided that the rate of ester hydrolysis was much greater than the rate of enolate formation, this side reaction would not be a problem.

The acid catalysed hydrolysis was assessed by refluxing **9** in hydrochloric acid overnight. Analysis of MS-ES data revealed that lactam formation was occurring, although it was evident that there was a significant decrease in the rate this reaction. Whilst not useful synthetically, this result did suggest that the tri-propionic acid (if isolated) would probably be sufficiently stable for use in radiolabelling evaluations. This reduced tendency towards lactamisation as compared to AAZ3A has subsequently also been noted by Botta and co-workers.[7] Base catalysed ester hydrolysis of **9** was achieved by stirring with 3.1 equivalents of sodium hydroxide in THF : water (1 : 1) for 17 hours. There was no evidence of racemisation at the α-carbon position, as deduced by analysis of ^{1}H and ^{13}C NMR spectra.

Synthesis of Ligand L⁴

The N-methylated (*SSS*)-propionic ligand, **L⁴**, was synthesised from **9** in a manner akin to that for the synthesis of the acetate analogue **L³**. The N-methylation reaction was less efficient, which is probably a result of the increased steric demand of the propionate substituent, hindering alkylation under the very mild conditions. Efforts to improve the yield by increasing the solvent polarity resulted in the formation of the quaternary ammonium salt. Ester hydrolysis of **11** was carried out under basic (sodium hydroxide) conditions, following the success already obtained with this approach (Scheme 2.7). In theory, acid catalysed hydrolysis is also feasible for this ligand.

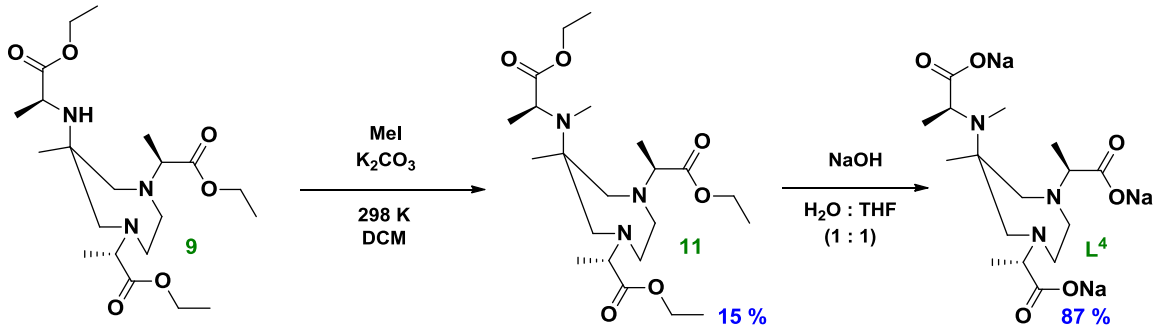

Scheme 2.7 *Conditions used for methylation, and subsequent ester hydrolysis to synthesise ligand **L⁴**.*

Synthesis of Ligand L⁵

The synthesis of ligand **L⁵** was relatively straightforward and made use of the tri-ester **5**. A series of functional group transformations on a commercially available reagent yielded the *para*-acetamide benzylic bromide derivative (**16**), which was inserted at the exocyclic amine of **5**. This reaction required harsher conditions (353 K, two equivalents caesium carbonate, acetonitrile) than those needed for the formation of **7** and **11**. This was followed by ester hydrolysis using trifluoroacetic acid to give ligand **L⁵** (Scheme 2.8), as the protonated bis-trifluroacetate salt.

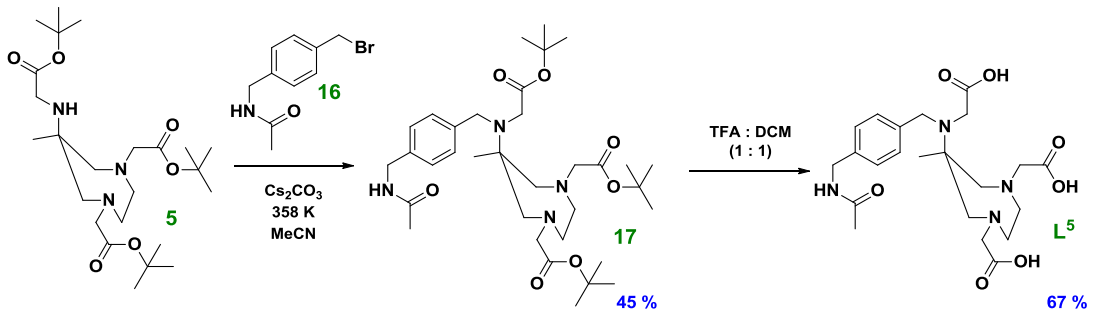

Scheme 2.8 *Conditions used for alkylation, and subsequent ester hydrolysis to synthesise ligand **L⁵**.*

2 pH Potentiometric ^{1}H NMR Analysis of Ligand L^{2}

There is considerable interest in optimising the conditions and procedures used to create a more efficient radiolabelling protocol. Optimisation of the radiolabelling conditions is often ligand specific, whereas improvements to the procedure are universally applicable.[20] The efficiency of a radiolabelling protocol is not only determined by the quantitative measurements of yield and rate. Qualitatively, the way in which the radiolabelled complexes are prepared and how these affect further use of the radiolabelled complex also needs to be taken into account. For example, if the radiolabelled complexes are intended for *in vivo* use, it is considerably more 'efficient' if the radiolabelling is done at a pH and temperature close to physiological conditions. Therefore, although there is expected to be an increase in the rate of radiolabelling with temperature, increasing the temperature to the maximum allowed (363 K in water) is not always the most practicable.

As already stated a key consideration is the pH at which the radiolabelling is carried out. Ligands, like those described in the previous section, have donor groups which can be protonated and deprotonated depending on the prevalent pH. The protonated nature of these groups has a significant effect on the rate of complexation. Therefore determining and understanding the pK_a values of the ligands is very helpful in defining the best conditions for complexation.

In many cases, changes to the protonation state of the donor groups are signalled by changes in the chemical shift of ligand protons. By following the changes in proton shift with pH, it is possible to estimate certain ligand pK_a values within the pH range of interest.

It is appropriate at this point to introduce a labelling system for the differently protonated species of the ligand. It is difficult to state unequivocally what the optimal protonation state of the ligand should be, because the exact speciation of the metal ion under the radiolabelling conditions is not known and this will influence how the ligand and metal interact on approach. Envisioned as being the ideal state for complexation, the triply negative tribasic state is designated L^{3-}, with protonation of the amines being formulated in the label as a salt species, i.e. $[HL^{3-}]^{2-}$ is the singly N-protonated species.

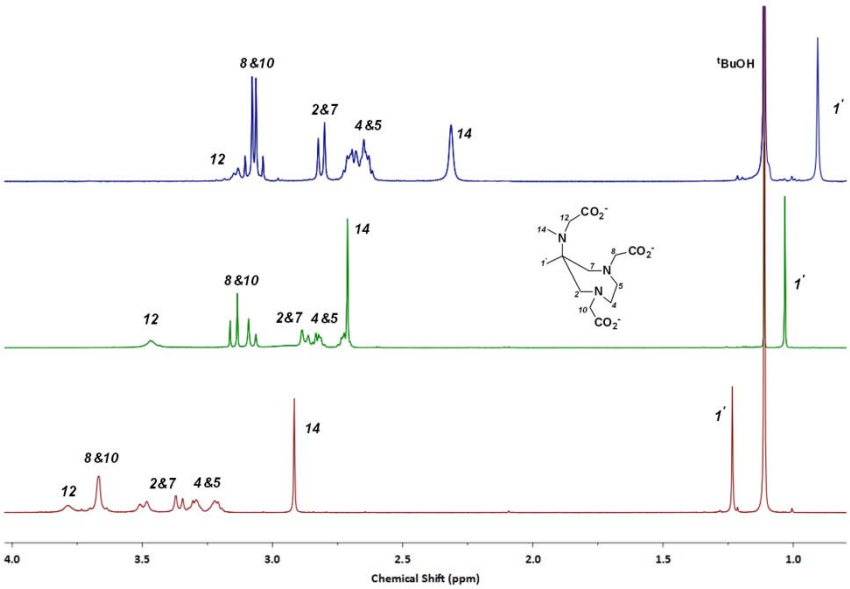

Figure 2.2 *^{1}H NMR spectra (298.1 K, D_2O, 700 MHz) of ligand **L^{2}** at pH 12.0 (blue), 7.2 (green) and 2.0 (red). The structure shown is intended solely to illustrate the atom labelling scheme, and does not reflect the protonation state or conformation of the ligand. ^{t}BuOH was added as reference, δ_H =1.10 ppm.*

The ^{1}H NMR spectrum of **L^{2}** has a number of resonances, which were assigned with the help of 2D NMR spectroscopy (COSY, HSQC and HMBC). The spectrum of **L^{2}** at pH 12.0, 7.2 and 2.0 (Figure 2.2) has the signals of interest assigned. The diastereotopic methylene protons H^4 and H^5 gives rise to two multiplets which form an AA'BB'-multiplet. Diastereotopic methylene protons of H^2 and H^7 form an AA'BB'-doublet, due to the absence of neighbouring C-H groups. An AB-doublet is generated for the diastereotopic acetate CH_2 protons (of H^8 and H^{10}). For each isolated ring CH_2 proton of the 7-membered ring (H^2 and H^7) the signal which resonates to higher frequency was determined to be the proton adopting a pseudo-equatorial site in the major conformer. A more detailed account of this orientation assignment is provided in Chapter 4 Section 2.2.1. The quaternary methyl ($H^{1'}$), remaining acetate (H^{12}) and N-methyl (H^{14}) substituents all appear as singlets (Figure 2.2).

The protonation constants of **L^{2}** were determined in the pH range 2 – 13 by measuring the pH dependent ^{1}H NMR shifts of the non-exchangeable protons. A solution of **L^{2}** in D_2O, containing *t-butyl*-alcohol as a reference, was prepared and the ^{1}H NMR spectrum recorded at 700 MHz at 295.2 ± 0.2 K. The pH of the sample was then increased (and recorded) by the addition of deuterated sodium hydroxide, and the ^{1}H NMR spectrum recorded under the same conditions. Once a pH of ~ 12.5 had been reached, deuterated hydrochloric acid was used to reduce the pH of the solution, and

further ^{1}H NMR spectra were recorded to confirm the accuracy of the previously recorded data. A pH dependent shift variation was observed for $H^{2\&7}$, $H^{4\&5}$, $H^{1'}$, acetate protons ($H^{8\&10}$ and H^{12}) and the N-Me substituent, H^{14} (Figure 2.2). The chemical shift (ppm) for each of these resonances was plotted against pH (Figure 2.3). For the spin-coupled proton signals of $H^{8\&10}$, $H^{4\&5}$ and $H^{2\&7}$, the mean chemical shift was compared as a function of pH.

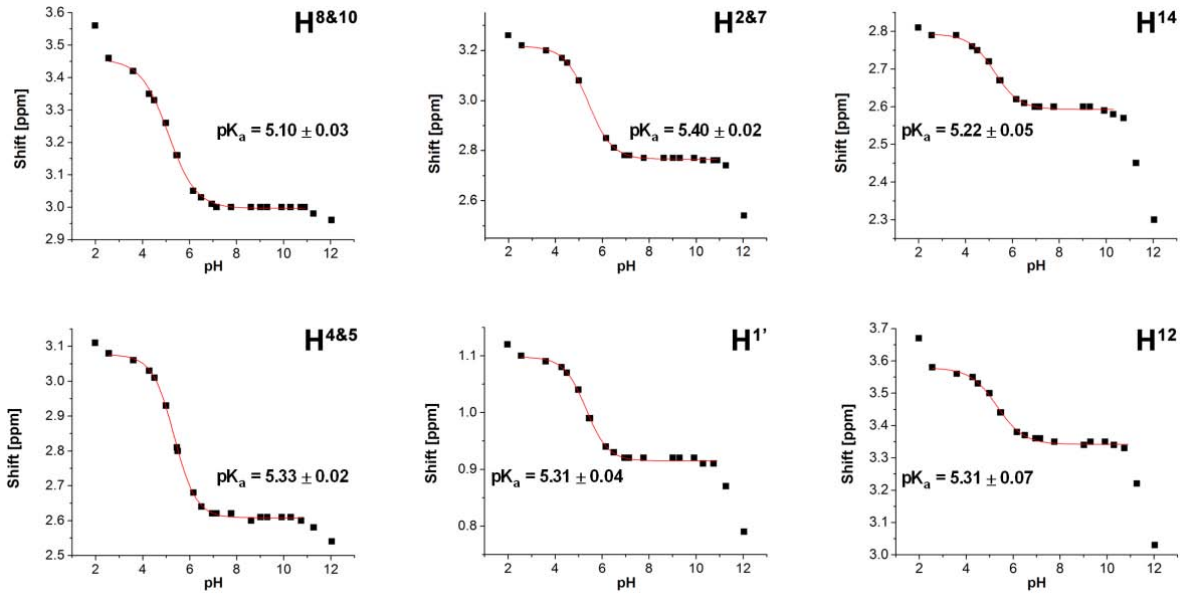

Figure 2.3 *Variation in chemical shift for ligand* ***L*** ^{1} *as a function of pH (meter reading), at 700 MHz and 295 K in* D_2O*. See Figure 2.2 for proton labelling scheme. Protonation constants shown are determined using the pH meter reading, and thus require correction to give the* pK_a*s. The plots have been fitted using standard iterative least squares minimisation methods, and the errors quoted relate to the fitting only.*

All the ^{1}H NMR titration curves (Figure 2.3) display distinctive changes over well-defined pH values, related to the stepwise N-protonation of the ligand. The protonation/deprotonation steps which take place, occur rapidly on the NMR timescale, such that the observed chemical shifts are a weighted average of the chemical shifts of the two species involved in that protonation step. In assessing these changes, the following equation has been used: pD = pH (meter reading) + 0.41.[21] The mean protonation constant in D_2O (pK_a) is 5.70 (± 0.1) for the equilibrium shown and 11.7 (± 0.15) for the first pK_a value, in each case adjusted for the pD/pH change. The experimentally determined pK_a values are listed in Table 2.1, along with values for other relevant compounds.

Table 2.1 *Comparison of the experimentally determined pK_a values (298 K) for* ***L²*** *with representative ligands of similar structure.*

	$L^{2\,a}$	$H_3DAZA^{b,1}$	$H_3AMPED^{c,22}$	$L^{1\,d,12}$	$L^{2\,d,7}$
$pK_{a,1}$	11.7 (0.15)	9.2	9.54	9.97 (0.03)	10.90 (0.04)
$pK_{a,2}$	5.70 (0.1)	6.5	6.70	6.42 (0.05)	5.14 (0.05)
$pK_{a,3}$	< 3	3.2	1.91	3.75 (0.05)	3.71 (0.06)
$pK_{a,4}$	-	-	-	1.94 (0.05)	2.17 (0.08)

[a]Determined by NMR (D_2O, 700MHz, 295 K). [b]Determined by pH-metric titration (298 K, 0.1 M KCl).[c]Determined by NMR titration (D_2O, 298 K, no inert electrolyte, no errors published).[d]Determined by potentiometric analysis (298 K, I = 0.15 M NaCl).

As the pH was decreased, a shift for each signal was observed to higher frequency, as expected with the increased level of protonation. Starting from basic pH, the addition of acid produces a downfield shift of the methylene protons with an inflection point at pH ~ 11.3. This is assigned to the protonation of an amine consistent with the observed shift to higher frequency of the chemical shifts associated with to the ring protons. Within the range pH 7 – 10 there is no apparent change in the ligand protonation state, with the mono-protonated form dominant, $[HL^{3-}]^{2-}$. A second inflection was observed at pH ~ 5.3. This is also assigned to the protonation of an amine, and was characterised by a further shift to higher frequency of the ring proton resonances. A third incipient inflection was observed at *ca.* pH 3.0, which probably corresponds to protonation of one of the carboxylic acids. The di-protonated species $[H_2L^{3-}]^{-}$, is the dominant species over the range pH 3.5 – 5.

The protonation sequence can be assigned tentatively on the basis of the pH dependence of ^1H NMR chemical shifts and the pK_a values of related literature compounds. It is well known that protons close to a basic site shift to higher frequency (become deshielded) following protonation.[23, 24] This effect is greater with decreasing number of bonds (distance) between the protonation site and the proton, allowing the site to be assigned by considering the relative shift of the proton resonances. However, due to the conformational flexibility of 7-membered rings, assigning the protonation sequence based on chemical shifts can be problematic because protonation can induce significant conformational changes that may influence the chemical shifts of even more remote ligand protons.[25, 26]

Botta et al have assigned the protonation sequence of **L²**, based on the hypothesis that "*the first protonation step in part occurs at the nitrogen atom of the ring and in part at the exocyclic primary amine. Following the second protonation step, the first proton is then transferred to the exocyclic nitrogen.*"[7] Zsolt et al[12] made the same assignment for the most basic pK_a of **L¹** (AAZTA), as did Hegetschweiler and co-workers for 6-amino-1,4-diazepine.[1] No explanation was offered for this assignment that implies a non-specific distribution of the added proton atom over the three amino groups. This protonation sequence in which the exocyclic amine protonates before a endocyclic amine is 'universally' applied to ligands featuring the DAZA core, and was first proposed by Hegetschweiler and co-workers.[1] The assignment was based on a model which takes into account suitable de-shielding constants, and can be used to identify the different tautomeric forms of the partially protonated species.[25, 26] The protonation sequences of **L¹** and **L²**, by Botta et al, were assessed based on the pH dependence of the ^{1}H NMR chemical shifts.[7] None of these examples have taken into account possible protonation induced conformation changes to the 7-membered ring, and the possible de-/shielding effects that these changes may have. [22, 25, 26]

The importance of such effects can be assessed by considering the possible effect of protonation on ring conformation. For heterocyclic ligands such as 9-N_3 (Figure 2.4), amine protonation is not expected to have a significant effect on the ring conformation, due to the rigidity of the ring. However, protonation of an endocyclic amine of **L²** (in its L^{3-} state) is likely to give rise to a bifurcated hydrogen bond (similar to that observed for 9-N_3) distributed over each endocyclic amine.[27] Such a protonation is expected to have a significant effect on the preferred ring conformation, relative to the deprotonated species. Protonation at the exocyclic amine could also have a significant effect on the ring conformation, because of the competition between the tertiary carbon substituents for the sterically less demanding equatorial position. Protonation of the exocyclic nitrogen increases its effective steric bulk in aqueous media, enhancing the preference of the protonated N-substituent to take up an equatorial position.[22] Thus prior to N-protonation the methyl group may adopt this position, but switch to an axial site following N_{exo} protonation, modifying the structure of the preferred conformer. Indeed, discontinuities in conformational analysis (based on NMR shielding effects) have been attributed to conformational changes that result from amine protonation for similar cycloheptane structures.[25, 26]

The structure of **L²** could be viewed as a combination of DACHDA[28] (H_2DACHDA = 1,4-diaza-cycloheptane-1,4-diacetic acid) and dmGly[29] (N,N-dimethylglycine) (Figure 2.4). However, the first

pK_a values for these ligands are 9.83 and 9.94 (298 K) respectively, which is not particularly helpful in discerning the protonation sequence of **L²**. The first protonations of DACHDA and dmGly are very similar. The fact that this is not the case for the first two protonation steps of DAZA based ligands, can be understood in terms of the simple electrostatic interactions between the positive charges located at the amino-groups which hinders the second protonation event.[30]

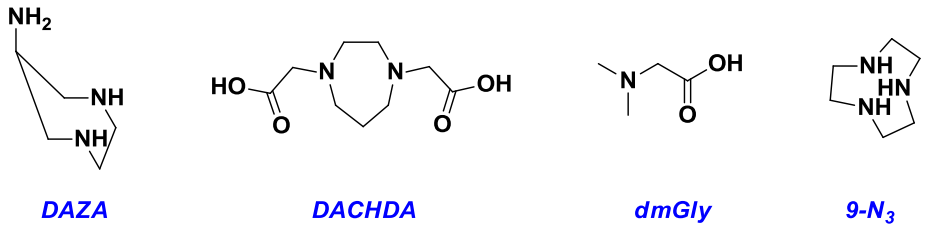

Figure 2.4 *Structures of DAZA[1], DACHDA[28] and dmGly[29] which are structural 'components' of* ***L²****. The triamine ligand 9-N_3 is also shown, to which reference is made in the text.*

Which amine protonates first – starting from basic pH – is debatable. Indeed there is inconclusive data as to the location of the proton, with some proposing that the protonation occurs partially at all three amines.[1, 7, 12, 22] The fact that there are shifts to higher frequency experienced for all the rings protons as well as H^8 and H^9 at the first and second protonation steps, makes it difficult to assign the two steps to particular nitrogen atoms.

We propose that the first protonation occurs at the endocyclic amines, generating a bifurcated hydrogen bond similar to that observed in the first protonation step of 9-N_3 based systems.[27] It is likely that the bifurcated proton will be better stabilised and accommodated in this case. Furthermore, the presence of the negatively charge carboxylate groups will serve to reduce the local overall charge. The second protonation step is accompanied by shifts of $H^{1'}$, H^{12} and H^{14} to higher frequencies, which are consistent with protonation of the exocyclic amine. The other protons also shift to higher frequencies, which could be related to conformational changes, resulting from protonation of the exocyclic amine.[22, 25]

The pH-chemical shift plots of **L²** (Figure 2.3) reveal some important information. In the pH range 5 – 11, the ligand exists exclusively as a single species which is the single protonated ammonium species $[HL^{3-}]^{2-}$, with the proton probably 'spread' across endocyclic amines as a bifurcated hydrogen bond. Between pH 4 and 7, ligand **L²** exists as a mixture of the mono- and di-protonated species, $[H_2L^{3-}]^{-}$.

The latter becomes the exclusive species between pH 3 and 4. Although less favourable for radiolabelling, it should be noted that there is still a significant portion of $[HL^{3-}]^{2-}$ at pH 5. Radiolabelling with ^{68}Ga(III) was to be examined inside the range pH 2 – 7, in which case a large portion of which will have the mono-protonated form of **L²**, $[HL^{3-}]^{2-}$, as a dominant species. The fastest rates of radiolabelling are expected to occur with this species.

3 Radiochemical Evaluations

In this section the suitability of ligands **L$^{1-5}$** for chelation of ^{68}Ga(III), primarily in terms of the radiolabelling efficiency and kinetic stability of the complexes, is evaluated. In the first instance the optimal labelling conditions for the ligands are identified (Section 3.1), with subsequent stability evaluation of the systems deemed suitable based on the radiolabelling results (Section 3.2). Further radiochemical evaluation studies (concentration dependent kinetics and competition experiments) on ligands displaying satisfactory stability are presented in Section 3.3.

3.1 Radiolabelling Studies with Ligands L$^{1-5}$

Gallium-68 has a relatively short half-life (68 minutes), which means it is useful in imaging applications for approximately 2 hours after generator elution. Taking into account the number of steps required from generator elution to *in vivo* injection (i.e. elution, eluate purification, radiolabelling, radiolabel purification, pH adjustment, Injection), an efficient and rapid radiolabelling protocol is of the upmost importance. Typically, radio-labelling is carried out for a maximum of ten minutes, to ensure that there is sufficient time for the remaining procedures to be conducted.

As a result, there is considerable focus on the development of ligands which are able to bind ^{68}Ga(III) rapidly and form a complex with high kinetic stability. Ideally, a chelator is sought which binds ^{68}Ga(III) quantitatively in less than 10 minutes at room temperature. Quantitative radiolabelling eliminates the need for complex purification of the radiolabel prior to *in vivo* administration. In theory, such a labelling protocol would allow for the development of easy to use ‘kits’ in clinical practice.[31-33] The idea with the kit is that the ligand, and any other chemical substances required (such as buffer), are lyophilised into a suitable vial. Radiolabelling would then be carried out by simply adding the ^{68}Ga container eluate, and mixing the contents at room temperature.[32, 33] Low temperatures are also preferred in the sense that useful ligands may be conjugated to temperature

sensitive biomolecules. Radiolabelling efficiency also shows a dependency on pH, and most chelators operate best within a given pH window. As is the case with temperature, pH should be chosen keeping in mind the sensitivity of biomolecules that may be used. For example, quantitative labelling of DOTA with ^{68}Ga, whilst producing radiolabelled complexes of exceptionally high kinetic stability, requires heating at 368 K for 30 min at pH 4.6.[34] The long radiolabelling time allows for considerable radioactive decay of the radiolabel, whilst the high temperature and low pH are unsuitable for many biomolecules of interest in imaging. Despite these drawbacks, DOTA is still the 'industry standard' for ^{68}Ga-PET. Whilst it is the most applied ligand in clinical PET imaging practice, it does not possess characteristics which make it ideal for radiolabelling with ^{68}Ga. A basic understanding of the coordination chemistry of DOTA and ^{68}Ga is required to understand why they are a somewhat unsuitable pairing in some regards. The reader is referred to Chapter 1 Section 5.2 for a more detailed discussion of this 'mis-match'. In practice, a ligand which radiolabels with a > 90 % yield at 368 K in less than 10 minutes (to give a stable radiolabelled complex) is still potentially useful.[20]

In order to evaluate the suitability of the synthesised ligands, the dependence of radiolabelling on ligand concentration, temperature and pH was determined. Typically, the concentration of the chelator greatly exceeds that of the ^{68}Ga(III), and therefore concentration kinetics is less important. This aspect was therefore assessed once both the pH and temperature had been optimised, for ligands deemed suitable for ^{68}Ga-PET. The ligands (**L$^{1\text{-}5}$**) evaluated in this work are shown below (Figure 2.5).

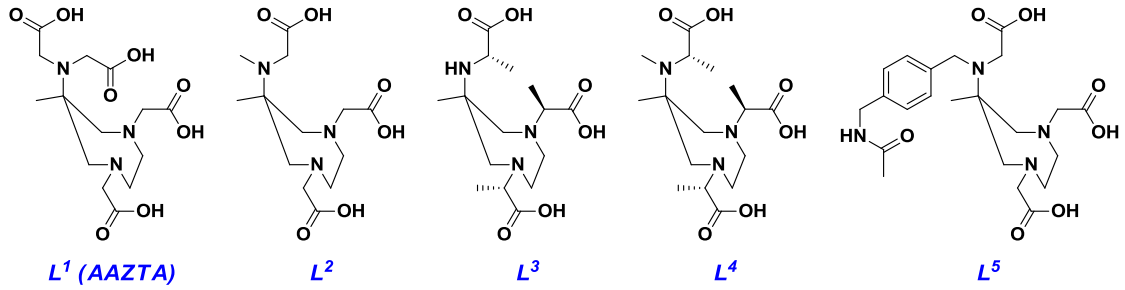

Figure 2.5 *First generation ligands synthesised for evaluation as potential ^{68}Ga-PET imaging agents.*

The generator eluate contains $^{68}GaCl_3$ which exists as freely available ^{68}Ga(III) for pH < 3.6. However, when the pH exceeds ~ 3.6 the water insoluble hydroxide, $^{68}Ga(OH)_3$, begins to form. In order to prevent this from occurring a suitable anion can be added, which weakly binds the ^{68}Ga(III), thereby slowing the formation of the hydroxide but still allowing the radiolabel to form. Popular choices

include acetate, succinate, glutamate, lactate, oxalate and tartrate as well as the anions present in TRIS and HEPES buffer solutions.[35] These anions can be formulated as buffers to give a desired pH, thereby serving a dual purpose. The radiolabelling results section has been divided into two parts. The first, deals with radio-labelling at pH < 3.6 with no buffer present, and the second, considers the radio-labelling at pH > 3.6 in the presence of a suitable buffer.

The radiolabelling yield is defined here as the percentage of the total radioactivity (^{68}Ga) associated with the ligand, and was measured using a TLC radio-imager. This is different to the radiochemical yield (decay corrected) which also takes into account the decay of the ^{68}Ga(III) radio-isotope. The background radiochemical noise, determined in a series of control experiments, is typically ~ 4% of the total measureable radioactivity on a radio-imaged TLC plate. For this reason radiolabelling yields measured to >96 % are assumed to have reached completion unless there is clear evidence that this is not the case, i.e. a noticeable peak on the radioactivity population distribution map.

3.1.1 Radiolabelling at pH < 3.6

There are obvious benefits to labelling of the generator eluate directly; most notably fewer steps permitting less radioactive decay. However, the strongly acidic conditions of the eluate (pH ~ 1.0) are not conducive to complex formation. Indeed, when tested, no radiolabelling was observed under these conditions for any of the ligands, even at 368 K. This can be attributed to the protonated nature of the ligand under these conditions, which hinders electrostatic encounter with the charged metal ion species and suppresses formation of the Ga-ligand bonds.

Ad hoc adjustment of the cation-exchanger eluate pH using a suitable base was time consuming, and a protocol involving addition of a predetermined amount of base proved inefficient because the resulting pH was not reproducible. The pH can also be increased by suitable dilution. However, there is a careful balance to be struck between the final volume and radioactivity content. For a given amount of generator eluate, the final volume needs to be small enough to make further studies (stability and *in vivo* assays) feasible, but sufficient to provide the necessary increase in pH. A 12.5 fold dilution of the cation-exchanger eluate with Milli-Q ultrapure water produced a labelling solution with a pH ~ 2.3, and sufficient radioactivity to make further evaluations possible.

The results of the radiolabelling experiments at pH ~2.3 for each ligand at 298, 323 and 368 K are shown below (Figure 2.6).

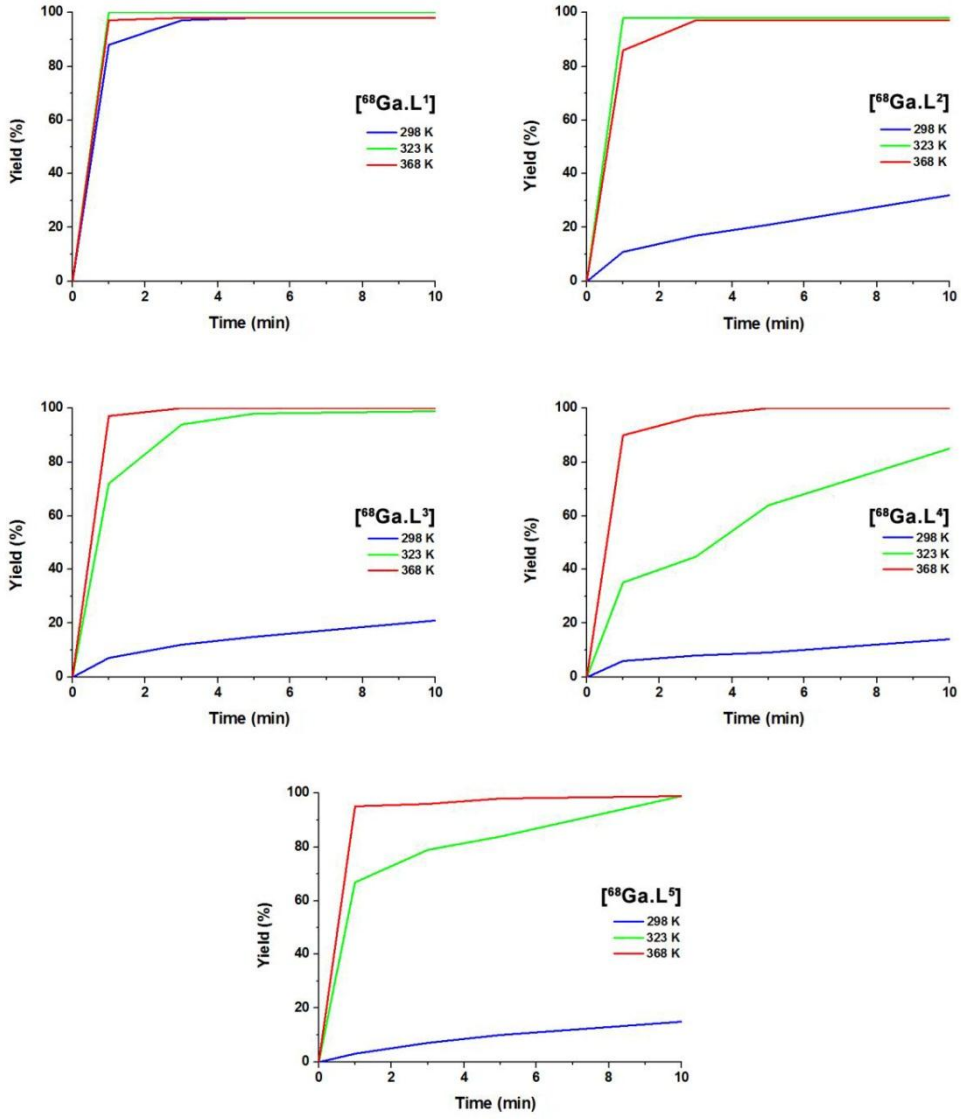

Figure 2.6 *Temperature dependent radiolabelling kinetics of ligands* $\boldsymbol{L^{1\text{-}5}}$ *at pH 2.3, shown as the percentage of the radioactivity which is associated with the radiolabelled complexes at 1, 3, 5 and 10 minute time intervals. Activity ~ 100 MBq* ^{68}*Ga(III) at t = 0 minutes. [*^{68}*Ga] = 0.18 nM. [L*^{n}*] = 10 µM.* V_{tot} *=5 mL.*

As expected, increasing the temperature improves the radiolabelling yield. The most efficient radiolabelling is observed for $\mathbf{L^1}$, which produces a quantitative yield within 3 minutes at 298 K. The other ligands require 323 K and 10 min to produce the same result, with the exception of $\mathbf{L^4}$ which labels quantitatively at 363 K. The superior radio-labelling efficiency of $\mathbf{L^1}$ is likely due to having a

greater number of carboxylic acids which foster more efficient ^{68}Ga complexation. Differences in the labelling kinetics of the other 4 ligands are small, which is unsurprising considering their structures all feature three carboxylic acids and a tri-basic core. Slower labelling rates associated with **L^4** and **L^5** may be related to increased steric bulk about the exocyclic amine, hindering arrangement of the donor groups for metal-complexation.

To further assess the influence of pH in absence of a buffer we considered a larger dilution. A 100 fold dilution of the cation-exchanger eluate with Milli-Q ultrapure water produced a labelling solution with a pH ~ 3.3. Although this larger dilution meant resulting radiolabelled solutions had a low radioactivity to volume ratio (insufficient for stability studies and *in vivo* assays), the results still provided useful insight into the influence of pH on radiolabelling kinetics.

The results of the radiolabelling experiments at pH ~ 3.3 for **L^2**, **L^3** and **L^5** at 298, 323 and 368 K are shown in Figure 2.7. The radiolabelling data for **L^1** and **L^4** is not shown, because no significant change was measured.

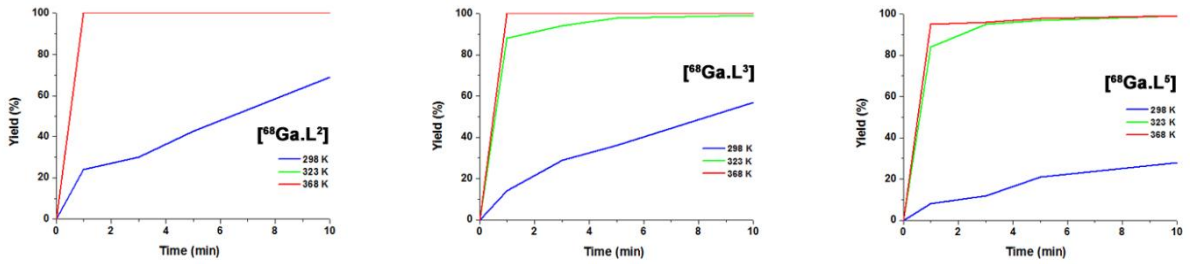

Figure 2.7 *Temperature dependent radiolabelling kinetics of ligands **L^2**, **L^3** and **L^5** at pH 3.3, shown as the percentage of the radioactivity associated with the radiolabelled complexes at 1, 3, 5 and 10 minute time intervals. Activity ~ 12 MBq ^{68}Ga(III) at t = 0 minutes. [^{68}Ga] = 0.02 nM. [L^n] = 50 µM. V_{tot} =5 mL.*

Again, an increase in the labelling efficiency is observed with increasing temperature. Also evident is a significant increase in the radiolabelling efficiency with the increased labelling pH. This is most noticeable for **L^2** and **L^3** at room temperature where the labelling yield approximately tripled in value. This increase can be understood in terms of the reduced degree of protonation of the donor groups at higher pH, which facilitates complexation more readily.

The labelling protocols discussed so far were, at face value, very successful. In all but one instance (**L^4** – which radiolabelled quantitatively at 298 K) > 99 % radiolabelling could be achieved within 10

minutes at 323 K. This is a very good result taking into account the strongly acidic conditions. However, there is an inherent problem of stability and speciation for some of the ligands complexes.

Firstly, the radiolabelled complexes of **L**^{4} and **L**^{5} were unstable in Phosphate Buffered Saline (PBS) at physiological pH (7.4). Complete de-complexation was observed within 10 minutes after placing the radiolabelled complex in the buffer solution at room temperature. Radiolabelled **L**^{1} (AAZTA) was more stable under the same conditions, with 80 % of the radiolabelled species intact after 2 hours at physiological pH and 310 K. Stability at physiological pH is essential and, as a result, the complexes of **L**^{1}, **L**^{4} and **L**^{5} synthesised under these conditions are unsuitable. Secondly, radiolabelling of **L**^{1} and **L**^{2} produced multiple radiolabelled species (Figure 2.8). In the context of radio-labelling the formation of multiple species is also undesirable. In the case of **L**^{2} one of the species accounts for ~ 90 % of the chelated ^{68}Ga, and as a result this system is still of interest (Figure 2.8). However, radiolabelling of **L**^{1} results in the formation of three species, two in nearly equivalent amounts and a third minor species (i.e., a ratio of 2 : 2 : 1). This ligand is therefore also not suitable for ^{68}Ga-PET, when radiolabelled under these conditions. The origins and nature of these multiple radiolabelled species are discussed in more detail in Chapter 4 Section 1. No instability was observed for the radiolabelled complexes of **L**^{2} and **L**^{3}, formed at pH 2.3, at physiological pH and temperature.

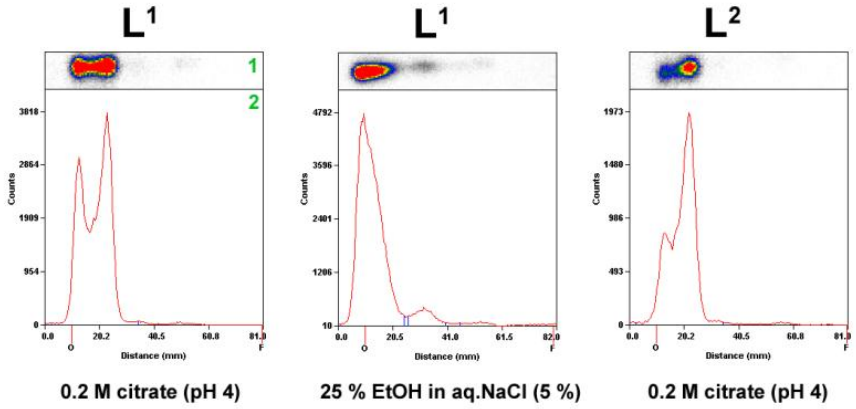

Figure 2.8 *Selected radio-imaged TLC plates from the radiolabelling of ligands **L**^{1} and **L**^{2} with ^{68}Ga. Region (**1**) is the radio-imaged TLC plate orientated horizontally, with the baseline (denoted by '**O**') on the left. Region (**2**) shows the radioactivity population distribution curves. In each case there is no unchelated ^{68}Ga, and all peaks originate from radiolabelled complexes of the respective ligand. Radiolabelling was carried out at 368 K and pH 2.3 for 10 min, using the standard protocol for this pH. TLC plates were eluted using the indicated solutions. The two '**L**^{1}' plates are of the same radiolabelling experiment, spotted on different TLC plates and eluted with different solutions. These were required to discern the three radiolabelled species present.*

3.2.2 Radiolabelling at pH > 3.6

From consultation of the ^{1}H NMR pH titration curve of **L^{2}** (Chapter 2, Section 2, Figure 2.3), the N,N'-diprotonated species is dominant at pH < 3.5. The equilibrium with the N-monoprotonated ligand (pK_a 5.7 (±0.1)) most probably involves a significant ligand conformational change. Given that we had already observed an increase in the radiolabelling efficiency with a relatively small increase in pH, there is good reason to believe that a further increase in pH might encourage a higher labelling yield. Furthermore, the presence of this conformational equilibrium may also play a role in explaining the formation of the radiolabelled species observed previously. By increasing the pH further, insight into the nature of these species might be gained.

A disadvantage of the protocols described in Section 3.2.1, is the large 'end-volume' of the radiolabel (i.e. 5 mL). The radioactivity : volume ratio is appropriate for further evaluations. However, it is not economical as a large portion of the radioactivity goes to waste (only 200 µL is used per stability evaluation, and 800 µL per an *in vivo* study). An advantage of making use of a buffer system is the potential to alter the pH in much smaller volumes.

Numerous buffer systems at varying concentrations and pH were considered for their ability to produce the desired pH and inhibit formation of the colloidal hydroxide, $^{68}Ga(OH)_3$. The HEPES and acetate buffers where chosen because they had the desired effect, and can be used to cover the pH range 4.0 – 6.5. These are popular choices because:

- The acetate buffer has FDA approval for use in humans, a useful buffering range and is effective in preventing formation of gallium hydroxide.[35]
- The HEPES buffer, whilst not yet approved for use in humans, has been used commercially for the synthesis of ^{111}In radiopharmaceuticals (where the HEPES is removed before the radiolabel is administered), and can produce radiolabelled complexes with very high specific activity.[35]

Radiolabelling was evaluated for **L$^{1\text{-}5}$** at pH 4.0 and 5.3 (using an appropriately prepared 0.2 M $CH_3COOH/NaCH_3COO$ buffer) and pH 7.0 (using an appropriately prepared 1.0 M NaHEPES solution).

Radiolabelling experiments were carried out for each ligand at 298, 323 and 368 K and at pH 4.0, 5.3 and 7.0. The results for the radiolabelling at 298 K for $\mathbf{L^{1-5}}$ are shown below (Table 2.2), as the time taken to reach the maximum yield.

Table 2.2 *Maximum radio-labelling yield (%) achieved and the time taken (minutes) at 295 K for* $\boldsymbol{L^{1-5}}$ *at pH 4.0, 5.3 and 7.0. Activity ~ 100 MBq, [*^{68}*Ga] ~ 0.66 nM (t = 0), [*L^n*] = 10 µM,* V_{tot} *= 1.4 mL.*

pH	Maximum radiolabelling yield (%) at 295 K Time taken to achieve maximum yield (min)				
	$\mathbf{L^1}$	$\mathbf{L^2}$	$\mathbf{L^3}$	$\mathbf{L^4}$	$\mathbf{L^5}$
4.0	97* 1	98* 1	99 3	95* 10	92* 10
5.3	96* 1	97* 1	98 3	95* 10	90* 10
7.0	96* 3	97* 1	98 3	92* 10	89* 10

*indicates the presence of more than on radiolabelled species

Control experiments were conducted to confirm that the weak associations between ^{68}Ga and the buffer anions did not result in 'bound-^{68}Ga' spots on the radio-imaged TLC plates. Indeed, there were no observable differences between the control experiments performed in the absence (pH < 3.6) and presence of the buffer (pH > 3.6). The increase in pH had a significant effect on the radiolabelling efficiency and in the cases of $\mathbf{L^4}$ and $\mathbf{L^5}$ changed the relative proportion of the radiolabelled species.

There was a noticeable perturbation to the ratio of observed radiolabelled complex speciation for $\mathbf{L^1}$ (9 : 9 : 1) and $\mathbf{L^2}$ (18 : 1) in comparison to that observed for labelling at pH ~ 2.3. Radio-labelling of $\mathbf{L^4}$ and $\mathbf{L^5}$ produced two radiolabelled species in ratios of 11 : 8 and 5 : 4 respectively, whereas at pH 2.3 and 3.3 only a single species was observed. These changes suggest that pH plays a key role in determining the constitution and speciation of the radiolabeled complexes. Ligand $\mathbf{L^3}$ maintained formation of a single radiolabelled complex, and showed no change in the R_f value of the complex on the TLC plate. The major species of $\mathbf{L^4}$ and $\mathbf{L^5}$ were unstable at physiological pH and temperature, whilst all other radiolabelled complexes were stable (under the same conditions).

Ligands $\mathbf{L^1}$ and $\mathbf{L^2}$ showed quantitative radiolabelling in less than one minute at room temperature. Labelling of ligand $\mathbf{L^3}$ was only slightly slower, reaching completion in 3 minutes. The radio-labelling of $\mathbf{L^4}$ and $\mathbf{L^5}$ was considerably slower, and elevated temperatures (303 K for 10 minutes) were

required to produce > 95 % radiolabelling. Nearly quantitative labelling at 303 K is a good result; however, investigation of both of these ligands (and $\mathbf{L^1}$) was discontinued due to the inherent speciation problems associated with formation of the radiolabelled complex.

3.3 Stability of Radiolabelled Complexes [^{68}Ga.$\mathbf{L^2}$] and [^{68}Ga.$\mathbf{L^3}$]

A labelling system is used where the italicised subscript after the radiolabelled complex indicates the pH at which it was formed. For example, $\boldsymbol{[^{68}Ga.L^1]_{2.5}}$, indicates that the ^{68}Ga-radiolabelled complex incorporating ligand $\boldsymbol{L^1}$ was formed at pH 2.5.

In order to fully evaluate the usefulness of these ligands for ^{68}Ga-radiolabelling, it is vital to assess the stability of the resulting radiolabelled complexes. Stability evaluations were performed at physiological pH (1.0 M PBS) and temperature (310 K) in the presence of DTPA, Fe(III), *apo*-transferrin and newborn calf serum. The stability of the radiolabels was assessed at 10, 20, 30, 60 and 120 min using the radio-imaged TLC method to determine the amount of radiolabelled product intact. Approximately 5 MBq of the radiolabelled solution was used for each experiment which translates to a ^{68}Ga concentration of 0.16 nM. The DTPA and Fe(III) were both prepared to give a final concentration of 0.8 µM during the challenge experiments, which is a 5000-fold excess with respect to the radiolabelled complex. The *apo*-transferrin used had a 0.005 % iron and a final concentration of 0.8 mg/mL which, taking into account the presence of two gallium biding sites, equates to a 130-fold excess with respect to the radiolabelled complex.

Based on observations and the results of the radiolabelling studies in the previous section, ligands $\mathbf{L^1}$, $\mathbf{L^4}$ and $\mathbf{L^5}$ had been deemed unsuitable, and were not evaluated further. Radiolabelling of ligand $\mathbf{L^2}$ also produced two species, however the minor species was only present as 2 - 10 % of the total chelated ^{68}Ga (depending on the radiolabelling pH), and was therefore still of interest. Ligand $\mathbf{L^3}$ is of particular interest because only a single radiolabelled species, which was stable under physiological pH and temperature, was observed.

The stability of the radiolabelled complexes produced at pH 2.3, 4.0, 5.3 and 7.0 was determined for ligands $\mathbf{L^2}$ and $\mathbf{L^3}$; Table 2.3 shows the stability of each complex with respect to the *apo*-transferrin experiment. No instability was observed for the radiolabelled complexes during the Fe(III) (0.8 µM), newborn calf serum and DTPA (0.8 µM) challenge experiments.

Table 2.3 *Stability of the investigated ligands at 120 minutes in a competition experiment in the presence of 130-fold excess apo-transferrin. Challenge experiment conducted at physiological pH and temperature.*

pH at which radiolabelled complex was synthesised	Percentage of Radiolabel/s intact after 120 min (%)	
	$[^{68}Ga.L^2]$	$[^{68}Ga.L^3]$
2.3	10	8
4.0	95	97
5.3	95	99
7.0	93	98

It was evident from the time interval radio-TLC data of $\mathbf{[^{68}Ga.L^2]_{4.0\text{-}7.0}}$, that any observed instability was due to decomplexation of the minor species. Careful examination of interval data suggested that the major species remained intact throughout. In contrast, a very poor stability profile for the radiolabelled complexes was observed following formation at pH 2.3.

No observable evidence (i.e. there was no noticeable evidence of ^{68}Ga signal greater than background activity, other than that of the complex) of complex instability was found for the radiolabelled complex $\mathbf{[^{68}Ga.L^3]_{4.0\text{-}7.0}}$ over 2 hours in all of the stability challenge experiments. In contrast, a very low stability profile for the radiolabelled complex was observed following formation at pH 2.3.

Of the first generation series of ligands, it is evident that $\mathbf{L^3}$ is the most suitable ligand for ^{68}Ga-PET. In terms of radiolabelling and stability (of the radiolabelled complex) it possesses the ideal characteristics and compares favourably with the best ligands in the literature. What sets this ligand apart from reported systems is its ability to undergo efficient radiolabelling over the pH range 4.0 – 7.0 at room temperature. Quantitative radiolabelling at lower pH (pH 2.3) is possible with elevated temperatures (10 min at 323 K); however the formed radiolabelled complexes are not sufficiently stable. Ligand $\mathbf{L^2}$ displays very similar radiolabelling characteristics and as a result is also a potential candidate, despite its radiolabelled complex speciation problem.

The radiolabelling efficiency displayed by $\mathbf{L^2}$ and $\mathbf{L^3}$ is considerably better than that of DOTA (a reference standard for ^{68}Ga radiolabelling) and comparable with the most promising chelators published (Figure 2.9). The macrocyclic ligand NOTA (Figure 2.9), has been quantitatively

radiolabelled at room temperature in the pH range 3.5 – 5.[36, 37] The phosphinic acid derivative, TRAP, also radiolabelled at room temperature but requires a lower ligand concentration than NOTA.[32, 33, 38] The acyclic ligand H_2DEDPA[39] (Figure 2.9), quantitatively labels within 10 minutes at room temperature and pH 4.5 (earlier time intervals have not been reported). Other promising acyclic chelates are CP256[40] which quantitatively radiolabels within 5 minutes at room temperature and pH 6.5, and HBED-CC[41] which displays acceptable radiolabelling when conjugated to an antibody (Figure 2.9). Of particular value is the fact that, unlike any of the ligands above, **L**^{3} can be radiolabelled over the pH range 4.0 – 7.0 at room temperature. *Note: all radiolabelling data and conditions quoted above are the optimum conditions, and give rise to radiolabelled complexes which are sufficiently stable for ^{68}Ga-PET.*

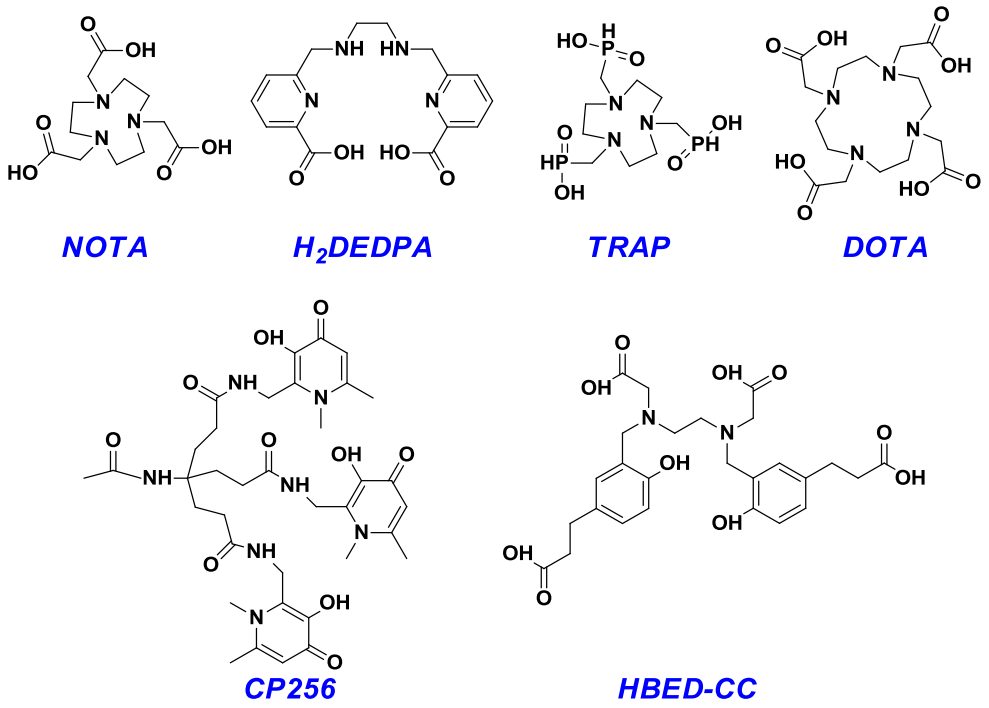

Figure 2.9 *Ligands NOTA, H_2DEDPA, TRAP, HBED-CC and CP256 which display favourable properties for ^{68}Ga-radiolabelling.*

3.4 Speciation of the ^{68}Ga-Radiolabelled Complexes

Accurate quantification of the relative amounts of the minor/major radiollabelled species was not always possible, due to the poor separation of the species on the TLC plate. However, it was possible to make some observations regarding the variation of their ratio with the labelling pH.

The heptadentate ligand $\mathbf{L^1}$ has more than the required number of donor groups to bind the Ga(III) ion, which is coordinatively saturated by a hexadentate ligand. This suggests that the multiple speciation may arise from the formation of constitutional isomers (Figure 2.10). More specifically, two radiolabelled species with $\mathbf{L^1}$ could arise from N_3O_3 and N_2O_4 binding modes of the ligand. Three species were observed for the radiolabelling of $\mathbf{L^1}$ at pH 2.3 with the two major species occurring in a 1 : 1 ratio. A third species accounted for 10 % of the observed species. When the pH is increased to 4.0 and 5.3 the presence of the minor species halved. It is proposed that the major species are constitutional isomers, because no change in their relative proportion was observed with change in pH or temperature.

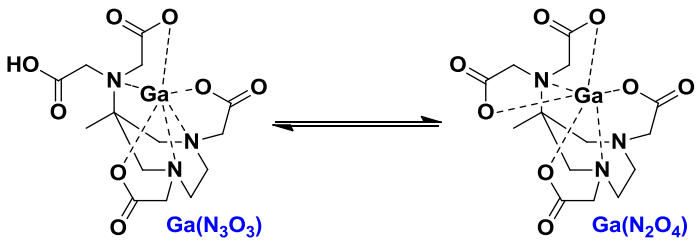

Figure 2.10 *Constitutional isomers that may arise from radiolabelling of* $\boldsymbol{L^1}$*; these two isomers are tentatively assigned to the two major species observed.*

Ligands $\mathbf{L^{2\text{-}5}}$ are hexadentate donors and thus this explanation is not applicable. Closer examination of the speciation profile and structures of these ligands leads to some interesting observations. The radiolabelled complex of ligand $\mathbf{L^3}$ is stable over the pH range 4.0 – 7.0 and only a single species is observed. Radiolabelled $\mathbf{L^2}$, may be considered slightly less suitable than $\mathbf{L^3}$ due to the presence of an unstable minor species (10 % of radiolabelled $\mathbf{L^2}$). Radiolabelling of $\mathbf{L^4}$ and $\mathbf{L^5}$ at pH 2.3 produces a single observable species each. However, the stability of their radiolabelled complexes is very poor at pH 7.4. It appears that as the steric bulk around the exocyclic nitrogen increases so the stability of the resulting radiolabel (produced at pH 2.3) decreases.

Considering the radiolabelling at higher pH, it was found that the relative speciation of $\mathbf{L^2}$ improved slightly, with the predominant species accounting for 96 % of the radiolabelled ligand. Radiolabelling of $\mathbf{L^4}$ and $\mathbf{L^5}$ at pH ≥ 4.0 resulted in the formation of multiple radiolabelled species, with ratios of 11 : 8 and 5: 4 respectively. In each case, the minor species is stable at physiological pH and temperature, whilst the other is not.

The possible origin and nature of these multiple radiolabelled species are discussed in more detail in Chapter 4 Section 1, but may be tentatively explained as follows. It is presumed, based on crystal structures of ligands with an AAZ core (See chapter 1 section 6 figure 1.13 for an example), that each ligand will try to assume a chair-like conformation in formation of a stable metal complex.[1, 3-5, 10, 14, 22] The most stable/prevalent conformation will be determined, in part, by the nature of the ring substituents. Radiolabelling at pH 2.3 produces more of the stable radiolabelled complex species when the steric bulk at the endocyclic amine is lower, suggesting that 'overloading' this amine disfavours formation of the chair-like conformation required to form a stable metal complex. It is tentatively proposed that as the steric bulk at the exocyclic amine increases, so the degree of ligand pre-organisation toward the favoured chair-like conformation is reduced, with the exocyclic amine functionality preferring instead an equatorial orientation. This is illustrated for ligands **L^2** and **L^5** (Figure 2.11). These structures represent possible binding conformations of the ligands, and not conformations of the protonated ligands. When the exocyclic amine is equatorial, the N_3O_3 donor set is not arranged for efficient metal complexation; but rather some form of relatively weak association with the ^{68}Ga consistent with the observed lower stabilities. Thus, we propose that the multiple radiolabelled species observed are also constitutional isomers featuring different ligand binding modes; loosely, such systems have been termed coordination isomers or linkage isomers.

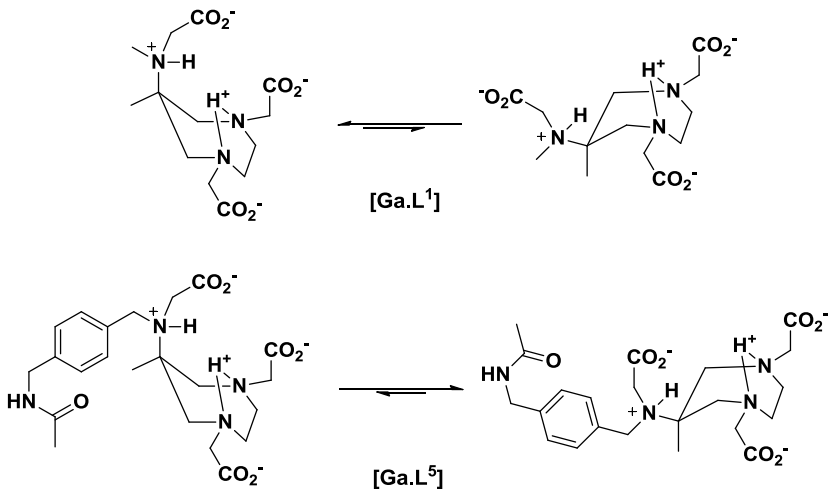

Figure 2.11 *Representation of the different possible binding conformations of ligands in **[Ga.L^1]** and **[Ga.L^5]**. Gallium metal has been excluded for clarity. The different species are shown to be in equilibrium, but in reality no exchange was observed with time. The equilibrium illustrates the potential of a given ligand to favour one conformation over the other, which may be determined by the relative steric demand of the quaternary carbon substituents.*

In Section 2 of this chapter the ^{1}H NMR pH titration curve of **L^{2}** was shown. It depicted a pK_as of approximately 11.7 and 5.70, associated with protonation of the endocyclic amines (bifurcated) and endocyclic amine respectively. When the exocyclic amine is protonated, it possesses greater steric bulk, and as a result the equilibria shown above will be shifted further to the right, since this is a conformation preferred by the free ligand. It could be argued that below pH 5.7, forces of repulsion between the two positive charges resulting from protonation of the exocyclic and endocyclic (shared bifurcated proton) amines, further favours an equatorial position of the exocyclic amine group and hence formation of the less stable radiolabelled isomer. Consistent with this postulate, it was found that for **[Ga.L$^{2\text{-}5}$]** there is an increase in the amount of the stable radiolabelled complex as the radiolabelling pH is increased beyond the endocyclic amine pK_a.

It is interesting to note that **[Ga.L^{4}]$_{2.5}$** and **[Ga.L^{5}]$_{2.5}$** appear to lie predominantly on the disfavoured side of the equilibrium, with the favoured (stable) radiolabelled complex being produced in greater amounts when the radiolabelling pH exceeds 4. Only a small perturbation of the radiolabelled complex speciation was observed for **[Ga.L^{2}]** with increasing radiolabelling pH, but there was nonetheless a considerable increase in the proportion of the stable isomer. A single radiolabelled complex species was observed for **[Ga.L^{3}]** over the entire pH radiolabelling range evaluated. However, only **[Ga.L^{3}]$_{4.0\text{-}7.0}$** were stable. This suggests that the different radiolabelled species of **L^{2}** and **L^{3}** are not fully distinguishable on TLC.

These observations, regarding changes in overall stability with changes in changes in radiolabelling pH, are consistent with the reduced steric bulk at the exocyclic amine favouring formation of the stable radiolabelled complex. In agreement with this, the proportion of the third radiolabelled species (< 10 %) of **L^{1}** diminished as the radiolabelling pH increased.

A further series of experiments was conducted to establish whether it was possible to alter the relative speciation of the radiolabel through induced conformational changes of the bound ligand. The radiolabelled complex was synthesised at pH 2.5, and then the pH of the solution was increased to 5. Buffer was not used to increase the pH, as this could possibly allow for re-complexation of 'released' ^{68}Ga(III). The relative ratio of the radiolabelled isomeric species was unaltered, indicating that the pH change was unable to induce a rearrangement to the more stable isomer. Thus the species formed were kinetically slow to undergo any dissociation/re-complexation process and conformational changes of the bound ligand are seemingly not possible, under these experimental

conditions. This is consistent with the formation of 'kinetically trapped', constitutionally isomeric complexes (Figure 2.10).

3.5 Further Radiochemical Evaluation of L^2 and L^3: Competition and Concentration Studies

The following evaluations were conducted by radiolabelling at pH 4.0 using a 0.2 M acetate buffer at room temperature.

3.5.1 NOTA Competition

Equimolar amounts (20 μM) of NOTA and the ligand of interest (**L^2** or **L^3**) were premixed in 1 mL of 0.2 M acetate buffer (pH 4), and radiolabelled with ~ 100 MBq ^{68}Ga (0.66 nM). The relative ratio of [Ga.NOTA] and **[Ga.L^n]** determined at 1, 3, 5, 10 and 120 min time intervals. Within 1 minute of the being added, all of the available ^{68}Ga was complexed. The relative proportions of the [Ga.NOTA] and **[Ga.L^n]** formed are a rough indication of the relative rate of radiolabelling of the ligands. The radiolabelled complexes formed were left at 298 K for two hours, and the relative proportions of the radiolabelled complexes re-measured. This gives an indication of the relative stability of the two radiolabelled complexes. The conditions (pH and ligand concentration) used were those optimised for NOTA, and thus offers an accurate evaluation of **L^2** and **L^3**.

For ligand **L^2**; 65 % of the available ^{68}Ga was complexed as **[Ga.L^2]**, with [Ga.NOTA] making up the difference. For ligand **L^3**: slightly less radiolabelled **L^3** formed, with 56 % of the available ^{68}Ga complexed as **[Ga.L^3]** and the remainder as [Ga.NOTA]. This indicates that NOTA, **L^2** and **L^3** have comparable radiolabelling kinetics under these conditions. No changes in the relative proportions of the complexes were detected over 2 hours in either case. Indicating that no trans-chelation had taken place, and the complexes were kinetically stable (under these conditions).

3.5.2 Metal Ion Competition

The radiolabelling efficiency of **L^2** and **L^3** was evaluated in the presence of increasing concentrations of calcium(II), iron(III) and copper(II) as their chloride salts. The standard labelling protocol at pH 4 was applied, i.e. [L^n] = 10 μM, [^{68}Ga] = 0.66 nM ~ 100 MBq, V_{tot} = 1.4 mL.

Calcium(II) is a biologically significant ion in typical extracellular concentrations of 2 mM.[42] Iron(III) is often a contaminant present in the generator eluate due to 'generator breakthrough' and the use of hydrochloric acid, and can be present in the generator stream at concentrations of 0.05 nM. Iron(III) in the generator eluate originates from the hydrochloric acid used. Copper(II) was also tested due to its exceptionally high affinity for tri-basic nitrogen ligands (Irving-Williams series). Along with the iron(III) studies, this competition provides some insight into the affinity of the ligands for gallium compared to these metal ions. In particular, the tolerance was determined, defined as the maximum amount of added metal ion which still allows quantitative labelling (at 298 K and within 10 minutes).

The presence of Ca(II) had very little effect on radiolabelling, with concentrations of 8.0 M being tolerated by $\mathbf{L^2}$ and $\mathbf{L^3}$. Radiolabelling in the presence of iron(III) was affected more with $\mathbf{L^2}$ and $\mathbf{L^3}$ tolerating 3.5 and 4.0 equivalents with respect to the amount of ligand present. The extent of radiolabelling decreased to ~ 75 % with the number of equivalents of iron(III) was increased to 5.0 and 10 equivalents, for $\mathbf{L^2}$ and $\mathbf{L^3}$ respectively. As expected, the presence of copper was the least tolerated, with $\mathbf{L^2}$ and $\mathbf{L^3}$ tolerating 1.25 and 1.2 equivalents with respect to the amount of ligand present. Taking into account the large excess of the metal ions (at least µM concentrations) in relation to the amount of ^{68}Ga(III) used (0.66 nM), $\mathbf{L^2}$ and $\mathbf{L^3}$ display a relatively high affinity for gallium over both calcium, copper and iron.

As an indication of the relative amount of ^{68}Ga present; the ligand is in a ~ 1.5×10^4 fold excess (assuming ^{68}Ga : $\mathbf{L^n}$ is 1 : 1 in the complex).

3.5.3 Dependence of Radiolabeling Yield on Ligand Concentration

The minimum ligand concentration required to provide quantitative labelling with ~ 100 MBq ^{68}Ga (~ 0.66 nM), within 10 minutes at 298 K and pH 4, was determined for $\mathbf{L^2}$ and $\mathbf{L^3}$. Both $\mathbf{L^2}$ and $\mathbf{L^3}$ radiolabelled quantitatively at a concentration of 5.0 µM, but the yield was reduced to 32 and 23 % respectively at a ligand concentration of 1 µM. This compares favourably with the acyclic chelators CP256[40] (10 µM, 298 K, pH 6.5) and HBED[41] (10 µM, 298 K, pH 4.6). This is also significantly better than macrocyclic chelators NOTA[32, 36] (100 µM, 298 K, pH 3.6), and the industry standard DOTA[32, 34] (10 µM, 368 K, pH 4.4). The tri-phosphinic acid ligand TRAP[32, 33, 38] is also comparable with quantitative labelling at a concentration of 100 µM, and an 80 % yield at a 3 µM (368 K, pH 3.3).

Note: All literature ligands are reported in their respective optimised conditions. Optimised labelling pH was not determined for ***L²*** *and* ***L³****.*

4 Summary

The results indicate that functionalisation of the exocyclic nitrogen plays a key role in determining the suitability of the ligand (in terms of radiolabelling efficiency and radiolabelled complex stability) for ^{68}Ga-PET, and that further synthetic effort should take this into account. The tri-propioniate ligand, **L³**, displayed quantitative radiolabelling at 298 K in less than 5 min over the pH range 4.0 – 7.0, with the formation of a single stable radiolabelled species. Similar radiolabelling efficiency was observed for **L²**, but formation of the stable radiolabelled complex is accompanied by the presence of a minor (< 10 %) unstable radiolabelled complex. Metal competition studies indicate a high relative affinity of both ligands for gallium over calcium(II), iron(III) and to a lesser extent copper(II). The acetate derivative of **L³** would also have been a interesting candidate, had its usefulness not been compromised by its tendency to undergo lactamisation in acidic aqueous media.

The protocol developed for radiolabelling at pH ≥ 4 is highly efficient and is simple to conduct. A significant benefit of ligand **L³** and the radiolabelling protocol used is that purification of the radiolabelled ligand is not necessary, because the acetate anion is approved for use in vivo and the radiolabelling yield quantitative. Therefore, for **L³**, it is possible to produce the radiolabelled complex, including generator elution and ^{68}Ga post-purification using the cation-exchanger method, within 10 minutes. This short time frame of preparation coupled with the small radiolabelling volume gives rise to high specific activities.

5 References

1. J. Romba, D. Kuppert, B. Morgenstern, C. Neis, S. Steinhauser, T. Weyhermuller and K. Hegetschweiler, *European Journal of Inorganic Chemistry*, 2006, 314-328.
2. S. Aime, L. Calabi, C. Cavallotti, E. Gianolio, G. B. Giovenzana, P. Losi, A. Maiocchi, G. Palmisano and M. Sisti, *Inorg Chem*, 2004, 43, 7588-7590.
3. S. Ge, A. Meetsma and B. Hessen, *Organometallics*, 2007, 26, 5278-5284.
4. S. Ge, A. Meetsma and B. Hessen, *Organometallics*, 2009, 28, 719-726.
5. S. Ge, S. Bambirra, A. Meetsma and B. Hessen, *Chemical Communications*, 2006, 3320-3322.
6. P. Comba, C. Haaf and H. Wadepohl, *Inorganic Chemistry*, 2009, 48, 6604-6614.
7. L. Tei, G. Gugliotta, M. Fekete, F. K. Kalman and M. Botta, *Dalton Trans*, 2011, 40, 2025-2032.

8. D. Imperio, G. B. Giovenzana, G.-l. Law, D. Parker and J. W. Walton, *Dalton Transactions*, 2010, 39, 9897-9903.
9. E. M. Elemento, D. Parker, S. Aime, E. Gianolio and L. Lattuada, *Organic & Biomolecular Chemistry*, 2009, 7, 1120-1131.
10. S. Aime, G. Bombieri, C. Cavallotti, G. B. Giovenzana, D. Imperio and N. Marchini, *Inorganica Chimica Acta*, 2008, 361, 1534-1541.
11. E. Gianolio, G. B. Giovenzana, D. Longo, I. Longo, I. Menegotto and S. Aime, *Chemistry*, 2007, 13, 5785-5797.
12. Z. Baranyai, F. Uggeri, G. B. Giovenzana, A. Benyei, E. Brucher and S. Aime, *Chemistry*, 2009, 15, 1696-1705.
13. G. Gugliotta, M. Botta and L. Tei, *Org Biomol Chem*, 2010, 8, 4569-4574.
14. R. S. Sengar, A. Nigam, S. J. Geib and E. C. Wiener, *Polyhedron*, 2009, 28, 1525-1531.
15. L. Manzoni, L. Belvisi, D. Arosio, M. P. Bartolomeo, A. Bianchi, C. Brioschi, F. Buonsanti, C. Cabella, C. Casagrande, M. Civera, M. De Matteo, L. Fugazza, L. Lattuada, F. Maisano, L. Miragoli, C. Neira, M. Pilkington-Miksa and C. Scolastico, *Chemmedchem*, 2012, 7, 1084-1093.
16. G. Gugliotta, M. Botta and L. Tei, *Organic & Biomolecular Chemistry*, 2010, 8, 4569-4574.
17. E. Gianolio, K. Ramalingam, B. Song, F. Kalman, S. Aime and R. Swenson, *Inorganic Chemistry Communications*, 2010, 13, 663-665.
18. E. Gianolio, G. B. Giovenzana, D. Longo, I. Longo, I. Menegotto and S. Aime, *Chemistry-a European Journal*, 2007, 13, 5785-5797.
19. C. Neis, T. Weyhermueller, E. Bill, S. Stucky and K. Hegetschweiler, *European Journal of Inorganic Chemistry*, 2008, 1019-1021.
20. P. J. Riss, C. Burchardt and F. Roesch, *Contrast Media Mol Imaging*, 2011, 6, 492-498.
21. P. K. Glasoe and F. A. Long, *Journal of Physical Chemistry*, 1960, 64, 188-190.
22. C. Neis, D. Petry, A. Demangeon, B. Morgenstern, D. Kuppert, J. Huppert, S. Stucky and K. Hegetschweiler, *Inorganic Chemistry*, 2010, 49, 10092-10107.
23. J. L. Sudmeier and C. N. Reilley, *Analytical Chemistry*, 1964, 36, 1698-1701.
24. J. E. Tackett and D. T. Sawyer, *Inorganic Chemistry*, 1964, 3, 304-307.
25. D. Kuppert, J. Sander, C. Roth, M. Wörle, T. Weyhermüller, Guido J. Reiss, U. Schilde, I. Müller and K. Hegetschweiler, *European Journal of Inorganic Chemistry*, 2001, 2525-2542.
26. J. W. Pauly, J. Sander, D. Kuppert, M. Winter, G. J. Reiss, F. Zürcher, R. Hoffmann, T. F. Fässler and K. Hegetschweiler, *Chemistry – A European Journal*, 2000, 6, 2830-2846.
27. T. Allscher, P. Kluefers and C. Neumann, *Acta Crystallographica Section E-Structure Reports Online*, 2009, 65, O1734-U1893.
28. J. R. Ascenso, M. A. Santos, J. Dasilva, M. Candida, T. A. Vaz and M. G. B. Drew, *Journal of the Chemical Society-Perkin Transactions 2*, 1990, 2211-2218.
29. T. Christensen, D. M. Gooden, J. E. Kung and E. J. Toone, *J Am Chem Soc*, 2003, 125, 7357-7366.
30. A. Zimmer, D. Kuppert, T. Weyhermuller, I. Muller and K. Hegetschweiler, *Chemistry-a European Journal*, 2001, 7, 917-931.
31. H. R. Maecke and J. P. Andre, *Ernst Schering Res Found Workshop*, 2007, 215-242.
32. J. Notni, K. Pohle and H. J. Wester, *EJNMMI Res*, 2012, 2, 28.
33. J. Notni, P. Hermann, J. Havlickova, J. Kotek, V. Kubicek, J. Plutnar, N. Loktionova, P. J. Riss, F. Rosch and I. Lukes, *Chemistry*, 2010, 16, 7174-7185.
34. G. J. Meyer, H. Macke, J. Schuhmacher, W. H. Knapp and M. Hofmann, *European Journal of Nuclear Medicine and Molecular Imaging*, 2004, 31, 1097-1104.
35. M. Bauwens, R. Chekol, H. Vanbilloen, G. Bormans and A. Verbruggen, *Nuclear Medicine Communications*, 2010, 31, 753-758.
36. I. Velikyan, H. Maecke and B. Langstrom, *Bioconjug Chem*, 2008, 19, 569-573.

37. A. S. Craig, D. Parker, H. Adams and N. A. Bailey, *Journal of the Chemical Society-Chemical Communications*, 1989, 1793-1794.
38. J. Simecek, M. Schulz, J. Notni, J. Plutnar, V. Kubicek, J. Havlickova and P. Hermann, *Inorg Chem*, 2012, 51, 577-590.
39. E. Boros, C. L. Ferreira, J. F. Cawthray, E. W. Price, B. O. Patrick, D. W. Wester, M. J. Adam and C. Orvig, *J Am Chem Soc*, 2010, 132, 15726-15733.
40. D. J. Berry, Y. Ma, J. R. Ballinger, R. Tavare, A. Koers, K. Sunassee, T. Zhou, S. Nawaz, G. E. Mullen, R. C. Hider and P. J. Blower, *Chem Commun (Camb)*, 2011, 47, 7068-7070.
41. M. Eder, B. Wangler, S. Knackmuss, F. LeGall, M. Little, U. Haberkorn, W. Mier and M. Eisenhut, *Eur J Nucl Med Mol Imaging*, 2008, 35, 1878-1886.
42. S. C. Conceicao, D. Weightman, P. A. Smith, J. Luno, M. K. Ward and D. N. S. Kerr, *British Medical Journal*, 1978, 1, 1103-1105.

Chapter 3

Second Generation AMPED Based Ligands for ^{68}Ga(III)

This chapter discusses the synthesis of a series of hexadentate aza-carboxylate ligands based on a modified AMPED scaffold (Section 1 and 2), followed by an assessment of their suitability for application in ^{68}Ga-PET (Section 3). In section 4, the behaviour of a ligand candidate from each series is assessed in vivo.

1 Introduction and Objective

The results obtained on the first generation chelators indicated that increasing steric bulk at the exocyclic amine hinders radio-labelling, favours the formation of multiple radiolabelled species and, consequently, reduces the stability of the resulting radiolabeled complex. It is believed that reducing the steric demand at the exocyclic amine facilitates formation of the more stable radiolabelled complex species. However, the extent to which steric bulk at the exocyclic amine could be reduced, has already been explored (Chapter 2).

In order to promote the ligand conformation that is most pre-organised for gallium binding, it was necessary to increase the steric bulk of the other substituent at the tertiary carbon (Figure 3.1). In the most extreme case, in which the exocyclic amine is protonated, the A-value for this substituent is expected to be between 6 and 10 kJ.mol^{-1}, depending on the number and size of the amino substituents.[1] This provided a reference point as to the nature of 1'. A phenyl and *t*-butyl group, with A-values of 12 and 20 kJ.mol^{-1} respectively, are both significantly larger than an exocyclic amine, and would therefore both serve the purpose. Despite the fact that *t*-butyl is expected to have a more profound effect, there were a few reasons why we opted to make use of the phenyl moiety. These include:

- There was some concern over what effect a very large increase in the steric bulk would have on reaction at the quaternary site (C^{1}), required for the formation of the 7-membered ring. (Chapter 2 Scheme 2.1). A smaller change in steric bulk would still provide the necessary shift in steric balance.
- The phenyl group would facilitate the use of experiments and analyses involving UV-visible spectroscopy (such as HPLC) to a much greater extent than the *t*-butyl group.

- The phenyl group provides scope for modification leading to bioconjugation (bifunctional chelators), by making use of the phenyl group as part of a spacer or linker moiety.

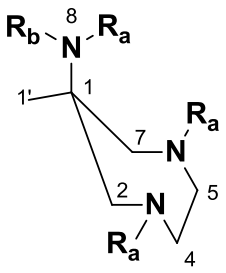

Figure 3.1 *Core structure numbering system for chelators based on 6-amino-1,4-diazepine. The N-substituents do not form part of the core structure. AMPED (1' = Me) and APPED (1' = Ph)*

Thus, the objective was to synthesise a series of chelators which would provide information on the effect of the modified scaffold (APPED: Figure 3.1), in comparison to chelators based on the AMPED core. The comparison can be made using NMR spectroscopic experiments and single crystal X-ray data. In addition, radiochemical experiments would provide information on the suitability of the chelators in terms of the rate of complexation and formation of the desired single species. Specifically, the synthesis of chelators akin to those which showed promise in Chapter 2 was undertaken (Figure 3.2). Therefore, the APPED analogues of ligands **L^4** and **L^5** were not considered. Although it had already been shown that the tetra-acid derivative of AMPED (**AAZTA: L^1**) was unsuitable for complexation of ^{68}Ga(III), it forms part of this series because its precursor is expected to form as a by-product.

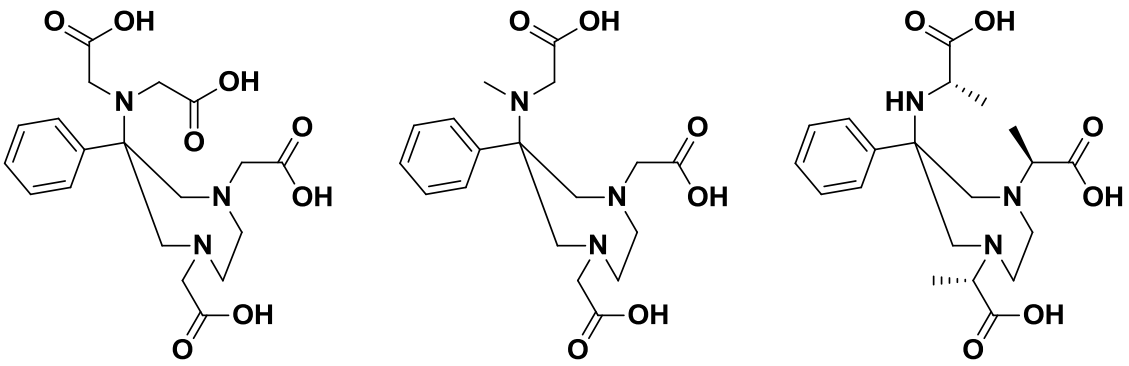

Figure 3.2 *Ligand targets (based on the APPED triamine) to evaluate the effect of introducing a phenyl moiety.*

2 Synthetic Aspects

There are a few examples in the literature of cyclic polydentate chelators featuring a modified AMPED core. A number of groups have ventured to use the quaternary site as a position from which targeting vectors could be attached (Figure 3.3(a)).[2-6] However, to date, there are no examples of alterations made to significantly increase the steric bulk at this site. There is a patent containing a bicyclic system (Figure 3.3(b)) which bridges the ethylene carbons C^4 and C^5.[7] However, the influence of this alteration on the ring conformation is unclear, and has not been discussed.

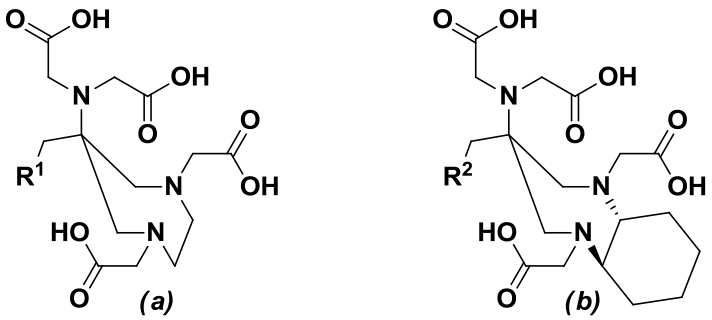

Figure 3.3 *General structures of polydenate chelators featuring a modified AMPED core.*[7, 8]

An identical modification has been made to the ethylene diamine bridge of DTPA, in an attempt to increase the rigidity of the ligand 'backbone'. ^{68}Ga-radiolabelled complexes, consisting of this modified DTPA, showed improved stability and radiolabelling with respect to the unmodified ligand.[9] The authors had perhaps hoped that this modification would have a similar effect on their AAZTA-system.

2.1 Proposed Syntheses of APPED

At first glance, the logical synthetic route would be to simply replace the nitroethane in the synthesis of the original AMPED system (Scheme 2.1 Chapter 2) with phenylnitromethane. Consultation with colleagues in the field who have attempted this synthesis previously and from our own experience suggested that this was not going to be straightforward. Reduction of the nitro group and deprotection of the benzyl protecting groups is carried out by hydrogenation in the presence of Pd/C (or $Pd(OH)_2/C$). Under these conditions, the 7-membered APPED ring is unstable, presumably due to hydrogenolysis of the endocyclic N–C bond. As a result, a new synthetic approach was required. It

seemed evident that deprotection to yield the free triamine (APPED) was going to be the key step and needed to be addressed as a priority, whilst N-functionalisation to yield the desired chelators should be less difficult.

Two possible routes to the APPED core were proposed: the first focused on making minimal changes to the established method, and relied upon modifying the nature of the deprotection step. The second route required a completely new strategy to avoid this deprotection step.

Whilst working with the AMPED system, it was established that it was possible to reduce the nitro functionality selectively using tin(II) chloride and 6M hydrochloric acid. This provided an alternative method for deprotection of the nitro group. However, concomitant cleavage of the benzyl substituents on the endocyclic nitrogens also needed to be undertaken. These benzyl groups are important to the efficiency of the ring formation reaction, and thus any changes should ideally maintain their aromatic nature. The use of methoxy substituted benzyl groups for amine protection has been demonstrated, and they can be easily deprotected in the presence of acid.[10] Therefore, by substituting the benzyl protecting groups with methoxy-functionalised benzyl groups, the exocyclic amine deprotection could be undertaken at the same time as the nitro-reduction (Scheme 3.1). More specifically, 2,4-dimethoxy benzyls where chosen, because the additional stabilization effect of the *ortho*- and *para*- methoxy groups on the positively charged benzylic intermediate should enhance the rate of the deprotection step.

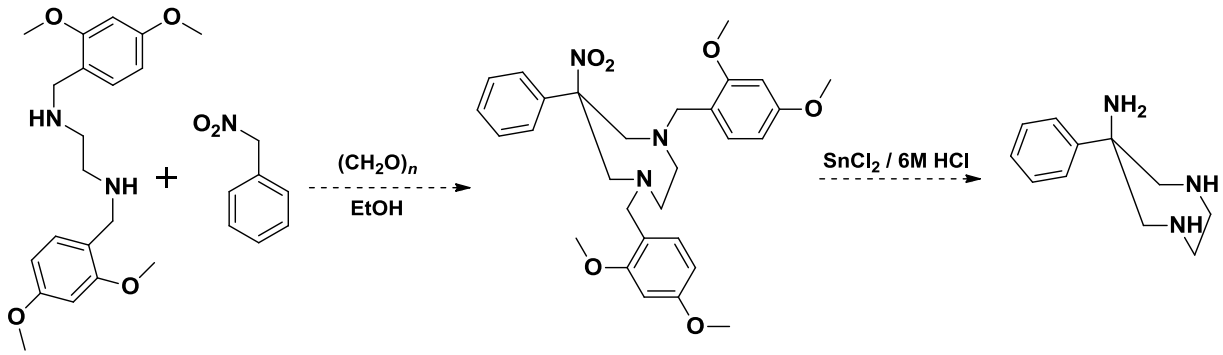

Scheme 3.1 *Proposed synthesis of APPED, using a modified protocol to that used for the synthesis of AMPED.*

The second option was to consider an entirely new approach, one more akin to the synthesis of polyaza macrocycles.[11, 12] The precursor 2-nitro-2-phenylpropane-1,3-diol, which owing to the presence of the di-hydroxyl groups may allow formation of the 7-membered ring by cyclisation with

an appropriate di-tosylamide (Scheme 3.2). The benefit of this method is that there is no need for the nitro and benzyl protecting groups. The route proposed is similar to that used for the synthesis of triazacyclononane. However, this did not guarantee success in this system, and the steric bulk close to the tosylate leaving group was considered problematic.

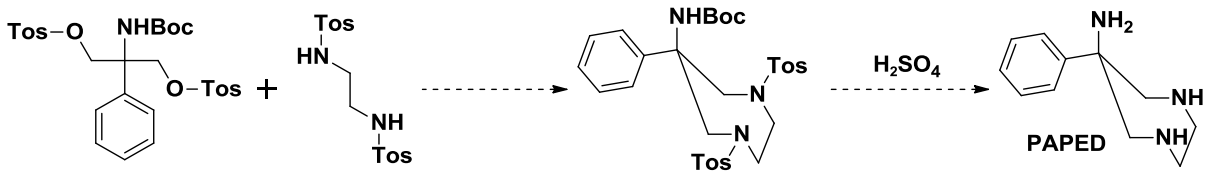

Scheme 3.2 *Proposed synthesis of APPED using a Tosyl cyclisation approach. Synthesis of starting materials is not shown.*

Faster progress was made with the method outlined in Scheme 3.1, and as a consequence the alternative route other was not continued further.

2.2 Synthesis of PAPED Based Ligands

The syntheses of phenylnitromethane (**21**) and the protected diamine (**20**) were undertaken using known functional group transformations. The former, by nitration of benzybromide using an aqueous suspension of silver nitrite.[13] For the latter, ethylenediamine was reacted with the synthesised 2,4-dimethoxy-benzylaldehyde to yield a di-imine, which was subsequently reduced to give the diamine (**20**) using sodium borohydride in a '2-step-1-pot' procedure (Scheme 3.3).

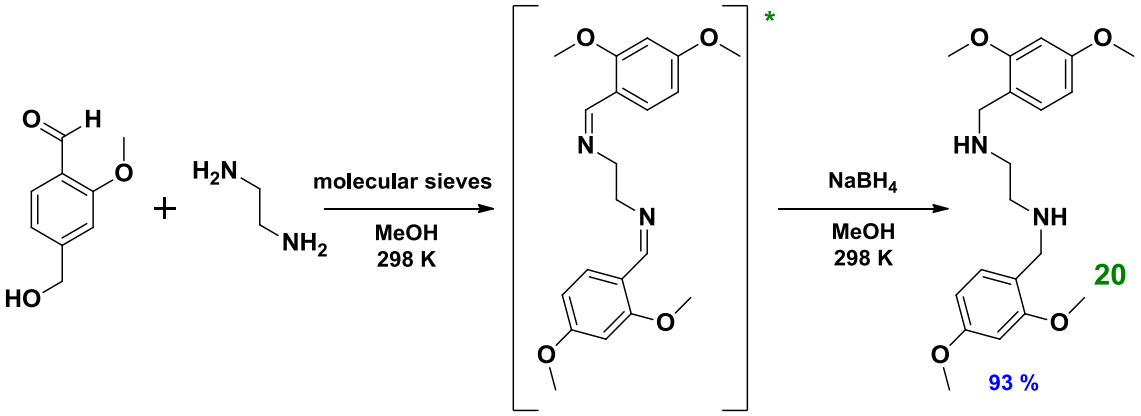

Scheme 3.3 *Synthesis of the modified protected ethylene diamine (**20**) *the diimine is an intermediate, but was not characterised.*

2.2.1 Synthesis of the Protected Triamine

The conditions first attempted for the nitro-Mannich type reaction to construct the 7 membered APPED ring were akin to those used for the AMPED system (Scheme 2.1). A product was isolated in a relatively poor yield of 22 %, following silica gel column chromatography. The 1D and 2D NMR spectra were consistent with the desired compound at first inspection. However the $[M+H]^+$ peak was found at one mass unit too low. Infra-red spectra revealed that the nitro symmetric and asymmetric stretching frequencies (1350 - 1530 cm^{-1}) were absent. Moreover, a broad band at ~ 3250 cm^{-1} suggested the presence of a hydroxyl functional group. Substitution of the nitro group by a hydroxyl group was consistent with the infra-red, mass spec and NMR data. Indeed, Crozet et al. have reported an example of rarely observed nitro-hydroxyl exchange in a tertiary nitroalkane.[14] It is believed that the nitro adduct is formed, followed by a fast S_N1 solvolysis reaction, in which the nitro group is substituted by a hydroxyl group in a two-step process (Scheme 3.4). Such a reaction requires the intermediary of a carbocation, which is stabilized under the polar protic conditions (wet ethanol solvent at a relatively high temperature). The conjugative stability of the nitro leaving group and the presence of the phenyl group, stabilising the carbocation, further promote this solvolysis reaction.

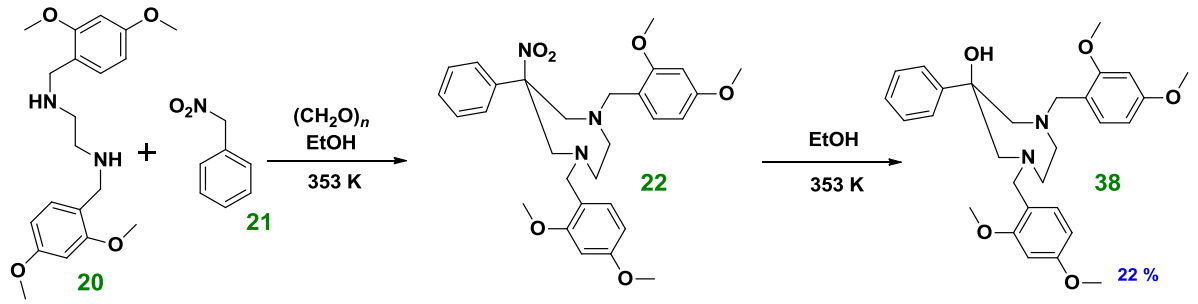

Scheme 3.4 *Formation of tertiary hydroxyl-compound (**38**) via S_N1 solvolysis of tertiary nitro-compound (**22**) following formation of the 7-membered ring. The tertiary nitro-compound (**22**) is shown as an intermediate, but was not isolated under these conditions.*

In order to inhibit this competitive solvolysis reaction, the polarity of the solvent was reduced (by using 50: 50, ethanol : toluene) and the temperature of the reaction was lowered to 308 K. As expected, the reaction progressed much more slowly, but the desired nitro-compound was isolated following silica gel column chromatography. It displayed an infra-red stretching frequencies (1540 and 1374 cm^{-1}) which could be assigned to the NO_2 symmetric and asymmetric stretches. The $[M+H]^+$

peak was observed by electrospray mass spectrometry, within the acceptable range of the theoretical mass, in a high resolution analysis. The constitution of **22** and **38** has been confirmed by means of single crystal X-ray diffraction. The solid state structures of these compounds are discussed in more detail in Chapter 4 Section 2.1.

Though unintentional, the synthesis of tertiary hydroxyl-compound (**38**) could prove useful. The use of **38** towards the synthesis of a ligand for ^{68}Ga is discussed in Section 2.2.4 of Chapter 3.

2.2.2 Reductive Deprotection the Tertiary Nitro-Compound, 22.

Earlier work, involving selective de-protection of the nitro group in the AMPED system, had been successful using tin(II)chloride in hydrochloric acid. This formed a logical starting point for nitro reduction, as the acidic conditions should also promote cleavage of the aryl substituents. Perhaps unsurprisingly, given the high temperatures and ionising conditions, exchange of the nitro group for a hydroxyl (this time accompanied by cleavage of the aryl substituents) was confirmed by mass spectrometry and infrared spectroscopic data. Attempts to suppress the solvolysis reaction, by reducing the temperature of the reaction and polarity of the solvent, were unsuccessful.

By using a temperature gradient it was possible to obtain a ~ 4 : 1 ratio in favour of hydroxyl derivative, however the yield was poor and the nature of the compounds made them exceedingly difficult to separate. Similarly unsuccessful reactions were carried out replacing tin with metals known to have similar nitro reducing abilities, namely zinc and iron.

The original reductive benzylation method used in the AMPED system (Scheme 2.1), using $Pd(OH)_2/C$ catalysed hydrogenation was attempted. However, it did not yield APPED or the nitro-reduced product. The hydrogenation was also attempted with Pd/C and ammonium formate, but also failed to yield any desired product. A new approach was needed, ideally one which involved sequential cleavage of the aryl substituents and nitro reduction. It had already been shown that the aryl substituents could be cleaved under acidic conditions, notwithstanding solvolysis of the nitro substituent. Given the relative ability of nitro and protonated amine functional groups to behave as a leaving group, it was considered prudent to undertake the nitro reduction first.

Ganem and co-workers[15] have described the reduction of nitro containing compounds using $NiB_2/NaBH_4$ prepared *in situ* from $NiCl_2$ and $NaBH_4$. When this reaction was applied to the tertiary

nitro-compound (**22**), none of the desired product was observed. Instead a product was isolated which was interpreted as a ring opened oxime, based on NMR, IR and MS data. We propose that this ring opening reaction occurs via a reduction of the nitro group to a nitroso species, followed by an anti-periplanar ring opening mechanism aided by protonation of the nitroso group (Scheme 3.5). The same product was isolated when selective reduction of the nitro group was attempted at 273 K using $LiAlH_4$ in tetrahydrofuran. A further possibility is that the reaction involves radical cleavage of the endocyclic C-N bond, potentially initiated by photolysis or triplet oxygen.

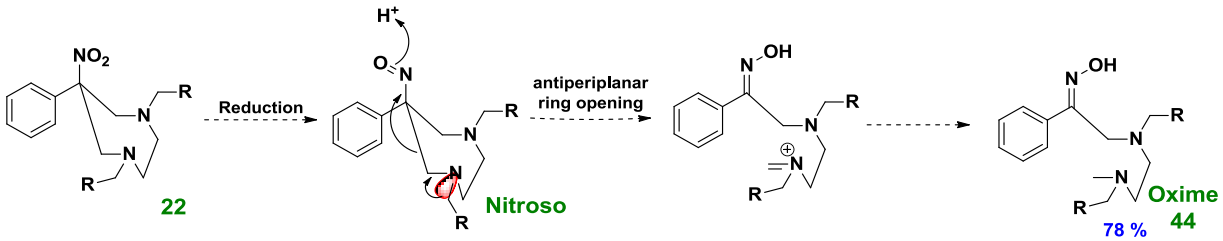

Scheme 3.5 *Proposed mechanism for the formation of the 'ring opened' oxime (**44**) when reduced with $NiB_2/NaBH_4$ or $LiAlH_4$. R = 2,4-dimethoxyphenyl.*

Raney nickel is a reagent commonly used for the hydrogenation of unsaturated carbons and desulfurisation reactions. Go and co-workers[16] have reported the use of Raney nickel in the presence of hydrogen for the reduction of alkyl nitro groups. This method was applied to **22** and found to selectively reduce the nitro functionality at room temperature in approximately 2 hours (Scheme 3.6). The reaction was carefully monitored using TLC to avoid formation of a by-product following nitro-reduction.

Given that the next step would yield the free tri-amine APPED (by cleavage of the aryl arms under acidic conditions), which are inherently difficult to purify and handle given its propensity to react with carbon dioxide, it was critical that the product isolated from the nitro reduction be of high purity. However, the exocyclic amine was susceptible to reaction with carbon dioxide at room temperature, and purification by silica gel column chromatography troublesome. A Boc protection of the amine was thought to be advantageous because it could be cleaved under the same acidic conditions used to cleave the aryl substituents, and engender a compound which should be readily purified by chromatography. The Boc protection to yield compound **45** was successful, and is reported as a 2-step reaction with the Raney nickel nitro reduction. The deprotected triamine, APPED (**46**), was obtained by stirring the carbamate (**45**) in trifluoroacetic acid and dichloromethane at 298 K overnight (Scheme 3.6).

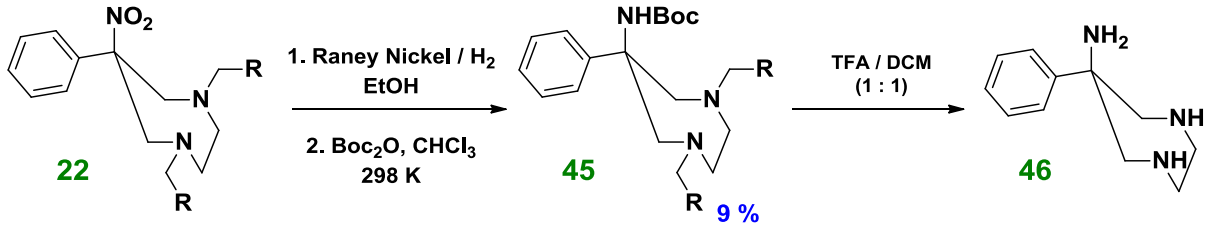

Scheme 3.6 *Synthesis of APPED (**46**) from the tertiary nitro-compound (**22**). First step involves nitro-reduction, to yield the tertiary amine, followed by Boc-protection to give the carbamate (**45**).In the second step, the Boc and aryl substituents are cleaved under acidic conditions. R = 2,4-dimethoxyphenyl.*

The triamine, APPED (**46**), was subsequently reacted with the appropriate α-bromo esters to give the protected ligand precursors in a very low overall yield (< 1%) with respect to the tertiary nitro compound, **22**. The major loss of product occurred at the deprotection step to yield **46**. Previous reactions to cleave the aryl substituents were efficient, which suggests that either the NHBoc deprotection is inefficient or the product (**46**) is unstable.

The possibility of varying the sequence of the deprotection and N-functionalisation steps was investigated. A synthetic route with the same number of overall steps, that avoided formation of **46** and the Boc-protection step was developed (Scheme 3.7).

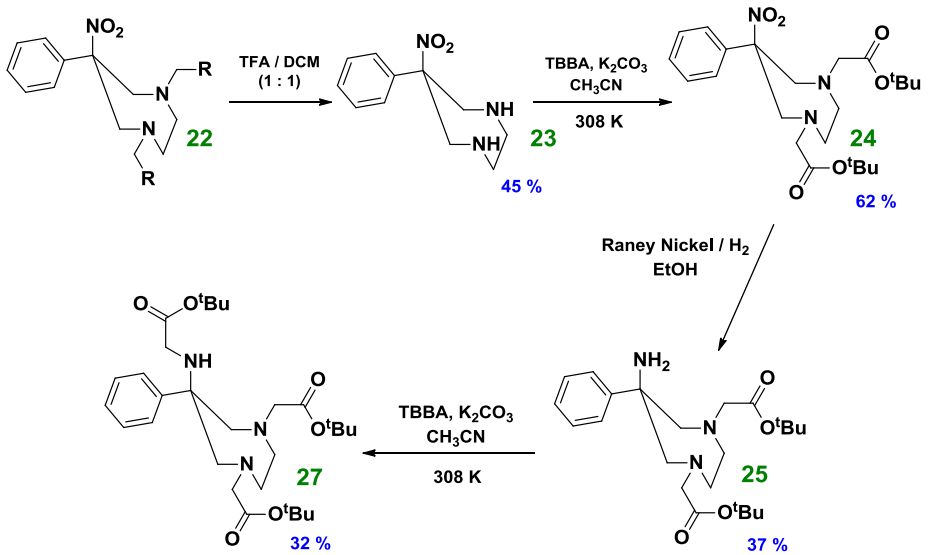

Scheme 3.7 *Synthetic route used for the stepwise deprotection and N-alkylation of the tertiary nitro compound (**22**). Shown as an example, is the synthesis of the triester derivative of APPED (**27**).*

In this revised sequence, the first step was cleavage of the aryl arms using trifluoroacetic acid, followed by N-alkylation with *t*-butyl bromo-acetate. The constitution of this intermediate, **24**, has been confirmed using single crystal X-ray diffraction. This was followed by nitro reduction using Raney nickel catalysis to yield **25** in sufficient purity. Alkylation of the resulting exocyclic primary amine gave the mono-N-substituted ester, **26**. The synthesis was carried out successfully with an improved yield. The major benefit of this method is the synthetic flexibility it introduces. Unlike every reported synthesis of chelators based on the AMPED core, the exo- and endo-cyclic amines can now be elaborated selectively and with relative ease. Whilst completing this work, the use of Raney nickel to achieve selective deprotection of the nitro group on the AMPED core has been reported elsewhere.[2]

2.2.3 Alkylation of the Exocyclic Amine

In the case of AMPED derivatives the exocyclic amine was very reactive and accessible to incoming nucleophiles. This characteristic was highlighted on a number of occasions. For example; alkylation with *t*-butyl bromo-acetate to yield tri-N-alkylated AMPED, **5** (Scheme 2.3), required mild conditions, and could not be undertaken without concomitant formation of the tetra-N-alkylated product, **3**. The reactivity and accessibility of the 'third' position of N_{exo} was also highlighted by the propensity of compound **5** to lactamise readily under the acidic conditions used to deprotect the ester groups (Chapter 2 Scheme 2.3). As discussed previously, this could be prevented by insertion of a methyl group onto the mono functionalised exocyclic amine. This methylation reaction also reflected the reactivity and accessibility of the exocyclic amine of AMPED. Relatively mild conditions (< 1 molar equivalent methyl iodide, dichloromethane solvent, 273 K) were required to hinder formation of a quaternary ammonium salt, resulting from over-methylation of the exocyclic amine.

These three reactions of the AMPED system make for an interesting comparison with the analogous reactions for the APPED system. The exocyclic amine of APPED derivatives appear to be significantly sterically hindered than the AMPED analogues. For example, when the APPED (core) is N-alkylated with *t*-butyl bromo-acetate under the same conditions, only the tri-N-alkylated product (**27**) was obtained. Formation of the tetra-N-alkylated product (**26**) required a higher temperature (343 K) and even then was only produced in a relatively low yield (12 %). This influence of the inserted phenyl substituent on the exocyclic amine, was also evident during methylation of the mono-substituted exocyclic amine of **7**. Considerably harsher conditions (1.5 equivalents of methyl iodide, acetonitrile solvent, 295 K) were required and no quaternary products where observed (Scheme 3.8).

Furthermore, lactamisation of **27** was considerably slower than that of the AMPED analogue (**5**) which suggests that the lone pair of electrons of the exocyclic amine is less accessible to the acetate substituent on the endocyclic amine, or that the conformation of the ring is less favourable to the formation of the lactam ring.

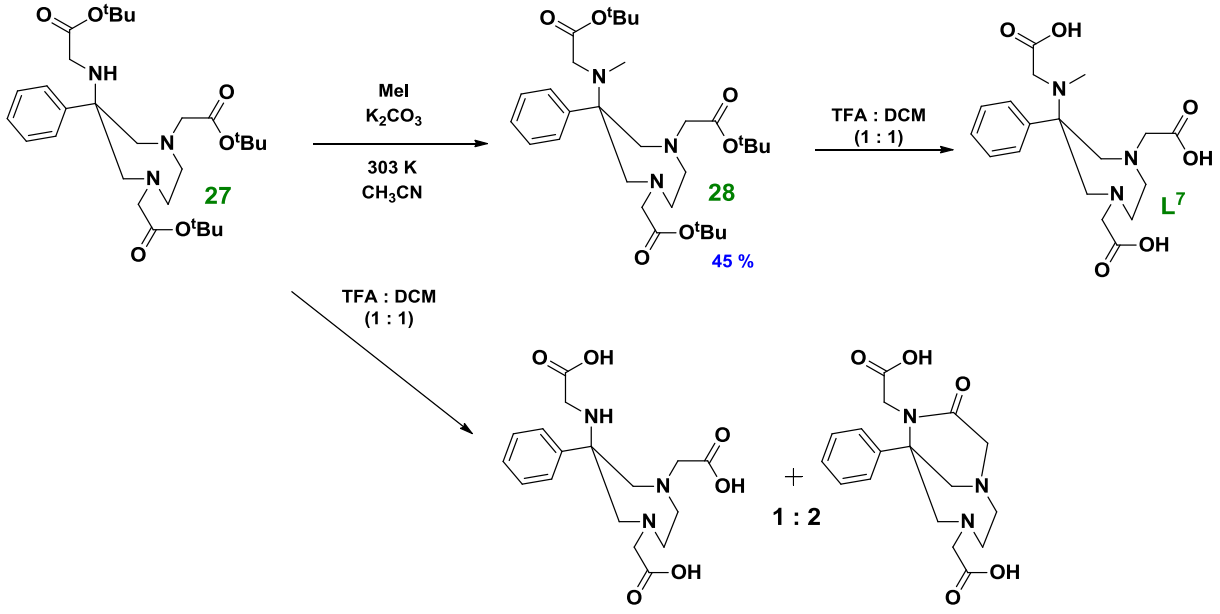

Scheme 3.8 *Synthesis of ligand* ***L*** ^{7} *from the triester (**27**), by methylation and subsequent ester hydrolysis. Also shown is the ester hydrolysis of **27**, which resulted in the formation of the desired tri-N-acid APPED derivative as well as the unwanted lactamised by-product.*

This observation suggested that synthesis of a chelator with a mono-N-substituted exocyclic amine which is stable enough to be used for ^{68}Ga-labelling is feasible with the APPED core. Mass spectroscopic data showed that both the lactamised and desired product were formed (in a 2 : 1 ratio) during ester deprotection of **27** using trifluoracetic acid. This is a significant improvement compared to the de-esterfication of the AMPED analogue under the same conditions (Scheme 2.3). These products were inherently difficult to separate, and thus an efficient synthesis which would prevent formation of the lactamised product was required. This was achieved by substituting the *t*-butyl esters for ethyl esters, (a method not dissimilar to that applied to the synthesis of **10**), which could be deprotected using sodium hydroxide in a 1 : 1 THF/water mixture (Scheme 3.9). The synthesis of ligand **L**^{8} was achieved following the same procedure, by substituting the ethyl bromo-acetate for enantiomerically pure (*R*)-trifluoromethyl-sulphonate.

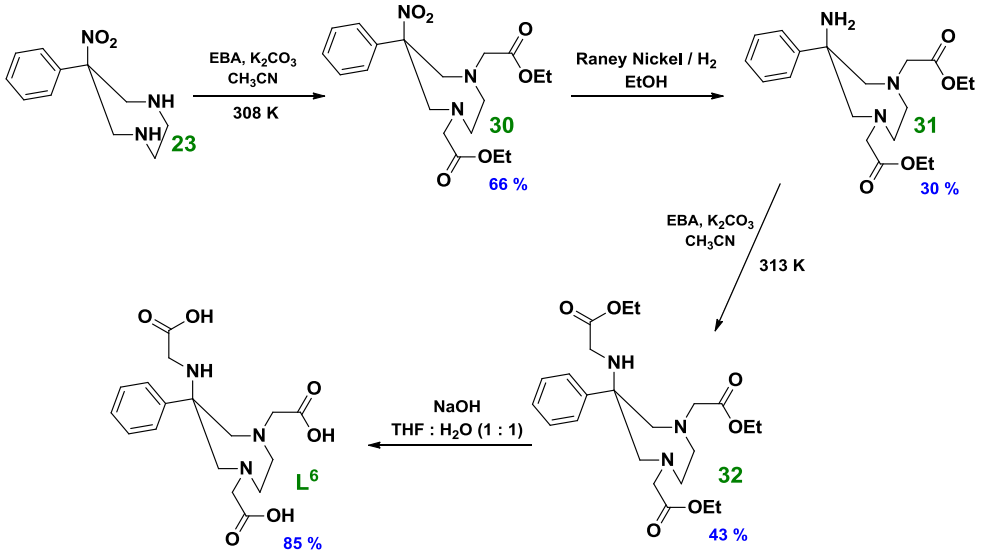

Scheme 3.9 *Synthetic protocol used for the preparation of ligand **L**[6]; designed to avoid formation of the lactamised by-product. Ligand **L**[8] was synthesised using the same route, substituting the ethyl bromo-acetate for (R)-trifluoromethyl-sulphonate.*

Acid catalysed ester hydrolysis of the tetra-N-alkylated derivative (**26**) was also troublesome. Mass spectroscopic data suggests that the desired product forms, accompanied by the formation of two other species. According to the $[M+H]^+$ peaks, these have been tentatively identified as fragments resulting from solvolysis at the tertiary carbon (C^1) and cleavage of the endocyclic N—C bond under the protic ionising conditions (Scheme 3.10). In Chapter 2, the tetra acid derivative of AMPED (**3**) was identified as largely unsuitable for ^{68}Ga(III) complexation. For this reason, the synthesis of the APPED analogue was not pursued by other methods.

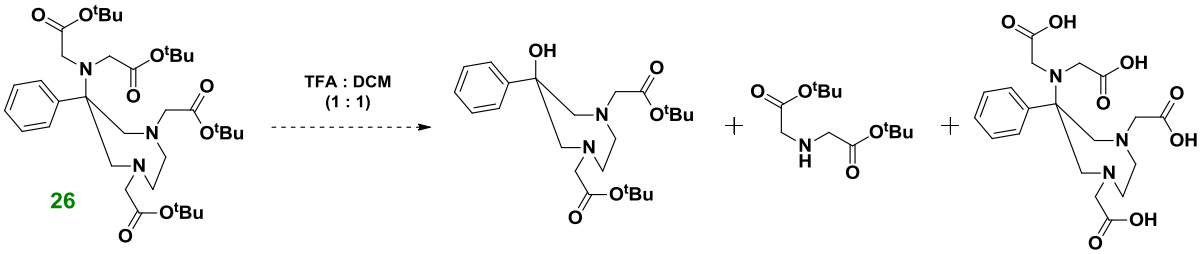

Scheme 3.10 *Proposed products resulting from the ester hydrolysis of the tetra-N-ester (**26**), based on LC ES$^+$ mass spectroscopic data.*

Figure 3.4 depicts the three novel N_3O_3 chelators synthesised, which are based on the novel APPED core structure. It is possible to synthesise these ligands via the triamine APPED core (**46**); a route

which is analogous to the synthesis of AMPED based ligands. However, from our experience this route is inefficient for the APPED system. We have found that the sequential deprotection and decoration of the exo- and endo-cyclic amines is considerably more efficient, and also provides a greater degree of synthetic versatility. In hindsight, there is also a strong case for the use of base-hydrolysable esters over the alternatives; specifically *t*-butyl esters should be avoided.

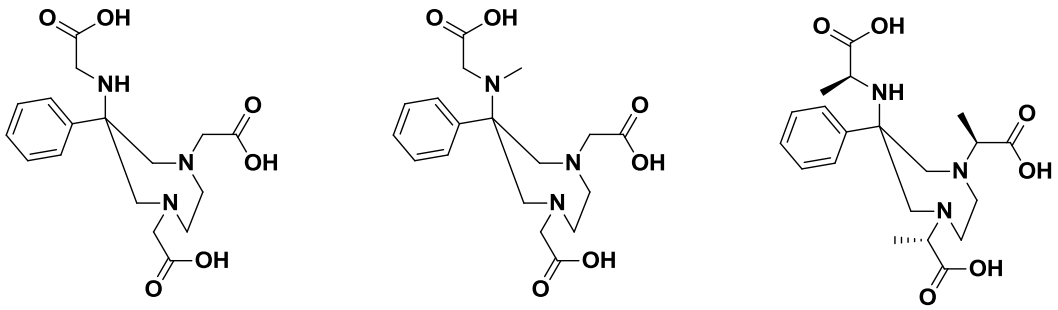

Figure 3.4 *Ligands featuring the novel APPED core synthesised for evaluation of their suitability for application in ^{68}Ga-PET.*

2.2.4 Synthesis of hydroxyl derivatives

The solvolysis reaction (Scheme 3.4) which resulted in the exchange of the nitro functional group for the hydroxyl was unplanned. However, the synthesis of an 'ether-like' analogue of **L^8**, does offer an interesting comparison to the N_3O_3 chelators described in this chapter. By virtue of its lower basicity (pK_a(NHR) ~ 6 vs pK_a(OR) ~ 16) the hydroxyl group is a weaker σ-donor than the amine, and as a result the dative bond which forms to gallium would be weaker. In this respect, it is reasonable to predict that the stability and radio-labelling kinetics would be less favourable. However, the hydroxyl group has a much smaller A-value than the amine (3 and 7 kJ/mol^{-1} respectively), giving an even greater bias to the phenyl moiety attached to the tertiary carbon (C^1). Of further benefit; the hydroxyl derivative is considerably easier to synthesise, and is not prone to internal lactamisation which plagued the AMPED and APPED system. The tri-akylated ligand (**L^9**), the 'ether-like' analogue of **L^6**, was synthesised in 4 steps from **22** (Scheme 3.12).

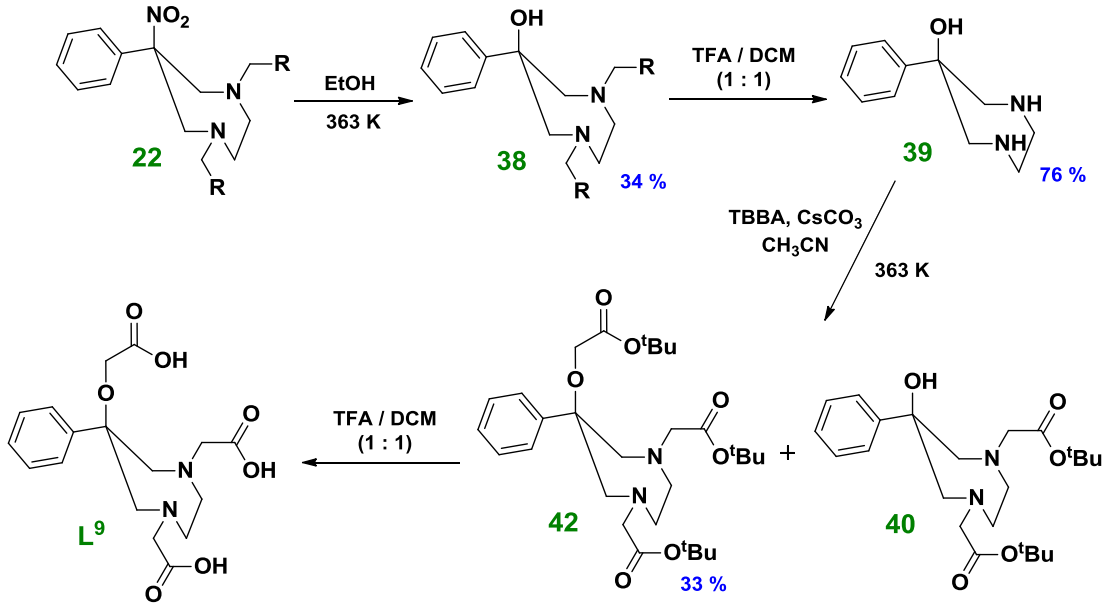

Scheme 3.12 *Synthesis of ligand* ***L*****[9]***, making use of the solvolysis-substitution reaction at the tertiary carbon of the reaction. R = 2,4-dimethoxyphenyl*

The nitro-hydroxyl exchange was attempted on different nitro intermediates, but found to work best by refluxing pure **22** in wet ethanol to give the hydroxyl analogue, **38**. The alkylation with *t*-butyl bromo-acetate requires harsh conditions, and the di-N-alkylated compound (**40**) was isolated as a by-product.

3 Radiochemical Evaluations

In chapter 2 the synthesis and radiochemical evaluation of a series of ligands based on the AMPED scaffold was discussed. Two of the ligands in particular, **L**^{2} and **L**^{3}, display ^{68}Ga-radiolabelling characteristics and stability (of the radiolabelled complex) which compare favourably with the best ligands in literature.[17-21]

This very promising system does have a couple of disadvantages, which have been attributed to structural characteristics of the ligands. In fact, the structural features which make **L**^{2} and **L**^{3} more suitable than the other ligands (**L**^{1}, **L**^{4} and **L**^{5}), are also the source of the disadvantages. More specifically, the reduced steric demand at the exocyclic amine was found to correlate favourably with radiolabelling efficiency and the enhanced stability of the radiolabelled complex. The best attributes were obtained for ligand **L**^{3}, which has a mono-functionalised exocyclic amine. However,

ligand **L^{3}** is hampered by its inherent tendency to lactamise under acidic conditions (Chapter 2 Section 1). Given that radiolabelling occurs over the pH range 4.0 – 7.0 the ability of the ligand to complex ^{68}Ga is not disadvantaged, because the rate of lactamisation is very slow in this pH range. Ligand **L^{2}** overcomes this problem, but it forms multiple radiolabelled species. Although the minor species only accounts for between 5 and 10 % of radiolabelled complex (depending on labelling conditions), the presence of multiple species is an undesirable feature. This limits the potential for bioconjugation, both in terms of the point of attachment (using the exocyclic amine may not be feasible) and the chelators that may be useful.

In Section 1 of this chapter the synthesis of ligands featuring a modified scaffold (APPED) was described, which has increased steric bulk at quaternary ring carbon (C^{1}). The hypothesis was that doing so would have two specific advantageous effects. Firstly, increased steric demand of this substituent would favour the chair-like conformation of the ligand in the Ga(III) complex, and thereby reduce the likelihood of formation of multiple radiolabelled species. This was especially a problem for radiolabelling at pH < 3.5, and in ligands where the exocyclic amine is di-N-alkylated. Secondly, the increased steric bulk close to N_{exo} would inhibit the internal lactamisation reaction which was the downfall of these promising ligands.

Synthetic observations indicate that introduction of the phenyl substituent did have the desired effect of reducing the rate of lactamisation (for structurally related ligands in each series). For example; ligand **L^{6}**, which is structurally related to the AMPED based ligand (AAZ3A: Figure 2.1) which was deemed too unstable under acidic conditions, is sufficiently stable to be considered. Furthermore, **L^{8}** also shows a slower rate of internal lactamisation than that observed for **L^{3}**.

The series of four chelators, **L$^{6\text{-}9}$** (Figure 3.5), featuring the modified AMPED core, was synthesised and evaluated for potential application in ^{68}Ga-PET. The suitability of these ligands has been assessed in the same manner as that described for ligands **L$^{1\text{-}5}$** (Chapter 2 Section 3). Firstly, the radiolabelling efficiency of the ligands was determined over the pH range 2.3 – 7.0 at 298, 323 and 368 K. Secondly, the stability of the radiolabelled complexes was evaluated at physiological pH and temperature in presence of *apo*-transferrin, DTPA, iron(III) and newborn calf serum. Ligands deemed suitable were evaluated in a series of competition experiments, and the dependence of the radiolabeling yield on ligand concentration investigated.

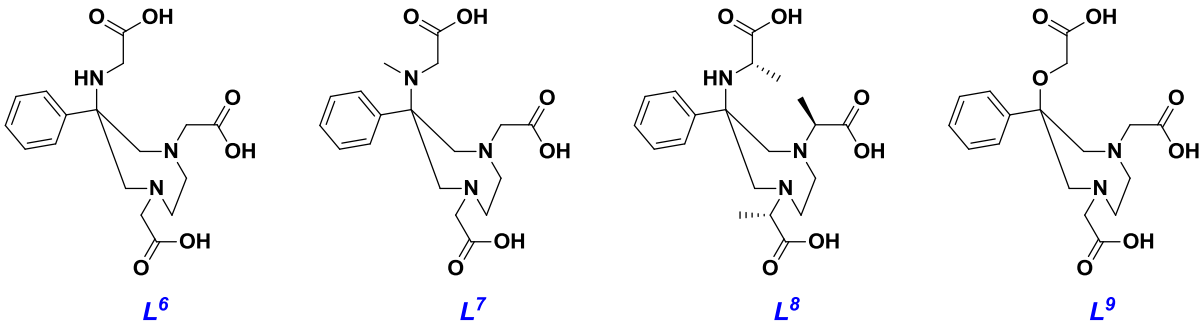

Figure 3.5 *Ligands featuring the modified AMPED core synthesised for evaluation as potential ^{68}Ga-PET imaging agents.*

3.1 Radiolabelling Studies with Ligands L^{6-9}

The radiolabelling (pH 4.0 - 7) and radiolabelled complex stabilities displayed by L^2 and L^3 were extremely favourable. Thus, the same or very similar characteristics are desirable in this series. Of further importance is to define the radiolabelled speciation characteristics, in comparison to their AMPED based analogues.

3.1.1 Radiolabeling at pH < 3.6

The radiolabelling of L^{6-9} was assessed at pH ~ 2.3 in the absence of a suitable buffer. Radiolabelling at pH 3.3 was not evaluated because only limited information could be extracted. Also, the protocol was unsuitable for the synthesis of radiolabelled complexes due to the resulting low radioactivity concentration of the solution. The results of the radiolabelling experiments for ligands L^{6-9} at 298, 323 and 368 K are shown below (Figure 3.6). Also shown for comparison is the radiolabelling kinetics for L^2 and L^3, the AMPED analogues of L^7 and L^8 respectively.

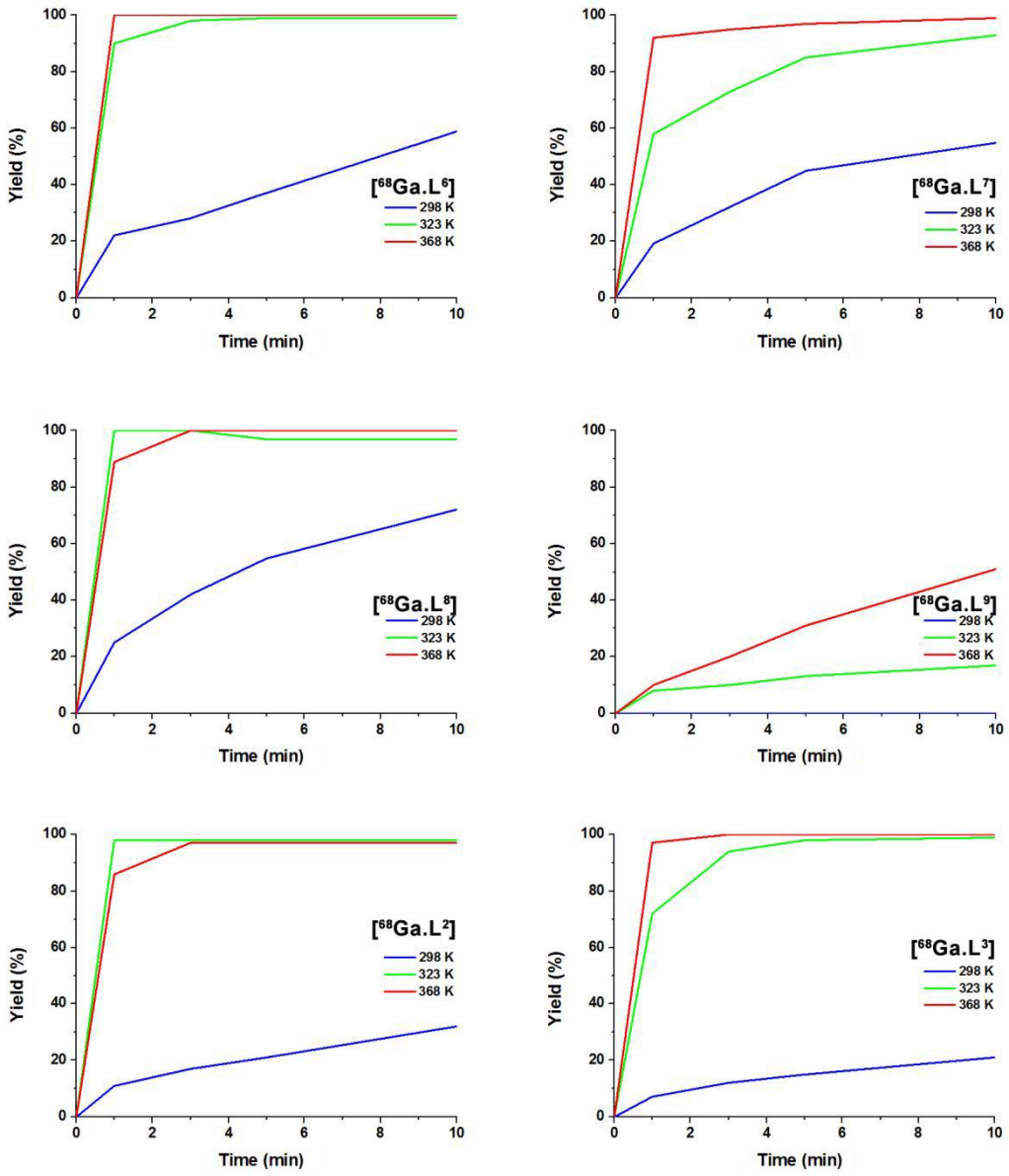

Figure 3.6 *Temperature dependent radiolabelling kinetics of ligands* $L^{6\text{-}9}$ *at pH 2.3, shown as a percentage of the radioactivity associated with the radiolabelled complexes, at 1, 3, 5 and 10 minutes intervals. ~ 100 MBq activity at t = 0 min.* $[^{68}Ga] = 0.18$ *nM.* $[L^n] = 10$ *µM.* $V_{tot} = 5$ *mL.*

There is a greater than two fold increase in the radiolabelling kinetics of L^7 and L^8 relative to L^2 and L^3 at 298 K. Ligand L^6 shows a similar radiolabelling profile at room temperature, and all three ligands show > 90 % labelling within 10 minutes at 323 K. In contrast, L^9 showed comparatively very slow radiolabelling even at 368 K, with a maximum radiolabelling yield of 55%. This considerable decrease in the radiolabelling kinetics with respect to its structural analogue, L^6, is likely to be a result of the reduced donor ability of the ether oxygen.

Examination of the eluted radio-TLC plates reveals some interesting information regarding the speciation of the radiolabelled ligands. Radiolabelling of ligand **L^{7}** at pH 2.3 gave rise to two radiolabelled species (ratio 9 : 1). Similarly, radiolabelled complexes **[Ga.L^{6}]$_{2.3}$** and **[Ga.L^{8}]$_{2.3}$** were also characterised by two species, but with considerable less biased ratios of 3 : 2 and 3 : 1 respectively.

Thus, in addition to the increase in the rate of radiolabelling through modification of the AMPED scaffold, we also note that there has also been a perturbation in the speciation of the radiolabelled complexes. Previously it was found that radiolabelling of ligand **L^{3}** at pH 2.3 resulted in formation of single radiolabelled complex species. Under the same conditions, the structural analogues **L^{6}** and **L^{8}** each give rise to two radiolabelled species with ratios of 3 : 2 and 3 : 1 respectively. Whether or not the change in the ratio of the isomeric species was in favour of the more stable species will be assessed in section 3.2 of this chapter. Radiolabelling with ligand **L^{7}** at pH 2.3 displayed improved radiolabelling kinetics compared to the AMPED analogue, **L^{2}**. However, there was no significant change to the speciation of the radiolabelled complex.

As a consequence of these speciation problems, the radiolabelled complexes of ligands L$^{6\text{-}8}$ formed at pH ~ 2.3 were considered unsuitable for application in ^{68}Ga-PET.

3.1.2 Radio-labelling at pH > 3.6

Radiolabelling experiments were carried out for ligands **L$^{6\text{-}9}$** at 298, 323 and 368 K and at pH 4.0, 5.3 and 7.0. Following the results obtained for ligands **L$^{1\text{-}5}$** where faster radiolabelling occurred above pH 3.6, a significant increase in the rate of radiolabelling rate was expected. The results for the radiolabelling at 298 K for **L$^{6\text{-}9}$** are compared (Table 3.1), examining the time taken to reach the maximum yield. Also shown are the results obtained for ligands **L^{2}** and **L^{3}** under the same conditions using identical buffer solutions in each case.

Table 3.1 *Maximum radio-labelling yield (%) achieved and the time taken (minutes) at 295 K for* $L^{2,3,6-9}$ *at pH 4.0, 5.3 and 7.0.* $[^{68}Ga]$*=0.66 nM.* $[L^n]$ *= 10 µM.* V_{tot} *= 1.4 mL. 100 MBq activity at t = 0 min.*

pH	Maximum radiolabelling yield (%) at 295 K [a] Time taken to achieve maximum yield (min)					
	L^6	L^7	L^8	L^9	L^2	L^3
4.0	97	65*	99	3	98*	99
	3	10	3	10	1	3
5.3	98	92*	99	6	97*	98
	3	10	3	10	1	3
7.0	97	20*	98	4	97*	98
	3	10	3	10	1	3

[a] *an asterisk indicates the presence of more than one radiolabelled species*

Ligand L^9 shows incomplete labelling at pH > 3.6, even at elevated temperatures, with very little enhancement of the radiolabelling yield observed at higher pH.

Surprisingly, radiolabelling of L^7 proved to be problematic. Quantitative labelling was not observed at any of the pH's evaluated, and only a ± 5 % change in the yield was observed with increasing the temperature to 368 K. Furthermore, the speciation of the radiolabelled ligand became less biased compared to radiolabelling at pH 2.5, with approximately equivalent proportions of the two species being formed.

Ligands L^6 and L^8 produced the expected change in rates compared to pH 2.5, achieving quantitative labelling at room temperature over the pH range 4.0 – 7.0 in less than 3 minutes. At face value, it may seem that insertion of the phenyl group onto the scaffold has had a negative impact on the rate radiolabelling at pH ≥ 4, compared to the AMPED analogues. However, closer examination of the time interval data shows that the radiolabelling yield at the 1 minute time interval was greater than 92 % for both ligands, over the pH range 4.0 – 7.0. This is only a very small difference compared to L^2 and L^3, and not significant taking into account that in each case radiolabelling would be conducted over 5 minutes, to ensure it goes to completion. Importantly, both L^6 and L^8 gave rise to a single radiolabelled species when each was labelled at pH 4.0, 5.3 and 7.0.

In terms of radiolabelling efficiency (rate and speciation) at pH ≥ 4, L^6 and L^8 display properties that are very similar to that of the very promising candidate ligand L^3. For these structures, the phenyl/methyl permutation has had little apparent influence on the near ideal radiolabelling

efficiency. The same is not true for **L^{7}**, where the modification has had a detrimental effect on the radiolabelling (pH > 3.6) efficiency and radiolabelled complex speciation as compared to **L^{2}**. Ligands **L^{7}** and **L^{9}** were deemed unsuitable and were not evaluated further. The poor radiolabelling behaviour of **L^{7}** may be a result of the crowded nature of N_{exo}, which hinder ligand rearrangement for metal binding.

3.2 Stability of Radiolabelled Complexes [^{68}Ga.L^{6}] and [^{68}Ga.L^{8}]

Despite the unfavourable speciation associated with the radiolabelling of ligands **L^{6}** and **L^{8}** at pH 2.3, the stability of the radiolabelled complexes has been assessed. The results may provide some insight into the nature of the different species; specifically, whether or not the phenyl/methyl permutation has resulted in an increase in the proportion of the more stable isomer.

As before, a labelling system is used where the italicised subscript after the radiolabelled complex indicates the pH at which it was formed. For example, **[^{68}Ga.L^{6}]$_{2.5}$**, indicates that the radiolabelled complex was formed at pH 2.5, and **[^{68}Ga.L^{6}]$_{4.0\text{-}7.0}$** indicates that the radiolabelled complex was formed at pH 4.0, 5.3 or 7.0.

The protocol used to evaluate the stability of **[^{68}Ga.L^{6}]** and **[^{68}Ga.L^{8}]** was exactly the same as that described for **[^{68}Ga.L^{6}]** and **[^{68}Ga.L^{8}]** (Chapter 2 Section 2.3). Briefly, the stability of the radiolabelled complexes was tested in a series of challenge experiments with DTPA (5000-fold excess), Fe(III) (5000-fold excess), *apo*-transferrin (130-fold excess) and in newborn calf serum. All solutions were prepared in 1.0 M PBS solutions, and the stability evaluations were carried out at physiological pH (7.4) and temperature (310 K). The relative amount of the intact radiolabelled complex and free ^{68}Ga was determined at 10, 20, 30, 60, 90 and 120 min, using a radio-TLC method with 0.5 M sodium citrate (pH 4) as the eluting solvent. Stability evaluations were performed in triplicate for each radiolabelled complex synthesised at pH 2.3, 4.0, 5.3 and 7. Two control experiments were performed in every case; one in the absence of the ligand, and the other in the absence of the challenge.

The stability of each complex with respect to the *apo*-transferrin challenge experiment is summarised in Table 3.2. No evidence of instability was observed for any of the radiolabelled complexes during the Fe(III), newborn calf serum and DTPA challenge experiments.

Table 3.2 *Stability of the investigated ^{68}Ga-radiolabeled ligands at 120 minutes in a competition experiment in the presence of 130-fold excess apo-transferrin. Challenge experiments were conducted at physiological pH (7.4) and temperature (310 K).*

pH at which radiolabelled complex was synthesised	Percentage of Radiolabel/s intact after 120 min (%)			
	$[^{68}Ga.L^{2}]$	$[^{68}Ga.L^{3}]$	$[^{68}Ga.L^{6}]$	$[^{68}Ga.L^{8}]$
2.3	10	8	19	47
4.0	95	97	97	98
5.3	95	98	99	96
7.0	93	94	97	99

Considering first $[^{68}Ga.L^{6}]_{2.5}$ and $[^{68}Ga.L^{8}]_{2.5}$, a significant degree of instability was observed in each case. Careful examination of the interval data and relative proportions of the radiolabelled species shows that the major radiolabelled species only was unstable, whilst the minor species remained completely intact. Overall $[^{68}Ga.L^{6}]_{2.5}$ and $[^{68}Ga.L^{8}]_{2.5}$, had 19 and 47 % of the combined radiolabelled ligand species intact after 120 min, respectively. This is in agreement with the results obtained for $[^{68}Ga.L^{2}]_{2.5}$, where the major isomer was exclusively unstable in the presence of *apo*-transferrin.

For the ligands L^{2}, L^{3}, L^{6} and L^{8} there is an apparent higher stability of the radiolabelled complexes formed at pH 2.5 from ligands which feature the APPED core. The relative ratios of the radiolabelled complex isomers for each ligand, formed at pH 2.5, suggests that the observed increase in stability arises from an increase in the relative proportion of the more stable species, i.e. the methyl-phenyl permutation has resulted in an increase in the amount of the more stable isomer formed.

No evidence (i.e. there was no noticeable evidence of ^{68}Ga signal greater than background activity, other than that of the complex) for complex instability was observed for the radiolabelled complexes $[^{68}Ga.L^{6}]_{4.0\text{-}7.0}$ and $[^{68}Ga.L^{8}]_{4.0\text{-}7.0}$ over 2 hours in all of the stability challenge experiments. The radiolabelled complexes $[^{68}Ga.L^{6}]_{4\text{-}7.0}$ and $[^{68}Ga.L^{8}]_{4\text{-}7.0}$ have very similar stability profiles to that of $[^{68}Ga.L^{3}]_{4\text{-}7.0}$.

In the case of L^{7}, the rate of radiolabelling at pH 2.3 increased slightly with respect to the AMPED analogue L^{2}, with the ratio of the radiolabelled species formed seemingly unaffected. However, radiolabelling of L^{2} at pH ≥ 4.0 was not quantitative, accompanied by the formation of two radiolabelled species. This is in contrast to L^{2}, where the relative proportion of the radiolabelled

species decreased above pH 4.0, and radiolabelling was quantitative at room temperature within 1 minute.

Modification of the AMPED core by insertion of a phenyl moiety has had differing effects on the radiolabelling efficiency, speciation and radiolabelled complex stability. Positively, the radiolabelling efficiency and stability of $[^{68}Ga.L^{6}]_{4\text{-}7.0}$ and $[^{68}Ga.L^{8}]_{4\text{-}7.0}$ have maintained the high standard set by L^{2} and L^{3}. In addition to this, there has also been an improvement in the speciation and stability of $[^{68}Ga.L^{6}]_{2.3}$ and $[^{68}Ga.L^{8}]_{2.3}$ compared to $[^{68}Ga.L^{3}]_{2.3}$. Unfortunately, the formation of multiple radiolabeled species, and resulting instability, associated with $[^{68}Ga.L^{6}]_{2.3}$ and $[^{68}Ga.L^{8}]_{2.3}$ means that the ligands L^{6} and L^{8} are unsuitable for ^{68}Ga-radiolabelling under these more acidic conditions. Thus, the useful pH range for radiolabelling is 4.0 – 7.0.

3.3 Trends in Speciation of the ^{68}Ga-Radiolabelled Complexes

From the results discussed in chapter 2, it was evident that there was a correlation between the formation/presence of multiple radiolabelled complex species for a given ligand and the steric bulk at the exocyclic amine, for radiolabelling in the pH range 4.0 – 7.0. Indeed a single radiolabelled complex species was observed for the mono-N_{exo}-functionalised ligand L^{3}. In addition, there was a general increase in the proportion of a second 'unstable' radiolabelled complex species with increasing steric bulk at the N_{exo} (chapter 2).

Competition between the methyl and N_{exo} groups for the equatorial position in the seven membered heterocyclic ring was thought to be associated with formation of radiolabelled constitutional isomers based on different conformations of the ligand. It was thought that the increased steric demand of N_{exo} caused it to prefer an equatorial orientation, disfavouring formation of the more stable chair-like conformation. The key hypothesis was that by increasing the steric demand at the quaternary carbon site, the N_{exo} group would be 'pushed' into an 'axial' position, which allows the nitrogen lone pair to bind to the metal cooperatively with the endocyclic nitrogens.

In good agreement with this hypothesis, it was observed that the radiolabelled complex speciation and stability profile of $[Ga.L^{6}]_{2.3}$ and $[Ga.L^{8}]_{2.3}$ was better than that of the AMPED derivatives $[Ga.L^{2}]_{2.3}$ and $[Ga.L^{3}]_{2.3}$, with introduction of the phenyl group promoting formation of the more stable radiolabelled species. This effect was not observed for ligand L^{7}, where the ratio appears to approximately the same as its AMPED based analogue ligand L^{2}. However, care should be taken with

an interpretation since the stability of **[Ga.L^7]$_{2.5}$** has not been determined, and thus whether the ratio of stable to unstable isomers is the same or been reversed, i.e. It is possible that the minor isomer of **[Ga.L^7]$_{2.5}$** is unstable, whilst the opposite was observed for **[Ga.L^2]$_{2.5}$**.

Multiple radiolabelled species were not observed for **[Ga.L^6]$_{4\text{-}7.0}$** and **[Ga.L^8]$_{4\text{-}7.0}$**. However this was not the case for **[Ga.L^7]$_{4\text{-}7.0}$**, for which the speciation profile and kinetics of radiolabelling got worse as the labelling pH was increased.

3.4 Further Radiochemical Evaluation of L^6 and L^8: Competition and Concentration Studies

Each evaluation reported in this section was carried out in exactly the same manner as those described in Chapter 2 Section 3.5. Specifically, each evaluation was performed at 298 K and pH 4 (0.2 M acetate buffer).

3.4.1 NOTA Competition

Equimolar amounts (20 μM) of NOTA and the ligand of interest (**L^6** or **L^8**) were premixed in 1 mL of 0.2 M acetate buffer (pH 4), and radiolabelled with ~ 100 MBq ^{68}Ga (0.66 nM). The relative ratio of [Ga.NOTA] and **[Ga.L^n]** determined at 1, 3, 5, 10 and 120 min time intervals. All available ^{68}Ga(III) was complexed within 1 minute, and no change to relative proportions of the radiolabelled complexes was detected over 2 hours at room temperature (at pH 4.0 and 7.4). This indicates that no trans-chelation had taken place, and the complexes are kinetically stable (under these conditions). Ligand **L^6** chelated 76 % of the available radioactivity, whilst **L^8** accounted for 53 %, with NOTA making up the difference in each case. Of the ligands evaluated thus far (i.e. **L^2**, **L^3**, **L^6** and **L^8**), **L^6** shows the fastest radiolabelling kinetics, as determined by this challenge experiment, with a rate three times faster than that of NOTA under the given conditions. Ligands **L^3** and **L^8** display the slowest rate of radiolabelling. This may be a consequence of the reduced 'mobility' of the carbocyclic arms due to steric inhibition involving rearrangement of the propionate substituents. The fast ^{68}Ga-radiolabelling kinetics of NOTA has been attributed to the pre-organisation of the ring conformation and associated donor groups to ^{68}Ga-complexation. The fact that **L^6** displays such fast radiolabelling kinetics (relative to the other AMPED based ligands) suggests that the introduction of the phenyl group may have pre-organised the ligand towards ^{68}Ga-complexation. Indeed, the fact that **L^8** labels faster than **L^3** is also consistent with this hypothesis.

3.4.2 Metal Ion Competition

The radiolabelling efficiency of $\mathbf{L^6}$ and $\mathbf{L^8}$ was evaluated in the presence of increasing concentrations of calcium(II), iron(III) and copper(II) as their chloride salts. The standard labelling protocol at pH 4 was applied, i.e. $[L^n]$ = 10 µM, $[^{68}Ga]$ = 0.66 nM ~ 100 MBq, V_{tot} = 1.4 mL, 10 min.

A tolerance to added Ca(II), similar to that of ligands $\mathbf{L^2}$ and $\mathbf{L^3}$, was observed for ligands $\mathbf{L^6}$ and $\mathbf{L^8}$, with concentrations of 8.0 M having no effect on the radiolabelling kinetics. This is 4000 times fold the concentration of Ca(II) *in vivo*.[22] Quantitative radiolabelling of $\mathbf{L^6}$ and $\mathbf{L^8}$ was achieved within 10 minutes in the presence of 4 equivalents of Fe(III) with respect to the concentration of the ligand. The degree of radiolabelling decreased to approximately 70 and 55 % in the presence of 5 and 10 equivalents of Fe(III) respectively. Ligands $\mathbf{L^6}$ and $\mathbf{L^8}$ were more sensitive to the presence of added Cu(II) than the AMPED based ligands tested. No radiolabelled complex was formed after 10 minutes in the presence of one equivalent of Cu(II), with respect to the ligand. However, each ligand radiolabelled quantitatively when the amount of Cu(II) was reduced to 0.75 equivalents. This equates to ~1.1×10^6 times more copper(II) than ^{68}Ga(III), indicating that there is a high degree of selectivity of the ligands for gallium(III) over copper(II) under these conditions. As an indication of the relative amount of ^{68}Ga present; the ligand is in a ~ 1.5×10^4 fold excess (assuming ^{68}Ga : $\mathbf{L^n}$ is 1 : 1 in the complex).

It is interesting to note that $\mathbf{L^6}$ and $\mathbf{L^8}$ apparently display a higher affinity for Cu(II), but lower sensitivity to Fe(III), compared to the AMPED based ligands.

3.4.3 Dependence of Radiolabelling Yield on Ligand Concentration

The influence of ligand concentration on radiolabelling with ~ 100 MBq ^{68}Ga (0.66 nM) was investigated over 10 min at 298 K and pH 4 (0.2 M acetate buffer) using the standard protocol.

Ligands $\mathbf{L^6}$ and $\mathbf{L^8}$ displayed quantitative radiolabelling within 10 minutes at a ligand concentration of 7.0 µM. At 3.5 µM ligand, the radiolabelling yields for $\mathbf{L^6}$ and $\mathbf{L^8}$ decreased to 51 and 80 % respectively, whilst no radiolabelled complex was observed for either ligand at 1.0 µM. Further experiments to accurately determine the limiting ligand concentrations (lowest concentration of the ligand able to give a quantitative yield under these conditions) have not been carried out. These values indicate that there is a greater dependence of the rate of radiolabelling on the ligand

concentration for **L^6** and **L^8** than for the AMPED based ligands **L^2** and **L^3**. These values compare favourably with the acyclic chelator CP256[18], which displays the lowest limiting concentration for quantitative ^{68}Ga radiolabelling in literature (10 µM, 298 K, pH 6.4, 10 min).

4 Preliminary *in vivo* Biological Examination of [^{68}Ga.L^2] and [^{68}Ga.L^8]

Preliminary investigations of the *in vivo* behaviour of radiolabelled complexes **[^{68}Ga.L^2]** and **[^{68}Ga.L^7]** have been carried out in male Spargue Dawley rats, along with [^{68}Ga.NOTA] for comparison. Dynamic, whole body and static brain autoradiography scans have been performed for each radiolabelled complex.

The data collected for the dynamic and brain scans of **[^{68}Ga.L^8]** failed to reconstruct, due to a corrupt data file. Furthermore, the rats used in the in vivo assessment of **[^{68}Ga.L^8]**, were considerably heavier than those used for **[^{68}Ga.L^2]** and [^{68}Ga.NOTA]. Therefore, the *in vivo* studies of **[^{68}Ga.L^2]** and [^{68}Ga.NOTA], are discussed separately from **[^{68}Ga.L^8]**.

4.1 µ-PET of [^{68}Ga.L^2] and [^{68}Ga.NOTA]

The radiolabelled complexes of **[^{68}Ga.L^2]** and [^{68}Ga.NOTA] were synthesised at pH 4.0 using the standard protocols described previously, and the pH adjusted to 7 using 0.1 M aqueous sodium hydroxide. Each radiolabelled complex was injected into two rats (~ 23 MBq, made up to 500 – 700 µL with 0.9 % saline solution) weighing between 330 and 380 g.

The dynamic scans confirm fast renal excretion of the radiolabelled complexes in both each case (Figure 3.7(i)). In the first frames (0 – 20 s), the radioactivity injection is visible by the high levels of the inferior vena cava, with simultaneous increasing uptake in the kidneys. Accumulation of [^{68}Ga.NOTA] in the kidneys occurs slightly faster than **[^{68}Ga.L^2]**, with the subsequent excretion to the bladder occurring at a slower rate. This is supported by the time averaged counts for the bladder (Figure 3.7(i)). In the last frames of 180 - 240 s for **[^{68}Ga.L^2]**, the final renal excretion to the bladder is marginally visible by the radioactivity in the ureter.

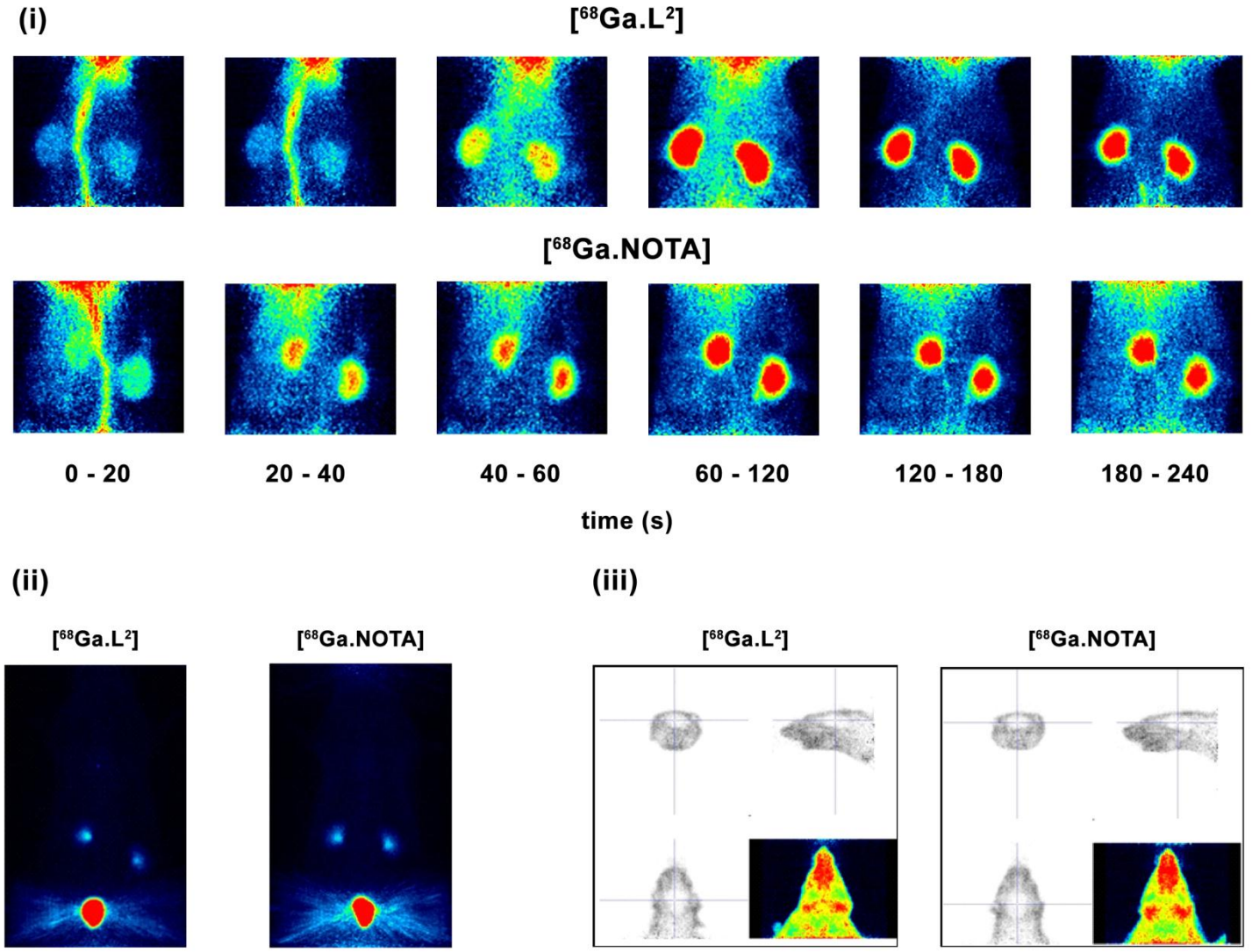

Figure 3.7 *in vivo ^{68}GA μ-PET scans following injection of ^{68}Ga labelled ligands L² and NOTA. Figure shows; (i) dynamic scans at various time intervals from 0 – 240 s postinjection, (ii) full body scans with the bladder (red) and kidneys (blue) visible, (iii) static brain scan showing accumulation in the nose and behind the eyes (red), and absencein the brain (white spot).*

Whole body scans were recorded 10 min post-injection, for a duration of 15 min (Figure 3.7(ii)). The full body scans for **[^{68}Ga.L^{2}]** and [^{68}Ga.NOTA] show strong accumulation in the bladder as a result of fast renal excretion. The very high radioactivity in the bladder prevents visualisation of any other structure or organs except the kidneys, which are slightly visible. This biodistribution profile demonstrates that the ^{68}Ga is not released from the radiolabelled complexes *in vivo*. Injection of unchelated ^{68}Ga usually results in the distribution of radioactivity throughout the whole animal, resulting from complexation by naturally occurring transferrin.[18]

Static scans of the brain were collected for the first 25 min post injection (Figure 3.7(iii)). Both radiolabelled complexes showed uptake in the nose tissue and Harderian glands behind the eyes; behaviour which is frequently observed for radiolabelled complexes. The uptake is considered non-specific, and the mechanism still awaits clarification. There was no observable uptake in the brain, as indicated by the white spot in brain region on the grayscale images.

The *in vivo* stability of **[^{68}Ga.L^{2}]** was supported by two features: its similarity to the biodistribution profile of the exceptionally stable [^{68}Ga.NOTA], the absence of any observable bone uptake, which is known to be a site of accumulation for weakly chelated gallium.[18, 23]

4.2 μ-PET of [^{68}Ga.L^{8}]

Assessment of **[^{68}Ga.L^{8}]** in vivo was carried out in two rats weighing 430 and 440 g. The first rat was injected with 31 MBq of **[^{68}Ga.L^{8}]** (made up to 800 μL with 0.9 % saline) synthesised at pH 4.0 (0.1 M acetate buffer), and adjusted to pH 7 using 0.1 M aqueous sodium hydroxide. The second rat was injected with 34 MBq of **[^{68}Ga.L^{8}]** (made up to 900 μL with 0.9 % saline) synthesised at pH 7.0 (1.0 M HEPES solution). In each case, the radiolabelled complexes were synthesised according to protocols described previously.

Whole body scans were recorded at 10 min post injection. Similar to **[^{68}Ga.L^{2}]** and [^{68}Ga.NOTA] there is substantial accumulation in the bladder and the absence of any observable bone uptake, indicating that in both cases the integrity of the radiolabelled complex is maintained *in vivo*. In both evaluations there is also evidence of, comparably much lower, accumulation at another site in the abdomen where the kidneys are expected to be found (Figure 3.8). In both **[^{68}Ga.L^{8}]** rats studies there was a single lower accumulation site instead of two as would be expected for kidney accumulation. Co-localisation in both kidneys was observed for **[^{68}Ga.L^{2}]** and [^{68}Ga.NOTA]. Further

studies are needed to fully characterise this accumulation. Interestingly, the accumulation occurs on opposite flanks in the two studies conducted. Furthermore, both $[^{68}Ga.L^{8}]_{4.0}$ and $[^{68}Ga.L^{8}]_{7.0}$ have shown similar *in vivo* behaviour suggesting that speciation is the same despite the different radiolabelling conditions. This is consistent with the results of the radiolabelling experiments.

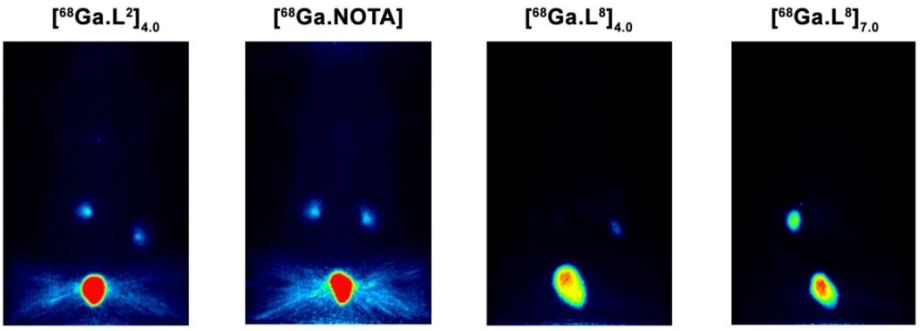

Figure 3.8 *in vivo ^{68}GA μ-PET full body scans 10 min post injection of ^{68}Ga labelled ligands **L²**, NOTA and **L⁸** (radiolabelled at pH 4.0 and 7.0). Full body scans of [^{68}Ga.NOTA] and **[^{68}Ga.L²]** show bladder and kidney accumulation. **[^{68}Ga.L⁸]** radiolabels accumulate in the bladder, and show additional retention in a region where the kidneys are expected to be located. Only one additional accumulation site is detected in each, which precludes a conclusive assignment.*

5 Summary

In Chapter 2, it was shown that ligand **L³** is a very promising candidate for ^{68}Ga-PET studies, with near ideal radiolabelling, complex speciation and stability profiles. However, the results suggested that synthesised and potential ligands were limited by their propensity to undergo internal lactamisation under acidic conditions. These inherent properties limit the ligands use both synthetically and in application.

The introduction of a phenyl substituent at the quaternary carbon, addresses some of the issues associated with ligand stability. Thus, **L⁶**, whose AMPED analogue was unstable with respect to lactamisation, was synthesised and could be used to form radiolabelled complexes. The two ligands **L⁶** and **L⁸**, which feature the modified core, give rise to stable, single radiolabelled complex species that form within 3 minutes at room temperature over the pH range 4.0 – 7.0. In addition to this, remarkable radiolabelling resilience was shown to the presence of added NOTA, iron(III), copper(II) and calcium(II) in μM concentrations (i.e., greatly exceeding the 0.66 nM concentration of ^{68}Ga).

Furthermore, the radiolabelled complexes were stable with respect to trans-complexation by NOTA over 2 hours at pH 4 and 7.4.

In agreement with the hypothesis, introduction of the phenyl group had a positive impact on the speciation and stability of radiolabelled complexes formed at pH 2.3 (for ligands with a mono-substituted exocyclic amine). Despite this improvement, radiolabelled complex speciation and stability is still a problem. This precludes their use for *in vivo* application following synthesis at pH 2.3. Unexpectedly, radiolabelled complexes formed using ligands with a di-substituted exocyclic amine displayed worse speciation and stability as a result of the introduction of the phenyl group. This suggests that there are other factors influencing the speciation of the radiolabelled complexes beyond competition for the equatorial site at the quaternary ring carbon.

The ligands featuring the modified APPED core offer an improvement on the AMPED based ligands. The structural modification has not been to the detriment of the radiolabelling properties of the mono-substituted exocyclic amine ligands nor their radiolabelled complex stabilities, and has improved the stability of the free ligands towards lactamisation. Of additional benefit, the synthetic methodology used to make these ligands is more selective, thereby allowing greater synthetic versatility.

Ligands featuring the modified APPED scaffold and a mono-substituted amine are better overall than their AMPED analogues, and compare favourably with the most promising literature compounds (including TRAP[20, 24, 25], CP256[18], H_2DEDPA[17, 23] and HBED[21] – see Section 3.2.2 of Chapter 2 for specific detail and structures). The rate of ^{68}Ga incorporation by $\mathbf{L^n}$ (n = 2, 3, 6, 8) is greater, at lower temperatures and concentrations, than established ^{68}Ga-PET ligands, DOTA[24, 26] and NOTA.[24, 27] The unique feature of these ligands is their ability to radiolabel over a wide pH range, which includes pH 7.0, within 3 minutes at room temperature, using comparably low concentrations of the ligands.

Assessment of **[^{68}Ga.L^n]** (n = 2 and 8) *in vivo* in rats, confirmed the *in vitro* stability studies, with renal clearance and rapid excretion to the bladder 10 minutes post injection.

6 References

1. E. V. Anslyn and D. A. Dougherty, *Modern Physical Organic Chemistry*, Univeristy Science Books, U.S.A, 2006.
2. L. Manzoni, L. Belvisi, D. Arosio, M. P. Bartolomeo, A. Bianchi, C. Brioschi, F. Buonsanti, C. Cabella, C. Casagrande, M. Civera, M. De Matteo, L. Fugazza, L. Lattuada, F. Maisano, L. Miragoli, C. Neira, M. Pilkington-Miksa and C. Scolastico, *Chemmedchem*, 2012, **7**, 1084-1093.
3. R. S. Sengar, A. Nigam, S. J. Geib and E. C. Wiener, *Polyhedron*, 2009, **28**, 1525-1531.
4. E. Gianolio, K. Ramalingam, B. Song, F. Kalman, S. Aime and R. Swenson, *Inorganic Chemistry Communications*, 2010, **13**, 663-665.
5. G. Gugliotta, M. Botta and L. Tei, *Organic & Biomolecular Chemistry*, 2010, **8**, 4569-4574.
6. E. Gianolio, G. B. Giovenzana, D. Longo, I. Longo, I. Menegotto and S. Aime, *Chemistry-a European Journal*, 2007, **13**, 5785-5797.
7. US Pat., 07988950, 2011.
8. S. Aime, L. Calabi, C. Cavallotti, E. Gianolio, G. B. Giovenzana, P. Losi, A. Maiocchi, G. Palmisano and M. Sisti, *Inorg Chem*, 2004, **43**, 7588-7590.
9. B. Koop, S. N. Reske and B. Neumaier, *Radiochimica Acta*, 2007, **95**, 39-42.
10. P. Nussbaumer, K. Baumann, T. Dechat and M. Harasek, *Tetrahedron*, 1991, **47**, 4591-4602.
11. T. J. Atkins, J. E. Richman and W. F. Oettle, *Organic Syntheses*, 1988, **50-9**, 652-662.
12. K. Wieghardt, W. Schmidt, B. Nuber and J. Weiss, *Chemische Berichte-Recueil*, 1979, **112**, 2220-2230.
13. R. Ballini, L. Barboni and G. Giarlo, *Journal of Organic Chemistry*, 2004, **69**, 6907-6908.
14. M. P. Crozet, S. Lapouge, M. Kaafarani and P. Vanelle, *Tetrahedron Letters*, 1994, **35**, 3055-3058.
15. J. O. Osby and B. Ganem, *Tetrahedron Letters*, 1985, **26**, 6413-6416.
16. M. Go, T. Ngiam and A. S. C. Wan, *Journal of Medicinal Chemistry*, 1981, **24**, 1471-1475.
17. E. Boros, C. L. Ferreira, J. F. Cawthray, E. W. Price, B. O. Patrick, D. W. Wester, M. J. Adam and C. Orvig, *J Am Chem Soc*, 2010, **132**, 15726-15733.
18. D. J. Berry, Y. Ma, J. R. Ballinger, R. Tavare, A. Koers, K. Sunassee, T. Zhou, S. Nawaz, G. E. Mullen, R. C. Hider and P. J. Blower, *Chem Commun*, 2011, **47**, 7068-7070.
19. J. Notni, K. Pohle, J. A. Peters, H. Gorls and C. Platas-Iglesias, *Inorg Chem*, 2009, **48**, 3257-3267.
20. J. Simecek, M. Schulz, J. Notni, J. Plutnar, V. Kubicek, J. Havlickova and P. Hermann, *Inorg Chem*, 2012, **51**, 577-590.
21. M. Eder, B. Wangler, S. Knackmuss, F. LeGall, M. Little, U. Haberkorn, W. Mier and M. Eisenhut, *Eur J Nucl Med Mol Imaging*, 2008, **35**, 1878-1886.
22. S. C. Conceicao, D. Weightman, P. A. Smith, J. Luno, M. K. Ward and D. N. S. Kerr, *British Medical Journal*, 1978, **1**, 1103-1105.
23. E. Boros, C. L. Ferreira, B. O. Patrick, M. J. Adam and C. Orvig, *Nucl Med Biol*, 2011, **38**, 1165-1174.
24. J. Notni, K. Pohle and H. J. Wester, *EJNMMI Res*, 2012, **2**, 28.
25. J. Notni, P. Hermann, J. Havlickova, J. Kotek, V. Kubicek, J. Plutnar, N. Loktionova, P. J. Riss, F. Rosch and I. Lukes, *Chem Commun*, 2010, **16**, 7174-7185.
26. G. J. Meyer, H. Macke, J. Schuhmacher, W. H. Knapp and M. Hofmann, *European Journal of Nuclear Medicine and Molecular Imaging*, 2004, **31**, 1097-1104.
27. I. Velikyan, H. Maecke and B. Langstrom, *Bioconjug Chem*, 2008, **19**, 569-573.

Chapter 4

Conformational Analysis of the Ring, and 'Cold' Gallium(III) Complexes

In this Chapter the trends observed in the radiochemical experiments are rationalised, and the structures of the 'cold' gallium complexes are investigated. Specifically, in section one, the rates of radiolabelling, radiolabelled complex speciation and their stability is addressed. In section two, crystallographic and NMR data are used to assess the influence of the phenyl substituent on the ring conformation in comparison to the analogous AMPED system. In section three, NMR spectroscopic and crystallographic data are used to discuss the 'cold' gallium complexes of the preferred ligands.

1 Conformational Analysis of the 7-Membered Ring

The radiolabelling studies detailed in Chapters 2 and 3 indicated that the most favourable chelators are those which possess a mono-substituted exocyclic amine. In fact, the results showed that further substitution resulted in a lower stability of the radiolabelled species, and was also directly linked to the formation of multiple radiolabelled species. Furthermore, there was a considerable decline in the forward rate of labelling and in the dissociative stability of the radiolabelled complexes, when labelling was carried out at pH < 3.5. At this pH, the diprotonated species is almost exclusively present. The pK_a which precedes formation of this species is assigned to protonation of the exocyclic amine, with deprotonation of this species to give mono-N-protonated species beginning at pH ~ 4 (Chapter 2 Section 2). Indeed, protonation of this group is expected to have a marked effect on the labelling kinetics, because the presence of the positive charge makes complexation more difficult. However, it does not explain why when the ligands were labelled at pH < 3.5 the stability of the radiolabelled complexes is compromised, and in some cases multiple radiolabelled species were observed. Notably, this was a problem for ligands based on AMPED, and to a lesser extent for ligands based on the APPED (Figure 4.1).

The conformational flexibility of saturated heterocyclic 7-membered rings is well documented, as are the ring substituent effects on the relative energy of the preferred conformers.[1-5] It is evident from the labelling studies that substituents at the N_{exo} position are playing an important role on radiolabelled complex stability and, presumably, on ligand conformation in solution. Understanding

these substituent effects and the different conformations is an important step in developing better ligands for use in ^{68}Ga-PET.

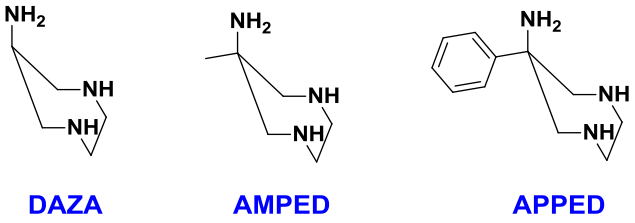

Figure 4.1 *Structures, and abbreviated names, of tri-amine ligands to which reference is made in the text.*

In Chapter 3 Section 2, it was shown that the presence of a phenyl group at the quaternary carbon of the ring had resulted in a significant decrease in the reactivity of N_{exo}. This decrease in reactivity is directly related to the increase in steric bulk about the quaternary carbon imparted by the phenyl group. An important consideration of the novel APPED core is the influence that the modification at this carbon has on the orientation of the ring substituents and the preferred conformation adopted by the ring. In this chapter, crystallographic and NMR data are used to assess the influence of the phenyl substituent on the conformation of the ring and ring substituent orientation, with comparison to the analogous AMPED system.

1.1 Cycloheptane to Diazepine

In the case of cycloheptane, the low energy conformations are made up of a series of twisted-chair (TC) and chair (C) conformations with relatively small energy barriers to the ring puckering which link conformers of the same family (Figure 4.2). The TC-conformation of cycloheptane is most favoured, and has a single unique isoclinal position as well as three distinct pseudo-axial and pseudo-equatorial positions.[2, 3, 6]

Figure 4.2 *Possible conformations of cycloheptane and other 7-membered rings. Chair and twisted-chair conformers are of lower energy than the boat and twisted-boat conformers.*

A preference towards a TC conformation is also observed for 1,4-diazepane (such as those studied here), of which there are four possibilities. The introduction of an exocyclic amine at the 1-position lowers the overall symmetry of the ring, and as a result increases the number of possible TC-conformers further.[2, 4] Due to the presence of destabilizing non-bonding interactions, arising from the eclipsed conformation of the N-CH_2-CH_2-N fragment, neither chair nor boat conformations are observed for 1,4-diazepane rings of free ligands.[2-4] In fact, Hegetschweiler noted that often the low stability of complexes containing ligands based on the DAZA core is a result of the unfavourable eclipsed orientation which is required for tri-dentate coordination of the DAZA core.[6, 7] Thus, strictly speaking, for the free ligands the chair and boat conformations exist only as high energy transition states.[2, 4] For free ligands based on the DAZA core, where the exocyclic amines have the same functionalisation and R^1 is variable, there are seven possible TC-conformers (Figure 4.3).

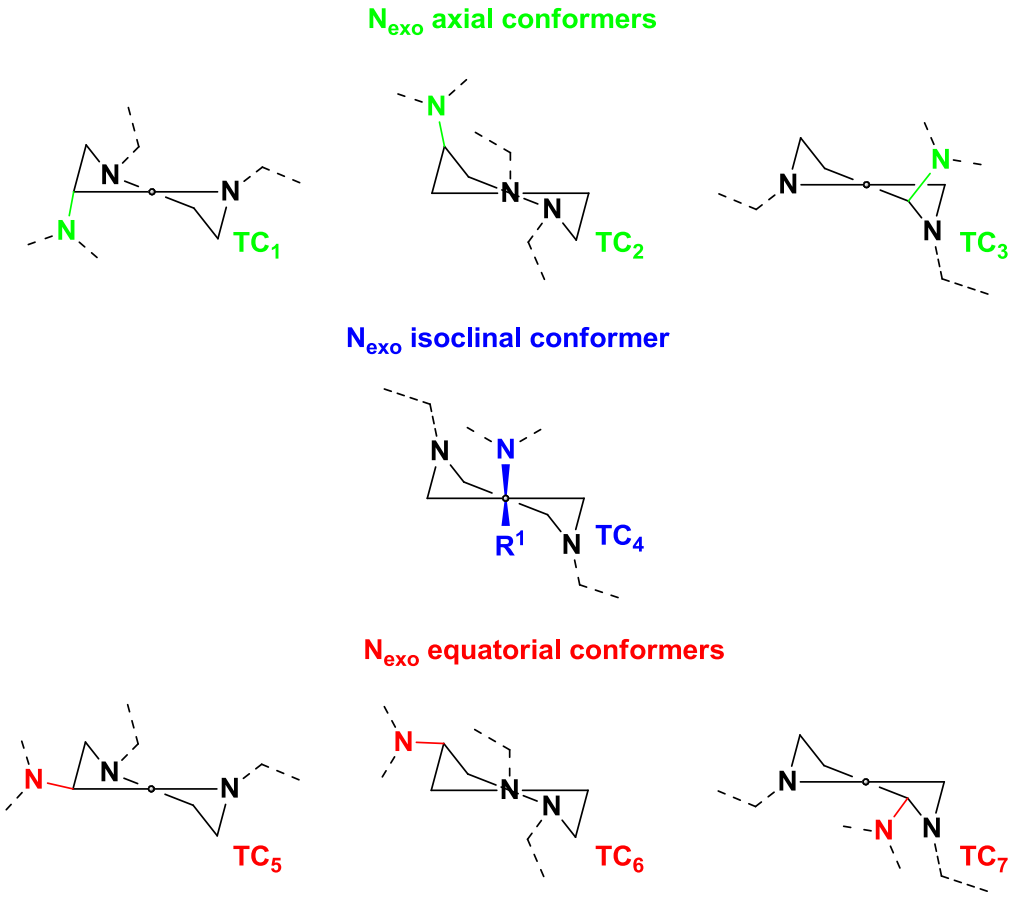

Figure 4.3 *Possible conformers of 6-R_1-6-amino-1,4-diazepane based ligands. Groups attached to the exocyclic amine are identical and arbitrary. Functionalisation of the endocyclic amine is also arbitrary. R^1 is only shown for the 'N_{exo} isoclinal' conformer.*[3, 6]

One of the conformers has the exocyclic amine in an isoclinal position (TC_4), and 3 each with the amine in axial (TC_{1-3}) and equatorial (TC_{5-7}) positions. An axially and equatorially positioned substituent is defined as having deviation (θ) from the mean plane of the ring of $0° \geq \theta \leq 30°$ and $60° \geq \theta \leq 90°$ respectively (where the mean ring plane is determined using all the atoms of the ring). Ring substituents between these two ranges ($30° > \theta < 60°$) are defined as isoclinal substituents.[2]

Hegetschweiler et al published the crystal structure of the triply protonated salts of DAZA and AMPED.[6, 7] In the crystal structure of $(H_3DAZA)^{3+}$, the exocyclic amine adopts an equatorial position in the TC-conformer shown by TC_6.[6] Two crystal structures have been obtained for $(H_3AMPED)^{3+}$ in which the exocyclic amine adopts an isoclinal position or an equatorial position, depicted in TC-conformers TC_4 and TC_7 respectively.[6] The fact that different conformations are observed for AMPED implies there are low energy barriers to exchange between conformers; however an influence of packing interactions cannot be excluded.[6]

In stable metal complexes of these ligands, the seven-membered rings are assumed to exist in a chair-like conformation, with the endocyclic amine occupying an axial orientation in order to allow ligation of the N_{exo}-lone pair, giving rise to a tri-dentate *fac*-N_3 coordination mode. Indeed, such a conformation has been observed for a number of complexes containing tri- and hepta-dentate ligands based on the DAZA core.[6, 8-13] Therefore, in order to produce a stable complex, the free ligand has to be able to populate a higher energy transition state chair conformation. There are two main concerns to accessing this high energy C-conformation. Firstly, the benefits of metal binding must outweigh the unfavourable destabilizing non-bonding interactions arising from the eclipsed nature of the N-CH_2-CH_2-N fragment inherent to the chair conformation preferred for metal binding. Secondly, the exocyclic nitrogen should adopt an axial position in the chair conformation.

It is worth noting at this juncture, that this ligand system behaviour is in stark contrast to the situation with chelators based on 9-N_3; in which the ring is conformationally rigid, with the strain already present in the free ligand. As a result, the conformational strain does not oppose metal binding, and the ligand is described as being pre-organised for metal complexation.[14] Due to the inherent characteristics of 7-membered rings, such pre-organization is not possible; however it is possible to consider some form of pre-orientation. To promote the rapid formation of a stable complex, the free ligand should be in a conformation such that the energy barriers to the desired metal bound chair conformation are kept to a minimum. In the case of DAZA, this involves ensuring that the exocyclic amine adopts an axial position in the free ligand.

The chair-conformer of the ligand which is expected to give rise to stable metal complexes is illustrated in Figure 4.4, C_{eq}, along with its ring inversion product, C_{ax}. The 'ring-flip' equilibrium between C_{ax} and C_{eq} is represented by a dashed line to show that conversion between the two takes place through one of the lower energy TC-conformations, TC_x (Figure 4.3). Which twisted-chair conformation is favoured is determined, in part, by the nature of the ring and N_{exo}-substituents used. In turn, this determines which of the chair conformations is of lowest energy. It is important to re-iterate that in the absence of a metal ion, conformations C_{ax} and C_{eq} are higher energy transition states between different twist-chair conformers. This scheme is meant only to highlight that two chair conformations are possible and are related by a ring inversion. In terms of metal complexation, C_{eq} is preferred because it presents a *fac*-N_3 coordination donor set with the N-substituents (e.g. acetate groups) held in closer proximity. The arrangement of the N-donors in C_{ax} means that, at best, two of the three N-groups could partake in metal binding. It is reasonable to predict that, if the formation of C_{ax} (from the free ligand: TC_x) is energetically more favourable than C_{eq}, then metal complexation by C_{eq} will be hindered. Under such conditions, the inherent structural strain within a $[M^{n+}(C_{eq})^{m-}]^{n-m}$ complex (arising from N_{exo} preferring an equatorial orientation) is expected to have negative implications on the stability of the complex. Therefore, it could be hypothesised that, in order to promote the desired C_{eq} conformer in the metal-ligand complex, a ligand TC-conformation which has the exocyclic amine either isoclinal or axial is preferred, i.e. TC-conformations represented by $TC_{1\text{-}4}$ (Figure 4.3).

In Figure 4.4, TC_x represents possible conformations of the seven-membered ring, with the R_1 and N_{exo} substituents taking up pseudo-axial, pseudo-equatorial or isoclinal positions. There are seven low energy conformations, which exist as energetically equivalent pairs (enantiomers) related by a ring puckering (Figure 4.3). The pair of twist chairs that is most stable, and hence favoured, is determined by the nature of the substituents R^1 and N_{exo}. The chair conformation most likely to form in a metal complex is that which has the lowest energy barrier with the preferred TC-conformer. One of the main factors which control the relative sizes of these energy barriers to the higher energy chair conformations will be the competition between R_1 and N_{exo} for the equatorial position.

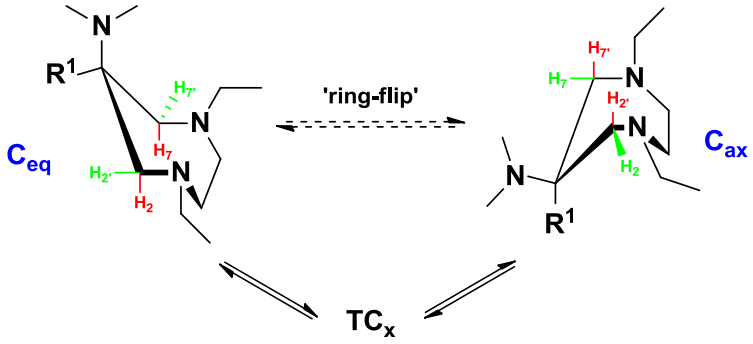

Figure 4.4 *Shows two possible chair conformations (C_{eq} and C_{ax}) for metal bound DAZA based ligands. The ring inversion equilibrium is shown as a dashed line to indicate that the conversion proceeds via a lower energy twisted chair conformer (TC_x). Note: C_{eq} and C_{ax} represent possible conformations of the ligand when bound to a metal. The free ligands will invariably adopt one of the lower energy TC conformations.*

If N_{exo} and R^1 had similar steric demands (or A-values: a measure of the steric bulk of a substituent), then a relatively flexible ring would ensue with a fairly disperse population of TC-conformers; the energy barrier to both chair conformers would be similar. In terms of metal complexation, such a situation is not necessarily unfavourable; however, a certain degree of 'pre-orientation' is beneficial. This is especially true, when it is considered that the N-CH_2-CH_2-N moiety must adopt an unfavourable eclipsed conformation, if the DAZA core is to serve as a tri-dentate ligand.

Simply put, in the absence of other interactions, the substituent with the greater steric demand should prefer to adopt the equatorial site. Thus, the chair conformation C_{eq} in Figure 4.2 will be favoured in the situation where R_1 has a greater A-value than N_{exo}, because its formation is of lower energy than that of C_{ax} from the twisted-chair conformation. Similarly, when N_{exo} is considerably more sterically demanding, it is expected that the energy barrier from the twisted chair (TC_x) to C_{ax} will be lower than that to C_{eq}. The substituent with the greater steric demand will prefer the equatorial position in the TC (and hence chair) conformers, and thus a less disperse conformer set is expected. In the presence of a more sterically demanding substituent, the conformational rigidity of the ring will also be increased.

Hegetschweiler explored suitability of tri-dentate ligands based on the DAZA core for metal ion complexation.[6, 7] They realised the importance of the orientation of N_{exo} in terms of complex formation and stability, and the possible effects of having this substituent in the 'wrong' (equatorial) orientation. They attempted to promote the more favourable axial orientation of the exocyclic

amine, with the aim of improving the metal binding ability of the tri-dentate ligand. Previous research involving TACH, showed that the 'wrong' (or unfavourable) equatorial orientation of the amine substituents could be changed by introduction of strategically placed methyl ring substituents (Figure 4.5).[15-17] The methyl groups of Me_3TACH promoted the axial orientation of the amine ring substituents (Figure 4.5).[6, 7, 16, 17]

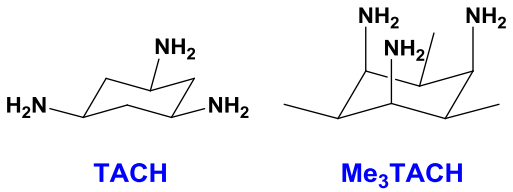

Figure 4.5 *Structures of tri-amine ligands TACH[15] and Me_3TACH[16, 17], showing the preferred orientation of the exocyclic amines at pH > 3. The axial arrangement of the amines in Me_3TACH, is more conducive to metal complexation, and forms a more stable complex.*

Similarly, addition of a methyl substituent at the 1-position of DAZA (to give AMPED) might promote an axial orientation of N_{exo}, and as a result improve the metal binding ability of the ligand.[6] Hegetschweiler's results indicated that although this modification was beneficial, there was only a small gain in the stability of AMPED complexes compared to the DAZA analogues.[6] Whilst the ligands described in this thesis are considerably different, in that they are hexa- and hepta-denate, they possess the same DAZA core as those described by Hegetschweiler. Thus, it was expected that similar principles would apply. Of course, the oxygen donors of the ligands reported here will assist with metal ion complexation, perhaps making the formation of metal-ligand complexes more favourable. Indeed, the results presented in Chapter 2 and 3 suggest that this is the case.

1.2 Influence of pH on Radiolabelling and Radiolabelled Complex Speciation

At low pH (< 3.5) the rate of labelling of the AMPED ligands deteriorated significantly, and in all cases the stability of the radiolabelled complexes was compromised. Obviously, deprotonation must precede formation of the M—N bond, and low pH slows complexation down as the proportion of the free amine decreases. However, there is a further factor relating to the relative steric bulk of R_1 and N_{exo} which should also be considered. According to the pK_a curve for methylated triacid AMPED ligand $\mathbf{L^2}$ (Chapter 2 Section 2), deprotonation of the exocyclic amine starts at pH ~ 4 and the equilibrium between the mono- and di-protonated ligand species is controlled by a pK_a of 5.7 (± 0.1).

When protonated, the A-value for the N_{exo}-substituent will increase from about 6 to 10 kJ/mol, in polar media, as the protonated N-H group can serve as a good H-bond donor to water molecules, increasing the local solvation shell.[18]

For ligands based on the AMPED core, at pH > 4 the R^1 (methyl) and N_{exo} (NR_XR_Y) substituents can be considered to have comparable A-values of 7 and 6 kJ/mol respectively.[18] Thus each complex conformer is likely to be populated significantly as they have comparable energies in their chair conformations.

The forward rate of radiolabelling and the subsequent radiolabelled complex stability observed at pH ≥ 4 are relatively high, whilst at pH < 3.5, both the rate of radio-labelling and the stability diminish significantly. Under these conditions N_{exo} becomes completely protonated and its A-value can be estimated to increase to 10 kJ/mol.[18] As a result, the desired chair conformation is no longer that of lowest energy. The ligand may still bind the metal in the C_{eq} conformation; however this would be in competition a lower energy C_{ax} conformation. This internal conflict, between the favoured conformation required by the metal (i.e. that conformation which allows for fast radiolabelling and the formation of stable complexes) and the lower energy conformation of the ligand, may have a negative impact on the stability of the complex formed, complex speciation and rate of ligand radiolabelling.

The relative population of the two conformers can be estimated using the Boltzmann population distribution equation – (1).

$$\frac{n_1}{n_2} \propto e^{-\left(\frac{\Delta E}{kT}\right)} \qquad (1)$$

kT^{298K} ~ 2.5 kJ/mol and $\Delta E^{pH < 3.5}$ ~ - 4 kJ/mol

$$\frac{n(C_{eq})}{n(C_{ax})} \sim 5 \text{ for pH} < 3.5$$

It is evident that the larger A-value of the N_{exo} substituent results in a significant preference for the less favoured conformer (C_{eq}). The A-values of the quaternary carbon substituents are not significantly different, and as a consequence the conformers are expected to have similar energies.

However, the rate of exchange between complex conformers C_{eq}-C_{ax} is controlled by an energy barrier, which must be crossed in order for the conformers to interchange. The size of the energy barrier is of upmost importance. A small energy barrier would allow for rapid interconversion of conformers and thus formation of the more favoured C_{eq} radiolabelled complex species would be disfavoured, i.e. complexation in the favoured ligand conformation would be able to rapid interconvert to the more favourable ligand conformation which has N_{exo} axially orientated. If the barrier to interconversion is large then the complex is essentially kinetically trapped with the bound ligand in the C_{ax} conformation, which prevents interconversion/rearrangement to the desired C_{ax} complex species.

At low pH (< 3.5) the ligands are present exclusively as the diprotonated species, with a proton on the exocyclic amine and the other forming a bifurcated hydrogen bond across the endocyclic amines. In this form, the ligand can be considered to approximate a metal complex of the ligand in the C_{eq} conformation. Specifically, the bifurcated proton mimics/models the presence of a metal ion by restricting motion in the region of the ethylene diamine bridge (N-CH_2-CH_2-N).

The energy barrier to C_{ax}-C_{eq} complex interconversion can be approximated using dynamic variable temperature ^{1}H NMR studies of ligand **L^2** at pH < 3.5, and these have been performed over the temperature range 298 – 358 K (See Figure 4.6).

The exchange between ligand conformers in which the substituents of the quaternary carbon exchange orientations is expected to proceed via a 'ring inversion'. This hinges about the C_2 and C_7 carbon atoms, i.e. inversion of the position C_2-C_1-C_7 fragment of the ring (Atom labelling scheme on Figure 4.7). Consistent with this axial-equatorial exchange of the quaternary carbon substituents, the diastereotopic protons of C_2 and C_7 also exchange orientations (Figure 4.7). The diastereotopic protons at C_2 and C_7 form a *AA'BB'*-doublet (Figure 4.6) at room temperature. As the temperature of a solution of the ligand is increased the rate of conformer exchange increases, and eventually a high energy transition state is achieved between the lower energy conformers. At this point, the two conformers are in rapid exchange on the NMR timescale, and as a result the protons of C_2 and C_7 are also rapidly exchanging orientations. This is manifested as a coalescence of the *AA'BB'*-doublet, and is an approximation of the energy required for ring-inversion, leading to conformer exchange (Figure 4.7).

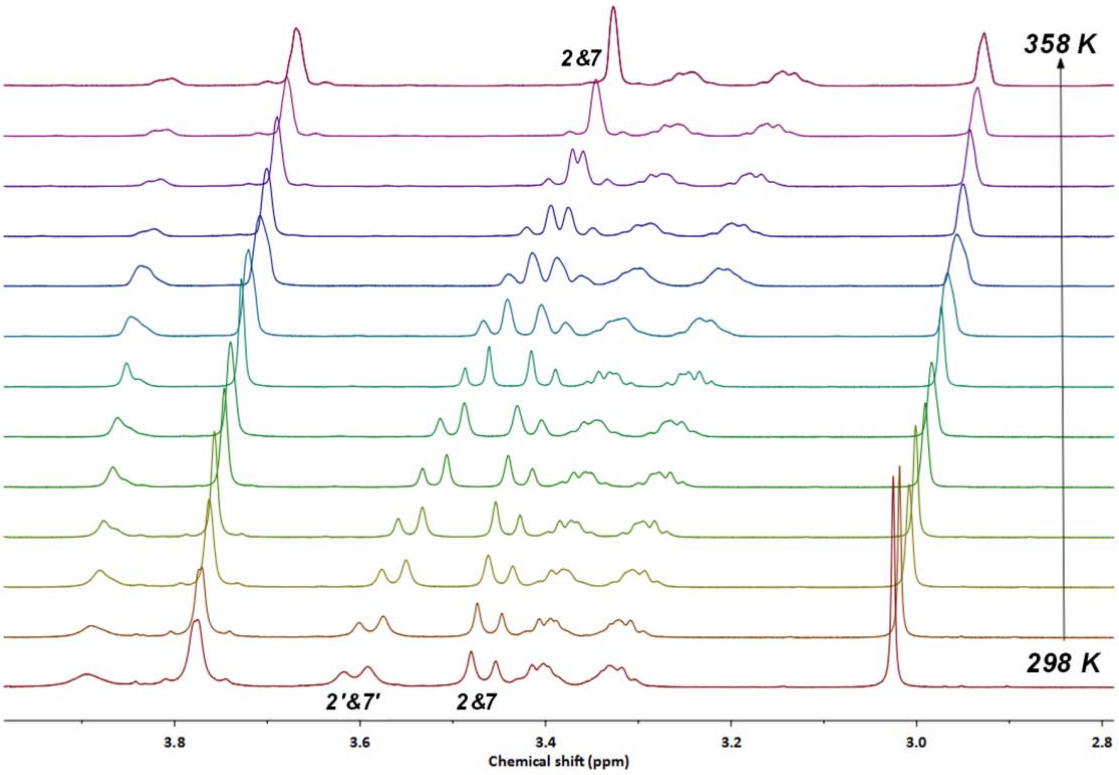

Figure 4.6 *^{1}H NMR spectra (D_2O, 600 MHz, pH 2.0) of **L^{2}**, recorded at 5 K intervals from 298 to 358 K. The peaks of interest are labelled*

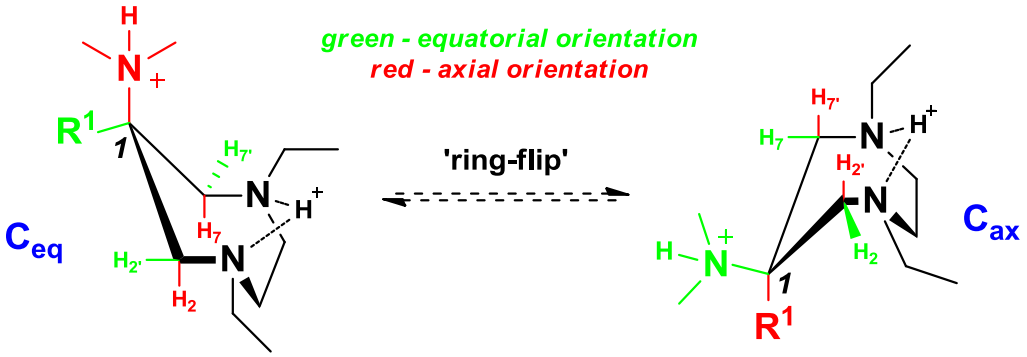

Figure 4.7 *Shows the atom labelling scheme to accompany the discussion of the VT ^{1}H NMR. The two conformers shown are in fast exchange above 358 K.*

The energy and rate of coalescence (conformer exchange) can be estimated using equation (2) and (3):

$$k_c = \frac{\pi}{2}\sqrt{\left(\Delta\vartheta^2 + 6{J_{AB}}^2\right)} \qquad (2)$$

$$\Delta G_c = RT_c[23 + \ln\left(\frac{T_c}{\Delta\vartheta}\right)] \qquad (3)$$

Where: k_c = rate constant for coalescence (sec^{-1})

T_c = temperature at which coalescence occurs (K)

Δv = limiting separation of the of the *AA'BB'*-doublets (Hz)

J_{AB} = coupling constant (Hz)

ΔG_c = Gibbs free energy of coalescence ($kJ.mol^{-1}$)

Close examination of the ^{1}H NMR spectra recorded at 358 K reveals the presence of small satellites on either side of the signal at 3.4 ppm. These indicate that the *AA'BB'*-doublet had not yet coalesced before the temperature limit of the solvent was reached. There are only very small changes in Δv (84 Hz at 298 K) and J_{AB} (-16 Hz at 298 K) between 298 and 308 K suggesting that, to a good approximation, the values at 298 K represent the limiting values. Values for the Gibbs free energy of activation and rate constant for coalescence were approximated using equations (1) and (2) to give $k_c > 146\ sec^{-1}$ and $\Delta G_c > 73\ kJ.mol^{-1}$ respectively.

The energy barrier to conformer exchange (> 73 $kJ.mol^{-1}$) is relatively large, and rate of exchange between them (146 sec^{-1}) slow. The consequence of this is that the formation of a radiolabelled complex with the ligand in this less favourable conformation, C_{ax}, is kinetically trapped despite the fact that the radiolabelled complex species is less stable, i.e. once complexed a significant energy input is required in order for the ligand to assume the preferred conformation. Furthermore, in order to obtain the desired radiolabelled complex directly, a significant energy input will be needed during radiolabelling. This is consistent with the observation that speciation (and hence resulting stability) did not change with increasing radiolabelling temperature and time, and once complete there was no observable exchange between the different species.

The presence of related ligand conformers has been observed for the tri-dentate ligand Me_3TACH. At high pH (~12) the amine ring substituents are all axially arranged, and thus pre-orientated for efficient and stable tri-dentate metal complexation.[6] As the pH is lowered to pH ~ 3, each of the

nitrogen atoms is protonated, which increases the steric bulk (A-value) of the substituents.[6, 7, 16] The Coulombic repulsion force also favours their equatorial reference. As a result, the ring adopts a conformation in which the amine substituents prefer sterically less demanding equatorial positions, which is an unfavourable arrangement for metal complexation.[6]

Whether the instability of complexes, slower radiolabelling rates and poor radiolabelling yields resulting from complexation with ligands preferring C_{ax} over C_{eq} arises from the formation of a complex in this conformation, or from the steric strain placed on the structure when it rearranges to C_{eq} (to facilitate metal complexation), is unknown. The fact that we frequently observe two distinguishable spots on the radio-TLC, suggests that the former is the case. In the C_{ax} conformation, we predict that the chelator shows 'EDDA-like' (EDDA = ethylenediamine-diacetic acid) complexation of Ga(III), in which N-acetate and endocyclic amines are involved in complexation of the metal (Figure 4.8). Alternatively, it is possible that 'EDDA-like' complexation involves the exocyclic amine, an endocyclic amine and their acetate groups. Bi-dentate coordination of the AMPED ligand has been observed for [Cu(H-AMPED)Br_3], where the free endocyclic amine assumes a more favourable non-eclipsed orientation with respect to the coordinated endocyclic amine.[6] In either case, this would account for the poor stability of the complexes formed at low pH, as well as the multiple radiolabelled species observed. This behaviour is also consistent with the finding that it was not possible to alter the speciation of a formed radiolabel by increasing the pH or temperature. i.e. once a given complex has formed from either C_{eq} or C_{ax}, conversion to the other conformer would have to proceed via a high energy process (the complex species are kinetically trapped). In order for this to occur, de-metallation would have to occur first.

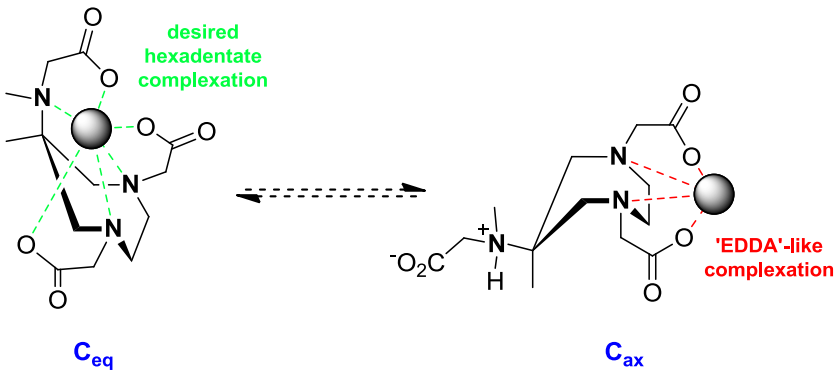

Figure 4.8 *Shows the proposed structures of the constitutional isomeric species formed during complexation of ^{68}Ga at pH < 3.5. The energy barrier to exchange between the species is large, and the rate of interconversion slow. At pH < 3.5 this equilibrium is predicted to be biased to the right.*

Turning our attention now to the kinetics and stability of the APPED based ligands, certain differences in behaviour were observed. The decline in the rate of labelling for pH 2.3, was similar to that observed for AMPED based ligands. In contrast, the radiolabelled complexes formed with APPED-derived ligands at pH 2.3 were more stable than their AMPED analogues and showed improved rates of radiolabelling. The increase in stability is associated with the formation of more of the stable radiolabelled complex species.

The differing steric demand of the quaternary carbon substituents can be used to rationalise the results obtained from the radiolabelling and stability experiments, of APPED and AMPED based ligands. The phenyl moiety has an A-value (12 kJ/mol) that is greater than that of a protonated N_{exo} (~10 kJ/mol).[18] Therefore, the population of the favoured conformer, C_{eq}, is expected to be greater for APPED than AMPED under the same conditions. As a result, more of the desired radiolabelled complex species is formed, giving rise to an overall greater stability. The 'EDDA'-like complexation (Figure 4.8) is expected to have a slower rate of formation than the desired hexadentate complexation. The phenyl group increases the likelihood for formation of the hexadentate complex, and therefore the APPED based ligands radiolabel more quickly than the AMPED based ligands at pH 2.3. This is also the reason why the APPED based ligands have a better stability profile.

It is evident that the relative steric bulk of quaternary substituents define the preferred ring conformation, and play vital roles in determining the stability of the complex formed, as the complexation of gallium is essentially irreversible. For ligands based on the DAZA core (such as AMPED and APPED based ligands) the radiolabelling pH also plays an important role in determining the stability of the complex formed.

2 Crystallographic and ^{1}H NMR Spectroscopic Analysis

Information regarding the conformation of the ring and relative orientations of the quaternary carbon substituents can be extracted from solid state single crystal structures and solution state NMR spectroscopy. In this section, these two techniques are used to investigate what effect introduction of a phenyl group has had on the ring conformation and relative orientations of the quaternary carbon substituents, by comparing AMPED and APPED based analogues.

2.1 Solid State Structure analysis

Two crystal structures of derivatives featuring the APPED core were obtained, along with a crystal structure of a compound featuring the AMPED core. Specifically, they relate to the protected tertiary nitro compounds (**1** and **22**) and the di-N_{endo}-t butyl acetate ester compound (**12**). In addition, a crystal structure of compound featuring the APPED core modified by the substitution of the N_{exo} for a hydroxyl group (**40**) was obtained.

Crystals suitable for single crystal X-ray diffraction were grown by slow evaporation from dichloromethane : ethanol (1 : 1) solutions, and the diffraction patterns obtained at 120 K. A diagrammatic representation of each structure is shown in Figure 4.9. The core structures are shown in Figure 4.10, with the endocyclic N-substituents and hydrogen atoms removed for clarity.

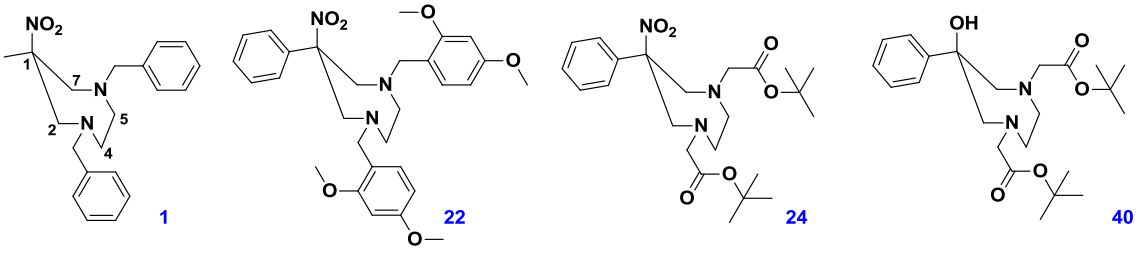

Figure 4.9 *Diagrammatic representations of ligand intermediates, **1**, **22**, **24** and **40**, for which single crystal structures have been determined. The single crystal structure of **24** displayed disorder in the positions of the methyl substituents of the t-butyl groups. Carbon atoms of the rings, relevant to the discussion, are labelled and applicable to all.*

Of particular interest is a comparison of the conformation of the 7-membered rings with specific reference to the relative positioning of the quaternary ring carbon substituent. A comparison between compounds **1** and **22** is most useful because it considers the effect of introducing the phenyl ring. A similar comparison between crystal structures of compounds **24** and **40** is of less interest here, but may provide insight into the effect of varying the size of the 'other' quaternary carbon substituent.

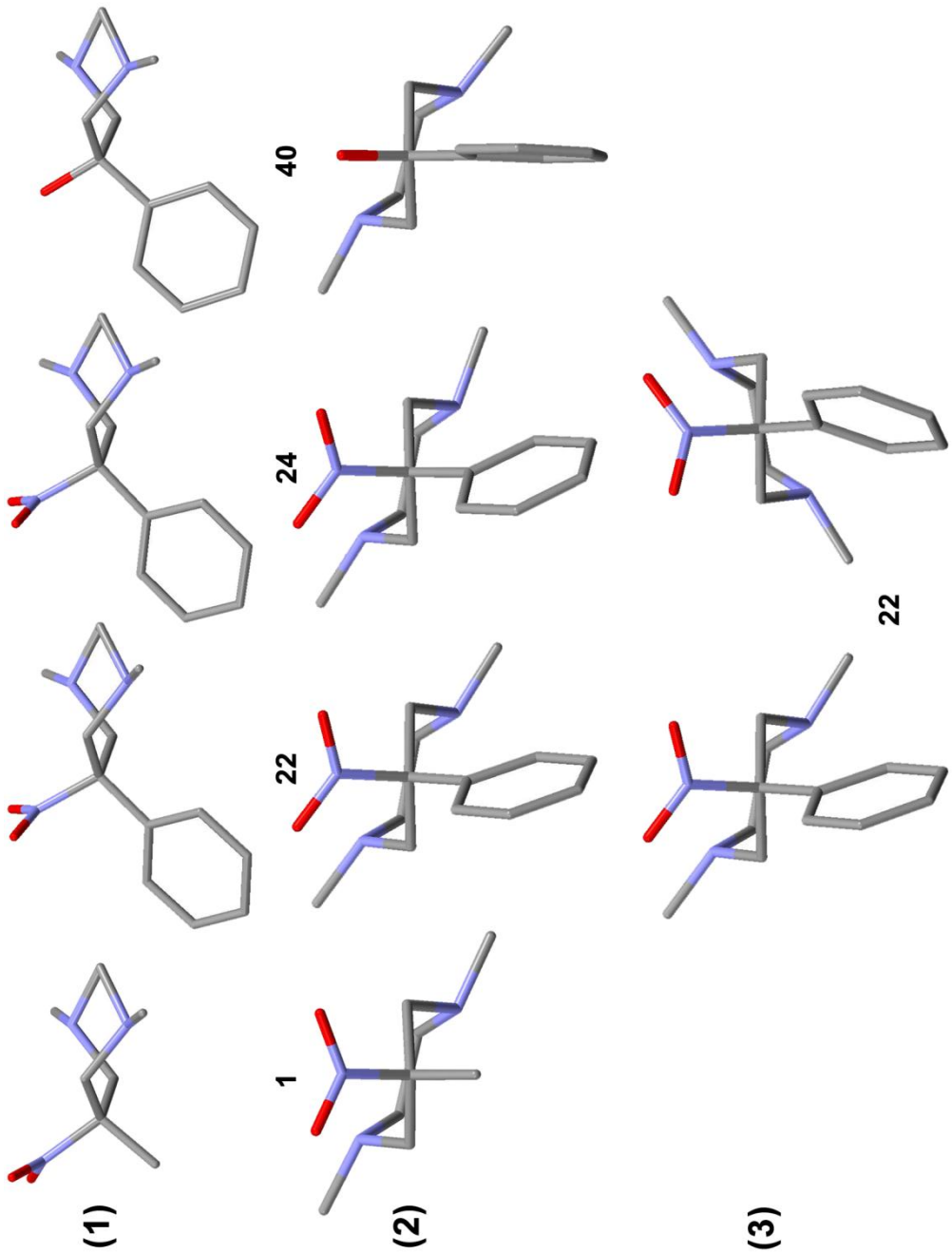

Figure 4.10 *Views of 1, 22, 24 and 40; taken (1) down a line joining C1 to a point which bisects the C^4-C^5 bond, showing the twisted-chair conformation of the seven-membered ring. Views (2) taken along the C^4-C^5 bond, showing the isoclinal orientation of the C^1 substituents. In each case only one of the two conformational enantiomers is shown. The enantiomeric pair of 22 are shown (3) as views down a line joining C^1 to a point which bisects the C^4-C^5 bond. The endocyclic nitrogen substituents and hydrogen atoms have been removed for clarity. See Figure for an atom labelling scheme.*

The views shown in Figure 4.10(1) are taken along a line drawn from C^1 to the middle of the C^4-C^5 bond, and highlight the twisted chair conformation of the 7 membered ring, and the positioning of the quaternary ring carbon as the isoclinal centre. This is the conformation depicted by TC_4 (Figure 4.3). Also shown is a view along the C^4-C^5 bond and parallel to a plane passing through C^4, C^5 and C^1, which illustrates the isoclinal orientation of the C^1-substituents and torsion of the N-CH_2-CH_2-N fragment (Figure 4.10(2)). In each case, the compounds crystallized as a pair of enantiomers, related through a puckering of the ring (See Figure 4.10(3) for an illustration).

The angles θ_1 and θ_2 denote the deviation of the non-carbon (nitro or hydroxyl) and carbon substituent from the mean plane of the ring (calculated using all of the atoms of the 7-membered ring) respectively, and ϕ denotes the torsion about the N^3-C^4-C^5-N^5 fragment (See Figure 4.9 for atom labelling). The important data is summarised in Table 4.1, along with other relevant examples from the literature. Also included are the relevant A-values (kJ.mol^{-1}) of the quaternary carbon substituents.

Table 4.1 *Synopsis of the structural parameters relating to the ring conformation for **1**, **22**, **24** and **40** (this work). Structural parameters of two, triply protonated salts of AMPED are also shown.*[6]

	1[a]	**22**[a]	**24**[a]	**40**[a]	**H_3AMPED**[a,6]	**H_3AMPED**[b,6]
θ_1(°)[c]	49.3	56.9	57.6	54.7	46.2	31.4
θ_2(°)[c]	47.6	43.4	41.9	43.8	56.3	90
ϕ(°)[d]	53.2	54.8	56.4	51.0	60.6	42.1
A-values[18]	Me: 7	Ph: 12	Ph: 12	Ph: 12	Me: 7	Me: 7
(kJ/mol)	NO_2: 5	NO_2: 5	NO_2: 5	OH: 3-4	NH_3^+: 7-9	NH_3^+: 7–9

[a] Structure adopts conformation TC_4 in which the C_1 is the isoclinal centre. [b] structure adopts conformation TC_7, in which the N_{exo} takes up an equatorial orientation. [c] θ_1 and θ_2 are the deviations of the, non-carbon and carbon respectively, quaternary carbon substituents from the mean plane of the ring. Mean plane calculated using all of the atoms of the 7-membered ring. [d] ϕ denotes the torsion about the N_3-C_4-C_5-N_5 fragment. Atom labelling scheme on Figure 4.9.

The most 'relaxed' (or favoured) arrangement of the N-CH_2-CH_2-N fragment has a torsion angle of 60°, and as expected the values for ϕ are not very different.[6, 7] It is interesting to note that the largest and smallest variations from this geometry are found for **24** and **40**, whilst the structurally similar compounds **1** and **22** are intermediary, and have similar values.

All θ_1 and θ_2 angles are greater than 30° but smaller than 60° consistent with their isoclinal assignment.[2] Although isoclinally positioned, a comparison of the respective θ_1 and θ_2 angles of **1** and **22** is useful. In **1**, the values of θ_1 and θ_2 are comparable, as would be expected from the similar steric bulk of the substituents of an isoclinal centre. However, in **22** the values of θ_1 and θ_2 indicate that the introduction has resulted in a shift (~ 8°) of the exocyclic nitrogen to a more pseudo-axial position, accompanied by a shift (~ 4°) of the other substituent to a more pseudo-equatorial positioning. The change is such that the exocyclic nitrogen is very close to the border (60° with respect to the mean plane of the ring) between an axial and isoclinal substituent.

Consistent with the greater A-value difference between the phenyl-methyl group change (ΔA ~ 5 $kJ.mol^{-1}$), compared to the nitro-hydroxyl group change (ΔA ~ 1 $kJ.mol^{-1}$), the changes in the relative θ_1 and θ_2 values are bigger between **1** and **22** compared to **24** and **40**. It is noteworthy that the **24** and **40** displays the opposite trend. Decreasing steric demand of one of the substituents results in it adopting a less axial orientation, i.e. in going from nitro to hydroxyl the A-value decreases slightly, but the hydroxyl group takes up a less axial orientation. This may be due to a 'secondary' influence. There is an intermolecular short contact between the hydroxyl group proton and the carbonyl oxygen of one of the ester arms. The O-H•••O distance of 2.685 Å is within range for moderate, mostly electrostatic, hydrogen bond.[19] It is possible that this interaction may alter the location of the hydroxyl group, to produce the unexpected trend. Furthermore, it is also possible that this interaction play a role in defining the smaller torsion angle (ϕ = 51.0°) observed for **40**, compared to the other structures.

The phenyl group in **40** is less rotated (4.10°) with respect to the other C^1-substituent, compared to **22** and **24** (31.3°and 27.8°respectively). This is possibly a result of the larger π-electron cloud present with the nitro group, causing electronic repulsion with the π-electron cloud of the phenyl moiety.

The changes, upon phenyl insertion, outlined in this section reflect the larger steric demand of the phenyl group. This is also seen in their respective A-values, were the difference between the endocyclic substituents is greater for **22** (Ph vs NO_2) than for that of **1** (Me vs NO_2). It should be emphasised that observations in the solid state are not necessarily applicable in solution. Furthermore, a di-functionalised amine will have a larger A-value (7-10 kJ/mol, depending on its protonation state and solvent) than that of a nitro group, and hence these observations are not necessarily true for the ligands used for metal ion complexation. This can be demonstrated by a comparison of the θ_1 and θ_2 values of **1** and H_3AMPED^{a}.[6] Consistent with the protonated exocyclic

nitrogen of H_3AMPED^a having a greater A-value than that of the nitro substituent of **1**; the exocyclic nitrogen of **1** adopts a more axial orientation (~3° further from the ring plane) whilst the methyl substituent takes up a more equatorial orientation (~9° closer to the ring plane) in comparison to H_3AMPED^a. In the case of H_3AMPED^b this effect is even more profound, with the exocyclic amine adopting an equatorial orientation.[6]

2.2 Solution state NMR studies

Information concerning the relative spatial orientations of the ligand protons can be gained from ^{1}H NMR NOESY experiments. In this section the ester precursors, rather than the ligands themselves, were analysed and compared in detail because the ^{1}H NMR NOESY experiments of the APPED based ligands in D_2O were poorly resolved. However, ^{1}H NMR NOESY experiments on the ligand precursors (esterified ligands) were considerably better defined. Critically, the splitting pattern of the ring protons was the same for the ester precursors and the free ligands (Figure 4.11). This suggests that the conformation of the ring is similar, and a discussion of the nOe correlations of the ligand precursors is of relevance.

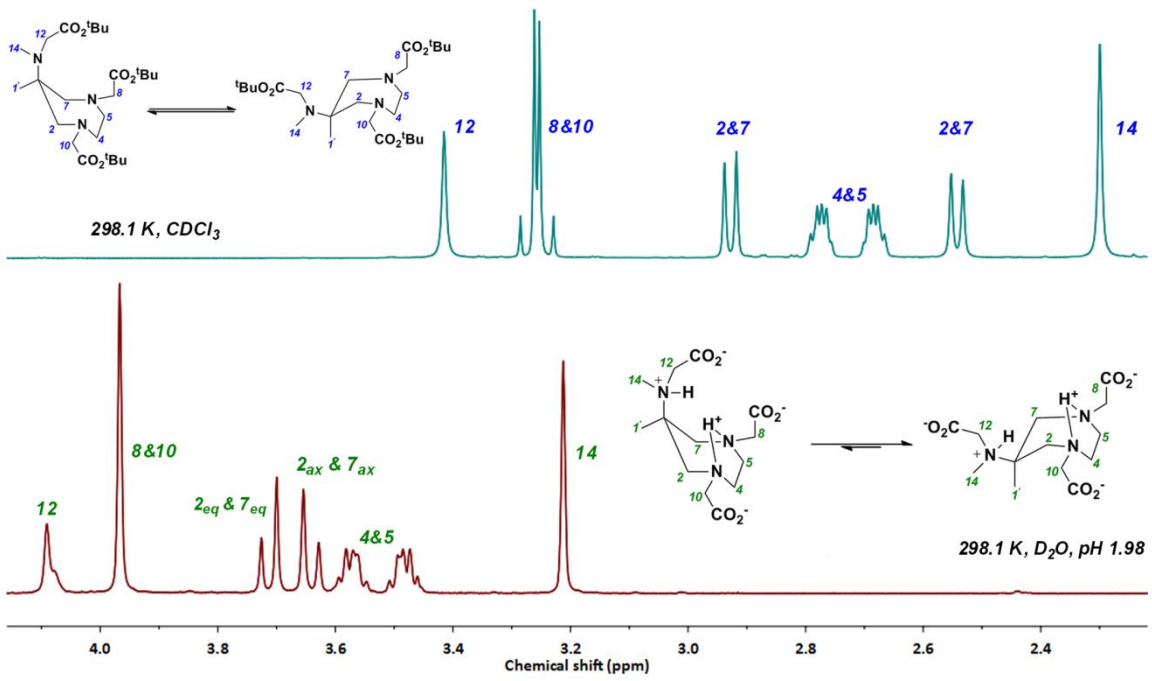

Figure 4.11 *^{1}H NMR spectra (700 MHz) of ligand **L^2** and its ^{t}Butyl-protected precursor, **3**, showing the commonality of the spectral features.*

Well resolved 2D NOESY NMR spectra were obtained for ligand **L^2** in D_2O. Before addressing the NOESY experiments of the ligand precursors, this experiment is discussed in isolation.

2.2.1 ^{1}H and 2D NOESY NMR Spectra of L^2

Invariably, for this and related compounds, two first order doublets were observed for the methylene groups at C^2 and C^7. See Figure 4.11 for atom labelling scheme and ^{1}H NMR spectrum. The splitting arises from geminal-coupling with ^2J = -16Hz. It was confirmed by ^{1}H NMR COSY correlations that each doublet is mutually coupled (Figure 4.11). The two protons which make up a doublet have the same orientations with respect to the ring, i.e. both axial or both equatorial. It is possible to assign the axial and equatorial orientation of the ring protons (H^2 and H^7) using ^{1}H NMR NOESY spectroscopy by making two key assumptions. Firstly, at low pH (~ 2.0) it is expected that the N_{exo} substituent with adopt a more equatorial orientation. Secondly, the strongest nOe correlation between $H^{2\&7}$ and quaternary methyl corresponds to a proton on $C^{2\&7}$ with the same orientation, because these will be nearest each other. The methyl group ($H^{1'}$) shows a stronger nOe correlation to the lower frequency $H^{2,7}$ resonance, which is therefore assigned to an axial orientation. Consistent with this; the N-methyl (H^{14}) and N-CH_2 (H^{12}) only correlate to the higher frequency $H^{2,7}$ resonance, which is therefore assigned to an equatorial orientation (Figure 4.12).

It was hypothesised previously, that at pH > 3.5 the exocyclic amine changes orientation (becomes axially orientated), as a result of a decreased A-value when it is deprotonated (pK_a ~ 5.7). Consistent with this is that; when the NOESY NMR experiment is repeated at pH 5 there is a significant change in the nOe correlations which are observed. Most importantly, the nOe correlations of $H^{1'}$, H^{14} and H^{12} with $H^{2,7}$ are reversed. At pH 5 the quaternary methyl ($H^{1'}$) is closer to the equatorial ($H^{2eq,7eq}$) protons, and the N-methyl (H^{14}) and N-CH_2 (H^{12}) only show an nOe correlation with axial ($H^{2ax,7ax}$) proton resonance. This strongly suggests that there is a change in the relative position of the quaternary carbon substituents associated with de/protonation of the exocyclic amine. The ^{1}H NMR spectrum recorded at pH 5 has broader proton peaks (than that measured at pH ~2), which may indicate that there is a rapid exchange (on an NMR time-scale) between different conformations of the ligand. Rapid exchange between conformations reflects a lowered energy barrier to interconversion, which is consistent with the exocyclic amine having a lower A-value when deprotonated.

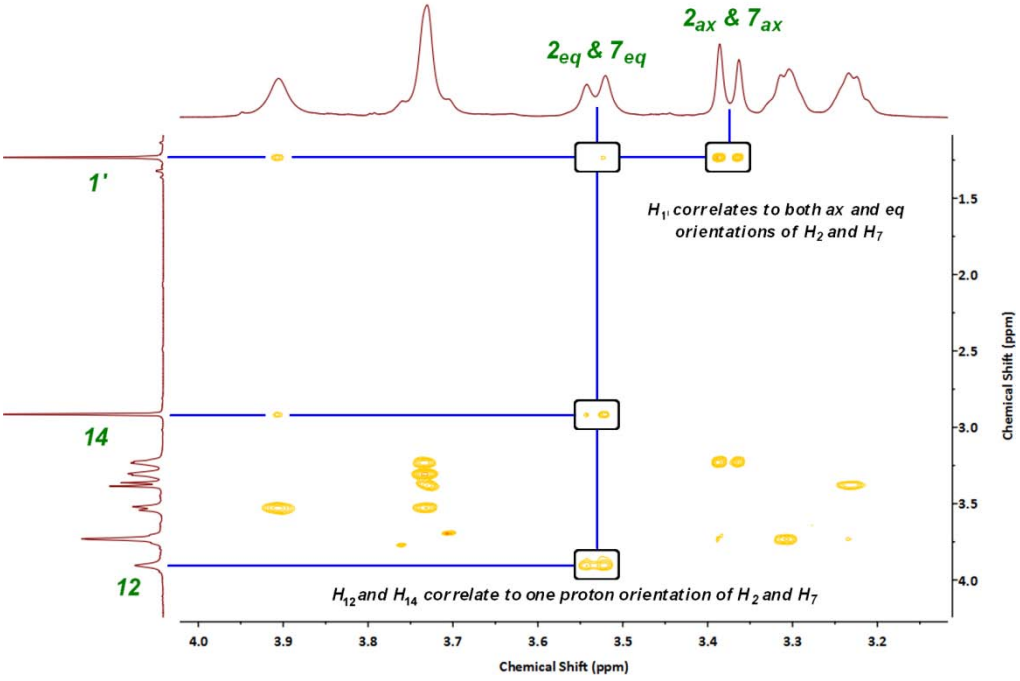

Figure 4.12 *2D NOESY-NMR (700 MHz, D_20, 298.1 K, pH 2.0) spectra of* ***L*** ^{2} *with the nOe correlations of interest highlighted, illustrating assignment of the orientation for protons attached to* C^2 *and* C^7.

2.2.2 ^{1}H and 2D NOESY NMR Spectra of Ligand Precursors

^{1}H NMR NOESY experiments again provided information of the mutual spatial orientation of protons. Although the absence of a correlation is not confirmation that two protons are not close in space, this technique can provide some insight into the relative positioning of the ring substituents. Of particular interest were the correlations that existed between protons attached to C^2 and C^7 with respect to protons at R^1 (H_b) and N_{exo} (H_a) (Figure 4.13). By analysing which correlations occur, and their relative strength, it was possible to make tentative inferences about the relative positions of the quaternary carbon substituents relative to the ring.

DAZA based compounds which have additional stereogenic centres on the N-substituents (for example **10** and **36**. Figure 4.14), will have increased asymmetry as a result. This means that protons H^{2ax}, H^{2eq}, H^{7ax} and H^{7eq} were diastereotopic and anisochronous. This allows for more intricate evaluation of the ^{1}H NMR and NOESY spectra. Furthermore, **10** and **36** only differ structurally in the nature of the group at the R_1-position and so offered a good comparison. Therefore, these two ligand precursors were chosen for the comparison (Figure 4.14).

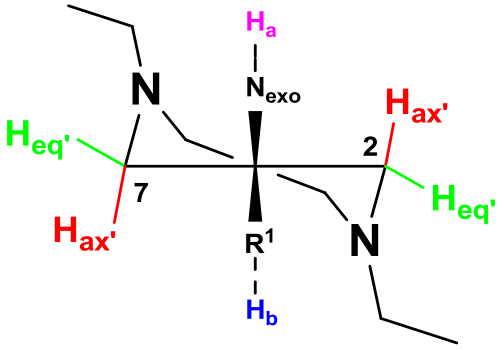

Figure 4.13 A representative *TC-conformations for ligand precursors **10** and **36**. (NOESY correlation of the protons shown provides useful information about the rigidity of the system. The structures have been drawn such that the quaternary carbon is located on the isoclinal centre, i.e. TC_4. This is not necessarily the case, and the diagram is meant purely for illustrative purposes from which the orientation of the quaternary carbon substituents can be discussed.*

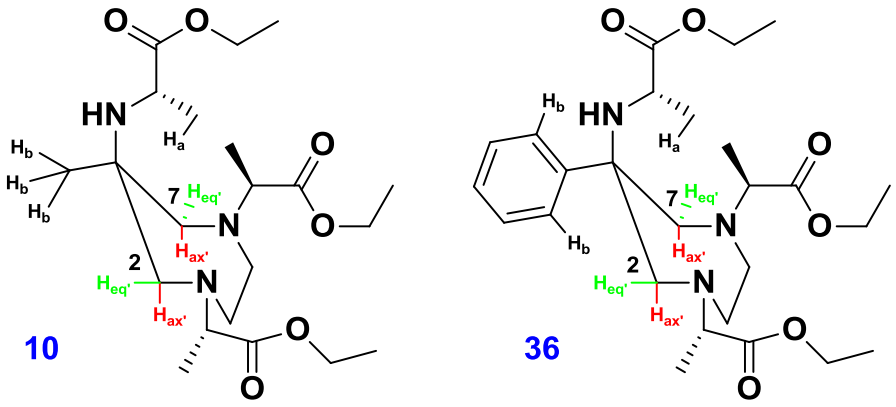

Figure 4.14 *Shows the structures of protected ligands **10** and **36**. Highlighted are the protons of interest for the NOESY experiments. Note that the chair conformation is only used for structure illustration, and does not imply a chair-like conformation in the solid state or solution.*

Of particular interest, were nOe correlations between H_a and $H^{2/7}$, and, H_b and $H^{2/7}$ (Figure 4.14). Looking first at **10**, six nOe-correlations were observed between this set of protons (Figure 4.15). Table 4.2 shows the ratio of these six correlations, determined by integration of the nOe correlation enhancement signal.

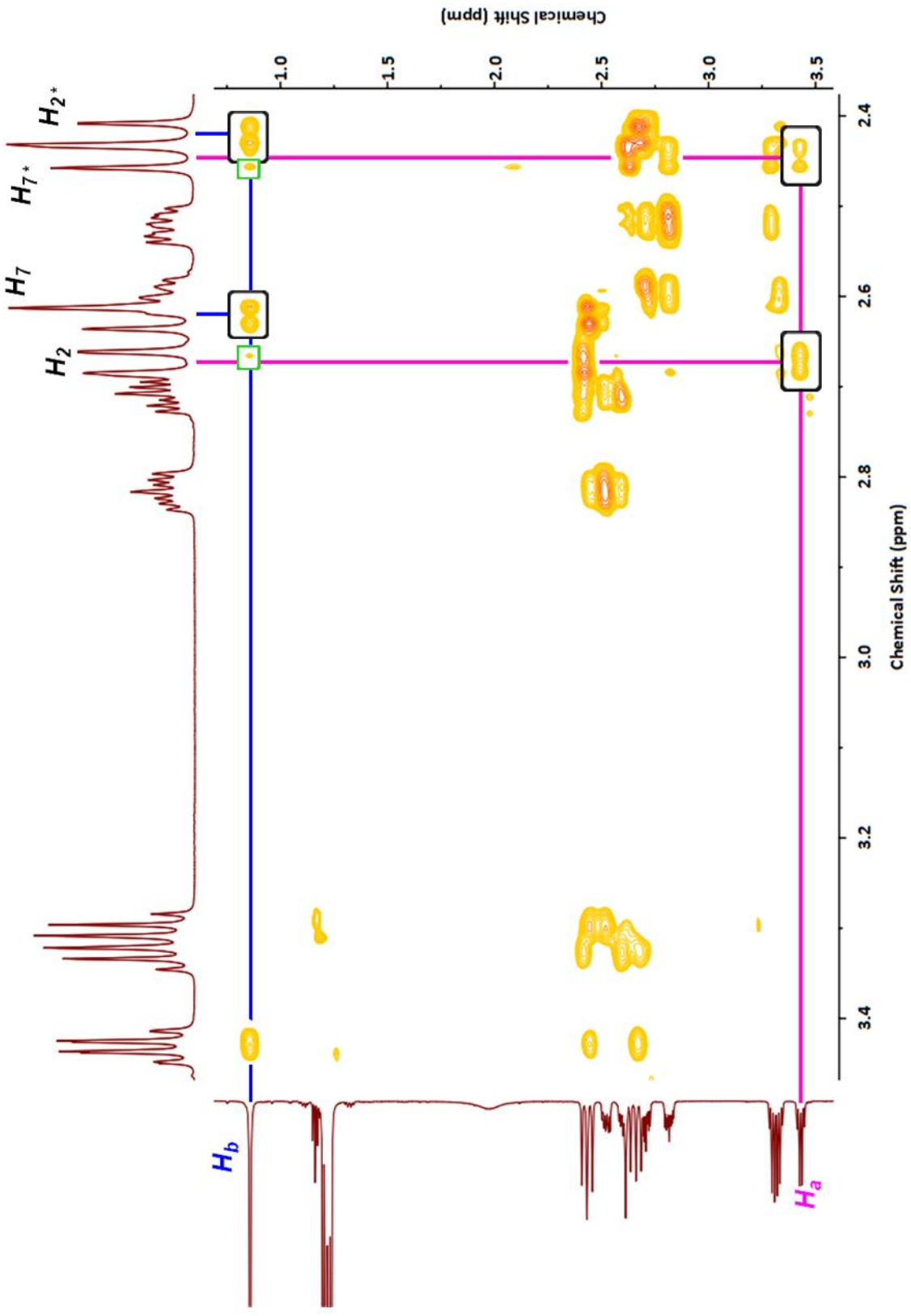

Figure 4.15 *2D NOESY-NMR spectrum ($CDCl_3$, 298 K, 600 MHz) of* ***10*** *with the nOe correlations of interest highlighted. See Figures 4.14 for proton labelling scheme.*

Table 4.2 *Shows the ^{1}H NMR NOESY correlations and integration, of compound **10,** for protons attached to C^{2} and C^{7}, with protons of the quaternary carbon substituents (H_a and H_b). The superscript '*' distinguishes different protons attached to the same carbon atom.*

NOESY correlation	Value (relative nOe enhancement)
H_b-H^{2*}	39
H_b-H^{7}	27
H_a-H^{2}	21
H_a-H^{7*}	11
H_b-H^{2} and H_b-H^{7*}	2

Specifically, nOe correlations were observed between H_a and one H^2 and H^7 proton. In terms of the H_b proton, there were correlations to the protons on C^7 and C^2 which do not correlate to H_a. The correlations of H_a were stronger than those of H_b. However, these are not strictly relevant because; there are three H_b protons and only a single H_a proton, and the two protons (H_a and H_b) differ in their position with respect to the quaternary carbon.

A view looking down C^1, onto the centre of the N-CH_2-CH_2-N bridge, is useful in understanding these correlations (Figure 4.16). From the diagram it is evident that H_b lies close in space to one of the axial protons, but not the other. Similarly, it is also evident that H_b lies close in space to one of the equatorial protons, but not the other. The equatorial and axial protons ($H^{2/7}$) it lies close to are attached to different carbons. A similar observation is made for H_a, but it is closer to the axial and equatorial protons which are furthest away for H_a. These observations have been confirmed by determining approximate H_b-$H^{2/7}$ and H_a-$H^{2/7}$ through space distances in the crystal structure of **1**. Specifically, the distances were measured from the nitro-group nitrogen (estimation of H_a) and first carbon atom of R^1 (estimation of H_b) to the protons of C^2 and C^7. The measurements indicated that, out of the four protons, the nitro-nitrogen to closest to one axial and one equatorial on different carbons, whilst the other substituent is closer to the other two protons.

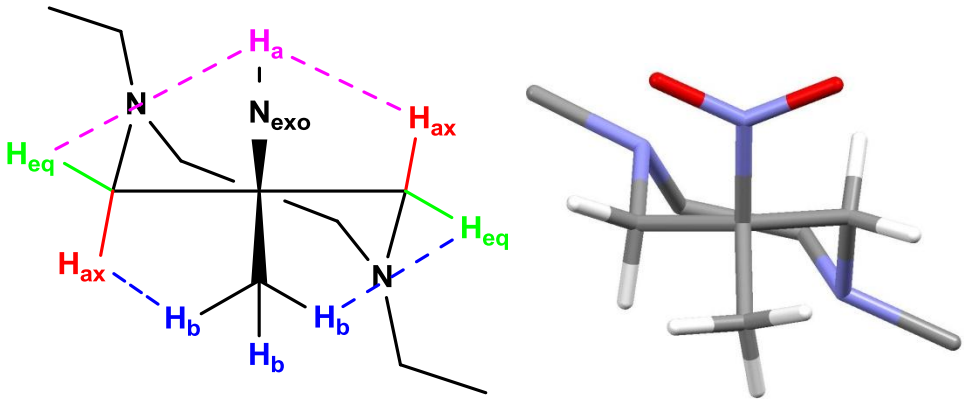

Figure 4.16 *Twist-chair conformer of an AMPED based ligand precursor illustrating the observed nOe correlations (dashed lines). Also shown is the crystal structure of **1**, for comparison. The proton H_a refers to a proton in the N_{exo}-substituent. Amine substituents removed or simplified, and protons not of interest here have been removed.*

To summarise, H_b has through space interactions to an axial orientated proton on one carbon, and an equatorially orientated proton on the other. The same is observed for H_a, but for the opposing ax-eq set of protons.

If we now turn out attention to similar NOESY correlations for **36**, a very different result was found (Figure 4.17). Table 4.3 shows the relative ratios for the NOESY correlations observed between H_b and $H^{2/7}$, and H_a and $H^{2/7}$.

Table 4.3 *Shows the NOESY correlations and relative integration, of compound **36,** for protons attached to C^2 and C^7, with protons of the quaternary carbon substituents (H_a and H_b). The subscript '*' distinguishes different protons attached to the same carbon atom.*

NOESY correlation	Value (relative nOe enhancement)
H_a-H^{7*}	4
H_b-H^{2*} and H_b-H^{7*}	31[a]
H_b-H^2	23
H_b-H^7	36

*It should be noted that, direct comparison of these correlations with those of **10** is not consistent. The reason being, that H_b is in a different position for the two compounds. (See Figure 4.8) Internal comparisons for **36** are more relevant because, H_b and H_a are in very similar position relative to the quaternary centre. However, these comparisons are purely qualitative as there are two H_b protons, but only a single H_a proton.[a] Signals too close to accurately determine individual values*

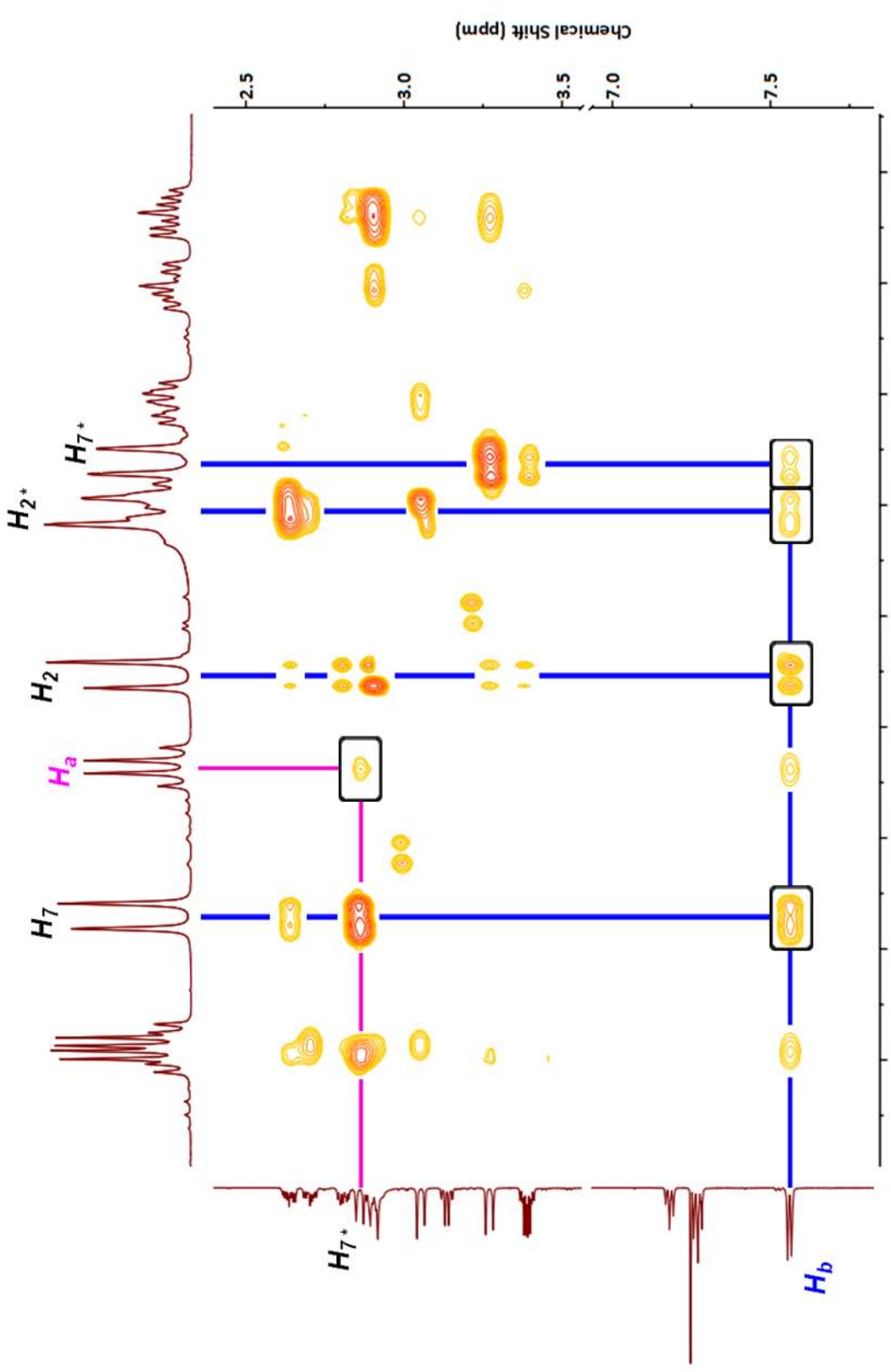

*Figure 4.17 2D NOESY-NMR spectrum ($CDCl_3$, 298 K, 600 MHz) of **36** with the nOe correlations of interest highlighted. See Figure 4.14 for the proton labelling scheme. A section of the vertical 1H NMR spectrum has been removed (3.5 – 7 ppm).*

There are nOe correlations between H_b and each H^2 and H^7 proton, whilst there is only a single very weak correlation between H_a and one H^2 proton (Figure 4.17). This behaviour contrasts with what was observed for the nOe correlations of **10**. The question raised is, "what conformational change, induced by the introduction of the phenyl group, allows the H_b (phenyl) to show nOe correlations with every proton attached to C^2 and C^7, yet reduces the number of nOe correlations of H_a (N_{exo}) to one?" It should be taken into account that H_b protons of **36** are expected to be closer to the ring than the H_b protons of **10**. However, this does not account for the apparent 'loss' in correlation associated with H_a.

Supported by evidence from crystal structures of **1** and **22**, the following hypothesis is tentatively offered to explain this behaviour. Introduction of the phenyl group results in a shift of the endocyclic nitrogen substituent to a more axial position. As a result, the through-space distance between H_a and the nearest H_{ax} and H_{eq} protons increases. In support of this, a larger N_{nitro}-$H_{ax/eq}$ distance was observed for the crystal structure of **22** compared to that of **1**. As a consequence, one of the distances (most likely that between H_a and the H_{eq} proton of C^2 or C^7) is too long to create a measureable nOe correlation, and is no longer observed. Accompanying the more axial orientation of N_{exo}, the other substituent takes up a more equatorial orientation. As a result of moving closer to the mean plane of the ring, the proton H_b is now closer to all four of the $C^{2\&7}$ protons and an nOe correlation is observed (Figure 4.18). Consistent with this hypothesis, the only correlation observed for H_a is to the proton which H_b shows the weakest correlation to.

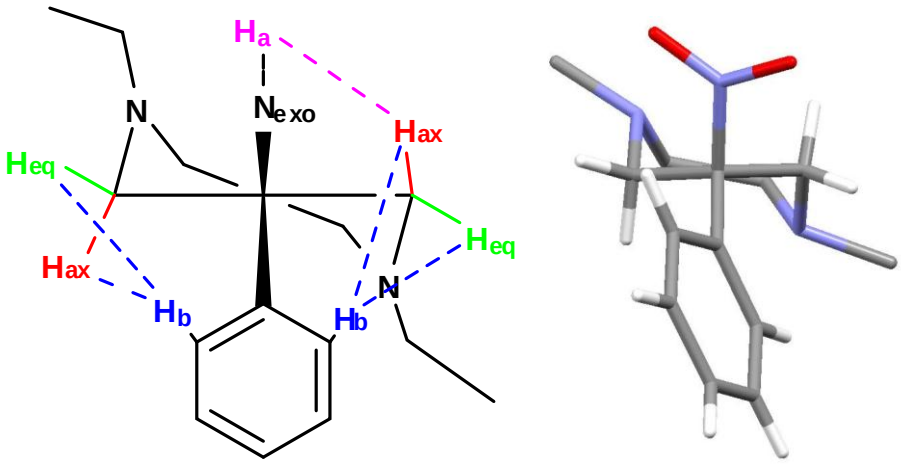

Figure 4.18 *Twist-chair conformer of a PAPED based ligand precursor illustrating the observed nOe correlations (dashed lines). Also shown is the crystal structure of* ***22****, for comparison. The proton* H_a *is in a CH attached to* N_{exo}*. Amine substituents removed or simplified, and protons not of interest here have been removed.*

The most significant feature of this analysis is the decrease in the number of correlations associated with H_a, and the increase in the number associated with H_b. In order to make this possible, H_b must be closer to, and H_a further from, the plane of the ring. This suggests N_{exo} adopts the favoured more axial site, and the other substituent takes up a more equatorial orientation in APPED- compared to AMPED-based compounds.

2.3 Summary

The Gibbs free energy barrier ($\Delta G^{\#}$) for interconversion between conformers with N_{exo}-equatorial (C_{ax}) and N_{exo}-axial (C_{eq}) is > 73 kJ/mol at pH < 3.5. This suggests that when the rate of metal complexation is fast with respect to the rate of interconversion of the isomers, the mixture of radiolabelled species observed (i.e. differing in stability and constitution) reflects the relative population of ligand conformers. When this conformational equilibrium is biased in favour of a major species, that favours cooperative lone pair ligation, a more stable single radiolabelled complex is obtained. Comparisons of compounds based on the APPED and AMPED cores, based on single crystal structural data and nOe NMR correlations, strongly indicate that introduction of the phenyl group promotes the axial orientation of the exocyclic nitrogen substituent. Increased population of the desired conformers, accounts for the better radiolabelling of APPED based ligands at pH < 3.5. Furthermore, nOe NMR correlations at pH 2.0 and 5.0 for ligand $\mathbf{L^2}$ suggest that the desired axial orientation of N_{exo} is preferred as the exocyclic amine becomes deprotonated. This accounts for the improved stability of the radiolabelled complexes at pH > 4 and, in part, the quicker radiolabelling.

3 'Cold' Gallium Complexes of [Ga.L^n]

3.1 Single Crystal X-ray Analysis of [Ga.L^n]

In terms of the complexation of 'cold' Ga(III), only those ligands deemed suitable following the radiochemical evaluations were of interest, i.e. ligands $\mathbf{L^2}$, $\mathbf{L^3}$, $\mathbf{L^6}$ and $\mathbf{L^8}$. Low resolution mass spectral analysis of these complexations carried out at pH 2.5, revealed formation of the $[MLH]^+$ species, and suggested that they were successful. However, attempts to crystallize the complexes were

unsuccessful and the ^{1}H NMR spectra in D_2O were broad, poorly resolved and could not be interpreted.

The radiochemical studies suggested that this may be related to the formation of multiple radiolabelled species, which could be avoided by carrying out the complexation at pH ≥ 4. However, complexations at pH > 3.6 require the use of a suitable buffer to prevent formation of the insoluble $Ga(OH)_3$. The disadvantage of this approach is that the addition of a buffer introduces 'impurities', which may hinder crystallization of the complexes. Instead, a reaction mixture containing equimolar amounts of $Ga(NO_3)_3$ and the ligand in water : methanol (2 : 1, 1.5 mL) was prepared, and the pH of the solution adjusted to pH ~ 4.5 using aqueous sodium hydroxide (0.1 M). The reaction was heated for 1 h at 333 K, and the mixture set aside. The Ga(III) complexes of **L^2**, **L^3, L^6** and **L^8** crystallised from solution as thin plates over the course of 36 h, and were examined by X-ray analysis at 120 K.

3.1.1 Solid State Structures of [Ga.L^n]

The Ga(III) complexes of **L^2** and **L^3** crystallize as hemi- and mono-hydrates respectively, whilst those of **L^6** and **L^8** do not contain any solvent of crystallization in the unit cell. In each complex, the Ga(III) ion is coordinated by the N_3O_3 donor set of the ligand to give charge neutral complexes. Views showing the conformation of the 7-membered ring, location of the Ga(III) ion and arrangement of the pendant acid arms are shown (Figure 4.19). The lattices of **[Ga.L^2]** and **[Ga.L^6]** contain enantiomeric complexes within the unit cell which have opposite ring conformations and helicities of the carboxylic pendant arms, either overall *Λ* or *Δ* (Table 4.4).

In each complex, two of the pendant arms have the same helicity, whilst the third has the opposite sense (Table 4.4). Crystals of **[Ga.L^6]** contain two nearly identical crystallographic independent molecules, which only differ significantly in the 15° *Λ*-twist (i.e., NCCO torsion angle) of one of the pendant carboxylic acid arms (Table 4.4). All other structural parameters show less than 5° of variation between the two conformers. The enantiomerically pure **[Ga.L^3]** and **[Ga.L^8]** are both overall *Λ*, and have a consistently high degree of N-C-C-O torsion within the pendant arms (Table 4.4). There is a comparatively small degree of helicity in ***Λ*-[Ga.L^n]** (n = 2 and 6), as indicated by the smaller N-C-C-O torsion angles.

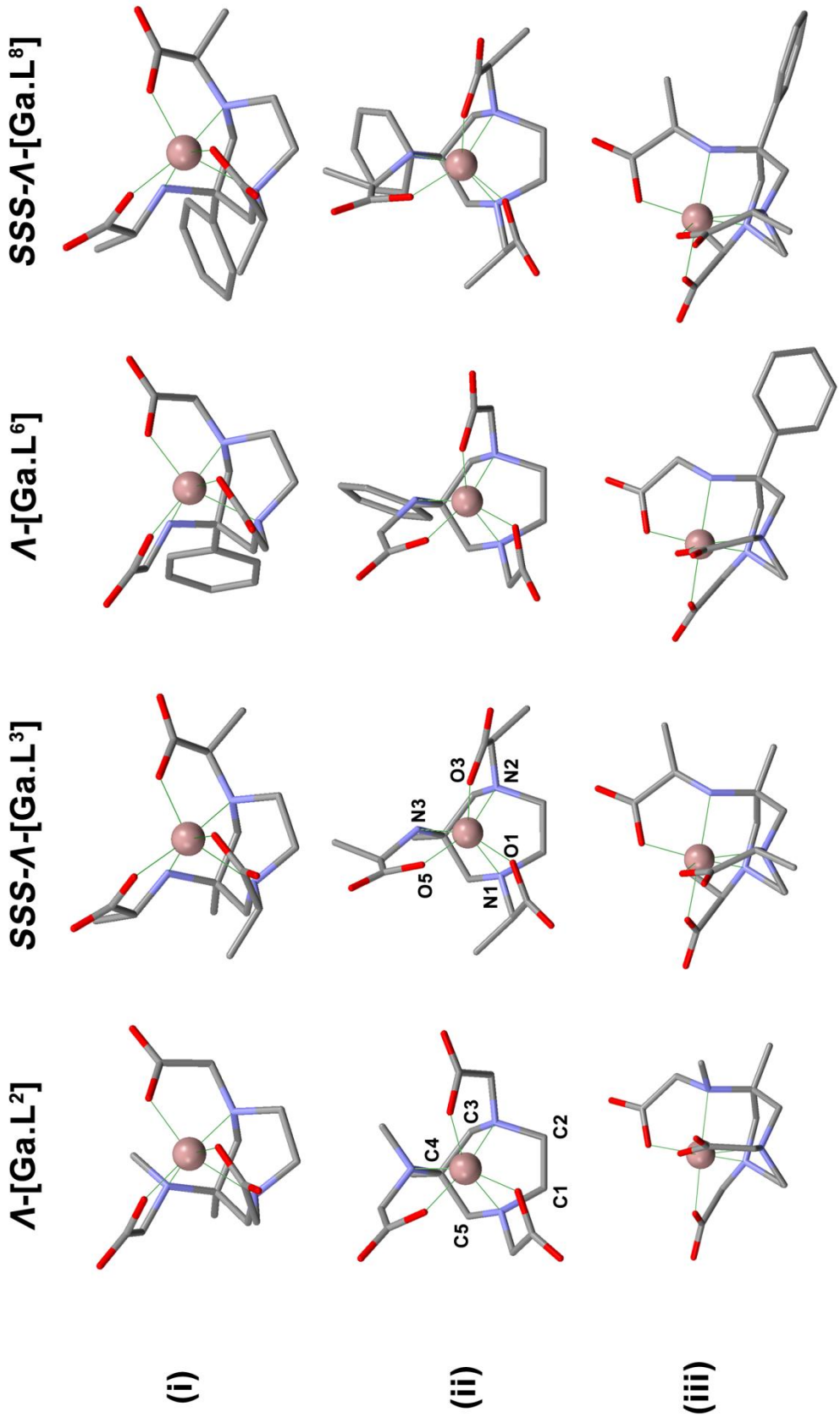

Figure 4.19 *Selected views of [Ga.L^n] (n = 2, 3, 6, 8). A single enantiomer is shown for [Ga.L^2] and [Ga.L^6], and only one of the crystallographic independent molecules of [Ga.L^6] is shown. Atom labelling scheme of the donors and rings carbons is shown, and the Ga(III) ion represented by a ball of arbitrary size. View (i) shows the encapsulation of the metal centre by the ligand framework; (ii) taken perpendicular to the N_3 plane, highlights the arrangement of the pendant arms relative to the N_3 donor set; (iii) taken along the C^1-C^2 diamine bridge, illustrates the relative positioning of the quaternary carbon substituents and pseudo-chair conformation of the ring.*

Table 4.4 *Torsion angles (°) for the N-C-C-O pendant arms of* ***Λ-[Ga.L^n]*** *(n = 2, 3, 6, 8).*

	Λ-[Ga.L^2]	**Λ-[Ga.L^3]**	**Λ-[Ga.L^6]$_a$***	**Λ-[Ga.L^6]$_b$***	**Λ-[Ga.L^8]**
N1-C-C-O1	-15.30	+21.48	+10.53	+6.05	+16.94
N3-C-C-O5	+10.24	-18.89	-7.63	+8.89	-18.35
N2-C-C-O3	-24.35	-21.77	-5.77	-20.93	-27.63

* *Subscripts 'a' and 'b' indicate the two constitutional isomers of* ***[Ga.L^6]****.*

Selected molecular parameters are presented in Table 4.5 for **[Ga.L^n]** (n = 2, 3, 6 and 8). As indicated by the N-Ga-O angles (≠ 180°) and non-parallel O_3 and N_3 faces, each complex adopts a distorted octahedral geometry of the ligand donor atoms around the Ga(III) centre, typical for the hexadentate ligand complexes of gallium.[20-22]

Table 4.5 *Selected N-Ga-O angles (°), and the angle formed between the planes of the N_3 and O_3 donor sets. See Figure 4.19 for atom numbering scheme.*

	[Ga.L^2]	**[Ga.L^3]**	**[Ga.L^6]***	**[Ga.L^8]**
N_3-O_3 angle (°)	3.03	3.55	4.24	2.91
N1-Ga-O3 (°)	157.25	148.73	152.42	146.82
N2-Ga-O5 (°)	165.16	158.28	161.53	156.20
N3-Ga-O1 (°)	159.68	155.40	157.84	155.07

values are the average of the two crystallographic independent molecules of* *[Ga.L^6]****.*

The octahedral distortion parameter (Σ) and the average trigonal distortion angle (Θ) illustrate the degree of distortion from an ideal octahedron, and are shown for **[Ga.L^n]** (n = 2, 3, 6 and 8) compared to [Ga.NOTA] in Table 4.6.

Table 4.6 *Octahedral distortion parameter (Σ) and the average trigonal distortion angle (Θ) for* ***[Ga.L^n]*** *(n = 2, 3, 6, 8) and [Ga.NOTA][23].*

	[Ga.L^2]	**[Ga.L^3]**	**[Ga.L^6]***	**[Ga.L^8]**	**[Ga.NOTA][23]**
Σ^a	9.27	8.72	10.3	11.8	6.26
Θ^b	10.7	16.9	13.8	13.6	6.45

** values from one of the two crystallographic independent molecules of* ***[Ga.L^6]*** *is provided. [a] Octahedral distortion parameter Σ = Σ(\|90–φi\|)/12 [Σ = 0° for an ideal octahedron; φi represents the 12 smallest L–M–L angles.][24]; [b] Average trigonal distortion angle Θ = Σ(\|60– i\|)/24 [Θ = 0° for an ideal octahedron; i represents the trigonal angles of the eight faces of the octahedron].[25]*

The parameters indicate that the geometry around the Ga(III) in the NOTA complex is less distorted octahedron than that of **[Ga.L^n]**. This may be a consequence of the non-uniform N_3 donor set of the 7-membered ring, and its lower symmetry of the ring relative to that of 9-N_3.

In general, the Ga-N_{endo} bonds are slightly longer for **[Ga.L^n]** than for [Ga.NOTA][23] by ~ 0.04 Å, whilst the average Ga-O distance is approximately the same (±0.01 Å). For **[Ga.L^n]** complexes, the N_{exo}-Ga distance is shorter than both the N_{endo}-Ga distances, which are comparable (Table 4.7). This is a feature consistently observed for metal complexes featuring a tridentate bound DAZA core, and is believed to reflect the flexibility associated with the exocyclic nitrogen group.[6, 7, 26] The Ga-N bond distances are considerably elongated compared to the M-O bonds, consistent with the difference in donor-acceptor strength of the Ga-N and Ga-O bonds (Table 4.7). There is significant variation in the Ga-O bond lengths which is likely to be a consequence of a number of factors, including the asymmetry of the ring (Figure 4.19(iii)).

Table 4.7 *Selected bond distances (Å) for **[Ga.L^n]** (n = 2, 3, 6, 8)* relating to the coordination sphere of the complex. Estimated standard deviation's in brackets. *See Figure 4.19 for atom labelling scheme.*

	[Ga.L^2]	[Ga.L^3]	[Ga.L^6]*	[Ga.L^8]
Ga-O1	1.939 (2)	1.967 (1)	1.948 (4)	1.969 (3)
Ga-O3	1.904 (2)	1.895 (2)	1.907 (4)	1.888 (3)
Ga-O5	1.933 (2)	1.934 (2)	1.917 (4)	1.925 (3)
Ga-N1	2.140 (2)	2.158 (2)	2.136 (4)	2.115 (3)
Ga-N2	2.138 (2)	2.150 (2)	2.142 (5)	2.204 (3)
Ga-N3	2.111 (2)	2.075 (2)	2.110 (4)	2.107 (3)

values are the average of the two crystallographic independent molecules of **[Ga.L^6].*

The only examples in the literature of complexes featuring a carboxylic acid functionalised DAZA ligand incorporate lanthanide metal ions.[9, 26] These complexes all crystallize as dimeric complexes, a consequence of the constrained environment of the DAZA core whose 'bite-size' is too small to encapsulate the lanthanide ion; and as a result the "face of the metal" is exposed.[9, 26] This is illustrated by the difference in distances of the of the lanthanide ion from the planes of the N_3 and O_4 donor sets in [Gd.AAZTA] (Table 4.8).[9] The Ga(III) ion is considerably smaller in size, and as a result a better fit for the 'bite' of the ligands, with more comparable distances between the metal centre and N_3 and O_3 planes (Table 4.8).

Table 4.8 *Distances (Å) between the metal ion and the mean plane of the N and O donor sets.*

	[Ga.L^2]	[Ga.L^3]	[Ga.L^6]*	[Ga.L^8]	[Ga.NOTA][23]	[Gd.AAZTA][9]
M-O$_{plane}$ (Å)	0.984	1.071	1.028	1.058	1.019	0.132
M-N$_{plane}$ (Å)	1.404	1.425	1.423	1.437	1.335	2.091

values are the average of the two crystallographic independent molecules of **[Ga.L^6].*

A comparison of the distances in Table 4.8 for the **[Ga.L^n]** complexes reveals some variation in the positioning of the Ga(III) ion relative to the N_3 and O_3 donor sets. It is interesting to note that although the Ga(III) ion lies closer to the N_3 donor set in [Ga.NOTA], it is better encapsulated by the ligands in **[Ga.L^3]** and **[Ga.L^6]**. This is not the case for **[Ga.L^2]** where the Ga(III) ion is slightly closer to the O_3 plane, and further from the N_3 plane, compared to [Ga.NOTA]. It is noteworthy that there is a considerabley greater degree of rotation of the phenyl group, relative the C-N_{exo} substituent, for **[Ga.L^8]** (68.0°) compared to **[Ga.L^3]** (16.7°). This is likely to be a result of the methyl group of the propionic acid pendant arm, which points in the same general direction as the phenyl substituent (Figure 4.19(III)).

3.1.2 Conformation of the 7-Membered Ring

It was expected that tridentate binding of the nitrogens in the DAZA core requires a near perfect chair conformation (Figure 4.20). Indeed, the vast majority of metal complexes involving tridentate DAZA show less than a 2° deviation from the perfectly eclipsed arrangement of the N-CH_2-CH_2-N fragment, which is characteristic of the chair conformation.[6-9, 11-13, 26, 27] In Figure 4.20 representative examples of complexes containing the DAZA core in the chair conformation are shown. Also characteristic of the chair conformation is that the torsion angles are approximately equal in size and opposite in sign at symmetry related sites of the ring (Table 4.9).

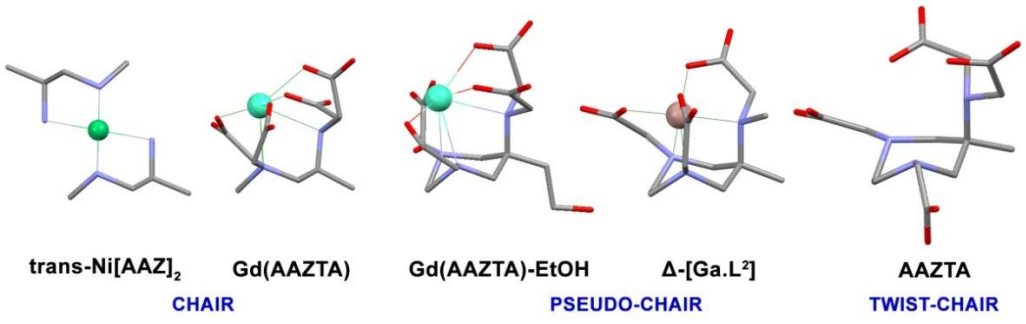

Figure 4.20 *Selected examples, and the conformation adopted by the ring of bound DAZA ligands and the AAZTA free ligand.*[6, 9, 26]

The gadolinium(III) and europium(III) complexes of the AAZTA-EtOH[26] ligand adopt a conformation with a N-CH_2-CH_2-N torsion angle of -28.17°, which is similar to that of the **[Ga.L^n]** complexes reported here (Table 4.9). The conformation of the 7 membered ring has been described as a pseudo-chair, however the torsion angles (and side-on view: Figure 4.20) suggest that the ring conformation is closer to that of the twisted-chair (TC) adopted by the free ligand AAZTA[9] (Table 4.9).

Table 4.9 *Torsion angles (°) for the seven membered rings of **Λ-[Ga.L^n]** (n = 2, 3, 6, 8) and relevant literature examples. See Figure 4.19 for atom labelling scheme.*

Bond torsion	Λ-[Ga.L^2]	Λ-[Ga.L^3]	Λ-[Ga.L^6]*	Λ-[Ga.L^8]	Eu(AAZTA-OH)[26]	AAZTA[a,9]	[Eu.AAZTA][b,9]
N1-C1-C2-N2 (°)	25.65	29.12	29.03	24.81	-28.17	-45.25	-2.95
C1-C2-N2-C3 (°)	-58.76	-56.92	-57.96	-58.51	58.43	40.26	76.97
C2-N2-C3-C4 (°)	103.20	101.86	101.38	101.65	-100.77	-96.37	-91.55
N2-C3-C4-C5 (°)	-68.32	-68.15	-64.22	-68.95	64.59	70.44	57.72
C3-C4-C5-N1 (°)	52.14	51.56	46.73	54.11	-48.25	-46.98	-57.87
C4-C5-N1-C1 (°)	-86.73	-82.50	-81.63	-84.79	80.89	67.49	92.06
C5-N1-C1-C2 (°)	99.60	98.90	101.26	96.52	-94.71	-91.12	-75.10

** one of the two crystallographic independent molecules of **[Ga.L^6]** is shown. There is no significant difference between the two ring conformations.[a]Twist-Chair conformation. [b]Chair conformation.*

A number of factors contribute towards defining the lowest energy conformation adopted by the ring. The reduced torsional strain (relative to the chair conformation) within the N-CH_2-CH_2-N fragment is favourable, perhaps made possible by the apparent 'willingness' of Ga(III) to adopt a distorted octahedral geometry.[20] In addition, the presence of the coordinating pendant arms is also expected to be influential. The torsion angles of the ring indicate that there is a notable structural commonality to the three structures reported here. The absence of any significant conformational change resulting from the Me/Ph permutation is evident. Indeed, it is tempting to speculate that this modification of the core structure has not only improved the degree of pre-organisation of the ligand for metal binding, but also enhanced the rigidity of the desired conformation.

3.2 Solution State Multinuclear NMR Studies of [Ga.L^n] (n = 2, 3, and 8)

The Ga(III) (d^{10}) ion is diamagnetic, and thus solution NMR studies of Ga(III) complexes are of interest. Crystalline material of **[Ga.L^n]** (n = 2, 3 and 8) was isolated from the complexation solution, re-dissolved in D_2O, and NMR studies carried out using a Varian 600 MHz NMRS at 298 K and pH ~ 5. Consistent with the solid state structure, mass spectrometry showed the presence of only a 1 : 1 complex (as the singly protonated species).

Single resonances were found in the ^{71}Ga (I = 3/2, 39.6 % natural abundance, quadrupolar moment = 0.112) NMR spectra of **[Ga.L^n]** (n = 2, 3 and 8), and are presented in Table 4.10, with chemical shifts relative to $[Ga(H_20)_6]^{3+}$. Also shown, are the 'width at half-height' ($\omega_{½}$) values which, for quadrupolar ^{71}Ga, are a sensitive function of the local molecular symmetry. For example, in the C_3-symmetric Ga(III) complex of NOTA, very little line broadening is observed ($\delta_{Ga(71)}$ = 171 MHz, $\omega_{½}$ = 210 Hz at 5.88 T) compared to that of the $[Ga(H_20)_6]^{3+}$ reference ($\omega_{½}$ = 53 Hz at 5.88 T).[28]

For [Ga.NOTA], the narrow line width of the ^{71}Ga NMR signal is consistent with a complex in which the metal ion donor set is tightly bound and highly symmetrical. Intrinsic line broadening in the spectra of quadrupolar nuclei ("Quadrupolar relaxation") is a result of interaction of the nuclear quadupole moment with the electric field gradient at the nucleus. The magnetic dipole and electric dipole are strongly coupled, because quadrupolar transitions change the electromagnetic environment. Therefore, relaxation of the nuclear electric quadupole, associated with changes in the local electric field gradient (due to molecular motion in the fluid state) also relaxes the nuclear spin. For octahedral complexes with facial N_3 and O_3 donor sets, the gradient in the *x*-*y* plane tends to zero and the resultant field gradient at the nucleus is highly anisotropic. This results in minimal quadrupolar relaxation, and hence, minimal line broadening.[28]

^{71}Ga-NMR $\omega_{½}$-values and the octahedral distortion parameters (Σ and Θ: Table 4.6), are all a measure of the relative symmetry in the different complexes. In terms of the relative order of the complexes, the parameters are in excellent agreement. This indicates that, the structures in solution and solid state are similar.

Table 4.10 *Variation of ^{71}Ga NMR spectral parameters (δ_{Ga} and $\omega_{½}$) for* ***[Ga.L^n]*** *(n = 2, 3, 8),* [Ga.(10N$_3$-triacetate)][28] *and $[Ga(H_20)_6]^{3+}$. Recorded at 182.91 Hz (14.09 T) and 298 K in D_2O, unless otherwise stated.*

Complex	δ_{Ga} (ppm)[a]	$\omega_{½}$ (Hz)
$[Ga(H_20)_6]^{3+}$	0	877
[Ga.L^2]	129	983
[Ga.L^3]	123	1174
[Ga.L^8]	124	1815
[Ga.(10N$_3$-triacetate)][b,28]	133	2000

[a]*Relative to $[Ga(H_20)_6]^{3+}$, i.e. $Ga(NO_3)_3$ in D_2O.* [b]*At 5.88 T and 298 K in D_2O.*

As an illustrative example the ^{1}H NMR spectrum of **[Ga.L^2]** is discussed below. The ^{1}H NMR (14.1 T) spectrum is particular well resolved, which makes it possible to unambiguously assign all protons, except for H^4 and H^5 (Figure 4.21), with the help of 2D COSY, HSQC- and HMBC-NMR experiments. The methyl signals, H$^{1'}$ and H^{14}, resonate as singlets at 1.03 and 2.43 ppm respectively. The remaining protons are all diastereotopic, with a coupling pattern that was typical of two *AB*-doublet for H^{2,7} (ring methylene protons), two *AB*-multiplets for H^{4,5} (ethylene bridge CH$_2$'s) and an *AB*-doublets for H^{8,10,12} (acetate CH$_2$'s) structure. The splitting pattern indicates that the complex has a very rigid structure.

With respect to the free ligand (at the same pH), the ^{1}H NMR signals of the two methyl signals (H$^{1'}$ and H^{14}) of the ligand in the bound complex show shifts to lower frequency, whilst remaining protons resonate to higher frequency (Figure 4.21 *top left*). In the free ligand, **L^2**, rapid exchange between enantiomers, on the NMR time-scale, was manifested as a single *AB*-doublet (4H) for H^8 and H^{10}, i.e. there are 2 pairs of equivalent diastereotopic protons. A similar splitting pattern is observed for H^2-H^7.

However, in the case of the bound ligand each 'pair' of diastereotopic protons resonate as separate *AB*-doublets, consistent with a lower time averaged symmetry. The same is observed for H^4-H^5, which resonate as more complex multiplets, due to the presence of vicinal and geminal proton coupling constants of different value. In the proton decoupled ^{13}C NMR spectra, the signals of the carbons which appeared as single resonances in the free ligand (C^4-C^5, C^2-C^7 and C^8-C^{10}) resolve into separate signals in the bound ligand, as expected.

In the case of C_3-symmetric complexes, for example [Ga.NOTA], it is possible to assign the *A* and *B ring* protons to their axial and equatorial orientations. Using 2D NOESY and Pureshift (homonuclear broadband decoupling) NMR experiments, together with the crystal structure of **[Ga.L^2]**, the diastereotopic protons of H_2 and H_7 were assigned to axial and equatorial orientations, as well as their correct location, with reference to the position adopted by the N_{exo}-acetate pendant arm (Figure 4.21 *top right*). The Pureshift ^{1}H NMR experiment collapses homonuclear signals into singlets (Figure 4.21 *bottom left*). This significantly improves signal 'separation' and makes interpretation of the 2D spectra more accurate. The Pureshift ^{1}H NMR spectrum of **[Ga.L^2]** has been plotted as the horizontal trace of the 2D NOESY plot.

According to the 2D NOESY plot, the N_{exo}-Me group (H^{14}) shows nOe correlations with a single proton on C^7 (δ_H = 3.46 ppm), C^8 (δ_H = 3.71 ppm) and C^{12} (δ_H = 3.21 ppm). From the crystal structure, it is evident that H^{14} is closest to an equatorially orientated proton on C^7, indicating that the signal at 3.46 ppm originates from H^{7eq}. One of the protons on C^{12} (δ_H = 3.89 ppm) has an nOe correlation to a proton of C^2 (δ_H = 3.59 ppm). Similarly, this indicates that the signal at 3.59 ppm originates from H^{2eq}. Consistent with these assignments and the crystal structure, $H^{1'}$ shows an nOe correlation with the other proton on C^2 (H^{2ax}). These correlations confirm the connectivity assignments made using 2D-HSQC and –HMBC NMR experiments. It was not possible to unambiguously assign the protons of H^4 and H^5, due to complexity and the similar chemical shifts of their *AB*-multiplets.

3.3 Summary

Solid state structures of the complexes reveal that the Ga(III) is a considerably better fit for the cavity of these ligands, than the larger Lanthanide ions. There is a high degree of commonality to the conformation of the ring in **[Ga.L^n]** (n = 2, 3, 6). The ring binds in a tridentate fashion, adopting a somewhat unusual pseudo-twisted-chair conformation. The conformation of the ring is expected to have less inherent strain than the more frequently observed Chair-conformation, due to the more staggered arrangement of the N-CH_2-CH_2-N fragment. The AMPED based examples, **[Ga.L^n]** (n = 2 and 3) have a less distorted octahedral geometry about the Ga(III) ion, as shown by crystallographic and ^{71}Ga-NMR spectroscopic data. The ^{1}H NMR spectra of the complexes are characterised by well resolved and sharp proton resonances, indicative of a rigid structure. The 2D NOESY NMR of **[Ga.L^2]** is fully consistent with the solid state crystal structure.

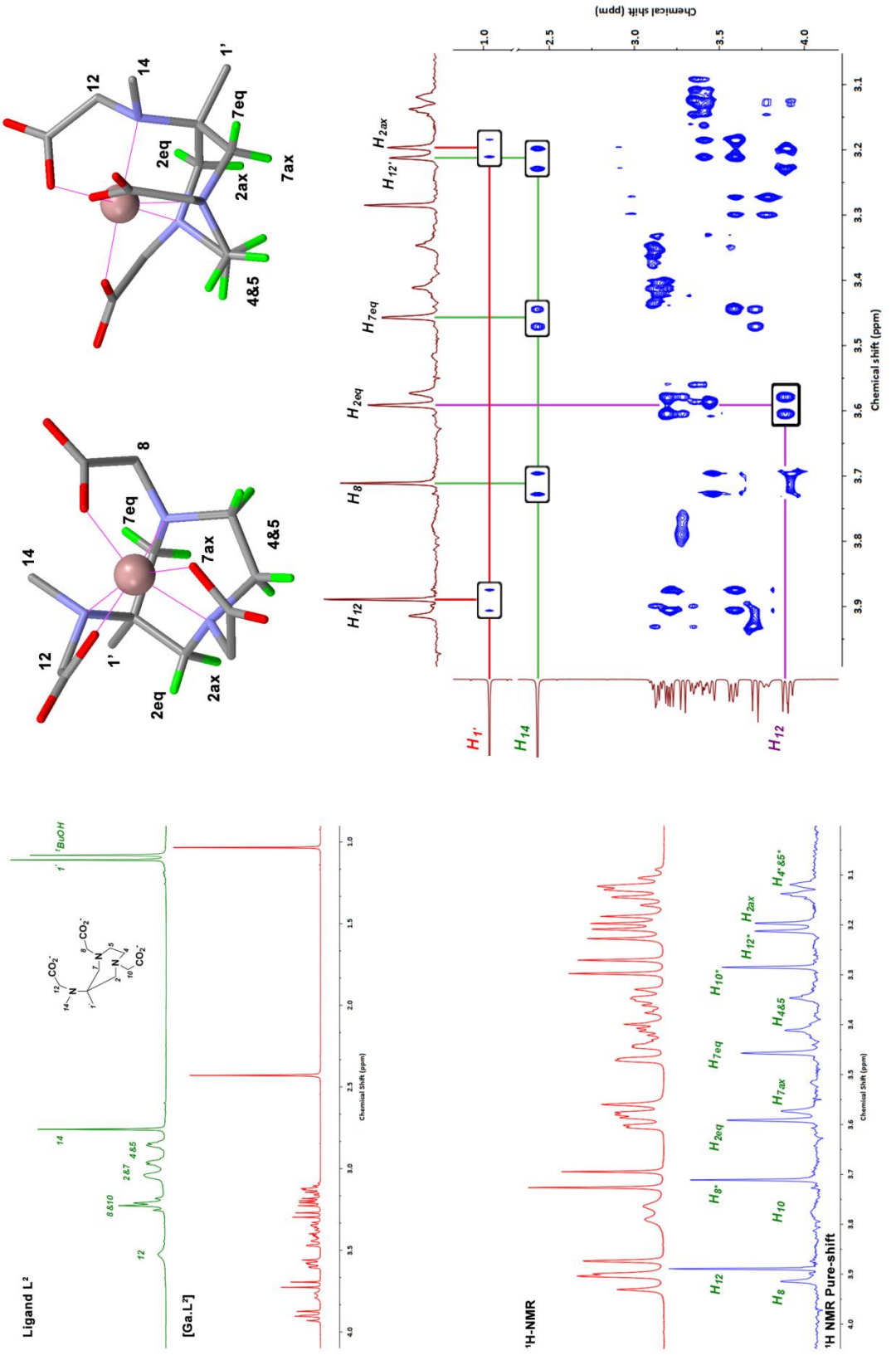

Figure 4.21 *NMR experiments used for the assignment of [Ga.L²], in particular the orientation of the methylene ring protons. Top left: Comparison of the free and Ga(III)-bound ligand L². Bottom left: Expansion of the ¹H NMR spectrum of [Ga.L²], and the Pureshift ¹H NMR spectrum with the proton resonances assigned. Top right: crystal structure views of [Ga.L²] with the protons labelled. Bottom right: NOESY plot with the nOe correlations of interest highlighted. 600 MHz, pH ~ 5, 298 K, D_2O.*

4 References

1. D. Cremer and J. A. Pople, *Journal of the American Chemical Society*, 1975, **97**, 1354-1358.
2. A. Entrena, J. Campos, J. A. Gomez, M. A. Gallo and A. Espinosa, *Journal of Organic Chemistry*, 1997, **62**, 337-349.
3. F. Freeman, J. H. Hwang, E. H. Junge, P. D. Parmar, Z. Renz and J. Trinh, *International Journal of Quantum Chemistry*, 2008, **108**, 339-350.
4. A. Entrena, J. M. Campos, M. A. Gallo and A. Espinosa, *Arkivoc*, 2005, 88-108.
5. I. K. Boessenkool and J. C. A. Boeyens, *Journal of Crystal and Molecular Structure*, 1980, **10**, 11-18.
6. C. Neis, D. Petry, A. Demangeon, B. Morgenstern, D. Kuppert, J. Huppert, S. Stucky and K. Hegetschweiler, *Inorganic Chemistry*, 2010, **49**, 10092-10107.
7. J. Romba, D. Kuppert, B. Morgenstern, C. Neis, S. Steinhauser, T. Weyhermuller and K. Hegetschweiler, *European Journal of Inorganic Chemistry*, 2006, 314-328.
8. A. J. Bortoluzzi, A. Neves and G. G. Terra, *Acta Crystallographica Section E-Structure Reports Online*, 2006, **62**, M2965-M2966.
9. S. Aime, G. Bombieri, C. Cavallotti, G. B. Giovenzana, D. Imperio and N. Marchini, *Inorganica Chimica Acta*, 2008, **361**, 1534-1541.
10. P. Comba, C. Haaf and H. Wadepohl, *Inorganic Chemistry*, 2009, **48**, 6604-6614.
11. S. Ge, A. Meetsma and B. Hessen, *Organometallics*, 2009, **28**, 719-726.
12. S. Ge, S. Bambirra, A. Meetsma and B. Hessen, *Chemical Communications*, 2006, 3320-3322.
13. S. Ge, A. Meetsma and B. Hessen, *Organometallics*, 2007, **26**, 5278-5284.
14. A. E. Martell, R. J. Motekaitis and M. J. Welch, *Journal of the Chemical Society-Chemical Communications*, 1990, 1748-1749.
15. L. Fabbrizzi, M. Micheloni and P. Paoletti, *Inorganic Chemistry*, 1976, **15**, 1451-1452.
16. S. Deangelis, A. Batsanov, T. J. Norman, D. Parker, K. Senanayake and J. Vepsalainen, *Journal of the Chemical Society-Chemical Communications*, 1995, 2361-2363.
17. D. Parker, K. Senanayake, J. Vepsailainen, S. Williams, A. S. Batsanov and J. A. K. Howard, *Journal of the Chemical Society-Perkin Transactions 2*, 1997, 1445-1452.
18. E. V. Anslyn and D. A. Dougherty, *Modern Physical Organic Chemistry*, Univeristy Science Books, U.S.A, 2006.
19. T. Steiner, *Angewandte Chemie International Edition*, 2002, **41**, 48-76.
20. G. Bandoli, A. Dolmella, F. Tisato, M. Porchia and F. Refosco, *Coordination Chemistry Reviews*, 2009, **253**, 56-77.
21. D. E. Reichert, J. S. Lewis and C. J. Anderson, *Coordination Chemistry Reviews*, 1999, **184**, 3-66.
22. T. J. Wadas, E. H. Wong, G. R. Weisman and C. J. Anderson, *Chem Rev*, 2010, **110**, 2858-2902.
23. A. S. Craig, D. Parker, H. Adams and N. A. Bailey, *Journal of the Chemical Society-Chemical Communications*, 1989, 1793-1794.
24. M. G. B. Drew, C. J. Harding, V. McKee, G. G. Morgan and J. Nelson, *Journal of the Chemical Society-Chemical Communications*, 1995, 1035-1038.
25. N. Ortega-Villar, A. L. Thompson, M. C. Munoz, V. M. Ugalde-Saldivar, A. E. Goeta, R. Moreno-Esparza and J. A. Real, *Chemistry: A European Journal*, 2005, **11**, 5721-5734.
26. R. S. Sengar, A. Nigam, S. J. Geib and E. C. Wiener, *Polyhedron*, 2009, **28**, 1525-1531.
27. R. A. Peralta, A. Neves, A. J. Bortoluzzi, A. Casellato, A. dos Anjos, A. Greatti, F. R. Xavier and B. Szpoganicz, *Inorganic Chemistry*, 2005, **44**, 7690-7692.
28. C. J. Broan, J. P. L. Cox, A. S. Craig, R. Kataky, D. Parker, A. Harrison, A. M. Randall and G. Ferguson, *Journal of the Chemical Society-Perkin Transactions 2*, 1991, 87-99.

Chapter 5

Conclusion and Future Work

1 Conclusion

A set of four structurally related ligands (**L^2**, **L^3**, **L^6** and **L^8**: Figure 6.1) has been prepared, which show considerable potential for practical application in the development of ^{68}Ga tracers for molecular imaging with PET. Three of the ligands quantitatively radiolabel within 3 minutes at room temperature over the pH range 4 – 7, to give a single radiolabelled species. The mild conditions make these ligands amenable to biomolecule conjugation. The very fast complexation and quantitative yields, which simply radiolabel purification, are major advantages for the application of the short-lived ^{68}Ga-radionuclide. The radiolabelled complexes are stable in the presence of excess DTPA, *apo*-transferrin, iron(III) and in newborn calf serum over 2 hours under physiological conditions. The bio-distributions of **[^{68}Ga.L^2]** and **[^{68}Ga.L^8]** confirm the stability of all complexes determined *in vitro* with a renal clearance pathway. The ligands display remarkable selectivity for gallium(III) over iron(III), calcium(II) and copper(II). Therefore, these ligands form a good basis for the development of ^{68}Ga-radiolabelled bioconjugates. Radiolabelling of the ligands below pH 3.5 is possible, but gives rise to multiple radiolabelled species of differing stability, which precludes their application *in vivo*. The presence of multiple species has been attributed to the formation of kinetically trapped complexes, resulting from different conformations of the free ligand. By substituting the quaternary methyl for a phenyl moiety, the population of the conformation which favours stable ^{68}Ga chelation is increased. However, radiolabelling under these conditions is still not practicable below pH 3.5. The Me-Ph permutation also serves to stabilise the preferred ligand design, by inhibiting internal lactamisation.

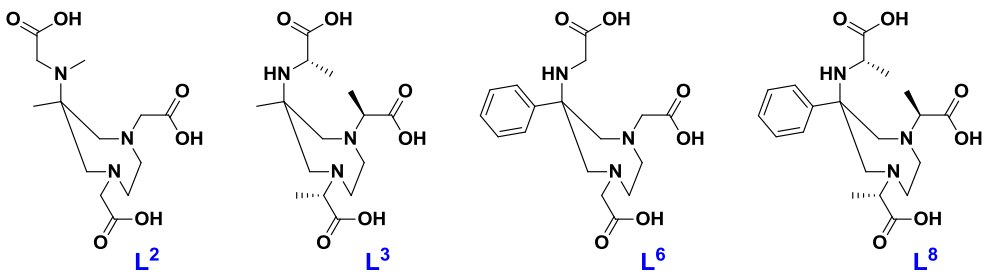

Figure 6.1 *Ligands with properties which make them very promising ligands for application in ^{68}Ga-PET.*

2 Future Work

In terms of carrying this research forward, it is hoped to develop derivatives of these ligands suited for bioconjugation. A significant amount of research has been carried out functionalising the quaternary carbon.[1-6] Using this approach has proved successful in terms of conjugation and maintaining the chelating ability of the ligand.[1-6] Other possible points of attachment include the exocyclic amine and α-carbon of the imino-acetate. Making use of the α-carbon of the iminoacetate as a point of attachment (**L**$^{11/12}$) has not yet been explored for AAZTA derivatives, but is a commonly applied method of conjugation applied to NOTA and DOTA ligand derivatives.[7, 8] On this basis, it would be fairly straightforward to propose some target compounds (Figure 6.2).

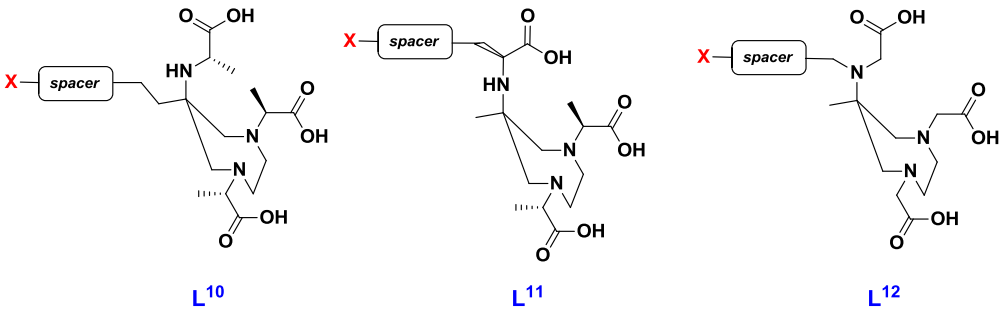

Figure 6.2 *Possible modifications to AMPED based ligands* ***L***^{2} *and* ***L***^{3} *to yield ligands suitable for bioconjugation.*

Using the AMPED scaffold as a basis may have some potential downfalls. Ligands **L**^{10,11} have an inherent tendency to lactamise, and **L**^{12} may encounter speciation problems. A sensible approach would be to make use of the modified scaffold (APPED), which has been shown to inhibit both of these problems. Of further benefit is the novelty of the scaffold, which will assist should a patent application be pursued.

Derivatisation of **L**^{6} and **L**^{8} at the *para*-position (**L**^{13}: Figure 6.3) of the phenyl group are very attractive targets, although they require significant synthetic effort. To test the suitability of the scaffold as a concept, it would be sensible to consider a simpler strategy. In particular, initial efforts should be focused on the synthesis of **L**^{14}. This structure will take advantage of the favourable properties of the novel APPED scaffold, which include improved ligand stability and the formation of a single radiolabelled species. Propionic acid pendant arms are proposed because they; increase the overall lipophilicity (which may reduce any untoward effects on the pharmacokinetics of the

targeting vector), and inhibit ligand lactamisation. Conjugates based on L^{13} would be interesting secondary targets, because they may be benefits of the having the spacer group isolated from the donor groups. Specifically, using the pendant propionate arm as the point of attachment may have a untoward effect on the stability and/or complexation kinetics of the ligand.

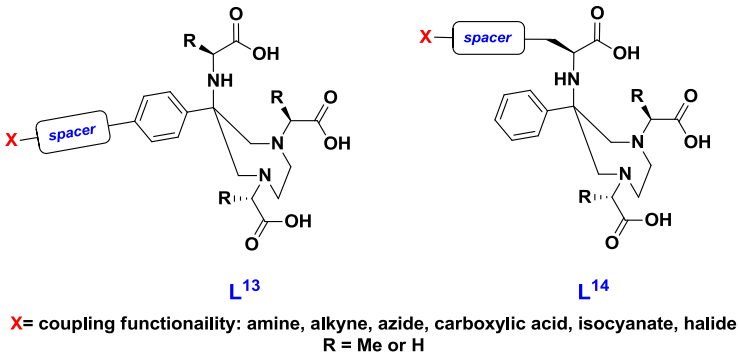

Figure 6.3 *Possible modifications to APPED based ligands* L^6 *and* L^8 *to yield ligands suitable for bioconjugation.*

Progress towards these BFC's has already started, with the synthesis of a hex-6-yne derivative of L^{12}. The unconjugated ligand displays very favourable radiolabelling properties, nearly identical to those of L^2 (its 'parent' ligand), and the radiolabelled complex is stable in the presence of excess *apo*-transferrin. Furthermore, the protected ligand has been coupled to pteroic (folic) acid via a copper catalysed click reaction. Certain tumour cells overexpress folate receptors, for which the pteroic acid has a high affinity.[9] Hydrolysis of the *tert*-butyl esters to give the bifunctional chelate is currently underway.

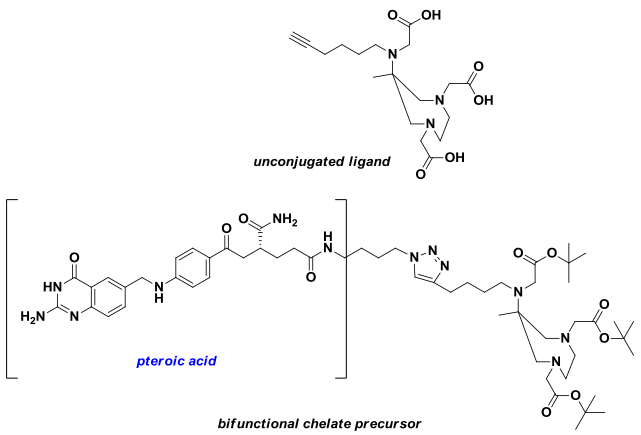

Figure 6.4 Shows the structures of the *unconjugated ligand, and pteroic acid conjugated ligand precursor currently being investigated as an AMPED based bifunctional chelator for* ^{68}Ga.

3 References

1. J. Martinelli, G. Gugliotta and L. Tei, *Organic Letters*, 2012, **14**, 716-719.
2. E. Gianolio, G. B. Giovenzana, D. Longo, I. Longo, I. Menegotto and S. Aime, *Chemistry-a European Journal*, 2007, **13**, 5785-5797.
3. G. Gugliotta, M. Botta and L. Tei, *Organic & Biomolecular Chemistry*, 2010, **8**, 4569-4574.
4. R. S. Sengar, A. Nigam, S. J. Geib and E. C. Wiener, *Polyhedron*, 2009, **28**, 1525-1531.
5. E. Gianolio, K. Ramalingam, B. Song, F. Kalman, S. Aime and R. Swenson, *Inorganic Chemistry Communications*, 2010, **13**, 663-665.
6. L. Manzoni, L. Belvisi, D. Arosio, M. P. Bartolomeo, A. Bianchi, C. Brioschi, F. Buonsanti, C. Cabella, C. Casagrande, M. Civera, M. De Matteo, L. Fugazza, L. Lattuada, F. Maisano, L. Miragoli, C. Neira, M. Pilkington-Miksa and C. Scolastico, *Chemmedchem*, 2012, **7**, 1084-1093.
7. R. C. Matthews, D. Parker, G. Ferguson, B. Kaitner, A. Harrison and L. Royle, *Polyhedron*, 1991, **10**, 1951-1953.
8. P. J. Riss, C. Kroll, V. Nagel and F. Rosch, *Bioorg Med Chem Lett*, 2008, **18**, 5364-5367.
9. C. J. Mathias, M. R. Lewis, D. E. Reichert, R. Laforest, T. L. Sharp, J. S. Lewis, Z. F. Yang, D. J. Waters, P. W. Snyder, P. S. Low, M. J. Welch and M. A. Green, *Nuclear Medicine and Biology*, 2003, **30**, 725-731.

Chapter 6

Experimental

This chapter described the procedures followed, instrumentation used, and compounds synthesised during the course of this project.

1 General Procedures

Commercially available reagents were used as supplied from the suppliers. Solvents were laboratory grade, dried using a suitable drying agent when required. Reactions requiring anhydrous conditions were carried out under an atmosphere of argon using standard Schlenk-line techniques. For all non-radioactive procedures, "water" refers to high purity water (< 0.04 $\mu S.cm^{-1}$) obtained from a PuriteSTILL Plus® purification system.

Thin-layer chromatography was carried using silica gel plates (Merck 5554). The plates were visualised, as appropriate, using UV (254/365 nm) irradiation or Dragendorff's reagent. Preparative column chromatography was carried out using silica gel (Merck Silica Gel 60, 230400 mesh).

pH Measurements were carried out at 295 K using Jenway 3320 or Jenway 3020 pH meter with a Sigma-Aldrich micro-pH combination electrode. Commercially available buffer solutions (Sigma-Aldrich) were used to calibrate the pH meter at pH 4.00 ± 0.02, 7.00 ± 0.02 and 10.00 ± 0.02 prior to use. For measurements conducted in D_2O, the pD was calculated from the pH meter reading using: pD = pH + 0.41.[1]

1D and 2D NMR spectra (^{1}H, ^{13}C and ^{71}Ga) were recorded on a Varian VXR-400 spectrometer (^{1}H at 399.97 MHz, 13C at 100.578 MHz), Varian VNMRS-700 spectrometer (^{1}H at 699.73 MHz, ^{13}C 175.95 MHz) or a 600 MHz Varian (Agilent) Premium Compact (^{1}H at 599.78 MHz, ^{13}C at 150.82 MHz, ^{71}Ga at 182.91 MHz). Unless otherwise stated, spectra were collected at 295 K in commercially available deuterated solvents, and referenced internally to the residual solvent proton resonances. All chemical shifts are given in ppm, with coupling constants and peak-width-at-half-heights in Hz. Splitting patterns are described as singlet (s), broad singlet (Br. s), doublet (d), triplet (t), quartet (q) or multiplet (m). A fairly common occurrence for the compounds characterised is the presence of

AA'BB'-coupling, arising from equivalent diastereotopic protons on symmetry related carbon atoms. Unless otherwise stated, proton resonances arising (entirely or in part) from A or A' are simply assigned as H^{A}. Similarly, proton resonances with contributions from B or B' are assigned as H^{B}. The use of superscript comma (′) in the assignment indicates that a resonance arises from more than one proton (i.e. $H^{2,7}$ is a proton resonance which arises from both H^{2} and H^{7}). The use of a superscript solidus (/) indicates that the assignment could not be defined with certainty (i.e. $H^{2/7}$ is a proton resonance that arises from either H^{7} or H^{2}).

Electrospray (ES) and high resolution (HS) mass spectrometry were performed on a Thermo-Finnigan LTQ FT system, operating in positive or negative mode as stated, using methanol as a carrier solvent. Ultra performance liquid chromatography (UPLC) electrospray mass spectrometry was performed on a LCT Premier XE mass spectrometer, operating in positive or negative mode as stated, equipped with an Acquity UPLC system. The Acquity photodiode array detector provides absorbance data from 210 nm to 400 nm. Carrier solvent is a methanol : water gradient (5 % methanol → 95 % methanol) elution, and a BEH C18 column (1.7 μm particle size, 2.1 x 50 mm dimensions).

Infra-red (IR) spectra were recorded on a Perkin Elmer Spectrum RX1 with ATR attachment.

Melting points were recorded on a Reichart-Köfler block and are uncorrected.

2 Single Crystal X-ray Studies

Single crystal X-ray data was collected on a Bruker SMART-CCD 6000 diffractometer (ω, 0.3 – 0.5 ° / frame) at 120 ±2 K. The temperature was controlled using an Oxford Cryostream open-flow nitrogen cryostat. The structures were solved by the Patterson method, and refinement by full-matrix least squares on F^{2} for all data using SHELXTL[2] and OLEX2[3] software. All non-disordered non-hydrogen atoms were refined with anisotropic displacement parameters. All hydrogen atoms were placed into calculated positions and refined in 'riding'-mode.

3 Radiochemical Procedures

All radiochemical investigations have been conducted by the author, at the Johannes-Gutenberg Universtat: Institut für Kernchemie, (Mainz, Germany) through collaboration with Professor Frank Rösch.

3.1 General

All chemicals used for the radiochemical experiments were procured from commercial suppliers in the highest available purity. Purite® water used was filtered through a Millex® Millipore filter membrane (0.54 µm) prior to use. No metallic implements or apparatus were used so as to avoid any metal contamination, and standard safety protocols strictly adhered to. For radio-TLC analysis, Merck Silica F254 TLC plates were used, and the eluted plates radio-imaged using a flatbed Canberra Packard Instant Imager. All radioactive ^{68}Ga solutions were kept inside lead blocks. Whenever possible, radioactive solutions and TLC plates were kept behind suitable lead shielding 'bricks'. All solids were weighed using a 5 decimal-place mass-balance. All solution volumes were measured using suitable Eppendorf® pipettes, except in the preparation of buffers were a volumetric flask was used.

In this study a 350 MBq ^{68}Ga/^{68}Ge-generator based on titanium dioxide, produced by Cyclotron Co., Obninsk, Russian Federation, was used. The generator was eluted with 8 mL of 0.1 M HCl. Prior to radiolabelling, post-processing of the generator eluate was carried out using a cation exchange technique described elsewhere.[4] Using this approach the eluate volume was reduced to 400 µL, and the presence of metal impurities (^{68}Ge and non-radioactive metals) lowered in the protocol that takes less than 5 min to complete. Following post-processing, the eluate was diluted, such that 400 µL contained ~ 100 MBq of radioactivity (at t = 0). In all radiochemical experiments the reactions/evaluations where carried out in sterile unused containers as specified.

All stabilities and radiolabelling yields have been evaluated using a radio-TLC plate method. Background radioactive signal can be as high as 5 % of the total radioactivity on the plate. Therefore, unless the population distribution map shows evidence of a 'radioactive spot' on the plate, any signal < 5 % is assumed to be background. For this reason radiolabelling yields > 96 % are deemed 'quantitative'.

3.2 Radiolabelling Protocols

The radiolabelling kinetics of the ligands was evaluated at 298, 323 and 368 K at pH 2.3, 3.3, 4.0, 5.3 and 7.0. Stock solutions of the ligands (1 mg/mL) were prepared in water. Radiolabelling experiments carried out at pH 4.0 and 5.3 were acetate buffered, and the experiments conducted at pH 7.0 were HEPES buffered. Various concentrations of the buffer solutions were evaluated for the

lowest concentration that had sufficient buffering ability upon addition of the post-processed ^{68}Ga solution. The acetate 'buffers' were prepared by combining calculated amounts of acetic acid and sodium acetate to give a 0.2 M buffer solution, adding sufficient HCl or NaOH to give the desired pH. The HEPES buffer was prepared by adjusting the pH of a 1.0 M sodium-HEPES solution to 7.2 using 1.0 M sodium hydroxide. Suitable dilution of the post-processed generator eluate was used to achieve pH 2.3 and 3.3. Preparations of the radiolabelling solutions for the different conditions are described below.

***pH 2.3*:**

The ligand (50 nmol) was added of water (4.6 mL) in a glass vial, and the mixture preheated at the desired temperature for 2 min. To this mixture the post-processed generator eluate (400 µL, ~ 100 MBq) was added and a timer started.

***pH 3.3*:**

Followed a similar protocol to that described for 'pH 2.3', except 50 µL (~ 12 MBq) of the post-processed generator eluate was used.

pH 4.0, 5.3 and 7.0:

The ligand (14 nmol) was added to 1 mL of the appropriate buffer solution (1 mL) in a 2 mL Eppendorf® vial, and the mixture preheated for 2 min at the desired temperature. To this mixture the post-processed generator eluate (400 µL, ~ 100 MBq) was added and a timer started.

Radiolabelling solutions were continuously agitated using a rotary shaker with a temperature control function. At 1, 3, 5 and 10 min time intervals after addition of the post-processed ^{68}Ga; 1 µL fractions of the reaction mixture were withdrawn using an Eppendorf® pipette and spotted, in duplicate, on separate TLC plates (Merck Silic Gel F254). To ensure correct interpretation of the radiolabelling the duplicate TLC plates were eluted separately with a 0.5 M sodium citrate buffer solution (pH 4.0) and a 90 % MeOH in 10 % aqueous NaCl solution. Using the citrate buffer, un-complexed ^{68}Ga forms a ^{68}Ga-citrate complex which elutes to the top of the TLC plate (R_f ~ 0.9), while the radiolabelled product remains on or close to the baseline. Using the 90 % MeOH saline solution the un-complexed ^{68}Ga remains on the baseline, whilst the radiolabelled product moves approximately half way up the TLC plate. Exact R_f values depend on the characteristics of the radiolabelled product, and were not recorded. From the eluted TLC plates it was possible to determine the ratio of complexed to un-complexed ^{68}Ga at the different time intervals. Each radiolabelling evaluation was repeated two

more times. Control experiments, in which the ligand is not added, were conducted in parallel with the radiolabelling experiments.

3.3 Stability Studies

No post-radiolabelling purification of the radiolabelled products was carried out because only ligands which showed quantitative radiolabelling were evaluated in the stability experiments.

The stability of the radiolabelled complexes was assessed in the presence of DTPA, Fe(III) (each 5000 equivalents), *apo*-transferrin (130 equivalents) and new born calf serum. The evaluations were carried out over 2 h at 310 K and pH 7.4 (1.0 M PBS), and the solutions agitated using a rotary shaker. All stability studies were performed twice and in duplicate for each ligand-radiolabelling pH combination of interest. Two control experiments where performed in each case; one in the absence of the ligand and the other in the absence of the challenge. These were used to establish the R_f values of the free ^{68}Ga, ^{68}Ga-transferrin and ^{68}Ga-DTPA complexes, as well as any complexation of the free ^{68}Ga in the new-born calf serum. Stock solutions of DTPA, $FeCl_3$ (both 1.0 μM) and apo-transferrin (1 mg/ml) were prepared in 1.0 M PBS (pH 7.4) solution. The newborn calf serum was used as received.

The challenge solution (200 μL) was preheated at 310 K for 10 minutes in a 2 mL Eppendorf® vial, and the radiolabelled complex (50 μL of the appropriate radiolabelling solution) added. At 15, 30, 60, 90 and 120 min time intervals following addition of the radioactivity, 2 μL fractions were withdrawn using an Eppendorf® pipette and spotted, in duplicate, on separate TLC plates. To ensure correct interpretation of the stability evaluation, the duplicate TLC plates were eluted separately with a 0.5 M citrate buffer solution (pH 4) and a 90 % MeOH 10 % NaCl solution. From the eluted TLC plates it was possible to determine the amount of intact radiolabelled complex at the different time points.

3.4 NOTA Competition Experiment

This evaluation was only undertaken for ligands deemed suitable for ^{68}Ga PET, as determined from their radiolabelling properties and radiolabelled complex stability.

The conditions used for the NOTA-challenge experiments were selected so that they reflected the optimum conditions for radiolabelling of NOTA. The challenge was performed at 298 K and pH 4 (0.2

M citrate buffer) over the course of 10 minutes, with a 20 µM concentration of both NOTA and the ligand of interest. Under the conditions used each ligand (in isolation) would show quantitative radiolabelling within 1 min at room temperature.

Equimolar amounts (28 nmol from 1 mg/mL stock solutions) of NOTA and the ligand were added to 1 mL of a 0.2 M acetate buffer solution (pH 4) in a 2 mL Eppendorf® vial, and the mixture left to equilibrate on a rotary shaker for 2 min at 298 K. The post-processed ^{68}Ga (400 µL) was added, and 1 µL fractions of the radiolabelling solution spotted on a TLC plate at 1, 3, 5, 10 and 120 min time intervals. The TLC plates were eluted using a 0.5 M citrate solution (pH 4). With this mobile phase the un-complexed ^{68}Ga elutes to the top of the plate, the [^{68}Ga.NOTA] complex about a third of the way up (R_f ~ 0.35) and the radiolabelled ligand L^n evaluated remains on, or close to, the base line. From the eluted TLC plates it was possible to determine the relative ratios of different complexes at each time interval. Control experiments were carried out in parallel in the absence of each and both ligands. All challenge experiments were repeated twice.

3.5 Metal Ion Competition Experiments

This evaluation was only undertaken for ligands deemed suitable for ^{68}Ga PET, as determined from their radiolabelling properties and radiolabelled complex stability.

Stock solutions of $CaCl_2$, $FeCl_3$ and $CuBr_2$ were prepared in 0.2 M acetate buffer pH 4. The challenge was performed at 298 K and pH 4 (0.2 M acetate buffer) over the course of 10 minutes, with a 10 µM (14 nmol) of the ligand. A known amount of the metal ion of interest (starting at 1 equivalent with respect to the ligand: 14 nmol) was added to the ligand, and the volume made up to 1 mL using 0.2 M acetate buffer (pH 4). The post-processed ^{68}Ga (400 µL) was added, and a 1 µL fraction of the radiolabelling solution spotted on a TLC plate at 1, 3, 5, 10 min time intervals. The TLC plates were eluted using a 0.5 M citrate solution (pH 4). The concentration of the metal ion was varied to establish the concentration of the metal ion which prevents quantitative radiolabelling in 10 min (‘limiting concentration’). Control experiments were carried out in parallel in the absence of the ligand and metal ion separately. All challenge experiments were repeated twice.

3.6 Concentration Kinetics Radiolabelling Experiment

This evaluation was only undertaken for ligands deemed suitable for ^{68}Ga PET, as determined from their radiolabelling properties and radiolabelled complex stability.

The concentration dependence of radiolabelling was determined by gradually reducing the ligand concentration from 20 µM. A stock solution (50 µM) of the ligand was prepared in 0.2 M acetate buffer (pH 4). 1 mL of the desired ligand concentration was prepared by suitable dilution using 0.2 M acetate buffer (0.2 M) and the solution equilibrated at 298 K for two minutes. The challenge was performed at 298 K and pH 4 (0.2 M acetate buffer) over the course of 10 minutes. The post-processed ^{68}Ga (400 µL) was added, and a 1 µL fraction of the radiolabelling solution spotted on a TLC plate at 1, 3, 5 and 10 min time intervals. The TLC plates were eluted using a 0.5 M citrate solution (pH 4). The concentration of the ligand was decreased until quantitative radiolabelling was no longer achieved. All experiments were repeated once.

3.7 µPET Studies

Animal imaging experiments were performed in Sprague Dawley rats (n = 2 per radiolabelled complex.

Body weights:

- 330 - 380 g, male for **[^{68}Ga.L^{2}]** and **[^{68}Ga.NOTA]**.
- 430 - 440 g, male for **[^{68}Ga.L^{8}]$_{4.0}$** and **[^{68}Ga.L^{8}]$_{7.0}$**.

The rats were placed under isoflurane anaesthesia (2% isoflurane, 98% oxygen). All experiments had previously been approved by the regional animal ethics committee and were conducted in accordance with the German Law for Animal Protection. (Tiergenehmigung Schmitt)

The complexes **[^{68}Ga.L^{2}]**, **[^{68}Ga.NOTA]** and **[^{68}Ga.L^{6}]$_{4.0}$** were prepared at pH 4 (0.2 M acetate buffer) using the entire undiluted post-processed generator eluate (~ 300 MBq; 400 µL). Apart from the amount of ^{68}Ga used, the radiolabelling protocol as previously described. Prior to injection, the pH was adjusted to pH 7. The labelling solution (~ 25 MBq) was made up to 0.8-0.9 mL using saline solution, and injected into the tail vein by bolus injection.

The complex **[^{68}Ga.L^{8}]$_{7.0}$** was prepared at pH 7 (1.0 M Na-HEPES buffer) using the entire undiluted post-processed generator eluate (~ 300 MBq; 400µL). Apart from the amount of 68Ga used, the radiolabelling protocol as previously described. The pH did not need to be adjusted prior to radiolabelling. The labelling solution (~ 25 MBq) was made up to 0.8-0.9 mL using saline solution, and injected into the tail vein by bolus injection.

µPET imaging was performed on a µPET Focus 120 small animal PET (Siemens/Concorde, Knoxville, USA). Animals were placed in head-first-supine position. After a 15 min transmission scan with an external ^{57}Co source, dynamic PET studies were acquired over 45 min in 2 D mode followed by a 15 min whole body scan.

For analysis the PET 'listmode' data were depicted into 14 - 20 frames with varying time frames and reconstructed using an OSEM algorithm. PMOD software (PMOD Technologies LTD.) was used to visualize the images.

4 Synthetic Procedures

4.1 Compounds Relating to the Syntheses of AMPED Based Ligands, L$^{1-5}$

1,4-Dibenzyl-6-methyl-6-nitro-1,4-diazepane**, 1.**[5]

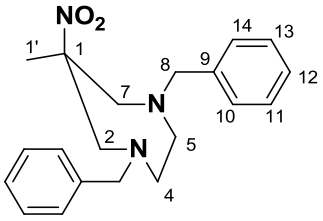

A solution of N,N'-dibenzylethylenediamine (2.00 g, 18.4 mmol) and *para*-formaldehyde (0.75 g, 25.0 mmol) in absolute ethanol (40 mL) was refluxed under an atmosphere of argon for 2 h. Nitroethane (0.94 g, 12.5 mmol) was added dropwise over 20 min, and the mixture boiled under reflux overnight under an atmosphere of argon. The solvent was removed under reduced pressure, and the resulting oil re-dissolved in chloroform (20 mL), filtered, and washed successively with aqueous potassium carbonate solution (2 x 20 mL, 0.1 M) and water (20 mL), dried over $MgSO_4$, filtered and solvent removed under reduced pressure. Purification by silica gel column chromatography

(dichloromethane) afforded an off-white solid (2.20 g, 78 %). R_F = 0.40 (SiO_2, dichloromethane). m.p. = 49.5 - 50 °C. **^{1}H NMR ($CDCl_3$, 400 MHz):** δ_H 1.34 (3H, s, $H^{1'}$); 2.60 (4H, m, $H^{4,5}$); 2.95 (2H, d, J 13, $H^{2/7}$); 3.59 (2H, d, J 13, $H^{2/7}$); 3.64 (2H, d, J 13, H^8); 3.78 (2H, d, J 13, H^8); 7.26-7.33 (10H, m, $H^{10,14}$). **HR MS ES+ (*m/z*):** found 340.2017 $[M + H]^+$; $C_{20}H_{26}N_3O_2$ requires 340.2025. The structure of **1** was confirmed by single crystal X-ray diffraction: $C_{20}H_{25}N_3O_2$, M_r = 339.43, monoclinic (C2/c); *a* = 32.4876(13) Å, *b* = 6.0545(2) Å, *c* = 20.2683(8) Å, *V* = 3710.1(2) Å^3,α = 90.00°, β = 111.467(10)°, γ = 90.00°, *Z* = 8; μ = 0.085 mm^{-1}, $D_{calc.}$ = 1.219 mg.mm^{-3}, *T* 120(2) K; 4452 independent reflections (R_{int} = 0.0342), R_1 = 0.0482, ωR_2 = 0.1252 ($I > 2\sigma(I)$). CCDC # 906039.

6-Methyl-1,4-diazepan-6-amine**, 2.**[5]

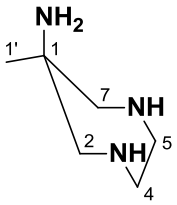

A catalytic amount of $Pd(OH)_2/C$ was added to a solution of the nitro-diamine **1** (0.10 g, 0.29 mmol) in methanol (20 mL), and the mixture agitated under an atmosphere of hydrogen for 48 h using a Parr hydrogenator (30 psi H_2). Thin layer chromatography (SiO_2, dichloromethane) was used to confirm complete reduction of the nitro group and cleavage of the benzyl N-sbstituents. Argon was bubbled through the solution for 15 min to purge remaining hydrogen, and the $Pd(OH)_2/C$ removed using a Celite® filter. The solvent was removed under reduced pressure to afford a yellow oil. (0.031 g, 81 %) R_f = 0.10 (CH_2Cl_2 / MeOH 19% / NH_3 1%, SiO_2). **^{1}H NMR ($CDCl_3$, 200 MHz):** δ_H 1.03 (3H, s, $H^{1'}$); 1.98 (4H, br. s, NH and NH_2); 2.68 (4H, br. s, $H^{2,7}$); 2.92 (4H, m, $H^{4,5}$). **MS ES+ (*m/z*)**: found 129.2 $[M+H]^+$;$C_6H_{16}N_3$ requires 129.1266. [Note: Compound **1** readily reacts with carbon dioxide in the atmosphere and should therefore be stored at < 0°C under an atmosphere of argon; or alternatively as the hydrochloride salt. As a consequence of this instability, compound **2** was always handled under argon, and subsequent reactions were carried out under an inert atmosphere.]

Tert-butyl 2,2'-(1,4-bis(2-tert-butoxy-2-oxoethyl)-6-methyl-1,4-diazepan-6-ylazanediyl)diacetate**, 3**.[5]

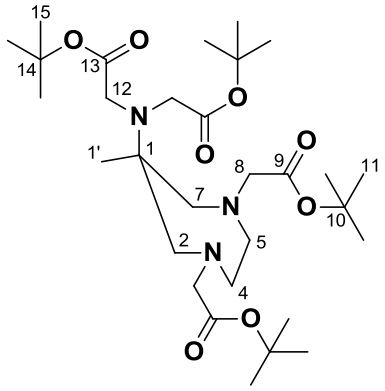

Tert-butyl-bromoacetate (0.272 g, 1.40 mmol) was added to a solution of **2** (0.030 g, 0.23 mmol) and potassium carbonate (0.193 g, 1.40 mmol) in acetonitrile (25 mL), and the mixture stirred for 24 h at 368 K under an atmosphere of argon. The solvent was removed under reduced pressure, and the resulting oil re-dissolved in chloroform (25 mL) and washed successively with aqueous potassium carbonate solution (2 x 25 mL, 0.1 M) and water (25 mL), dried over magnesium sulfate, filtered and solvent removed under reduced pressure. Purification by silica gel column chromatography (hexane → 5 % ethyl acetate) afforded a yellow oil (0.081 g, 60 %). R_f = 0.35 (hexane : ethyl acetate; 65 : 35). **^{1}H NMR ($CDCl_3$, 700 MHz):** δ_H 1.06 (3H, s, $H^{1'}$); 1.40 (36H, m, $H^{11,15}$); 2.58 (2H, d, J 14, $H^{2/7}$); 2.63 (2H, m, $H^{4/5}$); 2.73 (2H, m, $H^{4/5}$); 2.98 (2H, d, J 14, $H^{2/7}$); 3.23 (4H, s, H^{12}); 3.64 (4H, s, H^{8}). **HR MS ES+ (*m/z*):** found 586.4055 $[M + H]^+$;$C_{30}H_{56}N_3O_8$ requires 586.4059.

2,2'-(1,4-Bis(carboxymethyl)-6-methyl-1,4-diazepan-6-ylazanediyl)diacetic acid Bistrifluoroacetate salt**, $L^1.2CF_3COOH$**.[6]

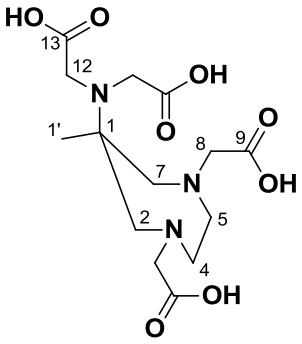

The tetra-ester **3** (0.200 g, 0.34 mmol) was dissolved in trifluoroacetic acid / dichloromethane (1 : 1, 2 mL) and left to stir for 2 days at room temperature. The solvent was removed under reduced pressure, the residue re-dissolved in dichloromethane : methanol (1 : 1, 2 mL) and evaporated. This procedure was repeated twice, and then with methanol. The resulting solid was dissolved in water

(10 mL) and washed with dichloromethane (10 mL). Removal of solvent under reduced pressure afforded the *bis*-trifluoroacetate salt of the title compound as a white solid (0.165 g, 82 %). **^{1}H NMR (D_2O, pD = 2.09, 700 MHz):** δ_H1.04 (3H, s, $H^{1'}$); 3.35 (2H, d, J 15, $H^{2,7}$); 3.59 (4H, m, $C^{2,7,4,5}$); 3.65 (4H, s, H^{12}); 3.71 (2H, m, $H^{4,5}$); 3.84 (2H, d 17, H^{8}); 3.84 (2H, d, J 17, H^{8}). **HR MS ES+ (*m/z*):** found 384.1 $[M + Na]^+$; $C_{14}H_{23}N_3NaO_8$ requires: 384.1383 **Elemental analysis (%):** found C (36.8) H (4.32) N (6.99) $[C_{14}H_{23}N_3O_8].2CF_3COOH$ requires C (36.7) H (4.28) N (7.13).

Tert-butyl 2,2'-(6-(2-tert-butoxy-2-oxoethylamino)-6-methyl-1,4-diazepane-1,4-diyl)diacetate, **5**.

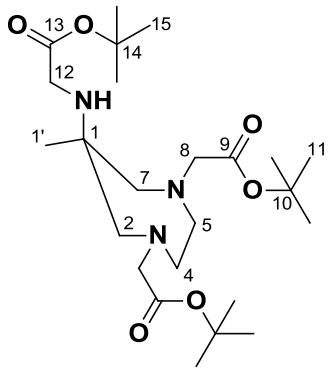

Tert-butyl-bromoacetate (0.113 g, 0.58 mmol) was added to a solution of **2** (0.030 g, 0.23 mmol) and potassium carbonate (0.25 g, 0.70 mmol) in acetonitrile (25 mL), and the mixture stirred for 24 h at 298 K under an atmosphere of argon. The reaction was monitored using UV-vis TLC, to follow formation of the unwanted tetra-alkylated by-product **3**. The solvent was removed under reduced pressure, and the resulting oil re-dissolved in chloroform (25 mL) and washed successively with aqueous potassium carbonate solution (2 x 25 mL, 0.1 M) and water (25 mL), dried over $MgSO_4$, filtered and solvent removed under reduced pressure. Purification by silica gel column chromatography (hexane → 25 % ethyl acetate) afforded a yellow oil (0.06 g, 22 %). R_f = 0.20 (SiO_2; hexane : ethyl acetate; 65 : 35). **^{1}H NMR ($CDCl_3$, 700 MHz):** δ_H 0.85 (3H, s, $H^{1'}$); 1.37 (27H, m, $H^{11,15}$); 2.54 (2H, d, J 14, $H^{2,7}$) 2.59 (2H, d, J 14, $H^{2,7}$); 2.72 (4H, m, $H^{4,5}$); 3.18 (2H, s, H^{12}); 3.22 (4H, s, H^{8}). **^{13}C NMR ($CDCl_3$, 176 MHz):** δ_C 22.79 ($C^{1'}$); 28.20 ($C^{11/15}$); 28.35 ($C^{11/15}$); 45.13 (C^{12}); 56.05 (C^{1}); 57.35 ($C^{2,7}$); 61.99 (C^{8}); 64.81 ($C^{4,5}$); 80.77 ($C^{10/14}$); 80.89 ($C^{10/14}$); 171.06 ($C^{9/13}$); 171.97 ($C^{9/13}$). **HR MS ES+ (*m/z*):** found 472.3380 $[M + H]^+$; $C_{24}H_{46}N_3O_6$ requires 472.3378.

(±)-2,2'-(6-Methyl-8-oxo-1,4,7-triazabicyclo[4.3.1]decane-4,7-diyl)diacetic acid, **6**.[7]

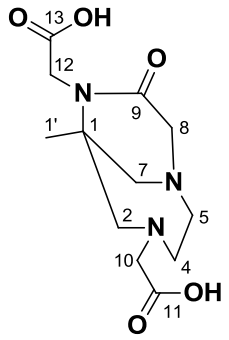

The triester **5** (0.100 g, 0.21 mmol) was dissolved in trifluoroacetic acid : dichloromethane (1 : 1, 2 mL) and left to stir for 2 days at room temperature. The solvent was removed under reduced pressure, the residue re-dissolved in dichloromethane : methanol (1 : 1, 2 mL) and evaporated. This procedure was repeated twice, and with methanol. The resulting solid was then dissolved in water (10 mL) and washed with dichloromethane (10 mL). Removal of the solvent under reduced pressure afforded, after drying *in vacuo*, a white solid (0.093 g). **^{1}H NMR (D_2O, pD = 2.07, 700 MHz):** δ_H 1.29 (3H, s, $H^{1'}$); 3.25 (1H, d, J 14, $H^{2,7}$); 3.39 (1H, d, J 14, $H^{2,7}$); 3.46 (2H, M, $H^{4/5}$); 3.59 (2H, m, $H^{2/7,4/5}$); 3.79 (6H, m, $H^{2/7,4/5,\ 8,\ 10}$); 4.11 (2H, s, H^{12}). **^{13}C NMR (D_2O, pD = 2.07, 176 MHz)**: δ_C 21.88 ($C^{1'}$); 43.75 ($C^{4/5}$); 50.67 (C^{1}); 53.66 (C^{8}); 57.58 ($C^{4/5}$); 58.56 ($C^{2/7}$); 60.49 ($C^{2/7}$); 115.40 ($C^{10/12}$); 117.06 ($C^{10/12}$); 166.15 ($C^{9/11/13}$); 170.65 ($C^{9/11/13}$); 173.50 ($C^{9/11/13}$). **MS ES+ (*m/z*):** found 308.2 $[M+H]^+$;$C_{12}H_{19}N_3NaO_5$ requires 308.1222

Tert-butyl 2,2'-(6-((2-tert-butoxy-2-oxoethyl)(methyl)amino)-6-methyl-1,4-diazepane-1,4-diyl)diacetate, **7**.

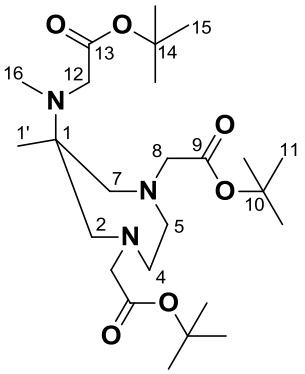

Iodomethane (0.030 g, 0.21 mmol) was added to a solution of **5** (0.100 g, 0.21 mmol) and postassium carbonate (0.029 g, 0.21 mmol) in anhydrous dichloromethane cooled in an ice-bath. After 15 min the mixture was allowed to warm to room temperature, and left for a further 5 h. The

solvent was removed under reduced pressure and the resulting oil re-dissolved in chloroform (20 mL), filtered, and washed successively with aqueous potassium carbonate solution (2 x 20 mL, 0.1 M) and water (20 mL), dried over $MgSO_4$, filtered and solvent removed under reduced pressure. Purification by silica gel column chromatography (hexane → 20 % ethyl acetate) afforded a yellow oil (0.042 g, 41 %). R_F = 0.30 (SiO_2, hexane : ethyl acetate; 80 : 20). **^{1}H NMR ($CDCl_3$, 700 MHz):** δ_H 1.05 (3H, s, $H^{1'}$); 1.42 (27H, m, $H^{11,15}$); 2.30 (3H, s, H^{16}); 2.55 (2H, d, J 14, $H^{2,7}$); 2.68 (2H, m, $H^{4/5}$); 2.79 (2H, m, $H^{4/5}$); 2.93 (2H, d, J 14, $H^{2,7}$); 3.24 (2H, d, J 17, H^8); 3.27 (2H, d, J 17, H^8); 3.41 (2H, s, H^{12}). **^{13}C NMR ($CDCl_3$, 176 MHz):** δ_C 23.75 ($C^{1'}$); 28.11 (C^{15}); 28.31 (C^{11}); 37.30 (C^{16}); 54.26 (C^{12}); 58.98 ($C^{4,5}$); 60.70 (C^1); 62.34 (C^8); 63.55 ($C^{2,7}$); 80.20 (C^{14}); 80.73 (C^{10}); 170.87 (C^9); 171.99 (C^{13}). **HR MS ES+ (*m/z*):** found 486.3540 $[M + H]^+$; $C_{25}H_{48}N_3O_6$ requires 486.3543.

2,2'-(6-((Carboxymethyl)(methyl)amino)-6-methyl-1,4-diazepane-1,4-diyl)diacetic acid Bistrifluoroacetate salt, **L^2.2CF_3COOH**.

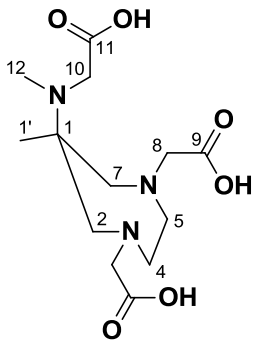

The triester **7** (0.150 g, 0.31 mmol) was dissolved in trifluoroacetic acid / dichloromethane (1:1, 2 mL) and left to stir for 2 days at room temperature. The solvent was removed under reduced pressure, the residue re-dissolved in dichloromethane and evaporated. This procedure was repeated twice, and then with methanol. The resulting solid was dissolved in water (15 mL) and washed with dichloromethane (15 mL). Removal of solvent under reduced pressure afforded, after drying the bis-trifluoroacetic acid salt of the title compound as a white solid (0.081 g, 83 %). **^{1}H NMR (D_2O, pD = 1.98, 700 MHz):** δ_H 1.22 (3H, s, $H^{1'}$); 2.91 (3H, s, H^{12}); 3.25 (2H, m, $H^{4,5}$); 3.31 (2H, m, $H^{4,5}$); 3.39 (2H, d, J 16, $H^{2,7}$); 3.52 (2H, d, J 16, $H^{2,7}$); 3.75 (4H, s, H^8); 3.90 (2H, s, H^{10}). **^{13}C NMR (D_2O, pD = 1.98, 176 MHz):** δ_c 15.43 ($C^{1'}$); 38.149 (C^{12}); 53.36 (C^1); 53.64 (C^{12}); 58.12 ($C^{4/5}$); 58.50 (^{8}); 67.42 ($^{2/7}$); 168.99 (C^9); 171.48 (C^{11}). **HR MS ES+ (*m/z*):** found 318.1677 $[M + H]^+$; $C_{13}H_{24}N_3O_6$ requires: 318.1665. **Elemental analysis (%):** found C (37.3) H (4.53) N (7.59) $[C_{13}H_{23}N_3O_6].2CF_3COOH$ requires C (37.4) H (4.62) N (7.70).

(2S,2'S)-Diethyl 2,2'-(6-((S)-1-ethoxy-1-oxopropan-2-ylamino)-6-methyl-1,4-diazepane-1,4-diyl)dipropanoate, **9**.

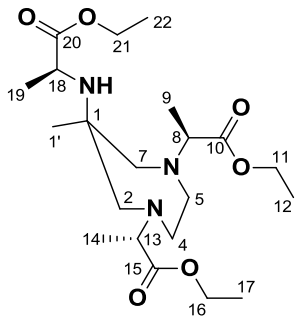

Ethyl (2R)-2-{[(trifluoromethyl)sulfonyl]oxypropanoate (0.98 g, 3.9 mmol) was added to a solution of potassium carbonate (0.54 g, 3.9 mmol) and **2** (0.10 g, 0.78 mmol) in acetonitrile (20 mL), and the reaction mixture stirred at 308 K for 18 h. The solvent was removed under reduced pressure and the resulting oil re-dissolved in chloroform (30 mL) and washed successively with aqueous potassium carbonate solution (2 x 30 mL, 0.1 M) and water (30 mL), dried over $MgSO_4$, filtered and solvent removed under reduced pressure. Purification by silica gel column chromatography (hexane : ethyl acetate, 95 : 5) afforded the title compound as a colourless oil (0.11 g, 34%). R_f = 0.40 (hexane : ethyl acetate; 65 : 35). **^{1}H NMR ($CDCl_3$, 600 MHz, ppm):** δ 0.88 (3H, s, $H^{1'}$); 1.25 (18H, m, $H^{9,14,19}$ & $H^{12,17,22}$); 2.46 (2H, t, J 15, $H^{2/7}$); 2.55 (1H, m, $H^{4/5}$); 2.63 (1H, m, $H^{4/5}$); 2.69 (2H, t, J 15, $H^{2/7}$); 2.73 (1H, m, $H^{4/5}$); 2.84 (1H, m, $H^{4/5}$); 3.34 (2H, m, $H^{8,13}$); 3.45 (1H, q, J 7, H^{18}); 4.12 (6H, m, $H^{11,16,21}$). **^{13}C NMR ($CDCl_3$, 151 MHz, ppm):** δ 14.40 ($C^{9/14/19}$ or $C^{12/17/22}$); 14.43 ($C^{9/14/19}$ or $C^{12/17/22}$); 15.24 ($C^{9/14/19}$ or $C^{12/17/22}$); 15.70 ($C^{9/14/19}$ or $C^{12/17/22}$); 16.52 ($C^{9/14/19}$ or $C^{12/17/22}$); 21.68 ($C^{9/14/19}$ or $C^{12/17/22}$); 20.34 ($C^{1'}$); 50.34 (C^{18}); 55.33 ($C^{4/5}$); 56.40 ($C^{4/5}$); 59.96 ($C^{11/16/21}$); 60.08 ($C^{11/16/21}$); 60.59 ($C^{11/16/21}$); 61.85 ($C^{2/7}$); 63.81 ($C^{8/13}$); 63.95 ($C^{8/13}$); 64.07 ($C^{2/7}$); 65.80 (C^{1}); 173.56 ($C^{10/15}$); 173.59 ($C^{10/15}$); 177.39 (C^{20}). **HR MS ES+ (*m/z*):** found: 430.2926 $[M + H]^+$; $C_{21}H_{40}N_3O_6$ requires 430.2917.

(2S,2'S)-2,2'-(6-((S)-1-Carboxyethylamino)-6-methyl-1,4-diazepane-1,4-diyl)dipropanoic acid trisodium salt **, $Na_3.L^3$**.

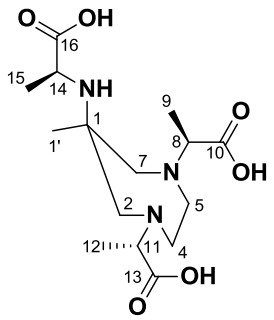

Sodium hydroxide (0.003 g, 0.072 mmol) dissolved in water (0.5 mL) was added to a solution of the tri-ester **9** (0.010 g, 0.023 mmol) in THF (0.5 mL), and the mixture stirred at 298 K. The reaction was monitored using LC-ESI MS, to follow ester cleavage. Once complete, the solvent was removed by lyophilisation. Water (5 mL) was added and removed by lyophilisation, and the procedure repeated two more times. The resulting solid was washed with ice-cold dichloromethane (0.5 mL), and dried *in vacuo* to afford the tris-hydrated tris-sodium salt of the title compound as a white solid (0.009 g, 92 %). **^{1}H NMR ($CDCl_3$, pD 12.24, 600 MHz, ppm):** δ 0.84 (3H, s, $H^{1'}$); 1.04 (3H, d, J 7, H^9); 1.06 (3H, d, J 7, H^{15}); 1.08 (3H, d, J 7, H^{12}); 2.22 (1H, d, J 15, H^2); 2.27 (1H, d, J 15, H^7); 2.59 (1H, m, $H^{4,5}$); 2.74 (1H, d, J 15, H^7); 2.78 (1H, d, J 15, H^2); 2.98 (1H, q, J 7, H^8); 3.06 (1H, q, J 7, H^{11}); 3.16 (1H, q, J 7, H^{14}). **^{13}C NMR ($CDCl_3$, , pD 12.24, 151 MHz, ppm):** δ 15.64 (C^9); 16.25 (C^{15}); 21.26 (C^{12}); 22.09 ($C^{1'}$); 52.33 (C^{14}); 55.91 (C^1); 57.29 ($C^{4/5}$); 57.45 ($C^{4/5}$); 59.70 (C^2); 60.29 (C^7); 66.50 (C^8); 66.75 (C^{11}); 181.22 (C^{10}); 181.25 (C^{13}); 184.42 (C^{16}). **HR MS ES+ (*m/z*):** found 368.1807 $[M + Na]^+$; $C_{15}H_{27}N_3NaO_6$ requires 368.1798. **Elemental analysis (%):** found C (38.6) H (6.73) N (8.94) $Na_3[C_{15}H_{24}N_3O_6].3H_2O$ requires C (38.7) H (6.50) N (9.03)

(2S,2'S)-Diethyl 2,2'-(6-(((S)-1-ethoxy-1-oxopropan-2-yl)(methyl)amino)-6-methyl-1,4-diazepane-1,4-diyl)dipropanoate, **11.**

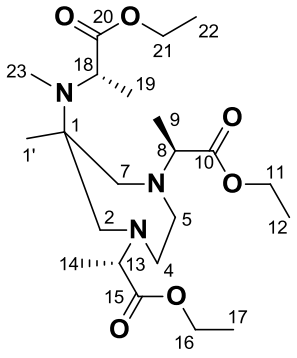

Methyl iodide (0.026 g, 0.18 mmol) was added to a solution of **9** (0.05 g, 0.12 mmol) and potassium carbonate (0.017 g, 0.12 mmol) in dichloromethane (15 mL), and the mixture stirred for 18 h at 303 K under an atmosphere of argon. The solvent was removed under reduced pressure and the resulting oil re-dissolved in chloroform (15 mL) and washed successively with aqueous potassium carbonate solution (2 x 15 mL, 0.1 M) and water (15 mL), dried over $MgSO_4$, filtered and solvent removed under reduced pressure. Purification by silica gel column chromatography (hexane → 15 % ethyl acetate) afforded the title compound as a yellow oil (0.007 g, 15 %). R_f = 0.45 (hexane : ethyl acetate; 65 : 35). **^{1}H NMR ($CDCl_3$, 600 MHz, ppm):** δ_H 1.05 (3H, s, $H^{1'}$); 1.24 (18H, m, $H^{9,14,19}$ & $H^{12,17,22}$); 2.38 (1H, m, H^4); 2.41 (3H, s, H^{23}); 2.45 (1H, d, J 14, H^7); 2.54 (1H, m, H^5); 2.62 (1H, d, J 14, H^2); 2.67 (1H, m, H^5); 2.84 (1H, m, H^4); 2.93 (1H, d, J 14, H^2); 3.06 (1H, d, J 14, H^7); 3.38 (1H, q, H^{13}); 3.42 (1H, q, H^8); 4.09 (7H, m, $H^{18,11,16,21}$). **^{13}C NMR ($CDCl_3$, 151 MHz, ppm):** δ_C 14.17 ($C^{12/17/22}$); 14.37 ($C^{12/17/22}$); 14.40 (C^9); 14.48 ($C^{12/17/22}$); 16.72 (C^{14}); 16.90 (C^{19}); 23.74 ($C^{1'}$); 29.99 (C^{23}); 54.34 (C^{18}); 54.42 (C^5); 55.49 (C^4); 59.93 ($C^{11/16/21}$); 59.95 ($C^{11/16/21}$); 60.07 ($C^{11/16/21}$); 61.67 (C^1); 63.29 (C^2); 63.61 (C^{13}); 64.30 (C^8); 65.06 (C^7); 173.53 ($C^{10/15}$); 173.70 ($C^{10/15}$); 175.21 (C^{20}). **HR MS ES+ (*m/z*):** found: 444.3071 $[M + H]^+$; $C_{22}H_{42}N_3O_6$ requires 444.3074.

(2R,2'S)-2,2'-(6-(((S)-1-Carboxyethyl)(methyl)amino)-6-methyl-1,4-diazepane-1,4-diyl)dipropanoic acid trisodium salt, **Na_3.L^4**.

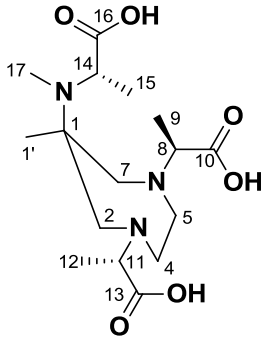

Sodium hydroxide (0.003 g, 0.072 mmol) dissolved in purite water (0.5 mL) was added to a solution of the triester **11** (0.010 g, 0.023 mmol) in THF (0.5 mL), and the mixture stirred at 298 K. The reaction was monitored using LC-ESI MS, to follow ester cleavage. Once complete, the solvent was removed by lyophilisation. Water (5 mL) was added and removed by lyophilisation, and the procedure repeated two more times. The resulting solid was washed with ice cold dichloromethane (0.5 mL), and dried *in vacuo* to afford the di-hydrated tri-sodium salt of the title compound as a white solid (0.008 g, 87 %). **^{1}H NMR (D_2O, pD 12.07, 600 MHz, ppm):** δ 0.92 (3H, s, $H^{1'}$); 1.06 (6H, d+d, $H^{9,12}$); 1.13 (3H, d, J 7, H^{15}); 2.29 (4H, d+s, $H^{2,17}$); 2.54 (4H, m, $H^{4,5}$); 2.66 (1H, d, J 15, H^7); 2.84

(1H, d, J 15, H^{7}); 2.97 (1H, d, J 15, H^{2}); 3.01 (1H, q, J 7, H^{8}); 3.12 (1H, q, J 7, H^{11}); 3.61 (1H, q, J 7, H^{14}). **^{13}C NMR (D_2O, pD 12.07, 151 MHz, ppm):** δ 13.77 ($C^{9/12}$); 15.30 (C^{15}); 16.35 ($C^{9/12}$); 18.67 ($C^{1'}$); 29.44 (C^{17}); 54.74 ($C^{4,5}$); 57.37 (C^{1}); 59.14 (C^{7}); 59.70 (C^{2}); 62.14 (C^{14}); 66.46 (C^{8}); 66.93 (C^{11}); 181.41 ($C^{10/12}$); 181.66 ($C^{10/13}$); 182.10 (C^{16}). **HR MS ES+ (*m/z*):** found 382.1950 $[M + Na]^+$; $C_{16}H_{29}N_3NaO_6$ requires 382.1954. **Elemental analysis (%):** found C (40.3) H (6.79) N (8.68); $Na_3[C_{16}H_{26}N_3O_6].2H_2O$ requires C (40.1) H (6.73) N (8.76).

Methyl 4-(aminomethyl)benzoate hydrochloride**, 13.HCl.**[8]

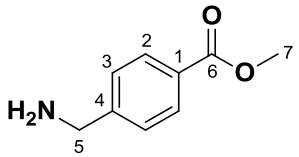

4-methylamine benzoic acid (3.00 g, 20 mmol) was dissolved in a mixture of methanol (30 mL) and 35 % hydrochloric acid (1 mL), and the solution stirred overnight at 348 K. Upon cooling to room temperature and standing for 3 h, needle-like white crystals formed which were filtered, washed with ice cold methanol (5 mL) and dried *in vacuo* to afford the hydrochloride salt* of the title compound (3.92 g, 98 %). **^{1}H NMR (CD_3OD, 700 Mhz):** δ_H 3.91 (3H, s, H^{7}); 4.22 (2H, s, H^{5}); 7.58 (2H, d, J 8, $H^{2/3}$); 8.06 (2H, d, J 8, $H^{2/3}$). **^{13}C NMR (CD_3OD, 176 MHz):** δ_C 166.16 (C^{6}); 138.34 (C^{4}); 131.62 (C^{1}); 130.27 (C^{3}); 129.05 (C^{2}); 52.97 (C^{7}); 42.76 (C^{5}). **HR MS ES+ (*m/z*):** found 166.0884 $[M+H]^+$;$C_9H_{12}NO_2$ requires 166.0868. *based on the synthetic procedure followed.

Methyl 4-(acetamidomethyl)benzoate**, 14**.z [9]

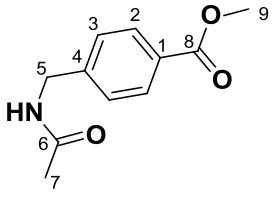

Acetyl chloride (0.39 mL, 5.4 mmol) was slowly added to a stirring solution of **13** (0.500 g, 2.5 mmol) and triethylamine (0.76 mL, 5.5 mmol) in THF at 273 K. The temperature was maintained for 15 min, and then gradually warmed to room temperature, and the mixture stirred overnight. The insoluble salts were removed by filtration, and solvent removed under reduced pressure to afford a white solid (497 mg, 97 %). **^{1}H NMR ($CDCl_3$, 700 MHz):** δ_H 2.11 (3H, s, H^{7}); 3.91 (3H, s, H^{9}); 4.45 (2H, s, H^{5}); 7.35 (2H, d, J 8, $H^{2/3}$); 7.98 (2H, d, J 8, $H^{2/3}$). **^{13}C NMR ($CDCl_3$, 176 MHz):** δ_C 170.63 (C^{6}); 166.24 (C^{8});

144.01 (C^1); 130.31 (C^2); 129.79 (C^4); 128.45 (C^3); 52.07 (C^9); 43.44 (C^5); 23.68 (C^7). **HR MS ES+ (*m/z*):** found 208.0958 $[M+H]^+$; $C_{11}H_{14}NO_3$ requires 208.0974.

N-(4-(Hydroxymethyl)benzyl)acetamide**, 15**.[9]

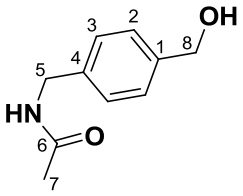

The *para*-acetamide benzylic ester **14** (2.000 g, 9.61 mmol) in THF (180 mL) was added dropwise to a 1.0 M solution of $LiAlH_4$ in THF (19.2 mL, 19.2 mmol) cooled to 195 K. The mixture was stirred for 10 min, and allowed to warm to room temperature. The reaction was quenched with sodium hydroxide (~ 25 mL, 10 M), filtered, and concentrated under reduced pressure. The crude residue was re-dissolved in dichloromethane (75 mL) and washed successively aqueous potassium carbonate (2 x 50 mL, 0.1 M) and water (2 x 50 mL), dried over magnesium sulphate, filtered and solvent reduced pressure. Purification by silica gel column chromatography (dichloromethane → 1 % methanol) afforded an off white solid (1.015 g, 59%). R_F = 0.25 (dichloromethane : methanol; 99 : 1). **^{1}H NMR ($CDCl_3$, 400 MHz):** δ_H 1.91 (3H, s, H^7); 4.32 (2H, s, H^8); 4.80 (2H, s, H^5); 4.90 (1H, br. s, H^{NH}); 7.30 (2H, d, J 8, $H^{2/3}$); 7.88 (2H, d, J 8, $H^{2/3}$). **HR MS-ES+ (*m/z*):** found: 180.1019 $[M+H]^+$; $C_{10}H_{14}NO_2$ requires 180.1025.

N-(4-(Bromomethyl)benzyl)acetamide, **16**.

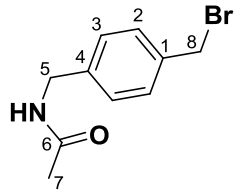

The *para*-acetamide benzylic alcohol **15** (1.000 g, 5.6 mmol) was dissolved in hydrogen bromide (37 % in acetic acid) and toluene (1 : 1, v : v, 100 mL), and stirred for 30 min at 298 K. The solvent was removed under reduced pressure, and the progress of reaction monitored using ^{1}H NMR, following the chemical shift of the methylene-bromo (H^8) protons. Purification by silica gel column chromatography (gradient elution: dichloromethane → 1 % Methanol) afforded an off white solid. (1.22 g, 90 %) R_F = 0.45 (dichloromethane : methanol, 99 : 1). **^{1}H NMR ($CDCl_3$, 700 MHz):** δ_H 2.04 (3H,

s, H^{7}); 4.45 (2H,s , H^{8}); 5.10 (2H, s, H^{5}); 5.92 (1H, br. s, H^{NH}); 7.29 (2H, m, $H^{2/3}$). **HR MS ES+ (*m/z*):** found 242.0180 $[M+H]^{+}$; $C_{10}H_{13}NOBr$ requires 242.0180.

Tert-butyl 2,2'-(6-((4-(acetamidomethyl)benzyl)(2-tert-butoxy-2-oxoethyl)amino)-6-methyl-1,4-diazepane-1,4-diyl)diacetate, **17**

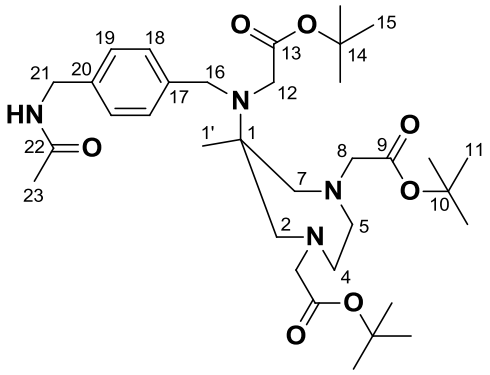

The *para*-acetamide benzylic bromide **16** (0.053 g, 0.22 mmol) was added to a solution of **5** (0.050 g, 0.11 mmol) and caesium carbonate (0.072 g, 0.22 mmol) in acetonitrile (25 mL), and the mixture stirred for 18 h at 353 K under an atmosphere of argon. The solvent was removed under reduced pressure and the resulting oil re-dissolved in chloroform (20 mL) and washed successively with aqueous potassium carbonate solution (2 x 20 mL, 0.1 M) and water (20 mL), dried over $MgSO_4$, filtered and solvent removed under reduced pressure. Purification by silica gel column chromatography (hexane → 35 % ethyl acetate) afforded the title compound as a yellow oil (0.030 g, 45 %). R_f = 0.65 (hexane : ethyl acetate; 50 : 50). **^{1}HNMR ($CDCl_3$, 700 MHz):** δ 1.13 (3H, s, $H^{1'}$); 1.33 (9H, s, H^{15}); 1.43 (18H, s, H^{11}); 1.99 (3H, s, H^{23}); 2.65 (2H, d, J 14, $H^{2,7}$); 2.69 (2H, m, $H^{4,5}$); 2.77 (2H, m, $H^{4,5}$); 3.11 (2H, d, J 14, $H^{2,7}$); 3.24 (2H, d, J 17, H^{8}); 3.28 (2H, d, J 17, H^{8}); 3.39 (2H, s, H^{12}); 4.06 (2H, s, H^{16}); 4.36 (2H, d, J 6, H^{21}); 7.16 (2H, d, J 8, H^{19}); 7.33 (2H, d, J 8, H^{18}). **^{13}C NMR ($CDCl_3$, 176 MHz):** δ 23.26 (C^{23}); 24.54 ($C^{1'}$); 27.96 (C^{15}); 28.20 (C^{11}); 43.61 (C^{21}); 52.15 (C^{12}); 53.05 (C^{16}); 59.11 ($C^{4,5}$); 61.20 (C^{1}); 62.42 (C^{8}); 65.36 ($C^{2,7}$); 80.03 (C^{14}); 80.73 (C^{10}); 127.66 (C^{19}); 128.64 (C^{18}); 136.19 (C^{20}); 140.98 (C^{17}); 169.65 (C^{22}); 170.91 (C^{9}); 172.82 (C^{13}). **HR MS ES+ (m/z):** found 633.4230 $[M + H]^{+}$; $C_{34}H_{57}N_4O_7$ requires 633.4227; found 655.4043$[M + Na]^{+}$; $C_{34}H_{56}N_4NaO_7$ requires 655.4047.

2,2'-(6-((4-(acetamidomethyl)benzyl)(carboxymethyl)amino)-6-methyl-1,4-diazepane-1,4-diyl)diacetic acid Tristrifluoro acetate salt, **L^5.CF_3COOH**.

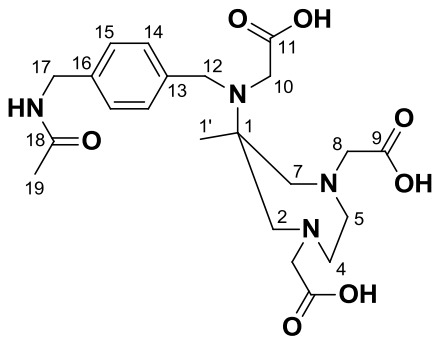

The triester **17** (0.020 g, 0.032 mmol) was dissolved in trifluoroacetic acid : dichloromethane (1 : 1, 2 mL) and left to stir for 2 days at room temperature. The solvent was removed under reduced pressure, the residue re-dissolved in dichloromethane : methanol (1 : 1, 2 mL) and evaporated. This procedure was repeated twice, and also with methanol. The resulting solid was dissolved in water (10 mL) and washed with dichloromethane (10 mL). Removal of solvent under reduced pressure afforded the tris- triflouroacetate salt as an off-white solid (0.020 g, 67 %). **^{1}HNMR (D_2O, pD 2.37, 700 MHz):** δ_H 1.32 (3H, s, $H^{1'}$); 3.33 (2H, m, $H^{4/5}$); 3.47 (2H, d, J 15, $H^{2/7}$); 3.49 (2H, m, $H^{4/5}$); 3.62 (2H, d, J 15, $H^{2/7}$); 3.74 (2H, d, J 17, H^8); 3.80 (2H, d, J 17, H^8); 4.03 (2H, s, H^{10}); 4.23 (2H, s, H^{17}); 4.33 (2H, s, H^{12}); 7.18 (2H, d, J 8, H^{15}); 7.36 (2H, d, J 8, H^{14}). **^{13}C NMR (D_2O, pD 2.37, 176 MHz):** δ_C 16.45 ($C^{1'}$); 21.81 (C^{19}); 42.65 (C^{17}); 43.08 (C^{10}); 53.25 ($C^{4/5}$); 54.62 (C^{12}); 58.76 (C^8); 59.35 ($C^{2/7}$); 66.91 (C^1); 127.68 (C^{15}); 128.75 (C^{16}); 131.38 (C^{14}); 139.89 (C^{13}); 170.93 (C^{11}); 171.21 (C^8); 174.12 (C^{18}). **HR MS ES+ (m/z):** found 465.2953 $[M + H]^+$; $C_{22}H_{33}N_4O_7$ requires 465.2941. **Elemental analysis (%):** found: C (42.9) H (4.51) N (6.72); $[C_{22}H_{32}N_4O_7].3CF_3COOH$ requires C (41.7) H (4.37) N (6.95).

4.2 Compounds Relating to the Syntheses of APPED Based Ligands, L^{6-9}

2,4-Dimethoxybenzaldehyde**, 19**.

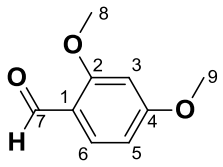

Manganese(II) dioxide (11.4 g, 10x by mass) was added to a solution of 2,4-dimethoxyl benzyl alcohol (1.140 g, 6.78 mmol) in chloroform (100 mL), and the mixture stirred at 298 K for 18 h. The mixture was filtered through Celite®, using ethanol (20 mL) and chloroform (20 mL) to wash the

filtered solids, and the solvent removed under reduced pressure. The residue was recrystallised from ethanol, and dried in vacuo, to afford the title compound as an off white crystalline solid (0.853 g, 76 %). m.p. 71 °C. **^{1}H NMR ($CDCl_3$, 700 MHz):** δ_H 3.86 (3H, s, $H^{8/9}$); 3.88 (3H, s, $H^{8/9}$); 6.43 (1H, s, H^3); 6.52 (1H, d, J 9, H^5); 7.80 (1H, d, J 9, H^6); 10.27 (1H, s, H^7). **^{13}C NMR ($CDCl_3$, 176 MHz):** δ_C 55.62 ($C^{8/9}$); 98.05 (C^3); 105.77 (C^5); 119.12 (C^4); 130.58 (C^6); 163.58 ($C^{1/2}$); 166.14 ($C^{1/2}$); 188.06 (C^7). **MS ES+ (*m/z*):** found 167.1 $[M + H]^+$;$C_9H_{11}O_3$ requires 167.0708.

N^1,N^2-Bis(2,4-dimethoxybenzyl)ethane-1,2-diamine, **20**.

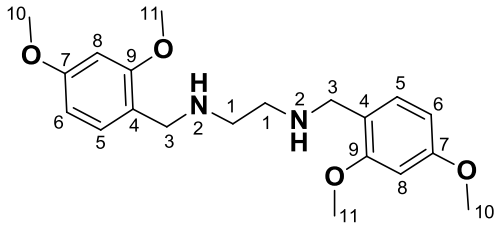

Under an inert atmosphere of argon, 2,4-dimethoxybenzaldehyde (3.00 g, 18 mmol) was dissolved in dry methanol (100 mL) containing 3 Å molecular sieves. The mixture was stirred at room temperature for 30 minutes before N,N'-ethylenediamine (0.59 g, 9.9 mmol) was added, and the mixture left to stir at room temperature overnight. The methanol was removed under reduced pressure and chloroform (200 mL) added, before the molecular sieves were removed by filtration. Removal of the chloroform under reduced pressure yielded the diimine as a yellow solid. The di-imine formed during this reaction is sensitive to water and was used in the next step without further purification and characterisation. Under an inert atmosphere of argon, sodium borohydride (2.70 g, 71 mmol) was added gradually over 30 minutes to a solution of the di-imine dissolved in dry methanol (40 mL). The solution was left to stir overnight at room temperature. The methanol was removed under reduced pressure and the solid re-dissolved in chloroform and washed successively with aqueous sodium hydroxide solution (0.1 M) and water. Removal of the chloroform under reduced pressure and subsequent drying *in vacuo* yielded a golden yellow oil which crystallized overnight to give a dark yellow solid. (3.03 g, 93 %) m.p. 56°C. **^{1}H NMR ($CDCl_3$, 500 MHz):** δ_H 2.72 (4H, s, H^1); 3.75 (4H, s, H^3); 3.78 (6H, s, H^{11}); 3.82 (6H, s, H^{10}); 6.44 (4H, m, $H^{5,6}$); 7.12 (1H, d, J 8, H^8). **^{13}C NMR ($CDCl_3$, 125 MHz):** δ_C 48.71 (C^1); 48.83 (C^3); 55.55 (C^{11}); 55.68 (C^{10}), 98.71 ($C^{5/6}$); 103.72 ($C^{5/6}$); 121.32 (C^4); 130.56 (C^8); 158.84 (C^9); 160.29 (C^7). **HR MS ES+ (*m/z*):** found: 361.2134 $[M + H]^+$; $C_{20}H_{29}N_2O_4$ requires 361.2127.

(Nitromethyl)benzene, **21.**[10]

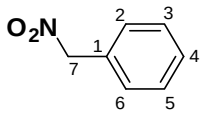

Silver nitrite (1.710 g, 40 mmol) was added to (bromomethyl)benzene (1.710 g, 10 mmol) in water (100 mL) contained in a flask covered in aluminium foil to exlude light. The mixture was stirred vigoursly at 298 K for 18 h. Ethyl acetate (100 mL) was added and the organic layer extracted. The aqueous layer was washed three more times with fresh ethyl acetate (50 mL), the organic layers combined and the solvent removed under reduced pressure. Purification by silica gel column chromtagraphy (hexane) afforded the title compound as a colourless oil (0.342, 325 %). R_f = 0.75. **^{1}H NMR ($CDCl_3$, 700 MHz):** δ_H 5.43 (2H, s, H^7); 7.48 (5H, m, $H^{2,3,4,5,6}$). **HR MS ES- (*m/z*):** found 136.0398 $[M - H]^-$; $C_7H_6NO_2$ requires 136.0399.

1,4-Bis(2,4-dimethoxybenzyl)-6-nitro-6-phenyl-1,4-diazepane, **22**.

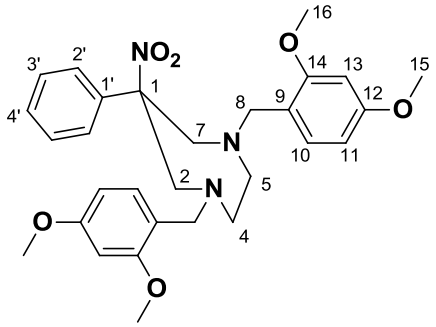

Nitromethylbenzene (0.32 g, 2.3 mmol) was added dropwise over 30 minutes to a solution of the N,N'-bis(2,4-dimethoxybenzyl)ethane-1,2-diamine **20** (0.83 g, 2.3 mmol) and paraformaldehyde (0.24 g, 8 mmol) in ethanol/toluene (50/50: 30 mL), and the reaction mixture stirred at 313 K overnight. The solvent was removed under reduced pressure and the resulting oil re-dissolved in chloroform (30 mL) and washed successively with aqueous potassium carbonate solution (2 x 30 mL, 0.1 M) and water (50 mL), dried over magnesium sulfate, filtered and the solvent removed under reduced pressure. Purification by silica gel column chromatography (hexane → 15 % ethyl acetate) yielded, after drying *in vacuo*, a white solid (0.134 g, 11 %). R_f = 0.55 (hexane : ethyl acetate; 65 : 35), m.p. 62 - 67 °C. **^{1}H NMR ($CDCl_3$, 700 MHz):** δ_H 2.85 (4H, m, $H^{4,5}$); 3.52 (2H, d, J 14, H^8); 3.73 (2H, d, J 14, $H^{2,7}$); 3.76 (6H, s, H^{16}); 3.77 (2H, d, J 14, $H^{2,7}$); 3.78 (6H, s, H^{15}) 3.85 (2H, d, J 14, H^8); 6.42 (4H, m, $H^{11,13}$); 7.17 (2H, d, J 9 , H^{10}); 7.28 (3H, m, $H^{3',4'}$); 7.37 (2H, t, J 4, $H^{2'}$). **^{13}C NMR ($CDCl_3$, 176 MHz):** δ_C 55.33 (C^{16}); 55.33 (C^{15}) 56.79 ($C^{2,7}$); 57.94 ($C^{4,5}$); 64.77 (C^8); 97.98 ($C^{1'}$); 98.38 (C^{11}); 104.00 (C^{13}); 119.62 (C^9);

124.87 ($C^{2'}$); 128.20 ($C^{4'}$); 128.55 ($C^{3'}$); 131.12 (C^{10}); 140.04 (C^{1}); 158.71 (C^{16}); 159.91 (C^{15}). **HR MS ES+ (*m/z*):** found 522.2603 $[M + H]^+$; $C_{29}H_{36}N_3O_6$ requires 522.2604. The structure of **22** was confirmed by single crystal X-ray diffraction: $C_{29}H_{35}N_3O_6$, M_r = 521.60, monoclinic ($P2_1/n$); a = 8.8932(2) Å, b = 19.1927(5) Å, c = 15.3402(3) Å, V = 2616.02(11) Å^3, β = 92.411(2)°, Z = 4, μ = 0.093 mm^{-1}, $D_{calc.}$ = 1.324 mg/mm^3, T 120(2) K; 7279 independent reflections (R_{int} = 0.0449), R_1 = 0.0478, ωR_2 = 0.1084 ($I > 2\sigma(I)$). CCDC # 906040.

6-Nitro-6-phenyl-1,4-diazepane , **23**.

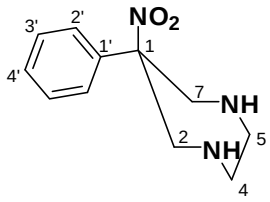

Trifluoroacetic acid (2 mL) was added to a solution of **22** (0.15 g, 0.29 mmol) in dichloromethane (2 mL), and the mixture stirred at room temperature. The reaction was monitored using LC-ESI MS, to follow removal of the dimethoxybenzyl substituents. Once complete, the solvent was removed by lyophilisation. Excess triflouroacetic acid was removed through repeated addition and removal of dicholormethane (3 x 10 mL) and subsequently methanol (3 x 10 mL). Filtration of a methanol solution (20 mL), using a 0.45 µm syringe filter, and subsequent removal of the methanol under reduced pressure yielded a brown oil. The oil was re-dissolved in chloroform : isopropyl alcohol (80 : 20, 20 mL) and washed successively with aqueous sodium hydroxide (2 x 20 mL, 0.5 M) and water (10 mL), dried over $MgSO_4$, filtered and solvent removed under reduced pressure to yield a pale yellow oil, (0.029 g, 45 %). **^{1}H NMR (CD_3OD, 600 MHz)**: δ_H 1.44 (4H, m, $H^{4,5}$); 3.71 (2H, d, J 15, $H^{2,7}$); 4.30 (2H, d, J 15 $H^{2,7}$); 7.35 (1H, t, J 8 $H^{4'}$); 7.38 (2H, t, J 8, $H^{3'}$); 7.42 (2H, d, J 8, $H^{2'}$). **^{13}C NMR (CD_3OD, 151 MHz)**: δ_C 45.78 ($C^{4,5}$); 53.89 ($C^{2,7}$); 94.44 ($C^{1'}$); 124.88 ($C^{4'}$); 124.96 ($C^{3'}$); 128.23 ($C^{2'}$); 135.16 (C^{1}). **HR MS ES+ (*m/z*):** found: 222.1240 $[M + H]^+$; $C_{11}H_{16}N_3O_2$ requires 222.1243.

Tert-butyl 2,2'-(6-nitro-6-phenyl-1,4-diazepane-1,4-diyl)diacetate, **24**.

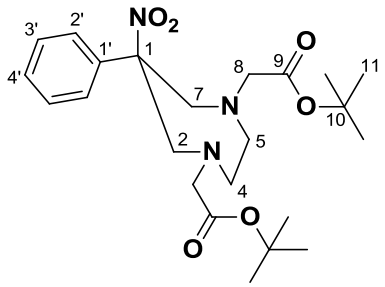

Tert-butyl bromoacetate (0.10 g, 0.52 mmol) was added dropwise to a mixture of potassium carbonate (0.072 g, 0.52 mmol) and **23** (0.029 g, 0.13 mmol) in acetonitrile (10 mL). The reaction mixture was stirred at 308 K for 24 hours, and the solvent removed under reduced pressure. The resulting oil was re-dissolved in chloroform (20 mL) and washed successively with aqueous potassium carbonate solution (2 x 20 mL, 0.1 M) and water (20 mL), dried over $MgSO_4$, filtered and solvent removed under reduced pressure. Purification by silica gel column chromatography (hexane : ethyl acetate, 95 : 5) yielded a white solid (0.036 g, 62 %). R_f = 0.49 (hexane : ethyl acetate; 65 : 35). m.p. 78 - 90 °C. **^{1}H NMR ($CDCl_3$, 700 MHz)**: δ_H 1.44 (18H, s, H^{11}); 2.93 (2H, m, $H^{4,5}$); 3.03 (2H, m, $H^{4,5}$); 3.38 (2H, d, J 17, H^8); 3.56 (2H, d, J 17, H^8); 3.63 (2H, d, J 15, $H^{2,7}$); 3.96 (4H, d, J 15, $H^{2,7}$); 7.24 (2H, d, J 8, $H^{2'}$); 7.31 (2H, m, $H^{3',4'}$). **^{13}C NMR ($CDCl_3$, 176 MHz)**: δ_C 28.20 (C^{11}); 55.93 ($C^{4,5}$); 60.33 (C^8); 62.87 ($C^{2,7}$); 81.15 (C^{10}); 97.99 ($C^{1'}$); 124.62 ($C^{2'}$); 128.52 ($C^{4'}$); 128.81 ($C^{3'}$); 138.68 (C^1); 170.90 (C^9). **HR MS ES+ (*m/z*):** found: 450.2612 $[M + H]^+$; $C_{23}H_{36}N_3O_6$ requires 450.2604. The structure of **24** was confirmed by single crystal X-ray diffraction: $C_{23}H_{35}N_3O_6$, M_r = 449.54, monoclinic ($P2_1/c$); a = 21.3378(19) Å, b = 11.5579(10) Å, c = 10.3203(9) Å, V = 2503.9(4) Å^3,β = 100.329(9)°, Z = 4; μ = 0.086 mm^{-1}, $D_{calc.}$ = 1.192 mg.mm^{-3}, T 120(2) K; 5463 independent reflections (R_{int} = 0.1564), R_1 = 0.0899 , ωR_2 = 0.1741 ($I > 2\sigma(I)$).

Tert-butyl 2,2'-(6-amino-6-phenyl-1,4-diazepane-1,4-diyl)diacetate, **25**.

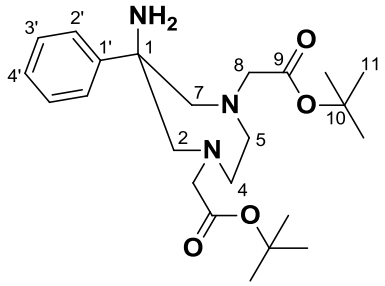

A water slurry of Raney nickel (0.010 g) was washed with methanol (3 x 25 mL) and ethanol added (10 mL). The suspension was transferred into a solution of **24** (0.050 g, 0.11 mmol) in ethanol (25

mL). The flask was evacuated and back-filled with hydrogen gas using four vacuum-purge cycles, and the mixture stirred at 298 K under an atmosphere of hydrogen. The reaction was monitored by UV-vis TLC for formation of the primary amine. Once complete (~ 3 h), the solution was decanted, and the solid washed with methanol (3 x 20 mL). The washings and decanted solution were combined, removed under reduced pressure and re-dissolved in methanol (25 mL). Remaining Raney nickel and insoluble by-products were removed by filtration through a base washed Celite® filter, and the solvent was removed under reduced pressure. The resulting oil was re-dissolved in chloroform : isopropyl alcohol (80 : 20, 20 mL) and washed successively with aqueous sodium hydroxide (2 x 20 mL, 0.5 M) and water (15 mL), dried over $MgSO_4$, filtered and the solvent removed under reduced pressure to yield a colourless oil (0.017 g, 37 %). **^{1}H NMR ($CDCl_3$, 700 MHz)**: δ_H 1.42 (18H, s, H^{11}); 2.16 (2H, br. s, NH_2); 2.61 (2H, d, J 14, $H^{2,7}$); 2.94 (4H, m, $H^{4,5}$); 3.31 (2H, d, J 14, $H^{2,7}$); 3.36 (4H, s, H^8); 7.21 (2H, t, J 8, $H^{4'}$); 7.30 (1H, t, J 8, $H^{3'}$); 7.60 (2H, d, J 8, $H^{2'}$). **^{13}C NMR ($CDCl_3$, 176 MHz)**: δ_C 28.18 (C^{11}); 56.93 ($C^{4,5}$); 58.19 (C^1); 61.76 (C^8); 69.25 ($C^{2,7}$); 80.88 (C^{10}); 125.23 ($C^{3'}$); 126.46 ($C^{4'}$); 128.09 ($C^{2'}$); 146.90 ($C^{1'}$); 170.87 (C^9). **HR MS ES+ (*m/z*):** found 420.2859 $[M + H]^+$; $C_{23}H_{38}N_3O_4$ requires 420.2862.

Tert-butyl 2,2'-(1,4-bis(2-tert-butoxy-2-oxoethyl)-6-phenyl-1,4-diazepan-6-ylazanediyl)diacetate **, 26**.

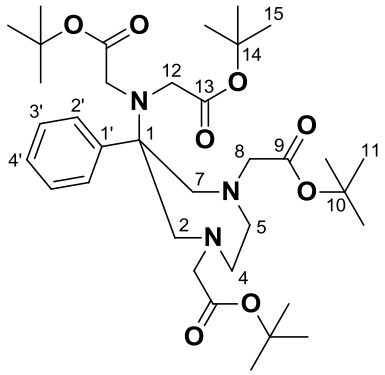

Tert-butyl-bromoacetate (0.14 g, 0.72 mmol) was added to a solution of **25** (0.050 g, 0.12 mmol) and potassium carbonate (0.13 g, 0.96 mmol) in acetonitrile (20 mL), and the mixture stirred for 18 h at 323 K under an atmosphere of argon. The solvent was removed under reduced pressure and the resulting oil re-dissolved in chloroform (20 mL) and washed successively with aqueous potassium carbonate solution (2 x 20 mL, 0.1 M) and water (2 x 20 mL), dried over $MgSO_4$, filtered and solvent removed under reduced pressure. Purification by silica gel column chromatography (hexane → 5 % ethyl acetate) afforded the title compound as a yellow oil (0.009 g, 12 %). R_f = 0.75 (hexane : ethyl acetate; 65 : 35). **^{1}HNMR ($CDCl_3$, 700 MHz):** δ 1.42 (18H, s, $H^{11/15}$); 1.43 (18H, s, $H^{11/15}$); 2.72 (2H,m, $H^{4,5}$); 2.84 (2H, m, $H^{4,5}$); 3.11 (2H, d, J 15, $H^{2,7}$); 3.29 (4H, d + d, $H^{2,7+8}$); 3.36 (2H, d, J 17, H^8); 3.59 (4H,

s, H^{12}); 7.17 (1H, t, J 8, $H^{4'}$); 7.27 (2H, t, J 8, $H^{3'}$); 7.73 (2H, d, J 8, $H^{2'}$). **^{13}C NMR ($CDCl_3$, 176 MHz):** δ 28.08 ($C^{11/15}$); 28.19 ($C^{11/15}$); 53.66 (C^{12}); 59.12 ($C^{4,5}$); 62.04 (C^{8}); 65.41 ($C^{2,7}$); 67.37 (C^{1}); 80.06 ($C^{10/14}$); 80.84 ($C^{10/14}$); 126.46 ($C^{4'}$); 127.08 ($C^{2'}$); 128.05 ($C^{3'}$); 147.73 ($C^{1'}$); 170.54 (C^{9}); 172.13 (C^{13}). **HR MS ES+ (m/z):** found 648.4247 $[M + H]^+$; $C_{35}H_{58}N_3O_8$ requires 648.4224; found 670.4068 $[M + Na]^+$; $C_{35}H_{57}N_3NaO_8$ requires 670.4043.

Tert-butyl 2,2'-(6-(2-tert-butoxy-2-oxoethylamino)-6-phenyl-1,4-diazepane-1,4-diyl)diacetate, **27**.

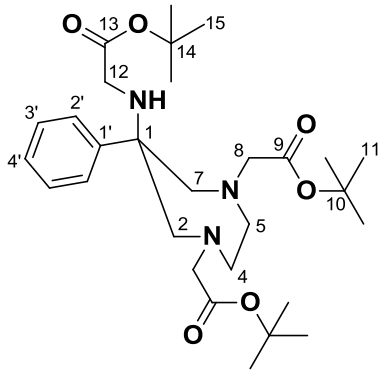

Tert-butyl-bromoacetate (0.29 g, 1.6 mmol) was added to a solution of **25** (0.050 g, 0.3 mmol) and potassium carbonate (0.31 g, 2.1 mmol) in acetonitrile (30 mL), and the mixture stirred for 18 h at 313 K under an atmosphere of argon. The solvent was removed under reduced pressure and the resulting oil re-dissolved in chloroform (20 mL) and washed successively with aqueous potassium carbonate solution (2 x 20 mL, 0.1 M) and water (20 mL), dried over magnesium sulfate, filtered and solvent removed under reduced pressure. Purification by silica gel column chromatography (hexane → 5 % ethyl acetate) yielded a yellow oil (0.051 g, 32 %). R_f = 0.60 (hexane : ethyl acetate; 65 : 35). **^{1}H NMR ($CDCl_3$, 700 MHz)**: δ_H 1.37 (18H, s, H^{11}); 1.38 (9H, s, H^{15}); 1.89 (1H, br. s, NH); 2.83 (2H, d, J 15, $H^{4,5}$); 2.87 (4H, s, $H^{2,7}$); 3.04 (2H, s, H^{12}); 3.27 (2H, d, J 15, $H^{4,5}$); 3.33 (4H, s, H^{8}); 7.14 (1H, t, J 7, $H^{4'}$); 7.24 (2H, t, J 7, $H^{3'}$); 7.45 (2H, d, J 7, $H^{2'}$). **^{13}C NMR ($CDCl_3$, 176 MHz)**: δ_C 28.10 (C^{11}); 28.21 (C^{15}); 45.57 (C^{12}); 56.44 ($C^{2,7}$); 61.62 (C^{8}); 62.08 ($C^{1'}$); 65.54 ($C^{4,5}$); 80.88 ($C^{10,14}$); 126.51 ($C^{2'}$); 126.67 ($C^{4'}$); 128.26 ($C^{3'}$); 144.48 (C^{1}); 171.01 (C^{9}); 171.75 (C^{13}). **HR MS ES+ (*m/z*):** found: 534.3556 $[M + H]^+$; $C_{29}H_{48}N_3O_6$ requires 534.3543.

Tert-butyl 2,2'-(6-((2-tert-butoxy-2-oxoethyl)(methyl)amino)-6-phenyl-1,4-diazepane-1,4-diyl)diacetate, **28**.

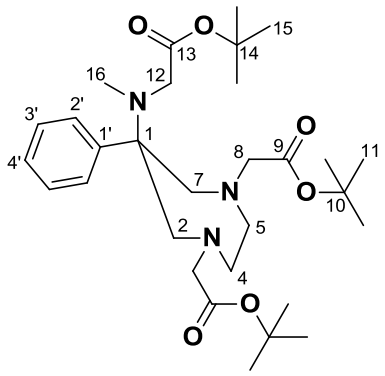

Methyl iodide (0.032 g, 0.023 mmol) was added to a solution of **27** (0.03 g, 0.056 mmol) and potassium carbonate (0.032 g, 0.023 mmol) in acetonitrile (30 mL), and the mixture stirred for 24 hours at 303 K, under an atmosphere of argon. The solvent was removed under reduced pressure and the resulting oil re-dissolved in chloroform (20 mL) and washed successively with aqueous potassium carbonate solution (2 x 20 mL, 0.1 M) and water (20 mL), dried over magnesium sulfate, filtered and solvent removed under reduced pressure. Purification by silica gel column chromatography (hexane → 5 % ethyl acetate) yielded a yellow oil (0.01 g, 45 %). R_f = 0.60 (SiO_2, hexane : ethyl acetate; 65 : 35). **^{1}H NMR ($CDCl_3$, 700 MHz)**: δ_H 1.38 (18H, s, H^{11}); 1.39 (9H, s, H^{15}); 2.23 (3H, s, H^{16}); 2.70 (2H, m, $H^{4,5}$); 2.80 (4H, m, $H^{4,5}$); 3.06 (2H, d, J 15, $H^{2,7}$); 3.13 (2H, d, J 15, $H^{2,7}$); 3.26 (2H, d, J 17, H^8); 3.30 (2H, d, J 17, H^8); 3.47 (2H, s, H^{12}); 7.11 (1H, t, J 8, $H^{4'}$); 7.21 (2H, t, J 8, $H^{3'}$); 7.63 (2H, d, J 8, $H^{2'}$). **^{13}C NMR ($CDCl_3$, 176 MHz)**: δ_C 28.12 (C^{11}); 28.20 (C^{15}); 45.57 (C^{12}); 38.40 (C^{16}); 54.73 (C^{12}); 58.84 ($C^{4,5}$); 62.19 (C^8); 64.11 ($C^{2,7}$); 66.55 ($C^{1'}$); 80.10 (C^{14}); 80.84 (C^{10}); 126.27 ($C^{4'}$); 126.94 ($C^{2'}$); 127.96 ($C^{3'}$); 148.05 (C^1); 170.63 (C^9); 172.37 (C^{13}). **HR MS ES+ (*m/z*):** found: 548.3704 [M + H]$^+$; $C_{30}H_{50}N_3O_6$ requires 548.3700.

2,2'-(6-((carboxymethyl)(methyl)amino)-6-phenyl-1,4-diazepane-1,4-diyl)diacetic acid Bistrifluoroacetate salt, **$L^7.2CF_3COOH$**.

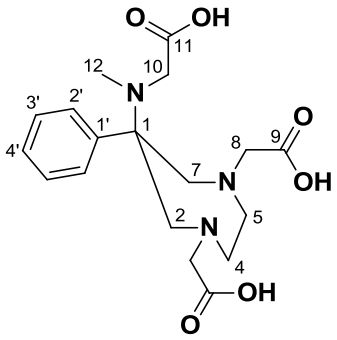

The triester **28** (0.050 g, 0.091 mmol) was dissolved in trifluoroacetic acid / dichloromethane (1 : 1, 2 mL) and left to stir for 2 days at room temperature. The solvent was removed under reduced pressure, the residue re-dissolved in dichloromethane : methanol (1 : 1, 2 mL) and evaporated. This procedure was repeated twice, and with methanol. The resulting solid was dissolved in water (10 mL) and washed with dichloromethane (10 mL). Removal of solvent under reduced pressure and drying *in vacuo* afforded a white solid (0.039 g, 71 %). **^{1}H NMR (D_2O, pH = 2.17, 600 MHz):** δ_H 2.62 (3H, s, H^{12}); 3.15 (2H, m, $H^{4,5}$); 3.44 (2H, m, $H^{4,5}$); 3.44 (2H, d, J 14, $H^{2,7}$); 3.67 (3H, m, $H^{4/5,10}$); 3.83 (3H, m, $H^{4/5,8}$); 3.88 (2H, d, J 14, $H^{2,7}$); 7.30 (1H, m, $H^{4'}$); 7.35 (2H, m, $H^{3'}$); 7.40 (2H, m, $H^{2'}$). **^{13}C NMR (D_2O, pH = 2.17, 151 MHz):** δ_c 32.60 (C^{12}); 51.89 ($C^{4/5}$); 53.19 ($C^{4/5}$); 58.73 (C^{10}); 59.00 (C^8); 63.00 ($C^{2,7}$); 71.85 (C^1); 128.87 ($C^{4'}$); 129.05 ($C^{3'}$); 129.44 ($C^{2'}$); 170.04 (C^9); 172.80 (C^{11}). **HR MS ES+ (*m/z*):** found 380.1818 $[M + H]^+$; $C_{18}H_{26}N_3O_6$ requires: 380.1822. **Elemental analysis (%):** found C (43.2) H (4.33) N (6.84); $[C_{18}H_{25}N_3O_6].2CF_3COOH$ requires C (43.5) H (4.48) N (6.92).

Diethyl 2,2'-(6-nitro-6-phenyl-1,4-diazepane-1,4-diyl)diacetate, **30**.

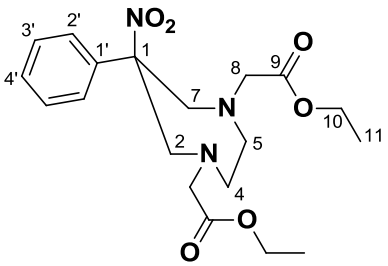

Ethyl bromoacetate (0.061 g, 0.52 mmol) was added dropwise to a stirred solution of potassium carbonate (0.072 g, 0.52 mmol) and **22** (0.029 g, 0.13 mmol) in acetonitrile (10 mL). The reaction mixture was stirred at 308 K for 24 hours, and solvent removed under reduced pressure. The resulting oil was re-dissolved in chloroform (20 mL) and washed successively with aqueous

potassium carbonate solution (2 x 20 mL, 0.1 M) and water (20 mL), dried over $MgSO_4$, filtered and solvent removed under reduced pressure. Purification by silica gel column chromatography (hexane → 20 % ethyl acetate) yielded a yellow oil (0.034 g, 66%). R_f = 0.27 (hexane : ethyl acetate, 65 : 35). **^{1}H NMR ($CDCl_3$, 700 MHz)**: δ_H 1.26 (6H, t, J 7, H^{11}); 2.96 (2H, m, $H^{4,5}$); 3.04 (2H, m, $H^{4,5}$); 3.49 (2H, d, J 18, H^8); 3.64 (2H, d, J 15, $H^{2,7}$); 3.67 (2H, d, J 18, H^8); 3.97 (2H, d, J 15, $H^{2,7}$); 7.24 (2H, d, J 8, $H^{2'}$); 7.32 (2H, m, $H^{3',4'}$). **^{13}C NMR ($CDCl_3$, 176 MHz)**: δ_C 14.26 (C^{11}); 55.85 ($C^{4,5}$); 59.41 (C^8); 60.40 (C^{10})62.70 ($C^{2,7}$); 97.76 ($C^{1'}$); 124.63 ($C^{2'}$); 128.62 ($C^{4'}$); 128.84 ($C^{3'}$); 138.41 (C^1); 171.53 (C^9). **HR MS ES+ (*m/z*):** found: 394.1968 $[M + H]^+$; $C_{19}H_{28}N_3O_6$ requires 394.1978.

Diethyl 2,2'-(6-amino-6-phenyl-1,4-diazepane-1,4-diyl)diacetate, **31**.

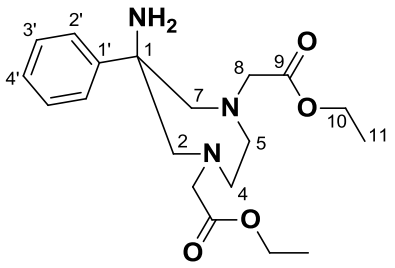

A water slurry of Raney nickel (0.010 g) was washed with methanol (3 x 25 mL) and ethanol added (10 mL). The suspension was transferred into a solution of **30** (0.050 g, 0.13 mmol) in ethanol (25 mL). The flask was evacuated and back-filled with hydrogen gas using four vacuum-purge cycles, and the mixture stirred at 298 K under an atmosphere of hydrogen. The reaction was monitored by UV-vis TLC for formation of the primary amine. Once complete (~ 3 h), the solution was decanted, and the solid washed with methanol (3 x 20 mL). The washings and decanted solution were combined, removed under reduced pressure and re-dissolved in methanol (25 mL). Remaining Raney nickel and insoluble by-products were removed by filtration through a base washed Celite® filter, and the solvent was removed under reduced pressure. The resulting oil was re-dissolved in chloroform : isopropyl alcohol (80 : 20, 20 mL) and washed successively with aqueous sodium hydroxide (2 x 20 mL, 0.5 M) and water (15 mL), dried over $MgSO_4$, filtered and the solvent removed under reduced pressure to yield a colourless oil (0.014 g, 30 %). **^{1}H NMR ($CDCl_3$, 700 MHz)**: δ_H 1.22 (6H, t+t, H^{11}); 2.12 (2H, br. s, NH_2); 2.63 (2H, d, J 14, $H^{2,7}$); 2.95 (4H, m, $H^{4,5}$); 3.30 (2H, d, J 14, $H^{2,7}$); 3.46 (4H, s, H^8); 4.10 (4H, q+q, J 7, H^{10}) 7.25 (2H, t, J 7, $H^{4'}$); 7.29 (1H, t, J 7, $H^{3'}$); 7.59 (2H, d, J 7, $H^{2'}$). **^{13}C NMR ($CDCl_3$, 176 MHz)**: δ_C 14.25 (C^{11}); 56.90 ($C^{4,5}$); 58.15 (C^1); 60.28 (C^{10}); 60.82 (C^8); 69.25 ($C^{2,7}$); 125.19 ($C^{4'}$); 128.11 ($C^{3'}$); 128.44 ($C^{2'}$); 146.62 (C^1); 171.47 (C^9). **HR MS ES+ (*m/z*):** found 364.2235 $[M + H]^+$; $C_{19}H_{30}N_3O_4$ requires 364.2236.

Diethyl 2,2'-(6-(2-ethoxy-2-oxoethylamino)-6-phenyl-1,4-diazepane-1,4-diyl)diacetate, **32**.

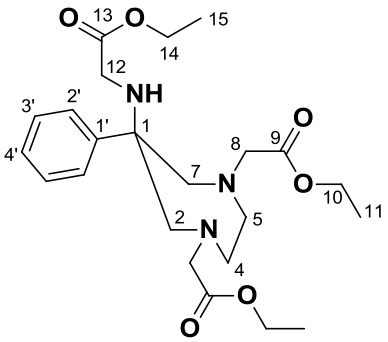

Ethyl-bromoacetate (0.068 g, 0.41 mmol) was added to a solution of **31** (0.030 g, 0.083 mmol) and potassium carbonate (0.080 g, 0.58 mmol) in acetonitrile (20 mL), and the mixture stirred for 18 h at 313 K under an atmosphere of argon. The solvent was removed under reduced pressure and the resulting oil re-dissolved in chloroform (20 mL) and washed successively with aqueous potassium carbonate solution (2 x 15 mL, 0.1 M) and water (15 mL), dried over $MgSO_4$, filtered and solvent removed under reduced pressure. Purification by silica gel column chromatography (hexane → 15 % ethyl acetate) afforded the title compound as a yellow oil (0.016 g, 43 %). R_f = 0.35 (hexane : ethyl acetate; 65 : 35). **^{1}H NMR ($CDCl_3$, 700 MHz)**: δ_H 1.24 (9H, t, J 7, $H^{11,15}$); 1.69 (1H, br. s, NH); 2.89 (2H, d, J 14, $H^{2,7}$); 2.94 (4H, s, $H^{4,5}$); 3.18 (2H, s, H^{12}); 3.34 (2H, d, J 14, $H^{2,7}$); 3.49 (4H, s, H^{8}); 4.13 (4H, q, J 7, H^{10}); 4.17 (2H, q, J 7, H^{14}) 7.19 (1H, t, J 8, $H^{4'}$); 7.29 (2H, t, J 8,$H^{3'}$); 7.50 (2H, d, J 8 , $H^{2'}$). **^{13}C NMR ($CDCl_3$, 176 MHz)**: δ_C 14.16 ($C^{11/15}$); 14.27 ($C^{11/15}$); 44.85 (C^{12}); 55.23 (C^{1}); 56.51 ($C^{4,5}$); 60.39 (C^{10}); 60.57 (C^{12}); 60.74 (C^{8}); 65.51 ($C^{2,7}$); 126.50 ($C^{2'}$); 126.75 ($C^{4'}$); 128.33 ($C^{3'}$); 144.17 ($C^{1'}$); 171.54 (C^{9}); 172.46 (C^{13}). **HR MS ES+ (*m/z*):** found: 450.2602 $[M + H]^+$; $C_{23}H_{36}N_3O_6$ requires 450.2604; found: 472.2423 $[M + Na]^+$; $C_{23}H_{35}N_3NaO_6$ requires 472.2424.

2,2'-(6-(Carboxymethylamino)-6-phenyl-1,4-diazepane-1,4-diyl)diacetic acid trisodium salt, **Na_3.L^6**.

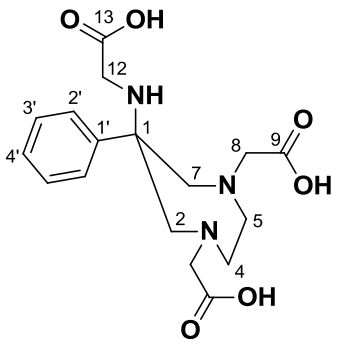

Sodium hydroxide (0.003 g, 0.069 mmol) dissolved in water (0.5 mL) was added to a solution of the triester **32** (0.010 g, 0.022 mmol) in THF (0.5 mL), and the mixture stirred at 298 K. The reaction was monitored using LC-ESI MS, to follow ester cleavage. Once complete, the solvent was removed by lyophilisation. Water (5 mL) was added and removed by lyophilisation, and the procedure repeated two more times. The resulting solid was washed with ice-cold dichloromethane (0.5 mL), and dried *in vacuo*, to afford the tetra-hydrated tri-sodium salt of the title compound as a white solid (0.010 g, 85 %). **^{1}H NMR (D_2O, pD 11.78, 600 MHz, ppm):** δ_H 2.61 (2H, m, $H^{4,5}$); 2.71 (3H, s, H^{10}); 2.76 (2H, m, $H^{4,5}$); 2.88 (2H, d, J 14, $H^{2,7}$); 3.09 (2H, d, J 16, H^{8}); 3.16 (4H, d+d, $H^{2,7,8}$); 7.419 (1H, t, J 7, $H^{4'}$); 7.29 (2H, t, J 7, $H^{3'}$); 7.34 (2H, d, J 7, $H^{2'}$). **^{13}C NMR (D_2O, pD 11.78, 151 MHz, ppm):** δ_C 46.32 (C^{10}); 56.72 ($C^{4,5}$); 61.99 (C^{1}); 63.51 (C^{8}); 65.09 ($C^{2,7}$); 126.73 ($C^{2'}$); 127.11 ($C^{4'}$); 128.51 ($C^{3'}$); 143.40 ($C^{1'}$); 179.23 (C^{11}); 179.35 (C^{9}). **HR MS ES+ (*m/z*):** found 366.1666 $[M + H]^+$; $C_{17}H_{24}N_3O_6$ requires 366.1665. **Elemental analysis (%):** found C (40.7) H (5.73) N (8.27); $Na_3[C_{17}H_{20}N_3O_6].4H_2O$ requires C (40.6) H (5.61) N (8.35).

(2S,2'S)-Diethyl 2,2'-(6-nitro-6-phenyl-1,4-diazepane-1,4-diyl)dipropanoate, **34**.

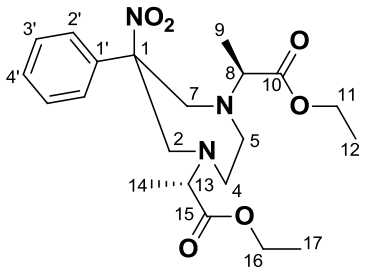

Ethyl (2R)-2-{[(trifluoromethyl)sulfonyl]oxy}propanoate (0.20 g, 0.78 mmol) was added to a stirred solution of potassium carbonate (0.11 g, 0.78 mmol) and **22** (0.029 g, 0.13 mmol) in acetonitrile (15 mL). The reaction mixture was stirred at 308 K for 24 h, and solvent removed under reduced pressure. The resulting oil was re-dissolved in chloroform (20 mL) and washed successively with aqueous potassium carbonate solution (2 x 20 mL, 0.1 M) and water (20 mL), dried over $MgSO_4$, filtered and solvent removed under reduced pressure. Purification by silica gel column chromatography (hexane : ethyl acetate, 95 : 5) afforded the title compound as a colourless oil (0.042 g, 77 %). R_f = 0.54 (hexane : ethyl acetate; 65 : 35). **^{1}H NMR ($CDCl_3$, 600 MHz, ppm):** δ 1.15 (3H, d, J 7, H^{9}); 1.24 (6H, t+t, J 7, $H^{12,17}$); 1.31 (3H, d, J 7, H^{14}); 2.67 (2H, m, $H^{4,5}$); 2.94 (1H, m, H^{5}); 2.98 (1H, m, H^{4}); 3.48 (1H, q, J 7, H^{13}); 3.51 (1H, d, J 15, H^{7}); 3.59 (1H, q, J 7, H^{8}); 3.70 (1H, d, J 15, H^{2}); 3.89 (1H, d, J 15, H^{2}); 3.96 (1H, d, J 15, H^{7}); 4.12 (4H, q, J 15, $H^{11,16}$); 7.31 (5H, m, $H^{2',3',4'}$). **^{13}C NMR ($CDCl_3$, 151 MHz, ppm):** δ 14.38 ($C^{12,17}$); 16.16 (C^{9}); 16.34 (C^{14}); 53.11 (C^{5}); 55.24 (C^{4}); 60.26 ($C^{11/16}$); 60.38

($C^{11/16}$); 63.38 (C^{2}); 63.48 (C^{8}); 63.87 (C^{7}); 63.93 (C^{13}); 98.14 ($C^{1'}$); 124.79 ($C^{2'}$); 128.45 ($C^{4'}$); 128.71 ($C^{3'}$); 139.39 (C^{1}); 173.21 ($C^{10,15}$); 173.56 ($C^{10,15}$). **HR MS ES+ (*m/z*):** found: 422.2301 $[M + H]^+$; $C_{21}H_{32}N_3O_6$ requires 422.2291.

(2S,2'S)-Diethyl 2,2'-(6-amino-6-phenyl-1,4-diazepane-1,4-diyl)dipropanoate, **35**.

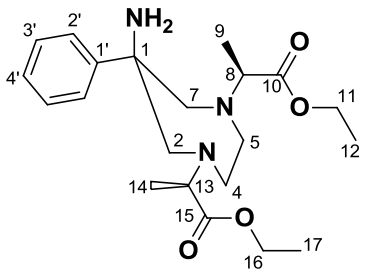

A water slurry of Raney nickel (0.010 g) was washed with methanol (3 x 25 mL) and ethanol added (10 mL). The suspension was transferred into a solution of **34** (0.050 g, 0.12 mmol) in ethanol (25 mL). The flask was evacuated and back-filled with hydrogen gas using four vacuum-purge cycles, and the mixture stirred at 298 K under an atmosphere of hydrogen. The reaction was monitored by UV-vis TLC for formation of the primary amine. Once complete (~ 3 h), the solution was decanted, and the solid washed with methanol (3 x 20 mL). The washings and decanted solution were combined, removed under reduced pressure and re-dissolved in methanol (25 mL). Remaining Raney nickel and insoluble by-products were removed by filtration through a base washed Celite® filter, and the solvent was removed under reduced pressure. The resulting oil was re-dissolved in chloroform : isopropyl alcohol (80 : 20, 20 mL) and washed successively with aqueous sodium hydroxide (2 x 20 mL, 0.5 M) and water (15 mL), dried over $MgSO_4$, filtered and the solvent removed under reduced pressure to yield a colourless oil (0.020 g, 44 %). **^{1}H NMR ($CDCl_3$, 600 MHz, ppm):** δ 1.23 (9H, m, $H^{12,17,\ 9/14}$); 1.29 (3H, d, J 7, $H^{9/14}$); 2.13 (2H, br. s, NH_2); 2.65 (1H, d, J 14, H^{2}); 2.74 (2H, d+m, $H^{7\ +\ 4/5}$); 2.82 (1H, m, $H^{4/5}$); 2.92 (1H, m, $H^{4/5}$); 3.00 (1H, m, $H^{4/5}$); 3.22 (2H, d+d, $H^{2,7}$); 3.47 (2H, q+q, $H^{8,13}$); 4.11 (4H, q+q, $H^{11,16}$); 7.22 (1H, t, J 7, $H^{4'}$); 7.31 (2H, t, J 7, $H^{3'}$); 7.60 (2H, d, J 7, $H^{2'}$). **^{13}C NMR ($CDCl_3$, 151 MHz, ppm):** δ 14.35 ($C^{12,17}$); 14.38 ($C^{12,17}$); 15.27 (C^{9}); 16.37 (C^{14}); 52.94 (C^{4}); 55.31 (C^{5}); 57.60 (C^{1}); 60.19 ($C^{11/16}$); 60.23 ($C^{11/16}$); 65.97 (C^{7}); 63.48 (C^{13}); 63.87 (C^{2}); 63.93 (C^{8}); 125.25 ($C^{2'}$); 126.51 ($C^{4'}$); 128.15 ($C^{3'}$); 146.09 ($C^{1'}$); 173.59 ($C^{10,15}$); 173.68 ($C^{10,15}$). **HR MS ES+ (*m/z*):** found 392.2567 $[M + H]^+$; $C_{21}H_{34}N_3O_4$ requires 392.2549.

(2S,2'S)-Diethyl 2,2'-(6-((S)-1-ethoxy-1-oxopropan-2-ylamino)-6-phenyl-1,4-diazepane-1,4-diyl)dipropanoate **, 36**.

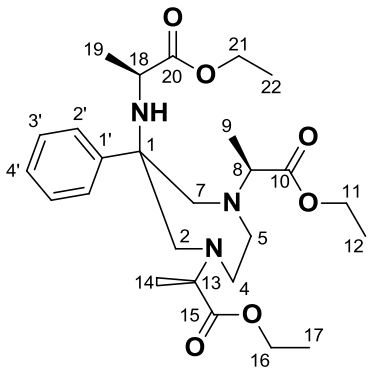

Ethyl (2R)-2-{[(trifluoromethyl)sulfonyl]oxy}propanoate (0.096 g, 0.38 mmol) was added to a solution of **35** (0.050 g, 0.13 mmol) and potassium carbonate (0.050 g, 0.38 mmol) in acetonitrile (15 mL), and the reaction mixture stirred at 308 K for 18 h. The solvent was removed under reduced pressure and the resulting oil re-dissolved in chloroform (20 mL) and washed successively with aqueous potassium carbonate solution (2 x 15 mL, 0.1 M) and water (15 mL), dried over $MgSO_4$, filtered and solvent removed under reduced pressure. Purification by silica gel column chromatography (hexane : ethyl acetate, 95 : 5) afforded the title compound as a colourless oil (0.030 g, 47 %). R_f = 0.65 (hexane : ethyl acetate; 65 : 35). **^{1}H NMR ($CDCl_3$, 600 MHz, ppm):** δ_H 1.16 – 1.31 (19H, m, $H^{9,14,19,12,17,22}$); 1.61 (1H, br. s, NH); 2.64 (1H, m, H^5); 2.70 (1H, m, H^4); 2.81 (1H, m, H^4); 2.86 (1H, d, J 13, H^7); 2.90 (2H, m, $H^{2,5}$); 3.05 (1H, d, J 13, H^2); 3.13 (1H, q, J 7, H^{18}); 3.27 (1H, d, J 13, H^7); 3.39 (2H, q+q, $H^{8,13}$); 4.01 (2H, q, J 7, $H^{11/16/21}$); 4.09 (2H, q, J 7, $H^{11/16/21}$); 4.14 (2H, q, J 7, H^5); 7.18 (1H, t, J 8, $H^{4'}$); 7.27 (2H, t, J 8, $H^{3'}$); 7.56 (2H, d, J 8, $H^{2'}$). **^{13}C NMR ($CDCl_3$, 151 MHz, ppm):** δ_C 14.07 ($C^{9/12/14/17}$); 14.37 ($C^{9/12/14/17}$); 14.37 ($C^{9/12/14/17}$); 14.42 ($C^{9/12/14/17}$); 17.38 (C^{22}); 21.78 (C^{19}); 51.11 (C^{18}); 52.83 (C^5); 55.01 (C^4); 60.05 (C^{21}); 60.09 ($C^{11/16}$); 60.31 ($C^{11/16}$); 62.28 (C^1); 63.38 ($C^{8/13}$); 63.51 (C^2); 63.85 ($C^{28/13}$); 65.03 (C^7); 126.49 ($C^{4'}$); 127.19 ($C^{2'}$); 127.84 ($C^{3'}$); 145.61 ($C^{1'}$); 173.64 ($C^{10/15}$); 173.71 ($C^{10/15}$); 177.13 (C^{20}). H**R MS ES+ (*m/z*):** found 492.3071 $[M + H]^+$; $C_{26}H_{42}N_3O_6$ requires 492.3074.

(2S,2'S)-2,2'-(6-((S)-1-Carboxyethylamino)-6-phenyl-1,4-diazepane-1,4-diyl)dipropanoic acid trisodium salt, **$Na_3.L^8$**.

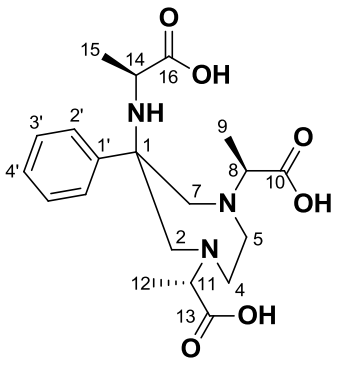

Sodium hydroxide (0.003 g, 0.063 mmol) dissolved in water (0.5 mL) was added to a solution of the triester **36** (0.010 g, 0.020 mmol) in THF (0.5 mL), and the mixture stirred at 298 K. The reaction was monitored using LC-ESI MS, to follow ester cleavage. Once complete, the solvent was removed by lyophilisation. Water (5 mL) was added and removed by lyophilisation, and the protocol repeated two more times. The resulting solid was washed with ice cold dichloromethane (0.5 mL), and dried *in vacuo* to afford the tri-sodium salt of the title compound as a white solid (0.091 g, 95 %). **^{1}H NMR (D_2O, pD 11.34, 600 MHz):** δ 0.87 (3H, d, J 7, H^9); 0.90 (3H, d, J 7, H^{15}); 1.09 (3H, d, J 7, H^{12}); 2.49 (1H, m, $H^{4/5}$); 2.60 (1H, m, $H^{4/5}$); 2.67 (2H, q, J 9, $H^{4,5}$); 2.73 (1H, q, J 7, H^{14}); 2.83 (1H, d, J 14, H^7); 2.96 (1H, q, J 7, H^8); 2.99 (1H, d, J 14, H^2); 3.10 (1H, d, J 14, H^2); 3.21 (1H, q, 7, H^{11}); 3.25 (1H, d, J 14, H^7); 7.14 (1H, t, J 8, $H^{4'}$); 7.23 (2H, t, J 8, $H^{3'}$); 7.37 (2H, d, J 8, $H^{2'}$). **^{13}C NMR (D_2O, pD 11.34, 151 MHz):** δ 14.87 (C^{12}); 15.70 (C^9); 21.35 (C^{15}); 53.50 (C^{14}); 54.70 ($C^{4/5}$); 56.07 ($C^{4/5}$); 61.37 (C^7); 62.08 (C^1); 62.18 (C^2); 66.58 (C^8); 67.07 (C^{11}); 126.92 ($C^{4'}$); 127.78 ($C^{2'}$); 127.96 ($C^{3'}$); 143.50 ($C^{1'}$); 181.65 ($C^{10/11}$); 181.94 ($C^{10/11}$); 183.84 (C^{16}). **HR MS ES+ (*m/z*):** found 430.1972 $[M + Na]^+$; $C_{20}H_{29}N_3NaO_6$ requires 430.1964. **Elemental analysis (%):** found C (45.4) H (6.33) N (7.77); $Na_3[C_{20}H_{26}N_3O_6].3H_2O$ requires C (45.5) H (6.12) N (7.97).

1,4-Bis(2,4-dimethoxybenzyl)-6-phenyl-1,4-diazepan-6-ol**, 38**.

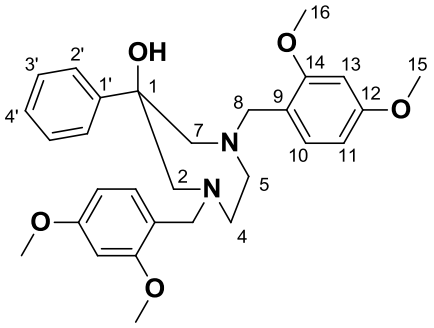

The protected APPED scaffold, **22**, (0.05 g, 0.10 mmol) was dissolved in ethanol (20 mL) and the solution refluxed. The solvolysis reaction was monitored using TLC (Hexane: Ethyl Acetate, 65 : 35). Once the nitro precursor (R_f = 0.55) had been consumed, solvent was removed under reduced pressure and the resulting oil re-dissolved in chloroform (50 mL) and washed successively with aqueous potassium carbonate solution (2 x 50 mL, 0.1 M) and water (50 mL), dried over $MgSO_4$, filtered and solvent removed under reduced pressure. Purification by silica gel column chromatography (hexane → 50 % ethyl acetate) yielded a yellow oil (0.017 g, 34 %). R_f = 0.45 (hexane : ethyl acetate; 50 : 50). **^{1}H NMR ($CDCl_3$, 700 MHz)**: δ_H 2.53 (2H, m, $H^{4,5}$); 2.76 (2H, d, J 13, $H^{2,7}$); 2.80 (2H, m, $H^{4,5}$); 3.18 (2H, d, J 13, $H^{2,7}$); 3.67 (2H, d, J 4, H^8); 3.74 (2H, d, J 4, H^8); 3.78 (6H, s, H^{16}); 3.79 (6H, s, H^{15}); 6.41 (2H, d, J 9, H^{11}); 6.44 (2H, s, H^{13}); 7.16 (2H, d, J 9, H^{10}); 7.20 (1H, t , J 8, $H^{4'}$); 7.30 (2H, t, J 8, $H^{3'}$); 7.48 (2H, d, J 8, $H^{2'}$). **^{13}C NMR ($CDCl_3$, 176 MHz)**: δ_C 54.0 ($C^{4/5}$); 55.3 (C^{16}); 55.3 (C^{15}); 56.8 (C^8); 67.6 ($C^{2,7}$); 74.7 ($C^{1'}$); 98.5 (C^{13}); 103.7 (C^{11}); 120.0 (C^9); 124.6 ($C^{2'}$); 126.4 ($C^{4'}$); 127.9 ($C^{3'}$); 131.0 (C^{10}); 146.1 (C^1); 158.8 (C^{12}); 160.0 (C^{14}). H**R MS ES+ (*m/z*):** found: 493.2724 $[M + H]^+$; $C_{29}H_{37}N_2O_5$ requires 493.2702.

6-Phenyl-1,4-diazepan-6-ol, **39**.

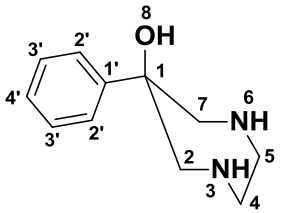

3,6-Bis(2,4-dimethoxybenzyl)-1-phenyl-3,6-diazepan-1-ol (0.100 g, 0.52 mmol) was dissolved in trifluoroacetic acid / dichloromethane (1:1, 2 mL) and left to stir for 2 days at room temperature. The solvent was removed under reduced pressure, the residue re-dissolved in dichloromethane and evaporated. This procedure was repeated twice. The residue was recrystallised from methanol/dichloromethane (1:1) to afford a white solid, (0.029 g, 76 %). **^{1}H NMR (CD_3OD, 700 MHz):**

δ_H 2.83 (2H, d, J 14, $H^{2,7}$); 2.92 (2H, m, $H^{4,5}$); 3.07 (2H, m, $H^{4,5}$); 3.19 (2H, d, J 14, $H^{2,7}$); 7.20 (1H, t, J 8 , $H^{4'}$); 7.37 (2H, t, J 8 , $H^{3'}$); 7.45 (2H, d, J 8 , $H^{2'}$). **^{13}C NMR (CD_3OD, 176 MHz):** δ_C 48.6 ($C^{4,5}$); 58.9 ($C^{2,7}$); 76.2 (C^{1}); 124.3 ($C^{2'}$); 126.6 ($C^{4'}$); 127.8 ($C^{3'}$); 145.4 ($C^{1'}$). H**R MS ES+ (*m/z*):** found: 193.1271 $[M + H]^+$;. Calculated for $C_{11}H_{17}N_2O$: 193.1341.

Tert-butyl 2,2'-(6-hydroxy-6-phenyl-1,4-diazepane-1,4-diyl)diacetate, **40**.

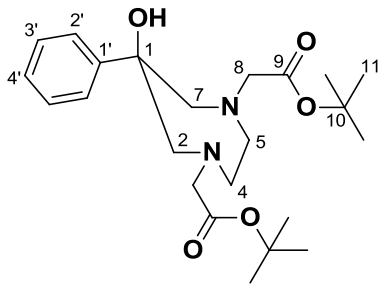

Tert-butyl-bromoacetate (0.20 g, 1.0 mmol) was added dropwise to a mixture of potassium carbonate (0.14 g, 1.0 mmol) and **39** (0.05 g, 0.26 mmol) in acetonitrile (15 mL), and the mixture stirred at 308 K for 18 h under an atmosphere of argon. The solvent was removed under reduced pressure and the resulting oil re-dissolved in chloroform (25 mL) and washed successively with aqueous potassium carbonate solution (2 x 25 mL, 0.1 M) and water (25 mL), dried over $MgSO_4$, filtered and solvent removed under reduced pressure. Purification by silica gel column chromatography (hexane → 20 % ethyl acetate) yielded white solid (0.084 g, 74 %). R_f = 0.15 (hexane : ethyl acetate, 65 : 35). m.p. 88 - 97 °C. Single crystals of **40** where grown by slow evaporation of saturated ethanol: dichloromethane solution. **^{1}H NMR ($CDCl_3$, 700 MHz)**: δ_H 1.43 (18H, s, H^{11}); 2.64 (2H, d, J 14, $H^{2,7}$); 2.94 (2H, m, $H^{4,5}$); 3.01 (2H, m, $H^{4,5}$); 3.38 (2H, d, J 14, $H^{2,7}$); 3.40 (2H, s, H^{8}); 5.02 (1H, br. s, H^{12}); 7.22 (1H, t, J 8, $H^{4'}$); 7.31 (2H, t, J 8, $H^{3'}$); 7.50 (2H, d, J 8, $H^{2'}$). **^{13}C NMR ($CDCl_3$, 176 MHz)**: δ_C 28.15 (C^{11}); 54.77 ($C^{4,5}$); 60.67 (C^{8}); 66.66 ($C^{2,7}$); 73.78 ($C^{1'}$) 81.12 (C^{10}); 124.57 ($C^{2'}$); 126.70 ($C^{4'}$); 128.05 ($C^{3'}$); 145.07 (C^{1}); 170.87 (C^{9}). **HR MS ES+ (*m/z*):** found: 421.2714 $[M + H]^+$; $C_{23}H_{37}N_2O_5$ requires 421.2702. The structure of **BW-31** was confirmed by single crystal X-ray diffraction: $C_{23}H_{36}N_2O_5$, M_r = 420.54, triclinic (P-1); a = 5.7906(7) Å, b = 9.5843(11) Å, c = 20.978(2) Å, V = 1145.6(2) Å^3,α = 81.025(10)°, β = 87.158(10)°, γ = 85.460(10)°, Z = 2; μ = 0.085 mm^{-1}, $D_{calc.}$ = 1.219 mg.mm^{-3}, T 120(2) K; 5749 independent reflections (R_{int} = 0.0595), R_1 = 0.0563 , ωR_2 = 0.1154 ($I > 2\sigma(I)$).

2,2'-(6-Hydroxy-6-phenyl-1,4-diazepane-1,4-diyl)diacetic acid trifluoroacetate, **41.CF_3COOH**.

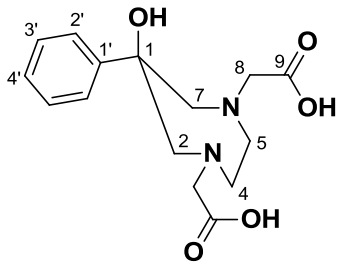

The diester **40** (0.050 g, 0.12 mmol) was dissolved in trifluoroacetic acid / dichloromethane (1:1, 2 mL) and left to stir for 2 days at room temperature. The solvent was removed under reduced pressure, the residue re-dissolved in dichloromethane and evaporated. This procedure was repeated twice, and also with methanol. The resulting solid was dissolved in water (15 mL) and washed with dichloromethane (15 mL). Removal of solvent under reduced pressure afforded the a white solid (0.026 g, 51 %). **^{1}H NMR (D_2O, pD 3.58, 700 MHz)**: δ_H 3.44 (2H, d, J 14, $H^{2,7}$); 3.72 (2H, m, $H^{4,5}$); 3.84 (2H, m, $H^{4,5}$); 3.89 (4H, s, H^8); 3.89 (2H, d, J 14, $H^{2,7}$); 7.33 (1H, m, $H^{4'}$); 7.34 (2H, br. s, $H^{2',3'}$). **^{13}C NMR (D_2O, pD 3.58, 176 MHz)**: δ_C 51.78 ($C^{4,5}$); 58.75 (C^8); 62.88 ($C^{2,7}$); 71.75 ($C^{1'}$); 124.09 ($C^{2'}$); 128.92 ($C^{4'}$); 129.08 ($C^{3'}$); 140.57 (C^1); 169.54 (C^9). **HR MS ES+ (*m/z*):** found: 309.1450 $[M + H]^+$; $C_{15}H_{21}N_2O_5$ requires 309.1450. **Elemental analysis (%):** found C (48.0) H (4.84) N (6.69); $[C_{15}H_{20}N_2O_5].CF_3COOH$ requires C (48.3) H (5.01) N (6.63).

Tert-butyl 2,2'-(6-(2-tert-butoxy-2-oxoethoxy)-6-phenyl-1,4-diazepane-1,4-diyl)diacetate, **42**.

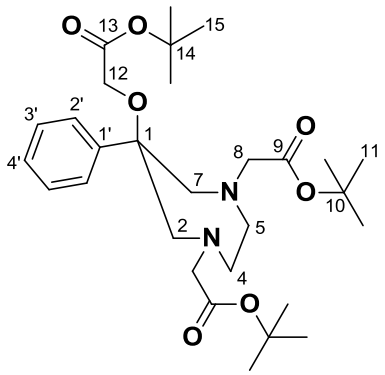

Tert-butyl-bromoacetate (0.10 g, 0.52 mmol) was added to a solution of **39** (0.02 g, 0.10 mmol) and caesium carbonate (0.10 g, 0.52 mmol) in acetonitrile (15 mL), and the mixture stirred for 18 h at 363 K under an atmosphere of argon. The solvent was removed under reduced pressure and the resulting oil re-dissolved in chloroform (15 mL) and washed successively with aqueous potassium carbonate solution (2 x 15 mL, 0.1 M) and water (10 mL), dried over $MgSO_4$, filtered and solvent

removed under reduced pressure. Purification by silica gel column chromatography (hexane → 20 % ethyl acetate) afforded a colourless oil (0.018 g, 33 %). R_f = 0.25 (hexane : ethyl acetate; 50 : 50). **^{1}H NMR ($CDCl_3$, 700 MHz)**: δ_H 1.42 (18H, s, $H^{11/15}$); 1.43 (9H, s, $H^{11/15}$); 1.46 (9H, s, H^{19}); 1.48 (9H, s, H^{16}); 2.50 (1H, d, J 7, $H^{8/12}$); 2.59 (1H, d, J 14, $H^{2/7}$); 2.66 (1H, d, J 7, $H^{8/12}$); 2.74 (1H, d, J 14, $H^{2/7}$); 2.89 (1H, m, $H^{4/5}$); 2.93 (1H, m, $H^{4/5}$); 3.01 (2H, m, $H^{4,5}$), 3.09 (1H, d, J 14, $H^{2/7}$); 3.36 (3H, m, $H^{2/7,8,12}$); 7.22 (1H, t, J 8, $H^{4'}$); 7.31 (2H, t, J 8, $H^{3'}$); 7.50 (1H, d, J 8, $H^{2'}$). **^{13}C NMR ($CDCl_3$, 176 MHz)**: δ_C 28.08 ($C^{11/15/19}$); 28.14 ($C^{11/15/19}$); 28.20 ($C^{11/15/19}$); 37.23 (C^{16}); 55.18 ($C^{4/5}$); 55.47 ($C^{4/5}$); 60.70 (C^{8}); 63.64 (C^{12}); 64.19 ($C^{2/7}$); 66.37 ($C^{2/7}$); 73.30 (C^{1}); 80.78 ($C^{10/14/18}$); 81.10 ($C^{10/14/18}$); 81.46 ($C^{10/14/18}$); 82.90 (C^{17}); 124.56 ($C^{2'}$); 126.67 ($C^{4'}$); 128.03 ($C^{3'}$); 145.23 ($C^{1'}$); 170.84 ($C^{9/13}$); 170.91 ($C^{9/13}$). **HR MS ES+ (*m/z*):** found: 535.3362 $[M + H]^+$; $C_{29}H_{47}N_2O_7$ requires 535.3383; found: 557.3192 $[M + Na]^+$; $C_{29}H_{46}N_2NaO_7$ requires 557.3203.

2,2'-(6-(Carboxymethoxy)-6-phenyl-1,4-diazepane-1,4-diyl)diacetic acid trifluoroacetate salt, **L^9.CF_3COOH**.

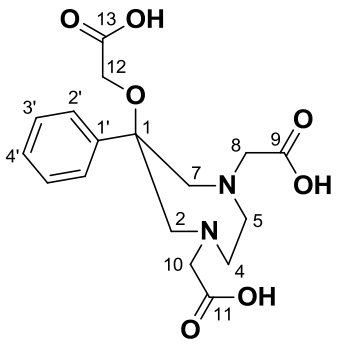

The triester **5** (0.020 g, 0.037 mmol) was dissolved in trifluoroacetic acid : dichloromethane (1 : 1, 2 mL) and left to stir for 2 days at room temperature. The solvent was removed under reduced pressure, the residue re-dissolved in dichloromethane : methanol (1 : 1, 2 mL) and evaporated. This procedure was repeated twice, and with methanol. The resulting solid was then dissolved in water (10 mL) and washed with dichloromethane (10 mL). Removal of the solvent under reduced pressure afforded, after drying *in vacuo*, a white solid (0.014 g, 81 %). **^{1}H NMR (D_2O, pD = 2.66, 700 MHz):** δ_H 2.70 (1H, m, $H^{4/5}$); 2.79 (1H, m, $H^{4/5}$); 2.98 (1H, m, $H^{2/7}$); 3.25 (3H, m, $H^{2,7,12}$); 3.36 (2H, m, $H^{2/7,\ 4/5}$); 3.52 (1H, m, $H^{4/5}$); 3.81 (4H, m, $H^{8,10}$); 4.01 (1H, d, J 12, H^{12}); 7.30 – 7.33 (5H, m, Ph H). **^{13}C NMR (D_2O, pD = 2.66, 176 MHz)**: δ_C 34.18 ($C^{4/5}$); 49.87 ($C^{2/7}$); 55.69 ($C^{4/5}$); 59.38 ($C^{8/10}$); 62.75 (C^{12}); 63.38 ($C^{2/7}$); 72.90 (C^{1}); 124.42 & 128.46 & 128.91 ($C^{2',3',4'}$) 141.27 ($C^{1'}$); 169.51 & 169.55 ($C^{9/11}$); 175.20 (C^{13}). **MS ES+ (*m/z*):** found 389.1337 $[M+Na]^+$; $C_{17}H_{22}N_2NaO_7$ requires 389.1325. **Elemental analysis (%):** found C (47.8) H (4.97) N (5.71); $[C_{17}H_{22}N_2O_7].CF_3COOH$ requires C (47.5) H (4.83) N (5.83).

(E)-Tert-butyl 1,4-bis(2,4-dimethoxybenzyl)-6-phenyl-1,4-diazepan-6-ylcarbamate, **44***.

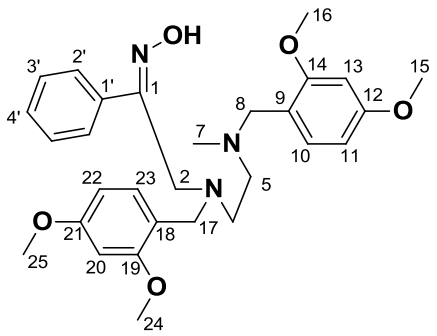

Sodium borohydride (0.013 g, 0.58 mmol) was added portionwise to a solution of nickel(II)chloride hexahydrate (0.025 g, 0.11 mmol) in anhydrous methanol (20 mL) cooled in an ice-bath, and the mixture stirred for 30 min. The protected amine **22** (0.100 g, 0.19 mmol) dissolved in anhydrous methanol (2 mL) was added to the reaction mixture, followed by sodium borohydride (0.028 g, 0.74 mmol) portionwise. The reaction mixture was allowed to warm to room temperature. The reaction was monitored using UV-vis TLC, to follow consumption of **22**. Once complete the reaction mixture was filtered through Celite®, and the insoluble borate salts washed with ice-cold methanol. The filtrates were combined, and the solvent removed under reduced pressure. The resulting residue was re-dissolved in chloroform (40 mL) and washed successively with aqueous potassium carbonate solution (2 x 30 mL, 0.1 M) and water (30 mL), dried over $MgSO_4$, filtered and the solvent removed under reduced pressure. Purification by silica gel column chromatography (hexane → 20 % ethyl acetate) afforded a colourless oil (0.075 g, 78 %). R_f = 0.35 (hexane : ethyl acetate; 50 : 50). **^{1}H NMR ($CDCl_3$, 500 MHz):** δ_H 2.16 (3H, s, H^7); 2.66 (2H, m, H^5); 2.74 (2H, m, H^4); 3.46 (2H, s, H^8); 3.67 (2H, s, H^{17}); 3.75 (6H, s, $H^{15/16,24/25}$); 3.79 (6H, s+s, $H^{15/16,24/25}$); 3.86 (2H, s, H^2); 6.41 (4H, m, $H^{13,14,22,23}$); 7.08 (1H, d, J 8, H^{20}); 7.18 (1H, d, J 8, H^{11}); 7.33 (3H, m, $H^{3',4'}$); 7.59 (2H, m, $H^{2'}$). **^{13}C NMR ($CDCl_3$, 125 MHz):** δ_C 42.52 (C^7); 51.24 (C^4); 53.23 (C^{17}); 53.43 (C^2); 54.34 (C^5); 55.40 ($C^{15/16,24/25}$); 55.50 ($C^{15/16,24/25}$); 55.77 (C^8); 98.64 ($C^{13/14/22/23}$); 98.71 ($C^{13/14/22/23}$); 104.09 ($C^{13/14/22/23}$); 104.28 ($C^{13/14/22/23}$); 117.15 (C^{18}); 119.16 (C^9); 126.31 ($C^{2'}$); 128.52 ($C^{3'/4'}$); 128.99 ($C^{3'/4'}$); 131.82 (C^{11}); 132.46 (C^{20}); 136.52 ($C^{1'}$); 154.26 (C^1); 159.03 (C^{10}); 159.34 (C^{19}); 160.24 ($C^{12/21}$); 161.01 ($C^{12/21}$). **HR MS ES+ (*m/z*):** found 508.2818 $[M + H]^+$; $C_{29}H_{38}N_3O_5$ requires 508.2811.*synthetic protocol adopted from[11].

(E)-2-((2,4-Dimethoxybenzyl)(2-((2,4-dimethoxybenzyl)(methyl)amino)ethyl)amino)-1-phenylethanone oxime, **45**.

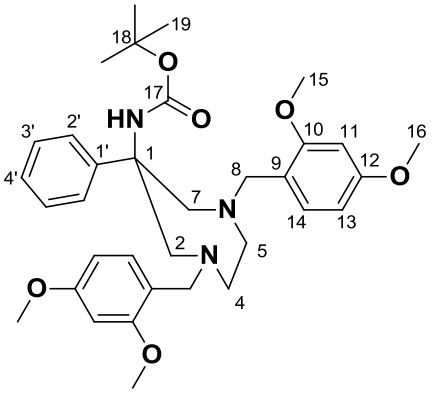

Synthesis of the NHBoc-protected primary amine, **45**, was carried out in two steps. In the first step the primary amine **22**‡ was formed by reduction of the nitro-functionality, followed by Boc-protection of the resulting primary amine.

A water slurry of Raney nickel (0.010 g) was washed with methanol (3 x 25 mL) and ethanol added (10 mL). The suspension was then transferred into a solution of **22** (0.050 g, 0.096 mmol) in ethanol (25 mL). The flask was evacuated and back-filled with hydrogen gas using four vacuum-purge cycles, and the mixture stirred at 298 K under an atmosphere of hydrogen. The reaction was monitored by UV-vis TLC for formation of the primary amine. Once complete (~ 3 h), the solution was decanted, and the solid washed with methanol (3 x 20 mL). The washings and decanted solution were combined, removed under reduced pressure and re-dissolved in methanol (25 mL). Remaining Raney nickel and insoluble by-products where removed by filtration through a base washed Celite® filter, and the solvent was then removed under reduced pressure. The resulting oil was re-dissolved in chloroform : isopropyl alcohol (80 : 20, 20 mL) and washed successively with aqueous sodium hydroxide (2 x 20 mL, 0.5 M) and water (15 mL), dried over $MgSO_4$, filtered and the solvent removed under reduced pressure to yield a colourless oil.

Di-*tert*-butyl dicarbonate (0.042 g , 0.19 mmol) was added gradually, to a solution of **22**‡ (from the previous step) and triethylamine (0.029 g, 0.29 mmol) in chloroform (15 mL), and the mixture stirred at room temperature. The reaction was monitored by LS-ES MS, to follow consumption of **22**‡. Once complete the solvent was removed and the residue re-dissolved in chloroform (15 mL) and washed successively with aqueous sodium hydroxide (2 x 15 mL, 0.5 M) and water (3 x 10 mL), dried over $MgSO_4$, filtered and the solvent removed under reduced pressure to yield a colourless oil.

Purification by silica gel column chromatography (hexane → 60 % ethylacetate) afforded a colourless oil (0.005 g, 9 %). R_F = 0.35 (hexane : ethylacetate, 50 : 50). **^{1}H NMR ($CDCl_3$, 700 MHz):** δ_H 1.36 (3H, s, H^{19}); 2.48 (4H, s, H^8); 2.72 (2H, m, $H^{4,5}$); 3.35 (2H, m, $H^{4,5}$); 3.46 (2H, d, J 13, $H^{2,7}$); 3.59 (2H, d, J 13, $H^{2,7}$); 3.73 (6H, s, $H^{15/16}$); 3.78 (6H, s, $H^{15/16}$); 6.37 (2H, d, J 8, H^{11}); 6.41 (2H, s, H^{13}); 7.14 (4H, m, $H^{3',4',10}$); 7.35 (4H, m, $H^{2'}$). **^{13}C NMR ($CDCl_3$, 176 MHz):** δ_C 28.25 (C^{19}); 55.33 ($C^{15/16}$); 55.53 ($C^{15/16}$); 57.19 (C^8); 57.33 ($C^{2/7}$); 57.84 (C^1); 68.77 ($C^{4/5}$); 78.61 (C^{18}); 98.65 (C^{11}); 103.73 (C^{13}); 120.21 (C^9); 125.17 ($C^{2'}$); 125.75 ($C^{3'}$); 125.92 ($C^{4'}$); 131.12 (C^{14}); 146.19 (C^{17}); 159.46 (C^{12}); 159.76 (C^{10}). **HR MS ES+ (*m/z*):** found 592.3406 $[M + H]^+$; $C_{34}H_{46}N_3O_6$ requires 592.3387; found 614.3221 $[M + Na]^+$; $C_{34}H_{45}N_3NaO_6$ requires 614.3206.

6-phenyl-1,4-diazepan-6-amine, **46**.

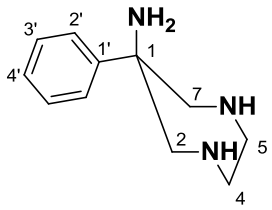

Trifluoroacetic acid (1 mL) was added to a solution of the protected diamine/amido **45** (0.010 g, 0.0.017 mmol) in dichloromethane (1 mL), and the mixture stirred at room temperature. The reaction was monitored using LC-ESI MS, to follow removal of the dimethoxy-benzyl substituents and deprotection of the primary amine. Once complete, the solvent was removed by lyophilisation. Excess trifluoroacetic acid was removed through repeated addition and removal of dichloromethane (3 x 2 mL) and subsequently methanol (3 x 2 mL), to afford a white solid (0.004 g*). **^{1}H NMR (CD_3OD, 600 MHz):** δ_H 3.37 (2H, m, $H^{4,5}$); 3.42 (2H, d, J 15, $H^{2,7}$); 3.56 (2H, m, $H^{4,5}$); 3.70 (2H, d, J 15, $H^{2,7}$); 7.29 (1H, t, J 8, $H^{4'}$); 7.35 (2H, t, J 8, $H^{3'}$); 7.38 (2H, d, J 8, $H^{2'}$). **^{13}C NMR (CD_3OD, 151 MHz):** δ_C 43.77 ($C^{4,5}$); 53.13 ($C^{2,7}$); 65.88 (C^1); 124.76 ($C^{2'}$); 125.00 ($C^{4'}$); 129.48 ($C^{3'}$). **HR MS ES+ (*m/z*):** found 192.1485 $[M + H]^+$; $C_{11}H_{18}N_3$ requires 192.1501. *Product isolated is of undetermined constitution. Presumed to be a trifluoroacetate salt.

4.3 Syntheses of 'Cold' Gallium(III) Complexes of L^n (n = 2, 3, 6, 8)

[Ga.L^n]; n = 2, 3, 6, 8.

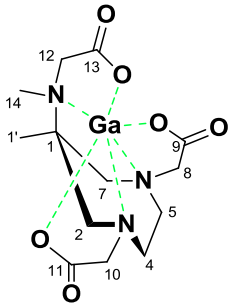

[Ga.L^2]

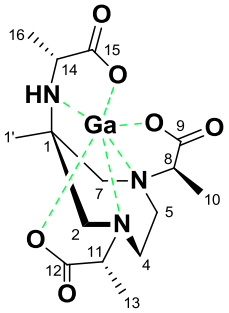

[Ga.L^3]

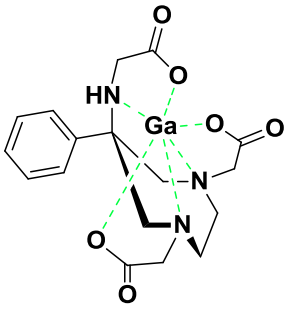

[Ga.L^6]

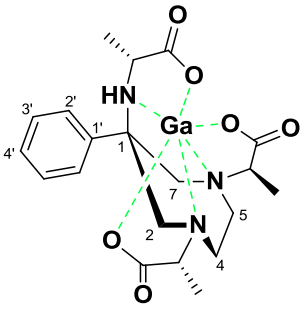

[Ga.L^8]

The general procedure for the synthesis of cold gallium complexes is as follows. The ligand in 2 mL of a methanol : water (1 : 2) mixture and equilibrated at 333 K. Gallium nitrate hexahydrate (1 equivalent) was added, and the pH adjusted to 4.5 using 0.10 M aqueous sodium hydroxide. The reaction mixture was stirred for 1 h, and allowed to cool slowly to room temperature. Single crystals of the complexes suitable for single crystal X-ray diffraction formed from solution upon standing over ~ 36 h. Crystalline material was isolated by filtration, and dried *in vacuo*. Yields and elemental constitution were not determined.

In ^{1}H NMR assignments Pureshift ^{1}H NMR experiments were used to provide better signal resolution. Due to signal overlapping coupling constants are not provided in some cases. The superscript '*' is used to denote proton resonances arising from protons attached to the same carbon atom, when the orientation (ax/eq) could not be assigned.

[Ga.L^2]:

^{1}H NMR (D_2O, pD 6.17, 600 MHz): δ_H 1.03 (3H, s, $H^{1'}$); 2.43 (3H, s, H^{14}); 3.12 (1H, m, $H^{4*/5*}$); 3.14 (1H, m, $H^{5*/4*}$); 3.20 (1H, d, J 16, H^{2ax}); 3.21 (1H, d, J 12, H^{12*}); 3.28 (1H, d, J 16, H^{10*}); 3.35 (1H, m, $H^{4/5}$); 3.41 (1H, m, $H^{5/4}$); 3.46 (1H, d, J 16, H^{7eq}); 3.57 (1H, d, J 16, H^{7ax}); 3.59 (1H, d, J 16, H^{2eq}); 3.71 (1H, d, J 19, H^{8*}); 3.77 (1H, d, J 16, H^{10}); 3.89 (1H, d, J 12, H^{12}); 3.91 (1H, d, J 19, H^8). **^{13}C NMR (D_2O, pD 6.17, 151 MHz):** δ_C 12.10 ($C^{1'}$); 37.96 (C^{14}); 53.01 (C^{14}); 58.22 ($C^{4/5}$); 59.80 (C^1); 60.41 (C^8); 61.31 (C^{10}); 63.57 (C^7); 64.00 (C^2); 174.10 & 174.67 & 174.82 ($C^{9,11,13}$). **HR MS ES+ (*m/z*):** found 384.0677 $[M + H]^+$; $C_{13}H_{21}N_3O_6Ga$ requires 384.0686. The structure of **[Ga.L^2]** was confirmed by single crystal X-ray diffraction: $C_{12}H_{20}N_3O_6.½H_2O$, M_r = 393.05, orthorhombic (Fdd2); a = 28.8536(7) Å, b = 27.2438(7) Å, c = 7.57981(19) Å, V = 5958.3(2) Å^3,α = 90.00°, β = 90.00°, γ = 90.00°, Z = 16; μ = 1.888 mm^{-1}, $D_{calc.}$ = 1.753 mg.mm^{-3}, T 120(2) K; 4319 independent reflections (R_{int} = 0.0417), R_1 = 0.0307, ωR_2 = 0.0657 ($I > 2\sigma(I)$). CCDC # 906036.

[Ga.L^3]:

^{1}H NMR (D_2O, pD 6.13, 600 MHz): δ_H 1.13 (3H, d, J 7, $H^{10/13/16}$); 1.21 (3H, s, $H^{1'}$); 1.36 (3H, d, J 7, $H^{10/13/16}$); 1.46 (3H, d, J 7, $H^{10/13/16}$); 2.83 (1H, d, J 15, H^{7ax}); 2.85 (1H, m, $H^{4*/5*}$); 3.07 (1H, m, $H^{4/5}$); 3.21 (1H, m, $H^{5*/4*}$); 3.42 (2H, m, $H^{5/4\ \&\ 7eq}$); 3.63 (1H, d, J 15, H^{2eq}); 3.78 – 3.84 (3H, m, $H^{8,11,14}$). **^{13}C NMR (D_2O,pD 6.13, 151 MHz):** δ_C 10.49 & 14.23 & 17.36 ($C^{10,13,16}$); 17.95 ($C^{1'}$); 41.15 ($C^{4/5}$); 46.68 ($C^{4/5}$); 49.66 (C^{14}); 56.94 (C^7); 60.64 (C^1); 64.77 (C^2); 64.44 & 66.38 ($C^{8,11}$); 176.96 & 178.42 & 179.07 ($C^{9,12,15}$). **HR MS ES+ (*m/z*):** found 412.1018 $[M + H]^+$; $C_{15}H_{25}N_3O_6Ga$ requires 412.0999. The structure of **[Ga.L^3]** was confirmed by single crystal X-ray diffraction: $C_{15}H_{24}N_3O_6.H_2O$, M_r = 430.11, monoclinic ($P2_1$); a = 7.58267(20) Å, b = 12.6657(3) Å, c = 9.2185(2) Å, V = 869.85(4) Å^3,α = 90.00°, β = 100.735(3)°, γ = 90.00°, Z = 2; μ = 1.627 mm^{-1}, $D_{calc.}$ = 1.642 mg.mm^{-3}, T 120(2) K; 4501 independent reflections (R_{int} = 0.0433), R_1 = 0.0322, ωR_2 = 0.0670 ($I > 2\sigma(I)$). CCDC # 906037.

[Ga.L^6]:

Insfficient amount of the complex was obtained to get a ^{1}H and ^{13}C NMR. Constitution has been confirmed by X-ray crystal structure analysis. **HR MS ES+ (*m/z*):** found 431.0599 $[M + H]^+$; $C_{17}H_{21}N_3O_6Ga$ requires 431.0608. The structure of **[Ga.L^6]** was confirmed by single crystal X-ray diffraction: $C_{17}H_{20}N_3O_6$, M_r = 432.08, triclinic (P-1); a = 10.6961(8) Å, b = 13.0778(12) Å, c = 12.8414(12) Å, V = 1652.8(2) Å^3,α = 116.076(9)°, β = 105.208(7)°, γ = 92.002(2)°, Z = 4; μ = 1.709 mm^{-1}, $D_{calc.}$ = 1.736 mg.mm^{-3}, T 120(2) K; 7571 independent reflections (R_{int} = 0.0881), R_1 = 0.0699, ωR_2 = 0.1553 ($I > 2\sigma(I)$). CCDC # 906038.

[Ga.L^{8}]:

^{1}H NMR (D_2O, pD 6.02, 600 MHz): δ_H 0.86 & 1.25 & 1.42 (9H, d, J 7, $H^{10,13,16}$); 2.94 (1H, m, $H^{4*/5*}$); 3.13 (1H, m, $H^{4*/5*}$); 3.33 (1H, m, $H^{5*/4*}$); 3.53 (1H, q, H^{14}); 3.56 (1H, m, $H^{5/4}$); 3.65 (1H, d, J 14 $H^{2*/7*}$); 3.75 (2H, d+d, $H^{7*/2*\ \&\ 7/2}$); 3.97 (2H, m, $H^{2/7\ \&\ 8*/11*}$); 4.17 (1H, d, J 16 $H^{8/11}$); 7.42 (5H, m, $H^{2',3',4'}$). **^{13}C NMR (D_2O, pD 6.02, 151 MHz):** δ_C 10.69 & 14.38 & 16.29 ($C^{10,13,16}$); 46.67 ($C^{4/5}$); 50.67 (C^{14}); 55.58 ($C^{2/7}$); 58.92 (C^{1}); 61.04 ($C^{4/5}$); 64.34 ($C^{2/7}$); 65.79 & 67.06 ($C^{8,11}$); 77.73 ($C^{1'}$); 126.47 & 129.32 & 129.96 ($C^{2',3',4'}$); 177.04 & 177.47 & 178.32 ($C^{9,12,15}$). **HR MS ES+ (*m/z*):** found 474.1149 $[M + H]^+$; $C_{20}H_{27}N_3O_6Ga$ requires 474.1156.

The structure of **[Ga.L^{8}]** was confirmed by single crystal X-ray diffraction: $C_{20}H_{26}N_3O_6$, M_r = 474.16, orthorhombic ($P2_12_12_1$); a = 7.3312(7) Å, b = 13.9288(12) Å, c = 19.6479(19) Å, V = 2006.3(3) Å^3,α = 90°, β = 90°, γ = 90°, Z = 4; μ = 2.262 mm^{-1}, $D_{calc.}$ = 1.570 mg.mm^{-3}, T 120(2) K; 2554 independent reflections (R_{int} = 0.0471), R_1 = 0.0477, ωR_2 = 0.1195 ($I > 2\sigma(I)$). *Not yet submitted to CCDC*.

5 References

1. P. K. Glasoe and F. A. Long, *Journal of Physical Chemistry*, 1960, **64**, 188-190.
2. G. M. Sheldrick, *Acta Crystallographica Section A*, 2008, **64**, 112-122.
3. O. V. Dolomanov, L. J. Bourhis, R. J. Gildea, J. A. K. Howard and H. Puschmann, *Journal of Applied Crystallography*, 2009, **42**, 339-341.
4. K. P. Zhernosekov, D. V. Filosofov, R. P. Baum, P. Aschoff, H. Bihl, A. A. Razbash, M. Jahn, M. Jennewein and F. Roesch, *Journal of Nuclear Medicine*, 2007, **48**, 1741-1748.
5. S. Aime, L. Calabi, C. Cavallotti, E. Gianolio, G. B. Giovenzana, P. Losi, A. Maiocchi, G. Palmisano and M. Sisti, *Inorg Chem*, 2004, **43**, 7588-7590.
6. S. Aime, G. Bombieri, C. Cavallotti, G. B. Giovenzana, D. Imperio and N. Marchini, *Inorganica Chimica Acta*, 2008, **361**, 1534-1541.
7. L. Tei, G. Gugliotta, M. Fekete, F. K. Kalman and M. Botta, *Dalton Trans*, 2011, **40**, 2025-2032.
8. P. M. O'Brien, D. R. Sliskovic, C. J. Blankley, B. D. Roth, M. W. Wilson, K. L. Hamelehle, B. R. Krause and R. L. Stanfield, *Journal of Medicinal Chemistry*, 1994, **37**, 1810-1822.
9. T. Hanano, K. Adachi, Y. Aoki, H. Morimoto, Y. Naka, M. Hisadome, T. Fukuda and H. Sumichika, *Bioorganic & Medicinal Chemistry Letters*, 2000, **10**, 875-879.
10. R. Ballini, L. Barboni and G. Giarlo, *J Org Chem*, 2004, **69**, 6907-6908.
11. J. O. Osby and B. Ganem, *Tetrahedron Letters*, 1985, **26**, 6413-6416.